PNRR - Missione 4, Componente 2, Investimento 1.5 - D.D. 3277 del 30.12.2021- Avviso pubblico per la presentazione di Proposte di intervento per la creazione e il rafforzamento di "ecosistemi dell'innovazione", costruzione di "leader territoriali di R&S" – Ecosistemi dell'Innovazione

Progetto SAMOTHRACE - Sicilian MicronanoTech Research And Innovation Center

CUP J43C22000310006 - codice identificativo ECS00000022

UNIVERSITÀ DEGLI STUDI DI MESSINA

Dipartimento Di Scienze Chimiche, Biologiche, Farmaceutiche Ed Ambientali

CORSO DI DOTTORATO DI RICERCA

IN BIOLOGIA APPLICATA E MEDICINA SPERIMENTALE

(XXXVIII CICLO)

Coordinatore: Chiar.ma Prof.ssa **Emanuela ESPOSITO**

SSD BIOS-01/B, BIOS-04/A

Sustainable strategies for the mitigation of anthropogenic impact: Valorization of algal biomass and multimodel experimental validation

DOTTORANDO

Dott.ssa **Barbara BILLÈ**

BARBARA BILLÈ
26.05.2026 14:33:47
GMT+02:00

SUPERVISORE:

Chiar.ma Prof.ssa **Marina MORABITO**

Firmato digitalmente da Marina Morabito
Data: 26.05.2026 15:32:56 CEST
Organizzazione: UNIVERSITA' DEGLI STUDI DI MESSINA/80004070837

CO-SUPERVISORE:

Chiar.ma Prof.ssa **Maria MAISANO**

Firmato digitalmente da Maria Maisano
Data: 26.05.2026 14:23:19 CEST
Organizzazione: UNIVERSITA' DEGLI STUDI DI MESSINA/80004070837

A.A. 2024/2025

Index

PREFACE

CHAPTER 1

Agricultural pesticides as emerging ecotoxicological stressors

1.1 General introduction

1.2 Environmental monitoring

1.3 Pesticides and the environment: A silent threat

- **1.3.1 Classification and major categories of pesticides**
- **1.3.2 Dithiocarbamates: Chemical properties, uses, and toxicity**
- **1.3.3 Thiram: Agricultural applications, environmental persistence, and ecotoxicological concerns**

1.4 Sentinel organisms in environmental impact assessment

1.4.1 *Arbacia lixula:* Sea urchin as a key bioindicator of marine ecosystems

- **1.4.1.1 Embryogenesis and larval development**
- **1.4.1.2 Skeletogenesis and sensitivity to contaminants**
- **1.4.1.3 Stress biomarkers and metabolic alterations**

1.4.2 *Danio rerio*: Zebrafish as a translational model

- **1.4.2.1 Overview of anatomy and physiology**
- **1.4.2.2 Embryonic development**
- **1.4.2.3 Experimental advantages and applications in ecotoxicology**

1.5 The thyroid axis in embryonic development: A shared evolutionary pathway

- **1.5.1 The thyroid system as a regulator of growth and development**
- **1.5.2 Evolutionary conservation of thyroid-related genes in invertebrates and vertebrates**
- **1.5.3 Chemical disruption and pesticide interference: the case of thiram**

1.6 References

CHAPTER 2

Valorization of algal waste biomass for the mitigation of environmental contaminants within a circular economy framework

2. General introduction

2.1 Environmental burden of algal waste biomass and its ecotoxicological implications

2.2 Hydrothermal Carbonization (HTC) as a sustainable strategy for biomass valorization and pollutant mitigation

2.2.1 Hydrothermal Carbonization process

2.2.2 HTC-Derived materials in environmental remediation

2.3 References

CHAPTER 3

Aims of the thesis

CHAPTER 4

The fungicide thiram alters the embryo-larval development of the black sea urchin Arbacia lixula by inducing multifactorial toxicological responses

4.1 Introduction

4.2 Material and methods

4.2.1 Gamete collection and experimental design

4.2.2 Toxicological dose-response modelling

4.2.3 Morphological analysis

4.2.4 Biochemical analysis

4.2.4.1 Neurotoxicity

4.2.4.2 Antioxidant activity

4.2.5 Metabolomic analysis

4.2.5.1 Metabolite extraction from sea urchin embryos

4.2.5.2 Metabolomics based on ^{1}H NMR

4.2.5.3 Metabolic pathway and enrichment analysis

4.2.6 Gene expression analysis (RT-qPCR)

4.2.7 Statistical analysis

4.3 Results

4.3.1 Mortality and developmental effects

4.3.2 Morphological observations

4.3.3 Biochemical assays

4.3.3.1 Neurotoxicity

4.3.3.2 Antioxidant activity

4.3.4 Metabolomic evaluation

4.3.4.1 Effects on metabolites

4.3.4.2 Pathway and enrichment analysis

4.3.5 Up-regulation of developmental and stress-related genes

4.4 Discussions

4.5 Conclusions

4.6 References

CHAPTER 5

Macroalgae-derived hydrochar as an eco-sustainable biofilter: adsorption properties and protective potential against thiram toxicity

5.1 Introduction

5.2 Materials and methods

5.2.1 Hydrothermal carbonization (HTC) process

5.2.2 Morpho-chemical analyses of hydrochar

5.2.3 Preparation of thiram solutions and exposure conditions

5.2.4 Biological assays and experimental setup using the sea urchin *Arbacia lixula*

5.2.5 Developmental assessment

5.2.6 Metabolomic investigation

5.2.6.1 Metabolite extraction from sea urchin embryos

5.2.6.2 NMR-based metabolomic profiling

5.2.7 Transcriptional analysis of stress-related genes

5.2.8 Statistical evaluation

5.3 Results

5.3.1 Morpho-chemical observations

5.3.2 Developmental outcomes

5.3.3 Metabolomic responses

5.3.3.1 Effects on metabolites

5.3.3.2 Multivariate metabolomic analysis

5.3.4 Gene expression patterns

5.4 Discussion

5.5 Conclusions

5.6 References

CHAPTER 6

Hydrochar-mediated rescue of thiram-induced developmental, metabolic, and thyroid disorders in Zebrafish (Danio rerio)

6.1 Introduction

6.2 Materials and methods

6.2.1 Preparation of hydrochar-based systems

6.2.2 Preparation of thiram solutions and exposure conditions

6.2.3 Zebrafish husbandry and breeding conditions

6.2.4 Embryo collection and exposure protocol

6.2.5 Zebrafish embryo acute toxicity test (ZFET)

6.2.6 Analysis of developmental phenotypes

6.2.7 Metabolomic investigation

6.2.7.1 Extraction of polar metabolites

6.2.7.2 ^{1}H NMR metabolic profiling

6.2.7.3 Pathway and network analysis

6.2.8 Gene Expression analysis of endocrine and stress markers

6.2.9 Statistical analysis

6.3 Results

6.3.1 Developmental toxicity and rescue effects

6.3.2 Metabolomic reprogramming and mitigation

6.3.2.1 Differential metabolite signatures

6.3.2.2 Multivariate statistical analysis of the polar metabolomic data

6.3.2.3 Pathway-level metabolic responses

6.3.3 Endocrine and stress-related transcriptional alterations

6.4 Discussion

6.5 Conclusions

6.6 References

CHAPTER 7

AHL-Derived liquid as a natural biostimulant: effects on Phaseolus vulgaris under stress conditions

7.1 Introduction

7.2 Materials and methods

7.2.1 Obtaining AHL solutions

7.2.2 NMR-Based metabolomic characterization of the AHL

7.2.2.1 Pathway mapping and enrichment analysis of AHL metabolites

7.2.3 Seed priming procedure and experimental design

7.2.4 Plant growth and anatomical traits

7.2.4 Plant water relations

7.2.6 Enzymatic antioxidant activities and lipid peroxidation

7.2.7 Statistical analysis

7.3 Results

7.3.1 NMR-Based metabolomic profile of the AHL

7.3.1.1 Pathway enrichment analysis

7.3.2 Effects of AHL seed priming on plant morphology

7.3.3 Stomatal conductance dynamics during recovery

7.3.4 Antioxidant enzyme activities and lipid peroxidation

7.4 Discussion

7.5 Conclusions

7.6 References

CHAPTER 8

8.1 General conclusions

8.2 Future prospective

LIST OF ABBREVIATIONS

AChE AcetylCholinEsterase

°C Degrees Celsius

µL Microliter

µm Micrometer

^{1}H NMR Proton Nuclear Magnetic Resonance

act Actin

AMPK 5' AMP-activated protein Kinase

BCAA Branched Chain Amino Acids

CAT Catalase

cDNA Complementary DNA

Cu/Zn-SOD Cooper/Zinc-SuperOxide Dismutase

D2O Deuterated water

Da Dalton

DNA DeoxyriboNucleic Acid

DSS Sodium 2,2-dimethyl-2-silapentane-5-sulfonate

DW Distilled Water

EC Emergent Contaminant

ECHA European Chemicals Agency

ED Endocrine Disrupting

EDC Endocrine Disrupting Compound

EFSA European Food Safety Authority

elfα Elongation factor α

FSW Filter Sea Water

GPx Glutathione Peroxidase

GSH Reduced Glutathione

GST Glutathione *S*-transferase

h Hour

H_2O_2 Hydrogen peroxide

LPO Lipid peroxidation

M Molar

MDA Malondialdehyde

mg Milligrams

MHz MegaHertz

min Minutes

mL Milliliters

mm Millimeter

mM MilliMolar

nmol nanomol

mRNA Messenger RiboNucleic Acid

ms Milliseconds

mV MilliVolt

Na/K ATPase Sodium/Potassium ATPase pump

NADH Reduced Nicotinammine Adenine Dinucleotide

NADPH Nicotinamide adenine dinucleotide phosphate

NOESY 1D Nuclear Overhauser Effect SpectroscopY One Dimensional

OECD Organization for Economic Co-operation and Development

PBS Phosphate Buffered Saline

ppm Parts per million

RNA RiboNucleic Acid

ROS Reactive Oxygen Species

rpm Revolutions per minute

rRNA Ribosomal RNA

RT Room Temperature

RT-qPCR Real Time-quantitative Polymerase Chain Reaction

Sal Salinity

SD Standard Deviation

sec Seconds

SW Sea Water

Tris-HCL Tris-Hydrochloride

ΔΨ m Relative value of the mitochondrial membrane potential

PREFACE

Environmental pollution associated with the extensive use of agrochemicals represents one of the most critical challenges for ecosystem integrity and environmental sustainability. Among chemical stressors, pesticides play a prominent role due to their widespread application, environmental persistence, and ability to affect non-target organisms through complex and often sublethal mechanisms. Increasing evidence indicates that traditional toxicological approaches, largely based on lethality, are insufficient to fully capture the ecological risks posed by these compounds, particularly during early developmental stages that are highly sensitive to chemical disruption. At this level, pesticide exposure may interfere with evolutionarily conserved developmental pathways, including thyroid hormone–related signalling, which plays a key regulatory role during embryogenesis in both invertebrates and vertebrates and represents a sensitive target of chemical stress. At the same time, the growing accumulation of organic waste biomass represents an additional environmental burden, requiring innovative strategies capable of coupling waste management with value recovery. In this context, circular economy frameworks offer a promising opportunity to transform residual biomasses into functional materials that can actively contribute to environmental protection and sustainability. This thesis is positioned at the intersection of these two challenges. It investigates the ecotoxicological effects of the dithiocarbamate fungicide thiram on aquatic non-target organisms and explores the valorization of waste algal biomass through hydrothermal carbonization (HTC) as a sustainable mitigation strategy. Importantly, HTC is addressed in this work not merely as a waste-treatment technology, but as an integrated

platform generating two functionally distinct products: a solid fraction (hydrochar), exploited as a bio-based adsorbent for environmental contaminants, and a liquid fraction (AHL), evaluated for its potential use as a biostimulant to enhance plant growth and stress tolerance. Accordingly, this thesis integrates ecotoxicological and plant physiological approaches within a unified framework: aquatic model organisms (*Arbacia lixula* and *Danio rerio*) are used to investigate thiram toxicity and the capacity of hydrochar to mitigate its adverse effects, while plant-based assays on *Phaseolus vulgaris* L. are specifically employed to evaluate the ability of the HTC-derived aqueous liquid (AHL) to enhance plant resilience under stress conditions. Overall, this thesis seeks to demonstrate that coupling ecotoxicological assessment with biomass valorization can lead to innovative and sustainable solutions, in which waste materials are transformed into functional tools for pollution mitigation and agricultural support, fully aligned with current environmental protection policies and the transition toward a bio-based circular economy.

CHAPTER 1

Agricultural pesticides as emerging ecotoxicological stressors

1.1 General introduction

Pesticide pollution represents one of the major threats to the environment and public health, as extensively documented at the global scale (Tang et al., 2021; Ullah et al., 2015; Wang et al., 2020). Over recent decades, the growing demand for agricultural production has driven the intensive use of plant protection products and biocides.

Although these substances have contributed to improved crop yields and the control of weeds and pathogens, their benefits have been accompanied by increasingly evident adverse environmental effects linked to frequent, widespread, and sometimes poorly regulated application.

Consequently, the need for corrective measures and international regulatory frameworks has become progressively more urgent. Despite the implementation of restrictions, bans, and regulatory controls, pesticide residues continue to be detected in multiple environmental compartments, including soils, surface and groundwater, sediments, and the atmosphere, often at concentrations that pose risks to exposed organisms and, indirectly, to humans (Malarvannan et al., 2014; EFSA, 2020).

This persistence largely reflects the intrinsic chemical properties of many pesticides and their metabolites, which may remain environmentally active for prolonged periods depending on molecular structure, degradation pathways, and site-specific ecological conditions (Feng et al., 2024; Tsen et al., 2021; Wei et al., 2021).

Environmental transport processes further exacerbate this issue: runoff and leaching transfer residues from soils to aquatic systems, while volatilization and spray

drift promote their dispersion far beyond the site of application (Carvalho, 2017; Tang et al., 2021).

A particularly critical aspect concerns the capacity of pesticides to disrupt ecological balance beyond their intended targets. Pesticide action is rarely fully selective; compounds designed to control specific pests or weeds may directly or indirectly affect non-target components of the biocenosis, leading to biodiversity loss and degradation of soil biological communities (Malik et al., 1999; John et al., 2017; Beketov et al., 2013; Lushchak et al., 2018).

Pollinating insects, aquatic macroinvertebrates, and soil microorganisms are among the most vulnerable groups, and adverse effects on these organisms can impair essential ecosystem services such as pollination and soil fertility maintenance (Hutter et al., 2018; Geiger et al., 2010; Sánchez-Bayo & Wyckhuys, 2019).

Moreover, the widespread emergence of pesticide resistance, driven by repeated and intensive application of the same active ingredients, forces target populations to develop tolerance, thereby requiring higher application doses or the introduction of new chemical formulations. This feedback loop further intensifies environmental contamination and ecological pressure (Sparks & Nauen, 2015; Bass et al., 2015).

The environmental consequences are multifaceted. In soils, pesticides can accumulate and interact with microbial communities and soil fauna, compromising fertility and biological equilibrium. In aquatic environments, runoff and leaching facilitate the transfer of residues into the water column, adversely affecting ecosystems often characterized by organisms highly sensitive to xenobiotic contamination (Eswaran et al., 2023; Ullah et al., 2015).

Equally significant is the presence of pesticide residues in agricultural products intended for human consumption. Although some plant species can metabolize pesticides into less toxic compounds, food crops may accumulate residues that are transferred along the food chain, ultimately reaching humans (Dogheim et al., 2001; Abbassy, 2001; Andersen and Poulsen, 2001; Poulsen and Andersen, 2003; Elgueta et al., 2017; Fantke et al., 2018).

Bioaccumulation and biomagnification further amplify toxic effects within trophic networks, disproportionately impacting apex predators and human populations exposed through diet and environmental contact (Pastor Ciscato et al., 2009; Caldas et al., 2006; EFSA, 2020). Importantly, toxic effects are not limited to acute lethality.

A growing body of evidence indicates that chronic or low-dose exposures can induce sub-lethal outcomes, including oxidative stress, endocrine disruption, immunosuppression, reduced fertility, and altered embryonic development (Ghoto et al., 2019; Kim et al., 2017; Gore et al., 2015).

Particular concern surrounds pesticides acting as endocrine-disrupting chemicals (EDCs), capable of interfering with key hormonal pathways such as the thyroid axis, which plays a fundamental role in embryonic development in both vertebrates and invertebrates. This aspect constitutes one of the central threads of the present research.

Globally, annual pesticide use exceeds 2.5 million tonnes (FAO, 2021), and monitoring programs consistently report the widespread presence of residues across diverse ecosystems. Despite regulatory advances, including European Regulation (EC) No. 1107/2009 and Directive 2009/128/EC on the sustainable use of pesticides, the problem remains unresolved.

Environmental persistence, bioaccumulation, and biomagnification have rendered pesticides ubiquitous across natural compartments, from freshwater systems to oceans, from soils to the atmosphere, and ultimately in everyday food products (Pacini et al., 2025; EFSA, 2020).

The current challenge therefore extends beyond reducing pesticide use through more sustainable agricultural practices; it also requires a deeper understanding of their biological and environmental effects. Ecotoxicology, which investigates the impacts of pollutants at molecular, cellular, organ, and population levels, plays a crucial role in this effort (Newman, 2014; Walker et al., 2020). At the same time, innovative and environmentally sustainable strategies are needed to mitigate pesticide contamination and its consequences for biodiversity.

1.2 Environmental monitoring

Environmental biomonitoring represents an indispensable tool for the integrated assessment of ecosystem health, particularly in complex and vulnerable environments such as marine and coastal systems. At the European level, the Marine Strategy Framework Directive (MSFD 2008/56/EC) defines Good Environmental Status as the capacity of marine ecosystems to maintain biodiversity, ecological functionality, and productivity while ensuring the sustainable use of resources over the long term (European Directive, 2008).

This framework, based on adaptive management and continuous monitoring, explicitly recognizes the need to complement traditional physico-chemical measurements with biological assessments of anthropogenic impacts (Elliott et al., 2022). Over recent decades, the intensification of human activities has progressively increased pollutant loads in aquatic environments, particularly in coastal areas receiving urban, agricultural, industrial, and sanitary discharges.

In many cases, wastewater treatment systems are not fully effective in removing complex chemical compounds, allowing the release of bioactive substances into marine environments even at low concentrations (Legislative Decree, 1999; Verlicchi et al., 2021). Within this context, emerging contaminants (ECs) have gained increasing attention. These predominantly anthropogenic substances are not yet fully regulated but can exert adverse effects on aquatic organisms and ecosystem health (Fig. 1) (Schoenfuss, 2021).

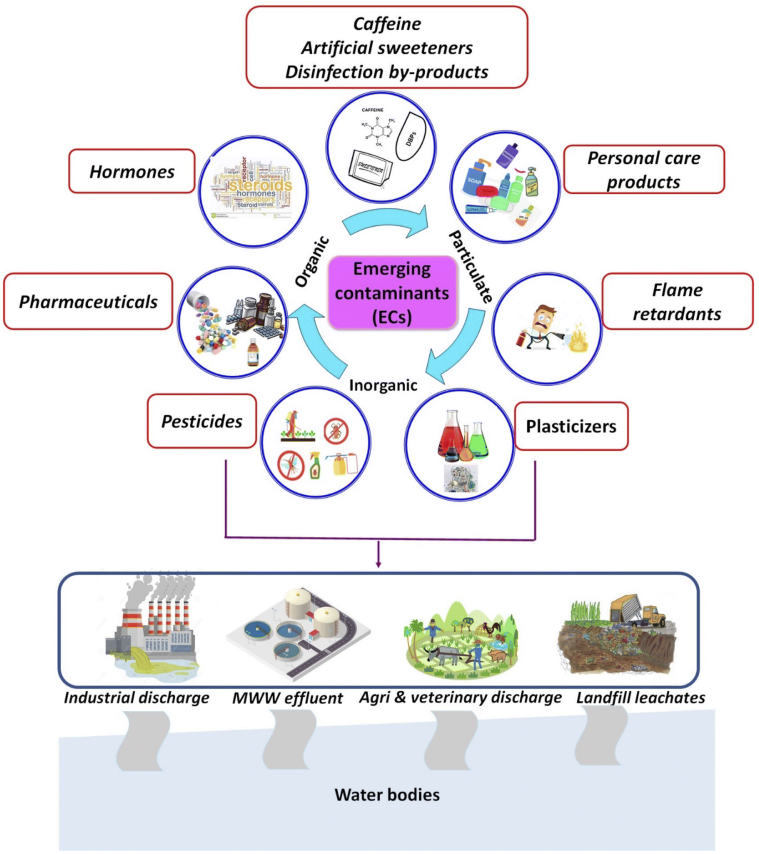


Fig. 1 - Conceptual classification of emerging contaminants (ECs) according to their chemical nature and use categories.

Among ECs, pesticides, pharmaceuticals, plasticizers, flame retardants, and microplastics are frequently detected in water, sediments, and biota. Particular concern surrounds Endocrine Disrupting Compounds (EDCs), capable of interfering with hormonal regulation even at extremely low concentrations (Fig. 2). Numerous studies show that such compounds can induce significant effects not only in adults but, more critically, during embryonic and larval stages, when endocrine regulatory systems are especially vulnerable (Tang et al., 2020; Thambirajah et al., 2022).

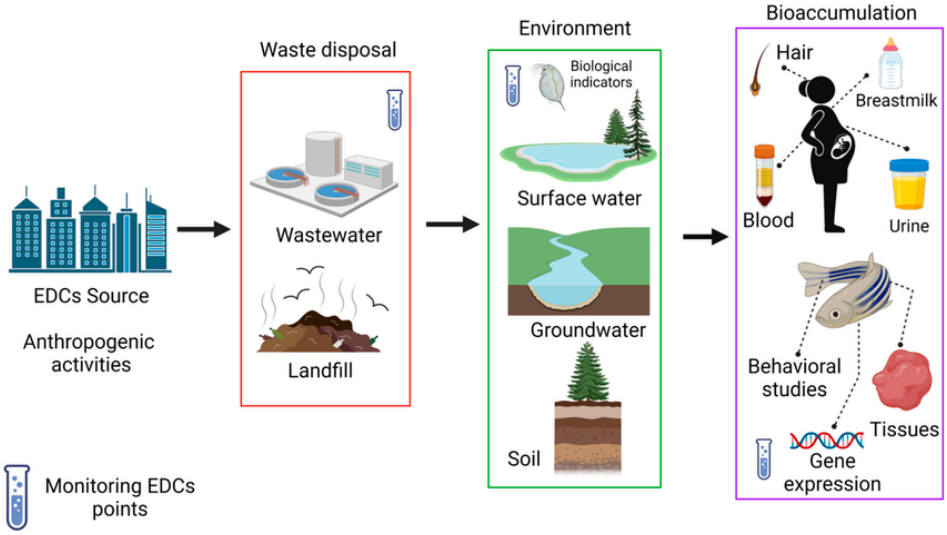


Fig. 2 - Schematic overview of the main anthropogenic sources of endocrine-disrupting compounds (EDCs).

Endocrine alterations may also impair gamete quality and fertility and, in some cases, produce transgenerational effects (Mallozzi et al., 2016; Menezo et al., 2019). Although environmental concentrations of many EDCs are typically within the ng/L–µg/L range, their continuous input, particularly near coastal discharge points, promotes chronic exposure, persistence, and bioaccumulation in resident organisms (Köck-Schulmeyer et al., 2021; Rout et al., 2021). These processes may lead to biomagnification along trophic webs, extending repercussions beyond target organisms and compromising ecosystem stability and, indirectly, human health (Álvarez-Ruiz et al., 2021; Anand et al., 2022; Wang et al., 2021).

Within Environmental Risk Assessment (ERA), parameters such as the Risk Quotient (RQ), defined as the ratio between the measured environmental concentration (MEC) and the predicted no-effect concentration (PNEC) for aquatic species, provide preliminary estimates of contaminant risk (Nika et al., 2020). However, these approaches often fail to capture real biological effects, especially in the presence of

contaminant mixtures or sub-lethal outcomes. The difficulty in directly linking chemical presence to biological responses underscores the need for integrative tools capable of bridging exposure and effect. In this context, biomonitoring based on biomarkers offers a critical connection between environmental contamination and biological impact. Biomarkers are measurable responses at molecular, biochemical, cellular, physiological, or organismal levels induced by environmental stressors (Lam & Gray, 2003). To be effective, they must provide early, sensitive, and reproducible signals capable of anticipating irreversible alterations and functioning as early warning systems (González-Fernández et al., 2015). Depending on specificity, biomarkers may respond selectively to particular contaminant classes or reflect general stress conditions, retaining evidence of exposure even after the contaminant is no longer detectable (De Pomerai, 1996; Sarkar et al., 2006).

In the present study context, the use of sentinel organisms across different phylogenetic levels enables a broader and comparative evaluation of contaminant effects. In marine systems, echinoderms such as *Arbacia lixula* represent highly sensitive models during embryonic development (Eliso et al., 2025; Maisano et al., 2015; Cappello et al., 2017) and are widely employed to assess alterations in skeletogenesis, metabolism, and redox balance following chemical exposure. In parallel, the teleost *Danio rerio*, owing to embryonic transparency and the evolutionary conservation of major endocrine pathways, serves as a reference vertebrate model for investigating endocrine effects, particularly those involving the hypothalamic–pituitary–thyroid axis (Vignet et al., 2019; Fetter et al., 2023). The combined use of these models allows integration across multiple levels of biological complexity, capturing both evolutionarily conserved responses and species-specific

sensitivities. In particular, the analysis of biomarkers related to thyroid axis regulation, an essential pathway in embryonic development in both vertebrates and invertebrates, provides a powerful approach to evaluating the impact of pesticides and EDCs on growth, differentiation, and organismal fitness. Methodologically, modern biomonitoring increasingly adopts a multi-biomarker approach that integrates morphological and histological analyses with biochemical, enzymatic, and molecular investigations (Vignet et al., 2019; Missawi et al., 2021; De Marco et al., 2022; Fasulo et al., 2010). Tissue-level alterations often represent early indicators of biological damage, while changes in gene expression and enzyme activity shed light on underlying stress-response mechanisms (McCarty & Munkittrick, 2008). These approaches are further complemented by –omics technologies, including ^{1}H-NMR-based metabolomics, which enable the simultaneous evaluation of multiple metabolic pathways and provide an integrated functional snapshot of physiological status (Lin et al., 2006; Cappello et al., 2018; Zhang et al., 2021; Sun et al., 2022). Overall, integrating traditional biomarkers with high-resolution analytical approaches in marine and freshwater sentinel organisms enables the early detection of sub-lethal effects induced by emerging contaminants. This strategy provides essential information not only at the individual level but also regarding potential population- and ecosystem-scale consequences. Such an approach is particularly relevant for clarifying how pesticides and EDCs disrupt key developmental and endocrine regulatory processes, thereby supporting the development of more effective strategies for environmental protection and the sustainable management of aquatic ecosystems.

1.3 Pesticides and the environment: A silent threat

Since the second half of the twentieth century, pesticide use has increased markedly and continuously, paralleling the intensification of agricultural practices and the expansion in the number of active ingredients available on the market (Fig. 3) (Shefali et al., 2021; Sotherton & Holland, 2003; Sharma et al., 2019).

This trend extends beyond agriculture: additional contributions arise from extra-agricultural applications in urban areas, gardens, infrastructure, and sports facilities, as well as from industrial activities and accidental events such as spills or improper storage, broadening release pathways and making chemical pressure more ubiquitous and difficult to control (KEMI, 2000; Hoffman et al., 2000; Carvalho, 2017).

Unlike many other anthropogenic contaminants, pesticides are intentionally released into the environment because they are designed to be biologically active and harmful to specific target organisms. This very property entails an intrinsic risk of adverse effects on non-target species and key ecological processes, both at the application site and following environmental transport (Geiger et al., 2010; Stehle & Schulz, 2015; Tang et al., 2021).

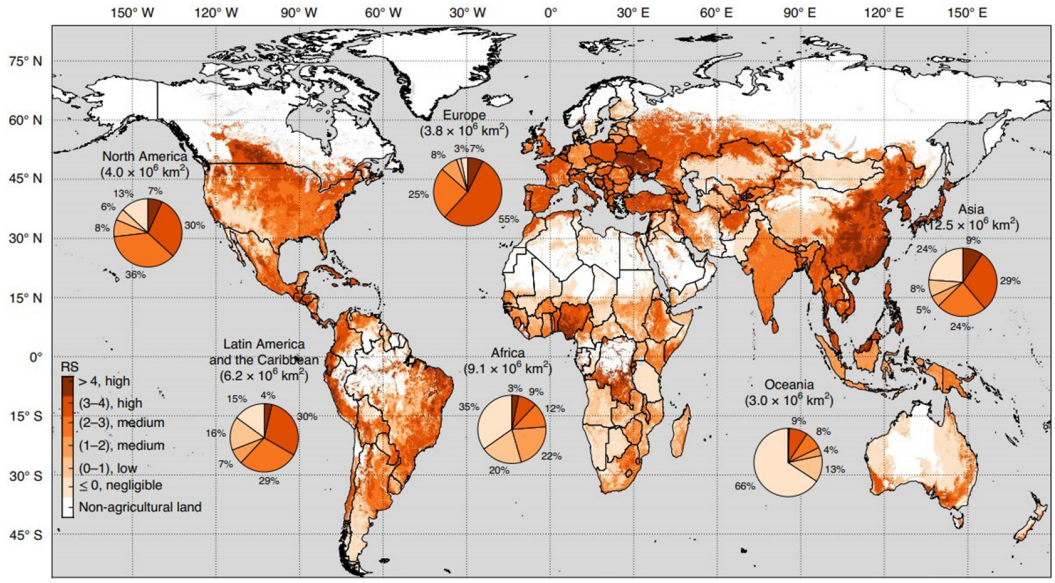


Fig. 3 - Global distribution of agricultural land use intensity and potential pesticide application pressure. The map shows regional differences in agricultural surface area and estimated relative pesticide input across continents, emphasizing hotspots of intensive agricultural activity that may represent major sources of pesticide contamination in freshwater and coastal ecosystems.

Their characterization as a "silent threat" is particularly evident in aquatic ecosystems, which act as final receptors for multiple contamination pathways. Pesticides and their transformation products reach rivers, lakes, lagoons, and coastal environments through atmospheric deposition, surface runoff, and leaching, with transport dynamics strongly influenced by precipitation, soil characteristics, and agronomic management practices (Kreuger, 1999; Carvalho, 2017; Stehle & Schulz, 2015). Monitoring programs and field studies across different regions worldwide have documented the presence of complex mixtures of herbicides, insecticides, and fungicides in surface waters and sediments. Frequently, both currently used compounds and substances banned or restricted years ago are detected, indicating persistence, secondary releases, and/or resuspension from environmental compartments (Miles & Pfeuffer, 1997; Ulén et al., 2002; Malaj et al., 2014; Stehle &

Schulz, 2015). In aquatic systems, the tendency of pesticides to adsorb onto particulate matter and accumulate in soft sediments can transform these compartments into reservoirs of chronic exposure for benthic communities and bottom-feeding organisms, facilitating trophic transfer and potential cascading effects throughout the food web (Landrum et al., 1996; Lotufo et al., 2000; Malaj et al., 2014).

A critical aspect, often underestimated in assessments based solely on measured environmental concentrations, is that toxicity depends on the bioavailable fraction and on the dose actually absorbed by the organism, rather than on the mere presence of the contaminant in the medium (Hamelink & Spacie, 1977; Landis & Yu, 1995).

Concentrations in water or sediment therefore represent useful but imperfect proxies of biological exposure: uptake rates and internal burdens vary substantially among species and life stages according to morphology, external coverings, respiratory surfaces, branchial physiology, feeding strategies, and trophic selectivity (Bruner et al., 1994a; Bruner et al., 1994b; Landrum & Fisher, 1998).

This variability explains why sub-lethal effects, including behavioural, immunological, reproductive, and developmental alterations, may occur even at relatively low environmental concentrations, particularly during windows of heightened susceptibility such as embryonic or reproductive stages, with potential repercussions for fitness and population dynamics (Moore & Waring, 2001; Mnif et al., 2011; Kim et al., 2017).

The “silence” of this threat is amplified by two additional factors. First, real-world exposure rarely involves single compounds: mixtures of pesticides with different modes of action can produce additive or synergistic effects, for example through increased biological permeability or biotransformation into more toxic metabolites,

thereby limiting the predictive value of single-compound assessments (Belden & Lydy, 2000; Cedergreen, 2014; Tang et al., 2021).

Second, environmental transformation processes, such as photolysis, hydrolysis, oxidation, and microbial metabolism, generate degradation products that are not always monitored and may be as persistent and toxic, or even more so, than the parent compounds.

For many of these transformation products, however, information on persistence, bioaccumulation, and no-effect concentrations remains incomplete, creating a significant gap in ecotoxicological risk assessment (Belfroid et al., 1998; Carvalho, 2017; Stehle & Schulz, 2015).

Taken together, pesticides represent a diffuse and often “invisible” chemical pressure, originating from multiple sources, mediated by transport and transformation processes, and capable of inducing chronic or indirect effects that extend beyond acute mortality to alter the structure and functioning of aquatic ecosystems in a lasting manner (Woin, 1998; Schulz & Liess, 1999; Malaj et al., 2014).

1.3.1 Classification and major categories of pesticides

Pesticides can be classified according to several criteria, including chemical structure, target organism, or field of application (Fig.4).

However, from an ecotoxicological perspective, one of the most informative classifications is based on the mechanism of action, as it allows identification of the biological processes affected and facilitates the interpretation of observed effects in non-target organisms and aquatic ecosystems (Matsumura, 1985; Ecobichon, 1991; DeLorenzo et al., 2001).

In general, insecticides primarily interfere with nervous system function, whereas herbicides and fungicides mainly target fundamental processes such as photosynthesis, cellular respiration, and the biosynthesis of essential macromolecules.

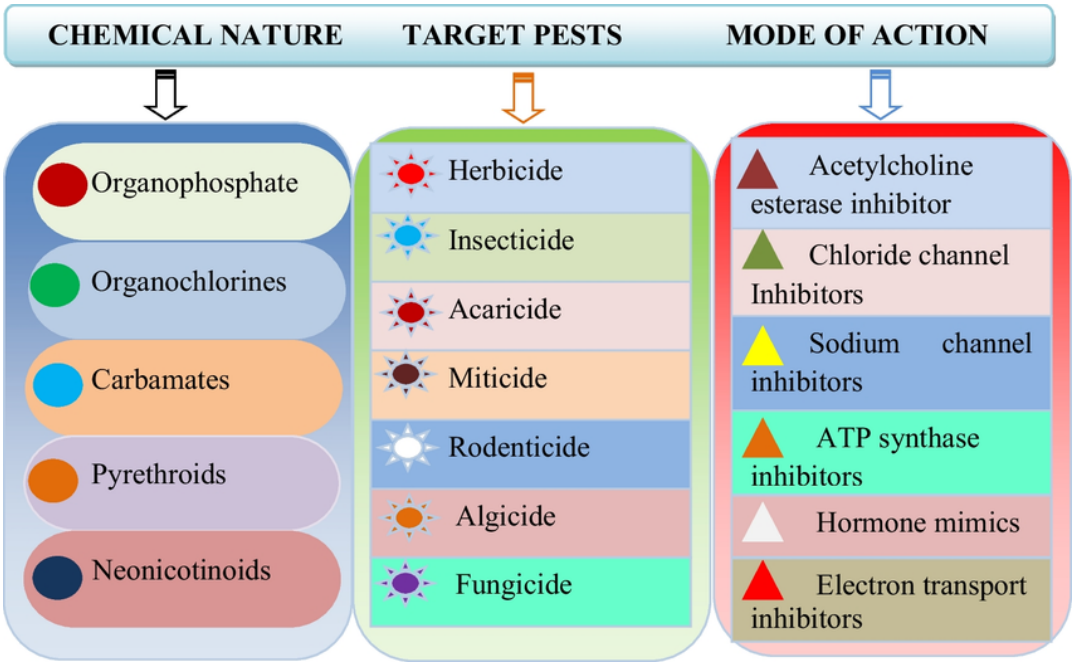


Fig. 4 - Classification of pesticide families based on chemical structure, target organisms, and primary mode of toxic action.

Insecticides

Many insecticides exert their toxicity by disrupting neuronal transmission through interference with transmembrane ion transport (Na^+, K^+, Ca^{2+}, and Cl^-), selective enzymatic activities, and the release or persistence of neurotransmitters at synaptic junctions (Ecobichon, 1991).

Organochlorine Insecticides

Organochlorine insecticides represent one of the historically most significant classes of pesticides and include chemically stable, weakly reactive compounds characterized by high environmental persistence and a strong tendency toward bioaccumulation. The most extensively studied compound in this group is DDT, whose molecular target has been identified as a subunit of ATPase involved in neuronal repolarization, a process essential for normal nervous system function (Younis et al., 2002). In addition to this primary mechanism, DDT alters neuronal membrane permeability to potassium and sodium ions by interfering with ion channels responsible for action potential propagation and inhibits calmodulin activity, thereby disrupting calcium transport required for neurotransmitter release (Matsumura, 1985).

Other organochlorines, including lindane and endrin, exhibit similar mechanisms of action but also function as antagonists of γ-aminobutyric acid (GABA) receptors, a key inhibitory neurotransmitter system in both insects and vertebrates (Wafford et al., 1989).

Organophosphorus and Carbamate Insecticides

Organophosphorus insecticides, including malathion and parathion, have been widely used as replacements for organochlorines in vector control programs following

their restriction or ban in many countries (Mulla & Mian, 1981). Their primary mechanism involves inhibition of acetylcholinesterase (AChE), the enzyme responsible for hydrolyzing acetylcholine at synaptic clefts. Binding to the active site of AChE forms a stable phosphorylated complex, causing acetylcholine accumulation and prolonged, often irreversible, neuronal stimulation (Ecobichon, 1991).

In some cases, toxicity is further enhanced by cytochrome P450-mediated bioactivation, which generates metabolites with greater inhibitory potency than the parent compound (Belden & Lydy, 2000). Carbamates act on the same molecular target but differ in reversibility: carbamylated AChE is less stable and can be rapidly regenerated through decarbamylation, resulting in generally less persistent toxic effects compared with organophosphorus compounds (Ecobichon, 1991).

Synthetic Pyrethroids

Synthetic pyrethroids constitute one of the most recent major classes of insecticides and are divided into two main types (type I and type II), associated with distinct toxicological syndromes. Both types primarily act on voltage-gated sodium channels in neuronal membranes, prolonging their open state and inducing repetitive neuronal firing, with effects comparable to those produced by DDT (Narahashi, 1986; Bradbury & Coats, 1989). Type II pyrethroids cause a more pronounced prolongation of sodium channel opening and also interact with the GABA-gated chloride channel complex, blocking chloride influx and enhancing neuronal excitability (Ecobichon, 1991). The overlap of these mechanisms with those of other neurotoxic insecticides raises concerns regarding additive or synergistic effects under conditions of multiple exposure.

Herbicides

Herbicides are designed to eliminate or damage unwanted plants by interfering with essential physiological processes, including photosynthesis, respiration, cell growth, nuclear division, and the biosynthesis of proteins, carotenoids, and lipids (Ecobichon, 1991). Glyphosate, the active ingredient in widely used formulations such as Roundup™, acts by inhibiting 5-enolpyruvylshikimate-3-phosphate synthase (EPSPS), a key enzyme in the biosynthesis of aromatic amino acids. EPSPS inhibition disrupts protein synthesis and leads to severe metabolic dysfunction.

Beyond this primary target, glyphosate also affects secondary physiological processes, including photosynthesis, chlorophyll degradation, and auxin metabolism (Cole, 1985; Sikorski & Gruys, 1997; Baylis, 2000). Chlorophenoxy herbicides, such as 2,4-D, 2,4,5-T, and MCPA, represent another important group and act as synthetic analogues of the plant growth hormone auxin.

At low concentrations, they may stimulate cell division and elongation, whereas higher doses induce rapid growth abnormalities, such as leaf and stem curvature, inhibition of root and shoot development, and increased leaf pigmentation, ultimately leading to desiccation, necrosis, and plant death (Grossmann, 2000).

These effects are mediated, among other mechanisms, by excessive ethylene production and the consequent inhibition of carbon assimilation.

Fungicides

Fungicides primarily act by disrupting energy production and cellular respiration in fungi, processes that are essential for spore germination and mycelial growth. Compounds such as dithiocarbamates (e.g., maneb and thiram) and R–S–CCl_3

derivatives (e.g., captan and dichlofluanid) exhibit multisite activity by inhibiting several enzymes involved in mitochondrial respiratory processes (Leroux, 1996).

Another relevant class includes phenylpyrrole fungicides, such as fenpiclonil and iprodione, which inhibit spore germination and induce morphological alterations of germ tubes. Although initially attributed to direct interference with oxidative phosphorylation, more recent studies indicate that their primary effect involves inhibition of cell wall glycan biosynthesis and accumulation of natural sugars, suggesting a disruption of glucose metabolism (Jespers & de Waard, 1995).

These effects closely resemble those induced by the herbicide dichlobenil in plants, indicating potential convergence of molecular targets and raising concerns about additive or synergistic effects when fungicides and herbicides co-occur in the environment (Delmer et al., 1987).

1.3.2 Dithiocarbamates: Chemical properties, uses, and toxicity

Dithiocarbamates (DTCs) are synthetic organosulfur compounds and represent one of the most widely used classes of agricultural fungicides, largely due to their favorable cost–effectiveness and broad-spectrum activity.

Compounds such as mancozeb, maneb, thiram, ziram, and propineb are extensively applied to fruits and vegetables to control fungal pathogens; however, their intensive use has raised concerns regarding residue persistence in food products and associated risks to human health and the environment.

Based on chemical structure, DTCs are classified into three main groups: dimethyl dithiocarbamates (DMDCs), ethylene-bis-dithiocarbamates (EBDCs), and propylene-bis-dithiocarbamates (PBDCs).

Ferbam, thiram, and ziram belong to the DMDC group: ferbam and ziram are iron and zinc salts of the dimethyldithiocarbamate anion, respectively, whereas thiram is an oxidized disulfide dimer of DMDC and, unlike the others, does not contain metal ions. These compounds are generally more soluble in organic solvents than other DTCs.

Propineb, the only PBDC, is a zinc salt of propylene-bis-dithiocarbamate and contains a propylene bridge linking two dithiocarbamate groups, conferring a polymeric structure and limited solubility (Bansal, 2022; Fanjul-Bolado et al., 2020).

EBDCs, including maneb, zineb, and mancozeb, are metal salts of ethylene-bis-dithiocarbamate: maneb and zineb are manganese and zinc salts, respectively, while mancozeb chelates both metal ions.

In general, EBDCs and PBDCs are polymeric, poorly soluble compounds that can degrade into more toxic metabolites such as ethylenethiourea (ETU) and propylenethiourea (PTU), with significant toxicological implications (Fig. 5).

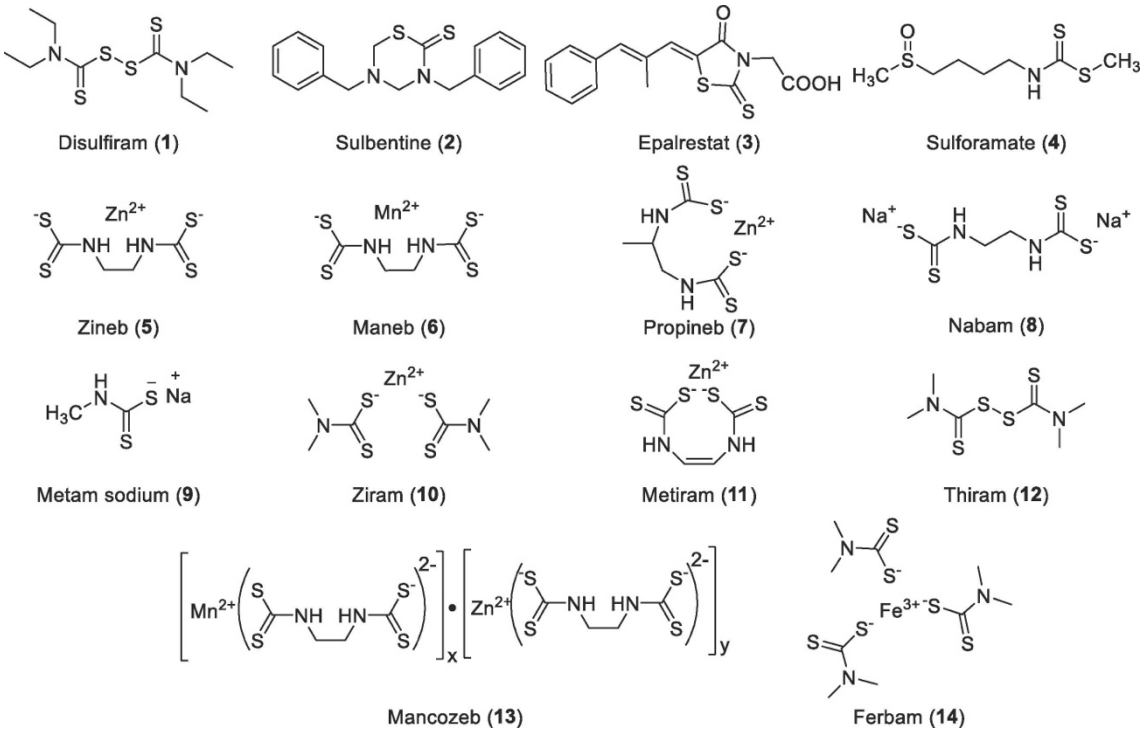


Fig. 5 - Chemical structure of different fungicide (dithiocarbamates): DMDCs (blue), from top to bottom, Ferbam, Thiram, Ziram, and Metiram; PBDCs (orange), Propineb; EBDCs (green), from (top) to (bottom) Maneb, Zineb, and Mancozeb.

These structural and chemical differences influence not only application patterns and environmental persistence, but also the analytical strategies required for their detection and for assessing dietary exposure risk (Fig.6) (Chung et al., 2022).

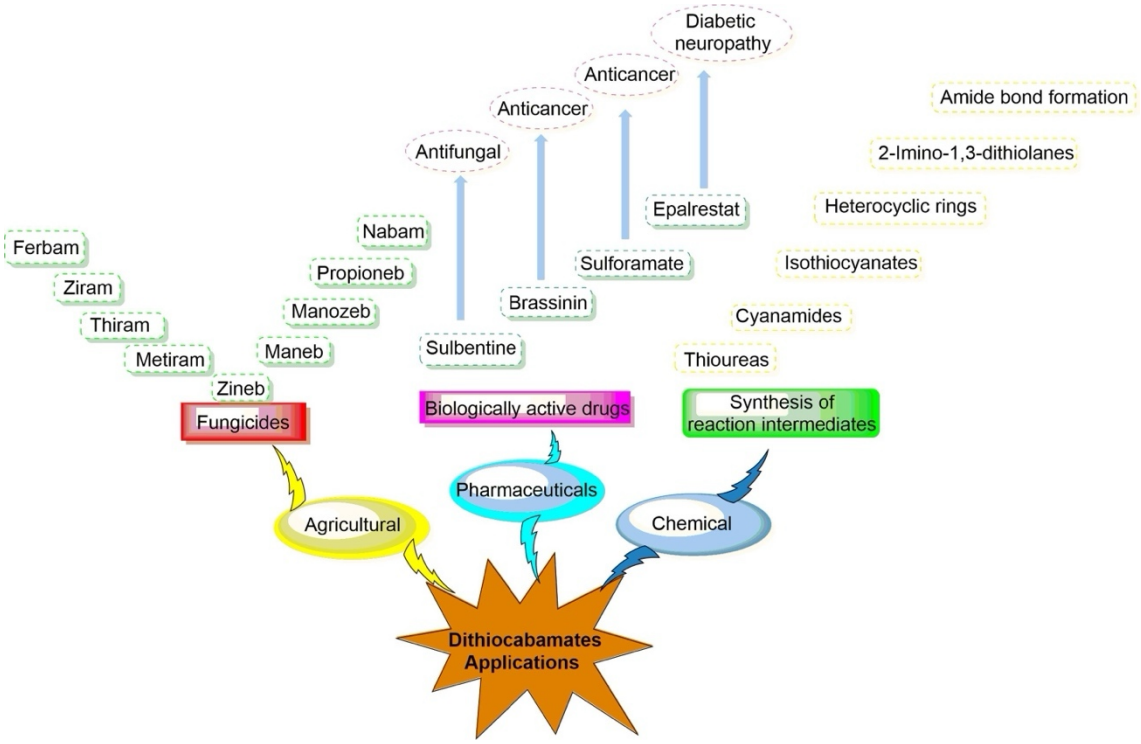


Fig. 6 - Representation of multifaceted applications of dithiocarbamates.

The development of dithiocarbamates began in 1931 with the filing in the United States of a patent for disinfectants with bactericidal and fungicidal activity, including thiram, which was granted in 1934 and later produced on a large scale (Tisdale, 1931). The success of thiram accelerated the spread of other DTC fungicides, such as EBDCs (maneb, zineb) and SMDCs (ferbam, ziram), which became widely used in subsequent decades (Liu et al., 2022; Jung et al., 1976).

Propineb was evaluated by FAO/WHO from 1977, approved in 2004, and not renewed in 2018, leading to its withdrawal from the European market (European Commission, 2018). In recent years, the European Commission has progressively withdrawn several DTCs, including maneb, mancozeb, metiram, and thiram, while maintaining them within the regulatory framework of maximum residue limits (MRLs). Currently, only ziram remains approved in the EU, with an expiry date of 31

January 2027, although it is considered a candidate for substitution (European Commission, 2009; European Commission, 2018).

In the EU, MRLs for dithiocarbamates are expressed as carbon disulfide (CS_2), a common degradation product, which prevents attribution of residues to a specific active substance. These limits are regularly updated in response to scientific advances, authorization changes, and evolving requirements for consumer protection and trade. Patent activity (Fig. 7) peaked between 2007 and 2015 and stabilized until 2020, reflecting efforts to improve DTC formulations and environmental performance (Stuke et al., 2020; Bristow, 2017; Van der Krieken et al., 2020; Van der Krieken et al., 2021).

Despite regulatory tightening and the phase-out of several compounds, the maintenance and updating of CS_2-based MRLs remain central to ensuring food safety and environmental protection in the European Union (Bellisai et al., 2023).

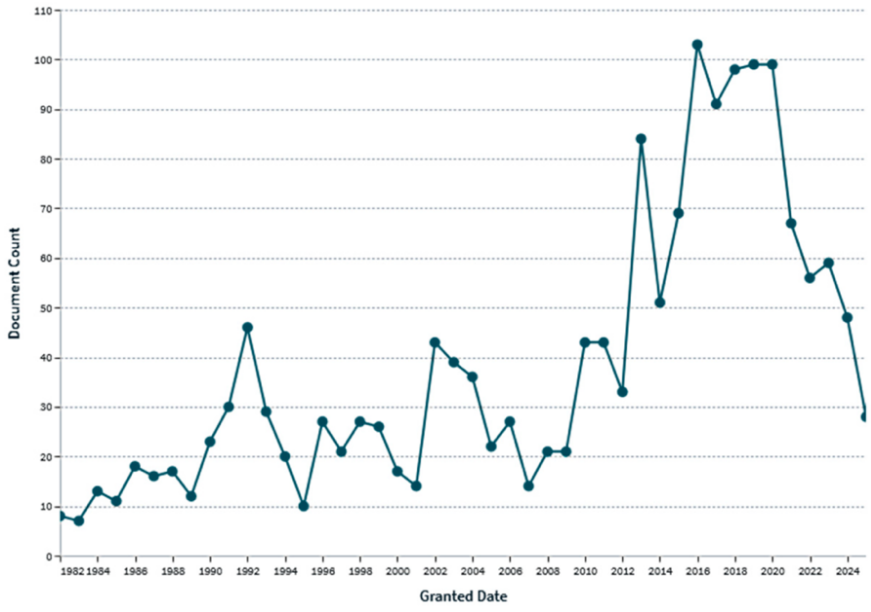


Fig.7 - Patent trend of dithiocarbamates use as fungicides over the years in Europe (Lens.Org).

From a structural perspective, dithiocarbamates (DTCs) are organosulfur compounds capable of chelating metal ions (Zn, Fe, Mn, Na), with the exception of thiram. Although metal coordination underpins their fungicidal efficacy, increasing toxicological concerns, particularly regarding long-term effects and persistence, have led to stricter regulatory scrutiny (Zoratto et al., 2022). Thiram, widely used as a seed and foliar fungicide (FAO, 2025), exhibits moderate acute toxicity in mammals (oral LD_{50} 210–2000 mg/kg) (NPIC, 2025) and may cause irritation and sensitization.

Chronic exposure has been associated with hepatic and renal alterations, neurotoxicity (New Jersey Department of Health, 2010), neuromuscular degeneration (Edwards et al., 1991), allergic reactions (NPIC, 2025), and inhibition of aldehyde dehydrogenase, producing a disulfiram-like reaction (Roberts et al., 2013).

Developmental studies report delayed ossification and fetal anomalies at high doses (WHO, 1988). Metiram, zineb, mancozeb, and maneb (EBDCs), as well as propineb (PBDC), generally show low acute toxicity (NPIC, 2025), but toxicological concern mainly derives from their degradation to ethylenethiourea (ETU) or propylenethiourea (PTU).

Chronic exposure has been associated with thyroid enlargement, altered thyroid hormone homeostasis, developmental toxicity, and possible reproductive and neurodevelopmental effects (WHO, 1988; Roberts et al., 2013; Kumar et al., 2019; EPA, 1993; Thiruchelvam et al., 2000; Rasglele et al., 2014; EFSA, 2016).

Zineb has been linked to thyroid histopathological changes and altered hormone levels (NPIC, 2025), while rodent studies suggest a potential increased risk of thyroid and liver tumors, although evidence remains insufficient for definitive carcinogenic classification (IARC, 2001).

Ziram shows moderate acute toxicity and potential dopaminergic neurotoxicity, with multisystem effects following chronic exposure (NPIC, 2025; Chou et al., 2008; Chen et al., 2023).

Ferbam displays low acute toxicity but has been associated with hematological and thyroid effects and occupational sensitization (WHO, 1988; EPA, 2005). Overall, while acute toxicity of DTCs is generally low, chronic exposure raises concerns involving the thyroid, liver, reproductive system, and central nervous system.

ETU, primarily derived from EBDCs, represents the principal toxicological driver due to its inhibition of thyroid hormone synthesis and compensatory TSH increase, with a single documented case in Bulgarian workers (Vergova et al., 1988).

ETU was initially classified as IARC Group 2B (IARC, 1987) and later reclassified as Group 3 based on lack of genotoxicity evidence and tumor findings limited to high-dose rodent studies (IARC, 2001).

PTU shares similar endocrine concerns, mainly at high experimental doses. Carbon disulfide (CS_2), produced by most DTCs at conversion rates of 10–40%, is unlikely to induce toxic effects at realistic exposure levels (WHO, 1988). A summary of the toxicological profiles of major DTCs and their metabolites is provided in Table 1.

Substance	Main Endpoints	Human Effects	Main Metabolites	Oral LD50 mg/kg (Rat)	References
Ferbam	Hepatotoxicity, Nephrotoxicity, Skin/Eye Irritation	Nausea, Headache, Respiratory Irritation, Chronic Liver and Thyroid Alterations	CS_2, ETU	~3300	WHO, 1988; IARC, 2001; EPA, 2005
Mancozeb	Thyroid Alterations, Reproductive/Developmental Toxicity, Neurotoxicity	Acute Irritation, Subclinical Hypothyroidism, Neurobehavioral Changes	CS_2, ETU	8000–10,000	WHO, 1988; IARC, 2001; Kumar et al., 2019
Maneb	Thyroid Alterations, Neurotoxicity (Experimental Parkinsonism)	Tremors, Cognitive and Thyroid Disturbances in Chronic Exposure	CS_2, ETU	5000–8000	WHO, 1988; IARC, 2001; EPA, 1993; Thiruchelvam et al., 2000
Metiram	Thyroid Toxicity, Reproductive Toxicity (Through ETU Formation)	Endocrine and Developmental Effects	CS_2, ETU	>6000	WHO, 1988; IARC, 2001; NIPC, 2025
Propineb	Skeletal Abnormalities, Thyrostatic Effect, Hepatotoxicity (Through PTU Formation)	No Direct Human Clinical Studies	CS_2, PTU	>5000	WHO, 1988; Resgele et al., 2014; EFSA, 2016
Thiram	Potential Neurotoxicity, Hepatoxicity, Dermal Irritation, Nephrotoxicity	Drowsiness, Confusion, Loss of Sex Drive, Incoordination, Slurred Speech, Weakness, Dermatitis, Conjunctivitis, Nausea, Cardiovascular Disturbances	CS_2	210–2000	WHO, 1988; NPIC, 2025; Roberts et al., 2013
Zineb	Thyroid Toxicity, Reproductive Toxicity (Through ETU Formation)	Tiredness, Dizziness, Weakness, Headache, Nausea, Fatigue	CS_2, ETU	1850–8900	WHO, 1988; IARC, 2001; NPIC, 2025
Ziram	Potential Neurotoxicity, Dopaminergic Neuron Toxicity	Reproductive Effects	CS_2	400–480	NPIC, 2025; Chou et al., 2008; Chen et al., 2023
ETU (Ethylene thiourea)	Thyroid toxicity, Goitrogenic, Experimental Carcinogenicity, Reproductive Toxicity	Hypothyroidism, Thyroid Hormone Disruption	—	1800–2000	WHO, 1988; IARC, 2001
PTU (Propylene thiourea/Propylthiouracil)	Thyrostatic Effect, Hepatotoxicity, Potential Mutagenicity	Hypothyroidism, Goiter, Hepatotoxicity	—	1300–1500	WHO, 1988; Brent et al., 2017
CS_2 (Carbon disulfide)	Neurotoxicity (CNS and PNS), Cardiovascular Effects, Reproductive Toxicity	Peripheral Neuropathy, Cognitive/Mood Disorders, Accelerated Atherosclerosis, Acute Headache/Dizziness	Thiocarbonates, Protein-bound Compounds	1200–3000	WHO, 1988;

Table 1. Toxicological profile of DTCs and relative main metabolites.

1.3.3 Thiram: Agricultural applications, environmental persistence, and ecotoxicological concerns

Thiram (tetramethylthiuram disulfide) is a dimethyl dithiocarbamate fungicide that has been widely employed for several decades in agricultural practice, mainly as a seed treatment and, to a lesser extent, in foliar applications (Fig.8).

Its primary use has been the prevention of seed- and soil-borne fungal diseases, including damping-off, seed rots, smuts, rusts, and infections caused by *Botrytis* spp., thereby improving germination rates and early seedling establishment (WHO, 2004; FAO/WHO, 2016).

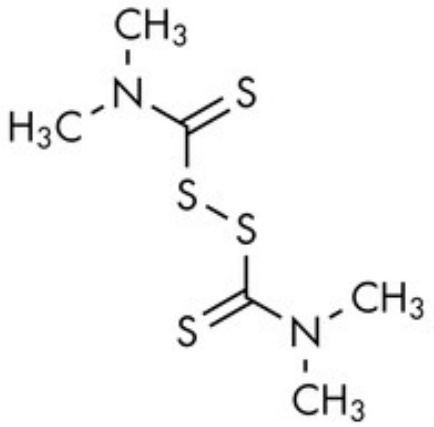


Fig. 8 - Chemical structure of thiram (tetramethylthiuram disulfide), a dithiocarbamate fungicide widely used in agriculture.

The fungicidal efficacy of thiram is linked to a multisite mode of action, based on the interaction with sulfhydryl (-SH) groups of fungal enzymes, leading to the inhibition of key metabolic pathways such as respiration and lipid metabolism.

This nonspecific mechanism has historically reduced the likelihood of resistance development compared with single-site fungicides (Matsumura, 1985; Ecobichon, 2001).

From an environmental perspective, thiram shows moderate persistence and a complex fate. In soils, it is subject to chemical hydrolysis, photodegradation, and microbial metabolism, processes that can reduce the parent compound relatively rapidly under favorable conditions.

However, its degradation results in the formation of sulfur-containing metabolites, including carbon disulfide (CS_2), which may persist longer and contribute to cumulative exposure in environmental compartments (FAO, 1997; EFSA, 2010).

Thiram generally exhibits low mobility in soils due to adsorption to organic matter, yet it can still reach surface waters through agricultural runoff, erosion, or spray drift, particularly following rainfall events shortly after application (Kreuger, 1999; DeLorenzo et al., 2001).

Once in aquatic systems, even transient concentrations may be sufficient to elicit biological effects, given the sensitivity of many non-target organisms. Ecotoxicological evidence indicates that thiram poses a significant hazard to a broad range of non-target species.

Primary producers such as algae and cyanobacteria are particularly sensitive, showing growth inhibition, impaired photosynthesis, and oxidative stress responses at concentrations close to those detected in agricultural runoff scenarios (Sabater & Carrasco, 2001a, 2001b; DeLorenzo et al., 2001).

These effects may propagate through the food web by altering primary productivity and community composition.

Aquatic invertebrates, including crustaceans and insect larvae, also exhibit high sensitivity, with both acute lethality and sub-lethal effects such as behavioral impairment, delayed development, and reduced reproductive success reported at environmentally relevant concentrations (Mulla & Mian, 1981; Moore et al., 1998).

In fish, thiram exposure has been associated with oxidative stress, enzymatic alterations, and neurobehavioral changes, raising concerns about population-level consequences under chronic exposure conditions (WHO, 2004; Kim et al., 2017).

Beyond direct ecotoxicity, thiram is of concern due to its potential endocrine-disrupting properties and systemic toxicity in vertebrates.

Experimental studies have shown that thiram can interfere with aldehyde dehydrogenase activity, producing a disulfiram-like effect, and may affect thyroid hormone homeostasis, neurodevelopment, and reproductive endpoints following repeated exposure (WHO, 2004; Mnif et al., 2011).

These findings are particularly relevant in the context of chronic, low-dose exposure scenarios, which are more representative of environmental and dietary exposure than acute toxicity tests.

Taken together, the widespread historical use of thiram, its capacity to generate persistent and toxic degradation products, and its documented adverse effects on multiple non-target taxa have prompted increasing regulatory scrutiny.

In the European Union, these concerns ultimately led to the non-renewal of thiram approval, reflecting a precautionary approach aimed at minimizing long-term risks to ecosystems and human health (EFSA, 2018).

Nonetheless, thiram residues and its transformation products may still be encountered due to legacy contamination and ongoing use in non-EU regions.

Consequently, thiram remains a paradigmatic example of a “silent” agrochemical threat, highlighting the need for integrated risk assessment approaches that consider environmental fate, mixture toxicity, sub-lethal effects, and sensitive developmental windows, as well as for the development of safer and more sustainable alternatives in crop protection (Fig.9).

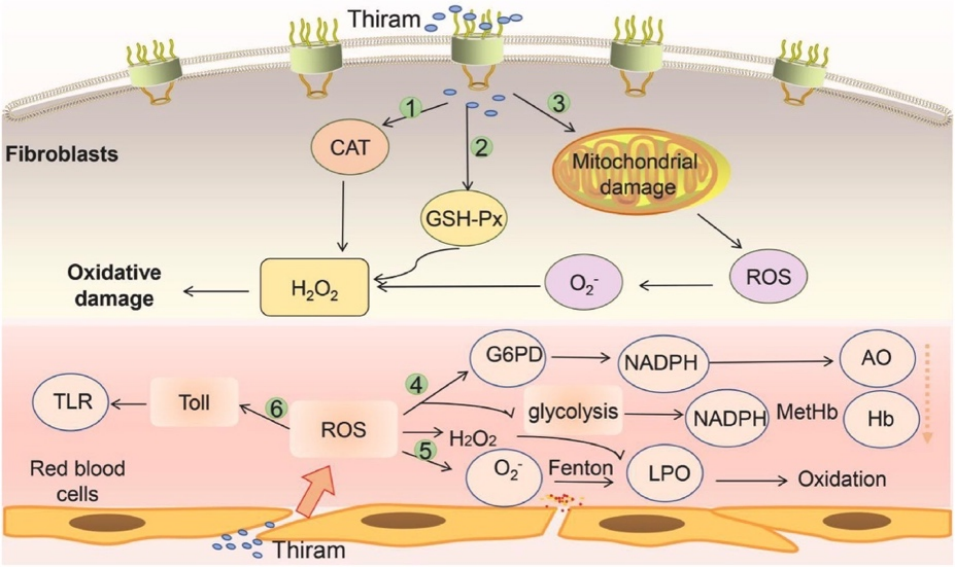


Fig. 9 - Mechanism of the effect of thiram on different cells

1.4 Sentinel organisms in environmental impact assessment

An organism can be considered a bioindicator or sentinel species when it develops measurable and reproducible responses to environmental stressors, providing reliable information on ecosystem quality.

Effective bioindicators should display high sensitivity to contaminants, resilience in degraded environments, wide distribution, ease of maintenance, and the ability to generate rapid and biologically meaningful responses (Bargagli et al., 1998; Ortiz-Zarragoitia & Cajaraville, 2006; Nasci et al., 2002).

These features make sentinel species central tools in modern ecotoxicology, particularly for detecting early and sub-lethal effects. Aquatic organisms at early life stages are especially vulnerable to environmental contaminants, including pesticides.

Embryos and larvae are generally more sensitive than adults, as ongoing processes of growth and differentiation can be disrupted even at low exposure levels (Braunbeck et al., 2019; Jezierska et al., 2022; Sogorb et al., 2023; Kádár et al., 2013; Bacchetta et al., 2012; Lee et al., 2012).

Thiram, in particular, has been shown to induce morphological abnormalities, metabolic alterations, and oxidative stress during embryogenesis (Özel et al., 2013), with lower concentrations sufficient to elicit toxicity compared with adult stages.

Growing awareness of the ethical implications of animal experimentation, reinforced by the REACH framework (Regulation EC No. 1907/2006), has encouraged the adoption of alternative strategies. Acute toxicity testing on adult organisms involves the use of large numbers of animals annually in the EU, exceeding one million individuals.

Embryotoxicity assays have therefore emerged as ethically more sustainable and scientifically sensitive approaches for detecting early and sub-lethal effects (Russell et al., 2022; Scholz et al., 2024; De Rossetto et al., 2014).

Embryotoxicology investigates the effects of chemical, physical, or biological agents on development. Alterations may manifest as developmental delay or arrest, or as structural defects affecting specific organs, resulting from genotoxic damage, metabolic interference, or endocrine disruption (Sogorb et al., 2023).

In the teleost *Danio rerio*, pesticide exposure, including thiram, induces dose-dependent effects on gastrulation, axis formation, cardiovascular development, and central nervous system differentiation, accompanied by changes in antioxidant enzymes, endocrine markers, and metabolic pathways (MacRae & Peterson, 2023; Morthorst et al., 2022).

Similar effects are observed in the echinoderm *Arbacia lixula*, where thiram disrupts larval skeletogenesis and alters redox and amino acid metabolism (Burić et al., 2020; Gianguzza et al., 2023). A unifying aspect across these models is the involvement of thyroid axis-related pathways.

Components regulating thyroid hormone synthesis, metabolism, and action, including thyrotropin, nuclear receptors, and deiodinases, are evolutionarily conserved among deuterostomes (Taylor & Heyland, 2018; Zwahlen et al., 2024).

In zebrafish, these pathways are essential for proper development, while in echinoderms homologous or functionally analogous systems have been identified. Thiram interference with these mechanisms may therefore dysregulate endocrine signaling during embryogenesis, compromising growth and differentiation.

Within this framework, in vivo and in vitro embryotoxicity assays provide powerful tools for investigating pesticide-induced toxicity. The integration of morphological, biochemical, and molecular endpoints enables mechanistic interpretation of toxic effects.

Moreover, the combined use of phylogenetically distinct models such as *Arbacia lixula* and *Danio rerio* enhances ecological relevance and improves the predictive power of environmental risk assessment (Van der Oost et al., 2023; Scholz et al., 2024).

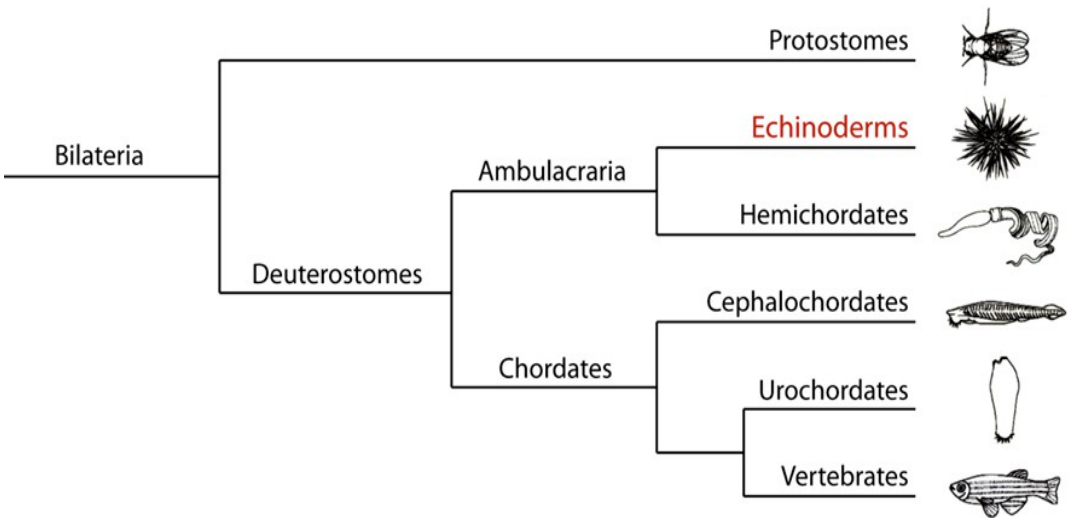


Fig 10. Echinoderms phylogeny

1.4.1 *Arbacia lixula:* Sea urchin as a key bioindicator of marine ecosystems

Echinoderms, and sea urchins in particular, are well-established model organisms in environmental and ecotoxicological research. They have been widely used to investigate the biological effects of contaminants, including nanoparticles and emerging pollutants, in marine systems (Gambardella et al., 2015; Maisano et al., 2015; Della Torre et al., 2014; Manzo et al., 2013; Manno et al., 2012).

Their benthic ecology results in prolonged exposure to sediment-associated micropollutants, which can be absorbed through epithelial contact or trophic transfer, making these organisms particularly responsive to local contamination.

Several biological and ecological traits further support their role as bioindicators, including broad geographic distribution, relatively sedentary habits, and marked sensitivity to chemical stressors. These features allow sea urchins to effectively reflect pollutant bioavailability and local environmental conditions (Zito et al., 2005).

Sea urchin embryos and larvae represent one of the most established experimental systems in biological research. External fertilization, high gamete production, small size (approximately 0.1 mm in diameter), optical transparency, and free-living development permit direct microscopic observation of developmental processes and precise detection of delays and malformations induced by chemical exposure (Zito et al., 2005).

Their synchronized development and ease of experimental manipulation facilitate biochemical and molecular analyses. Historically, studies on sea urchin embryos have contributed substantially to the understanding of fertilization and early embryonic cell cycle regulation (Manzo, 2004).

Another key advantage lies in their structural simplicity. Sea urchin larvae consist of a limited number of cell types (approximately 10–12) and largely single-cell-thick tissues, which simplifies the identification and interpretation of alterations in morphogenesis, skeletogenesis, and tissue differentiation following contaminant exposure (Davidson et al., 1998; Davidson et al., 2002).

Sea urchins are widely distributed across marine environments, including the Mediterranean Sea, where species such as *Paracentrotus lividus* are extensively employed in ecotoxicological assays.

Within this framework, the black sea urchin *Arbacia lixula* (Linnaeus, 1758) (Fig. 11) has emerged as a particularly relevant model species. Abundant in shallow Mediterranean rocky reefs, *A. lixula* combines ecological significance with experimental tractability, making it well suited for investigating developmental and physiological responses to environmental contaminants in marine ecosystems.



Fig11. Black sea urchin Arbacia lixula

Arbacia lixula typically inhabits shallow coastal environments, ranging from the intertidal zone down to approximately 50 m in depth. The species is most frequently associated with vertical rocky substrates that are subjected to intense hydrodynamic conditions, although it can also occur on horizontal rocky surfaces and, less commonly, on sandy bottoms interspersed with rock outcrops.

This ecological versatility contributes to its widespread presence in Mediterranean nearshore ecosystems. The reproductive biology of *A. lixula* in the northwestern Mediterranean was first systematically investigated by Fénaux (1968), who analyzed the gonadosomatic cycle and the seasonal occurrence of larval stages in the plankton over a three-year period at Villefranche-sur-Mer (French Riviera).

That study demonstrated a clear annual peak in the gonadosomatic index between May and June. This reproductive timing closely matched the subsequent appearance of echinopluteus larvae in the plankton, which were detected predominantly from July to November, corresponding to the warmest months of the year.

Fénaux interpreted this reproductive pattern as consistent with the thermophilous character of *A. lixula*, suggesting that elevated seawater temperatures play a key role in synchronizing gonadal maturation and larval release.

As observed in *Paracentrotus lividus*, reproduction in *A. lixula* involves the release of homolecithal eggs into the water column, where external fertilization takes place. Embryonic development proceeds rapidly, leading to the formation of a planktotrophic echinopluteus larva approximately 72 hours post-fertilization.

1.4.1.1 Embryogenesis and larval development

Embryogenesis in sea urchins is a classical and highly informative model in developmental biology (Fig. 12). After fertilization, the zygote undergoes a series of stereotyped and invariant cleavage divisions. The first and second cleavages are parallel to the animal–vegetal axis, while the third is perpendicular, producing blastomeres of similar size (Lyons et al., 2012).

Developmental asymmetry arises at the fourth cleavage, which generates eight mesomeres at the animal pole and, at the vegetal pole, four macromeres and four micromeres. During the fifth division, mesomeres and macromeres divide symmetrically, whereas micromeres divide unequally into four large and four small micromeres (Davidson, 2006; Peter & Davidson, 2015).

These blastomeres adopt distinct developmental fates: mesomeres form mainly oral and aboral ectoderm; macromeres give rise to endoderm, non-skeletogenic mesoderm (NSM), and a minor ectodermal component; large micromeres differentiate into primary mesenchyme cells (PMCs), responsible for larval endoskeleton formation; and small micromeres contribute to the germ line (McClay et al., 2018; Annunziata et al., 2019).

Cleavage synchrony progressively decreases after the fourth division, particularly in micromeres, whose slower cell cycle progression reflects lineage-specific regulatory programs (Peter & Davidson, 2015). Rapid divisions lead to morula formation, followed by cavitation into the blastula.

During gastrulation, PMCs undergo epithelial-to-mesenchymal transition (EMT) and migrate within the blastocoel to initiate endoskeleton deposition (Ettensohn, 2013; McClay et al., 2018). Concurrently, vegetal plate cells invaginate to form the

archenteron, which elongates and differentiates into the tripartite gut of the pluteus larva (Davidson & Erwin, 2015). Following gastrulation and early organogenesis, the pluteus becomes planktotrophic and feeds actively. Subsequent metamorphosis involves extensive tissue remodeling, leading to formation of the adult body plan through tightly regulated developmental transitions (Rafiq et al., 2014; Cary et al., 2020).

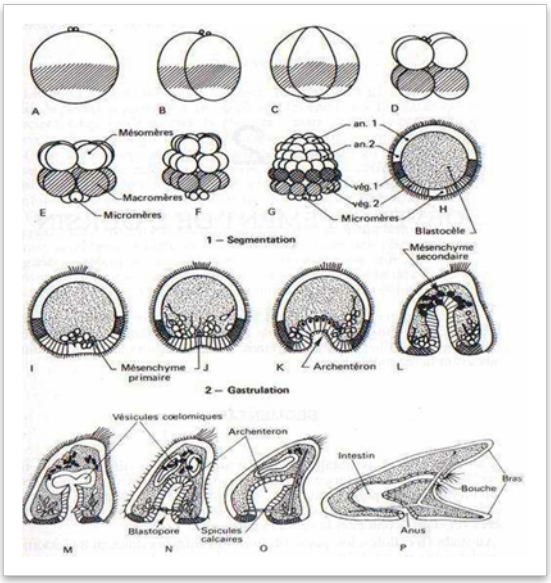


Fig 12. Sea urchin development. A: fertilized egg. B, C, D: first segmentations (2-4-8 blastomers). E, F, G: morula stage (16, 32, 64 blastomers). H: blastula section. I: primary mesenchyme cells migration. J, K, L: archenteron formation. M, N: coelomic vesicle formation. O, P: larvae pluteus development, bilateral symmetry acquisition, mouth opening and complete arms development.

Embryonic axis specification in sea urchins depends on the coordinated interaction of maternal determinants and zygotic signaling pathways, progressively elucidated through experimental studies and gene regulatory network (GRN) analyses.

As in other deuterostomes, establishment of the primary animal–vegetal (A–V) axis begins early and is largely driven by maternally deposited factors, later stabilized by inductive interactions during cleavage and blastula stages (Angerer & Angerer,

2003; McClay, 2011; Peter & Davidson, 2015). A pivotal event in A–V specification is the vegetal accumulation and nuclear translocation of β-catenin, regulated by Dishevelled-dependent Wnt signaling. The β-catenin/TCF complex activates vegetal transcriptional programs that promote endomesoderm specification and repress animal fates, positioning the vegetal pole as a key signaling center (Logan et al., 1999; Weitzel et al., 2004; Wikramanayake et al., 2012; McClay et al., 2018).

TGF-β family members further refine patterning along this axis: BMP2/4 signaling, modulated by antagonists such as Noggin and Chordin-like factors, helps define ectoderm–endoderm boundaries and restrict vegetal gene expression domains (Angerer et al., 2000; Lapraz et al., 2009; Su et al., 2009).

Downstream transcription factors, including Goosecoid, integrate these early positional inputs within the GRN and link A–V specification to subsequent morphogenetic events (Angerer et al., 2001; Peter & Davidson, 2011). Oral–aboral (O–A) axis specification involves additional metabolic and signaling asymmetries.

Localized differences in mitochondrial distribution and redox state generate spatially restricted redox signals that bias early polarity before zygotic gene activation (Coffman et al., 2004; Coffman & Denegre, 2007; Luo et al., 2013).

Molecularly, O–A patterning is centered on Nodal, whose expression becomes restricted to the oral ectoderm and integrates upstream Wnt/TCF inputs with downstream BMP signaling (Duboc et al., 2004; Flowers et al., 2004; Lapraz et al., 2006). Spatial confinement of nodal is ensured by feedback inhibitors such as Lefty and by antagonists including Antivin and Univin, sharpening the oral signaling domain (Duboc et al., 2008; Range et al., 2007; Yaguchi et al., 2006).

Nodal signaling activates oral ectoderm genes, including goosecoid, and additional downstream regulators such as the homeobox gene *not*, which consolidates oral identity and represses aboral programs (Li et al., 2012; Lapraz et al., 2006).

Upstream modulation by stress-responsive kinases, particularly p38 MAPK, promotes oral specification while repressing aboral gene expression, linking environmental and intracellular signals to embryonic patterning (Bradham & McClay, 2005; Wei et al., 2016).

Nodal signaling also contributes to left–right asymmetry, illustrating how early axial pathways are reutilized to generate multiple body axes through context-dependent deployment of shared modules (Duboc et al., 2005; Yaguchi et al., 2010; Hibino et al., 2021).

Overall, sea urchin axis specification emerges from the integration of maternal cues, metabolic asymmetries, and interconnected signaling pathways embedded within a conserved GRN architecture.

This modular yet robust organization ensures developmental precision while simultaneously creating potential points of vulnerability to environmental perturbations, an aspect of particular relevance in ecotoxicology and endocrine disruption research.

1.4.1.2 Skeletogenesis and sensitivity to contaminants

The formation of the embryonic endoskeleton by primary mesenchyme cells (PMCs) is one of the best-characterized processes in sea urchin embryogenesis. In the pre-hatching blastula, descendants of the large micromeres, after several additional cleavages, localize at the vegetal pole (Lyons et al., 2012).

PMCs then undergo an epithelial-to-mesenchymal transition (EMT), delaminate from the ectoderm, and ingress into the blastocoel (Wu et al., 2007).

This EMT is controlled by transcription factors including alx1 (Ettensohn et al., 2003), ets1 (Kurokawa et al., 1999), twist (Wu et al., 2008), snail (Wu and McClay, 2007), and foxN2/3 (Rho and McClay, 2011), and is accompanied by reduced integrin and cadherin expression, reflecting altered adhesion properties (Miller and McClay, 1997; Ettensohn, 1999; Lyons et al., 2012).

After ingression, PMCs divide once more, generating 32–64 cells depending on species (Ettensohn et al., 1997).

Following ingression, PMCs migrate and organize into two ventro-lateral clusters (VLCs) connected by oral and aboral chains, forming the sub-equatorial ring by mid-gastrula stage (Okazaki, 1965, 1975; Gustafson and Wolpert, 1999).

Migration is guided by interactions with extracellular matrix components such as EMC3 (Hodor et al., 2000) and fibronectin (Katow et al., 1990), as well as ectodermal signals (Duloquin et al., 2007; Röttinger et al., 2008; Cavalieri et al., 2011).

PMCs extend dynamic actin-rich filopodia (0.2–0.4 μm in diameter) that sense positional cues and contact the ectoderm (Karp and Solursh, 1985; Miller et al., 1995). Filopodial activity is initially random but becomes spatially biased toward sites of ring formation (Malinda et al., 1995).

As migration proceeds, PMCs fuse into a continuous syncytium, beginning approximately two hours after ingression and continuing during ring formation (Okazaki, 1965; Hodor and Ettensohn, 1998).

This fusion, also observed in cultured PMCs, reflects an intrinsic cellular property (Hodor and Ettensohn, 1998). Biomineralization begins within this syncytium, with deposition of a triradiate spicule rudiment at each VLC (Killian and Wilt, 2008).

The spicule matrix, composed of ~95% calcium carbonate, ~5% magnesium carbonate, and trace proteins, is secreted within a privileged extracellular compartment formed by syncytial filopodia (Wilt, 1999).

Initially deposited as amorphous calcium carbonate, it later converts to calcite during prism-to-pluteus stages, a transition regulated in part by occluded matrix proteins (Killian and Wilt, 2008; Gong et al., 2012).

Spicules elongate and branch in a species-specific but highly reproducible pattern, defining larval morphology and contributing to orientation and swimming (Ettensohn et al., 1997; Ettensohn, 2013).

Several morpho-effector proteins are embedded within the spicule matrix. SM50 (Benson et al., 1987), PM27 (Harkey et al., 1995), and SM30 (Killian et al., 2010) are PMC-specific proteins that accumulate before skeletogenesis and regulate mineral deposition (Wilt et al., 2008).

SM50, containing a C-type lectin domain and a C-terminal repeat conferring β-spiral structure, defines the privileged mineralization space. SM30 participates in exocytosis of matrix proteins and amorphous $CaCO_3$ (Urry et al., 2000).

MSP130, an acidic glycoprotein with glycine-rich domains, localizes to the Golgi and PMC surface and is implicated in calcium uptake from seawater during skeletogenesis (Anstrom et al., 1987; Harkey et al., 1992; Killian and Wilt, 2008).

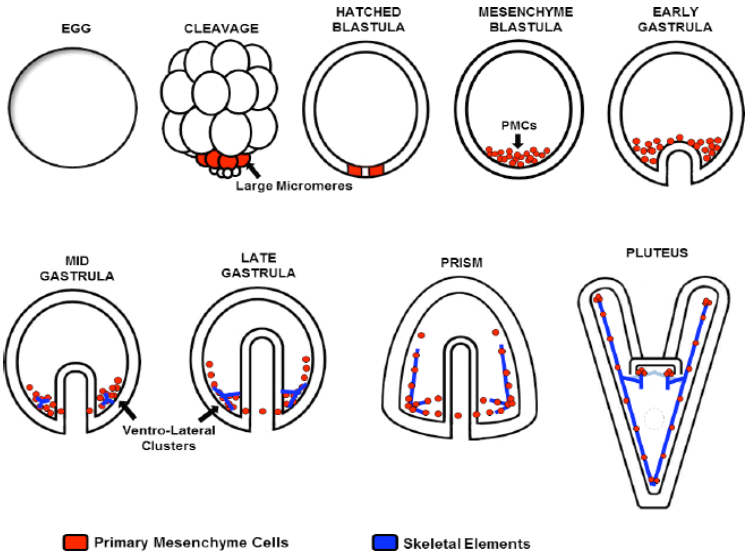


Fig 13. Schematic diagram of sea urchin embrionic development and skeletogenesis

1.4.1.3 Stress biomarkers and metabolic alterations

The toxic effects of environmental contaminants are not always evident, particularly at low or environmentally realistic concentrations. Under such conditions, conventional endpoints based solely on survival or gross pathology may fail to detect adverse effects, highlighting the importance of biomarkers as sensitive tools in environmental risk assessment.

A biomarker is defined as a xenobiotic-induced modification at the molecular, cellular, biochemical, or physiological level that can be quantitatively measured and reflects exposure, effect, or susceptibility to a contaminant (Gil & Pla, 2001; ENTOX/TIWET, 1996).

In this context, biomarkers provide integrative information on the health status of bioindicator organisms and the biological relevance of contamination (Fossi, 1998; van der Oost et al., 2022).

Biomarkers are central in toxicology and ecotoxicology because they detect tissue- and process-specific alterations before overt toxicity appears, reveal early subclinical effects, and account for inter- and intra-individual variability in sensitivity to xenobiotics (van Gestel & van Brummelen, 1996; Hook et al., 2014; Forbes et al., 2021).

In aquatic systems, morphological biomarkers have been extensively used to identify contaminant-induced structural alterations in critical organs and developmental stages, particularly in invertebrates such as bivalves and echinoderms (Ciacci et al., 2019; Cappello et al., 2020; Matozzo et al., 2021).

In sea urchins, sensitive stages include cleavage, gastrulation, larval development, and Skeletogenesis. Morphological biomarkers detect delayed or arrested

embryogenesis and skeletal malformations, which are consistently reported as reliable indicators of chemical stress (Carballeira et al., 2012; Gianguzza et al., 2014; Gambardella et al., 2015; Pinsino & Matranga, 2015).

Endpoints are typically classified as lethal (e.g., LC_{50}), sublethal (structural or functional impairments), or normal (absence of detectable abnormalities), allowing discrimination between general toxicity and subtle developmental disturbances (Carballeira et al., 2012; OECD, 2019).

At the molecular level, morphological and metabolic alterations often correspond to changes in gene expression affecting cell proliferation, differentiation, and tissue organization. In sea urchins, skeletogenesis represents one of the most sensitive developmental processes, making biomineralization-related genes valuable molecular biomarkers in embryotoxicity assays (Pinsino et al., 2011; Livingston et al., 2006; Sun & Ettensohn, 2020).

Key components include spicule matrix proteins SM30 and SM50, and the glycoprotein MSP130, which belong to coordinately regulated gene families. MSP130, localized on primary mesenchyme cells, is implicated in calcium uptake during skeletal formation and peaks around mid-gastrula stage.

SM50 expression increases markedly at the mesenchyme blastula stage and during active skeletogenesis, while SM30 is progressively upregulated from gastrulation to late pluteus stages (Guss et al., 1997; Pinsino et al., 2011; Killian et al., 2019).

In addition to structural proteins, signaling pathways regulating PMC migration and differentiation are sensitive targets of toxicant interference.

Fibroblast growth factor (FGF) signaling plays a central role in controlling cell migration, patterning, and differentiation during skeletogenesis, and its disruption leads to severe skeletal malformations (Duloquin et al., 2007; Röttinger et al., 2008; Morgulis et al., 2021).

Accordingly, components of the FGF pathway, together with biomineralization proteins, are proposed as molecular biomarkers of developmental stress in sea urchin embryos and larvae (Adomako-Ankomah & Ettensohn, 2013, 2014; Sun & Ettensohn, 2022).

Overall, integrating morphological, biochemical, and molecular biomarkers provides a robust framework for detecting early-life-stage effects of environmental pollutants.

In echinoderms, this multilevel approach enhances sensitivity and ecological relevance beyond traditional toxicity endpoints, enabling detection of subtle but biologically meaningful alterations.

1.4.2 *Danio rerio*: Zebrafish as a translational model

The zebrafish, *Danio rerio* (also historically referred to as *Brachydanio rerio*), is a tropical freshwater teleost belonging to the family Cyprinidae. The name "zebrafish" originates from the distinctive horizontal stripes extending along the body and fins. Sexual dimorphism is evident in adult individuals, with females generally exhibiting a larger abdominal region due to ovarian development, while males tend to show a slenderer morphology and slightly yellowish pigmentation (Fig.14).



Fig. 14 – Adult zebrafish male (bottom) and female (top). The species name derives from the characteristic horizontal stripes running along the body and fins. Females can be distinguished by a larger and more rounded abdominal region, whereas males typically display a slenderer body shape and a more pronounced yellowish coloration.

Danio rerio is geographically distributed across South and Southeast Asia, with natural populations documented primarily in India, Pakistan, Nepal, Bangladesh, and Myanmar. Although earlier reports suggested a broader African distribution, current evidence indicates that the native range of the species is largely restricted to the Ganges and Brahmaputra river basins and their associated floodplains (Dahm & Geisler, 2006; Spence et al., 2008; Engeszer et al., 2007; Parichy, 2015; Lawrence & Mason, 2023).

The natural habitats of zebrafish include small, slow-flowing freshwater bodies such as streams, rivers, irrigation canals, ponds, and shallow water reservoirs, often in proximity to rice paddies. These environments are typically characterized by clear or moderately turbid water, muddy substrates, and abundant aquatic vegetation, including macrophytes that provide shelter and foraging opportunities (Dahm & Geisler, 2006; Spence et al., 2008; Lawrence, 2007; Suriyampola et al., 2016).

Zebrafish are adapted to a relatively wide thermal range, with reported habitat temperatures spanning approximately 24–38 °C, reflecting their tolerance to fluctuating environmental conditions commonly encountered in monsoon-influenced regions (Lawrence, 2007; Ribas & Piferrer, 2014; Kimmel et al., 2021). The association of *D. rerio* with these habitats is likely linked to high food availability, reduced predation pressure, and favorable conditions for reproduction and early development (Spence et al., 2008; Parichy, 2015).

Zebrafish are omnivorous, and their natural diet consists primarily of zooplankton, phytoplankton, and both larval and adult stages of aquatic and terrestrial insects (McClure et al., 2006; Spence et al., 2008; Suriyampola et al., 2016).

In the wild, the reproductive period generally extends from April to August, although its precise timing varies according to latitude, altitude, hydrological regime, and climatic conditions, particularly rainfall and temperature (Engeszer et al., 2007; Spence et al., 2008; Lawrence & Mason, 2023).

These seasonal reproductive patterns are closely associated with monsoon cycles, which promote increased water levels and resource availability, thereby enhancing spawning success and larval survival.

1.4.2.1 Overview of anatomy and physiology

The zebrafish (*Danio rerio*) is a small-sized freshwater fish, typically reaching a total length of approximately 4–6 cm in adulthood. The body is streamlined and laterally compressed, with females generally exhibiting a more rounded and larger body shape compared to males, particularly in the abdominal region. Zebrafish are gregarious and usually live in shoals composed of 5 to 20 individuals, displaying synchronized swimming behavior, predominantly near the water surface (Spence et al., 2008; Parichy, 2015; Suriyampola et al., 2016). A pair of short barbels is present near the mouth. The general coloration consists of a silvery-golden base, an olive-green dorsal region, and a silvery-white ventral side. The flanks are characterized by alternating horizontal light stripes (white or golden-yellow) and darker cobalt-blue stripes, sometimes exhibiting violet hues.

These stripes extend longitudinally along the entire body from the head to the caudal fin and represent one of the most distinctive morphological features of the species. The caudal peduncle and caudal fin display alternating white and blue stripes; the dorsal fin is blue with a white margin, whereas the remaining fins exhibit a more olive-toned coloration. The mouth is oriented upwards, the pelvic fins lack pigmentation patterns, while the anal and caudal fins show continuous striped designs. The caudal fin is positioned relatively posteriorly along the body axis. The swim bladder is composed of two chambers and is connected to the terminal portion of the esophagus via a pneumatic duct, reflecting the physostomous condition typical of cyprinids (Fig.15) (Lawrence, 2007; Parichy, 2015). Based on two morphological characteristics, namely the presence of short dorsal fins with only seven branched rays and an incomplete or absent lateral line, Weber and de Beaufort (1916) originally

assigned *D. rerio* to the subgenus *Brachydanio*. However, subsequent taxonomic revisions proposed the unification of the genera *Danio* and *Brachydanio*, owing to the lack of consistent and reliable distinguishing characters between the two groups (Barman, 1991). This taxonomic interpretation has since been supported by molecular phylogenetic analyses, which confirmed the close evolutionary relationships among species previously assigned to the two genera (Fang et al., 2009; Tang et al., 2010; McCluskey & Postlethwait, 2015).

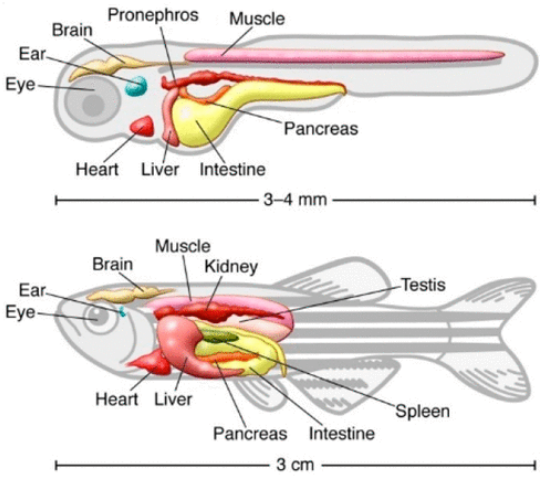


Fig. 15- Zebrafish anatomy. (A) larval stage; (B) adult stage.

Sexual dimorphism in zebrafish is relatively subtle and becomes clearly distinguishable only in adult individuals. Differences between males and females are particularly evident during the reproductive period, when females appear noticeably distended due to the presence of mature oocytes, resulting in a more rounded abdomen. In contrast, males tend to exhibit a slimmer body profile and more intense coloration, especially in the golden and blue stripes (Spence et al., 2008; Lawrence, 2007; Parichy, 2015; Ribas & Piferrer, 2014).

1.4.2.2 Embryonic development

Field studies describe zebrafish as an annual species whose reproductive period is primarily induced by temperature and typically coincides with the onset of the monsoon season (Talwar & Jhingran, 1991). Olfactory cues play a major role in the reproductive behavior of this species.

In particular, the release of male-derived pheromonal compounds has been shown to induce ovulation in females, although reproductive activity is also strongly influenced by photoperiodic cues.

Ovulation generally occurs shortly before dawn (Selman et al., 2005), and egg deposition begins during the first hours of daylight, although spawning is not strictly confined to this time window (Spence et al., 2008; Engeszer et al., 2007; Ribas & Piferrer, 2014).

Male courtship behavior takes place both before and during oviposition. During courtship, males swim alongside females in confined spaces while displaying erect fins. At the time of egg release, the male swims parallel to the female, often appearing to wrap around her body, and releases sperm synchronously with egg deposition (Spence et al., 2008; Parichy, 2015).

The mating ritual and the establishment and defense of spawning territories by males indicate a high degree of female mate choice, as females tend to spawn more frequently when paired with specific males.

Females are also selective with respect to oviposition sites, showing a preference for shallow substrates composed of small pebbles and rich in vegetation, which provide protection for both eggs and larvae.

Under standard laboratory conditions (28.5 °C), embryonic development proceeds rapidly, with hatching occurring within 48–72 hours post-fertilization (hpf) (Kimmel et al., 1995; Lawrence, 2007).

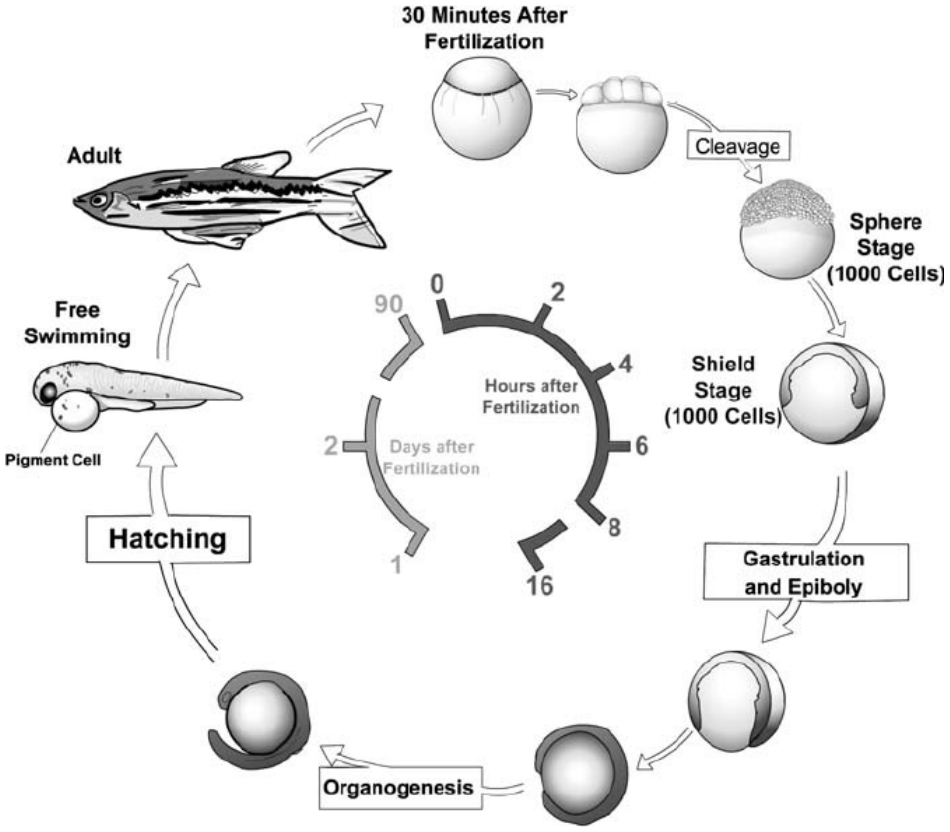


Fig.16 - Timeline of zebrafish embryonic and larval development. The schematic illustrates key developmental stages from fertilization through cleavage, gastrulation, organogenesis, hatching, and early larval stages, with corresponding time points expressed in hours and days post-fertilization.

Kimmel et al. (1995) divided zebrafish embryonic development into seven major stages, each characterized by distinct embryogenetic processes: the zygote period (0–45 minutes post-fertilization, mpf), the cleavage period (45 mpf–2¼ hpf), the blastula period (2¼–5¼ hpf), the gastrula period (5¼–10 hpf), the segmentation period (10–24 hpf), the pharyngula period (24–48 hpf), and the hatching period (48–72 hpf).

The majority of cell fate determination events occur during the blastula and gastrula stages. Prior to fertilization, cytoplasm and yolk are intermixed within the egg cell, which is surrounded by a transparent chorion.

At the one-cell stage, cytoplasm accumulates at the animal pole beneath the micropyle, forming the blastodisc, from which the embryo will develop. The fertilized zygote contains all the information necessary for development in the form of zygotic DNA, maternally deposited mRNAs, and proteins (Pelegri, 2003; Langdon & Mullins, 2011).

Zygote (0–¾ hpf)

The zebrafish egg has a diameter of approximately 0.7 mm, with the nucleus and cytoplasm positioned above a large mass of yolk (deuteroplasm). Fertilization triggers cytoplasmic movements that become visible within 10 minutes. Yolk-free cytoplasm migrates toward the animal pole, segregating the yolk-free blastodisc from the lighter, yolk-rich cytoplasm localized at the vegetal pole.

Cleavage (¾–2 hpf)

Cleavage is discoidal, as cell divisions occur exclusively within the blastodisc and do not extend into the yolk-rich cytoplasm. Following the first cleavage division, blastomeres divide at approximately 15-minute intervals. These meroblastic cytoplasmic divisions incompletely partition the blastodisc, and blastomeres remain connected by cytoplasmic bridges. The initial cleavage divisions are all longitudinal, whereas the first horizontal division produces a 64-cell embryo at approximately 2 hpf (Kimmel et al., 1995; Kane & Kimmel, 1993).

Blastula (2–5 hpf)

During this period, the mid-blastula transition (MBT) occurs, characterized by cell cycle lengthening and the onset of zygotic genome transcription. The yolk syncytial layer (YSL) forms, and epiboly begins, continuing throughout gastrulation. Cleavage plane orientation becomes increasingly variable. With the onset of the MBT, cell divisions lose synchrony, and cells within the embryo may be observed in different phases of the cell cycle simultaneously.

Marginal blastomeres, initially connected to the yolk by cytoplasmic bridges, collapse at approximately the tenth cell cycle, releasing their cytoplasm and nuclei into the yolk-rich cytoplasm and giving rise to the YSL. The YSL is a teleost-specific, extra-embryonic structure that persists throughout embryogenesis and plays a crucial nutritive and signaling role. Epiboly consists of the thinning and vegetal expansion of the blastodisc and YSL over the yolk surface. By the end of this stage, marginal cells of the enveloping layer (EVL) outnumber deep cells and form a flattened epithelial monolayer.

Gastrula (5–10 hpf)

Gastrulation begins with involution at the blastoderm margin, where a thickened marginal ring becomes evident. As no blastocoel is present during the blastula stage, a true archenteron does not form during gastrulation. Involution produces two distinct layers: the epiblast and the hypoblast.

Epiblast cells give rise to the epidermis, central nervous system, neural crest, and sensory placodes, whereas the hypoblast forms tissues traditionally assigned to mesodermal and endodermal lineages. Anteriorly, the paraxial hypoblast generates

muscles controlling eye, jaw, and gill movements, while posterior paraxial mesoderm forms a segmented plate that gives rise to somites. Thickening of the dorsal epiblast marks the formation of the neural plate, representing the first morphological indication of central nervous system development. Gastrulation ends with completion of epiboly and formation of the tailbud.

Somitogenesis (10–24 hpf)

A series of morphogenetic movements leads to somite formation. Primary organ rudiments become visible, the tailbud becomes prominent, the embryo elongates, and the first spontaneous body movements appear. Somites form sequentially along the trunk and tail, with internal cells differentiating primarily into myotomes.

Adjacent myotomes become separated by transverse myosepta composed of connective tissue. Somites also give rise to the sclerotome, which forms vertebral cartilage. The pronephric kidneys develop bilaterally near the third somite pair.

Neural tube formation in teleosts proceeds through a unique cavitation process, whereby a solid neural keel forms first and subsequently hollows to create the neurocoel. Pharyngeal arches and rhombomeres become visible, defining segmentation of the head region.

Pharyngula (24–48 hpf)

Seven pharyngeal arches develop from a primordial ventral-anterior region near the optic vesicle. The first two arches (mandibular and hyoid) form the jaws and operculum, while the remaining branchial arches give rise to gills.

Fin development begins as mesenchymal cells condense to form fin buds, which subsequently become capped by a prominent apical ectodermal ridge. Paired pectoral fin rudiments undergo progressive morphogenesis. The circulatory system forms during this stage, and the heart begins beating at its onset.

Hatching (48–72 hpf)

By this stage, morphogenesis of major organs is largely complete, with prominent changes occurring in the pharyngeal region. Initially, the mouth opening is positioned ventro-medially between the eyes, posterior to the head region. During the final 12 hours of embryogenesis, jaw morphogenesis dramatically shifts the mouth anteriorly, such that it ultimately protrudes between the eyes.

Hatching occurs at the end of this period, when larvae emerge from the chorion, a glycoproteinaceous envelope that has enclosed the embryo throughout development. Following hatching, larvae attach to submerged surfaces via specialized adhesive cells located on the head. Between 24 and 48 hours post-hatching, larvae begin feeding on small zooplankton (Eaton & Farley, 1974; Müller & van Leeuwen, 2014). Sexual maturity is typically reached between 3 and 6 months post-fertilization but varies considerably depending on environmental conditions and food availability (Spence et al., 2008; Lawrence, 2007).

Consequently, sexual maturity is more accurately assessed based on body size rather than chronological age. Several studies report that a standard length of approximately 23 mm represents a reliable threshold for sexual maturity (Eaton & Farley, 1974; Spence et al., 2008; Parichy et al., 2009).

Despite its widespread use as an ornamental aquarium species, zebrafish has become one of the most important vertebrate model organisms in genetics, developmental biology, medicine, pharmacology, and ecotoxicology (Scholz et al., 2008; Spitsbergen & Kent, 2008; Howe et al., 2013; MacRae & Peterson, 2015; Bugel et al., 2014).

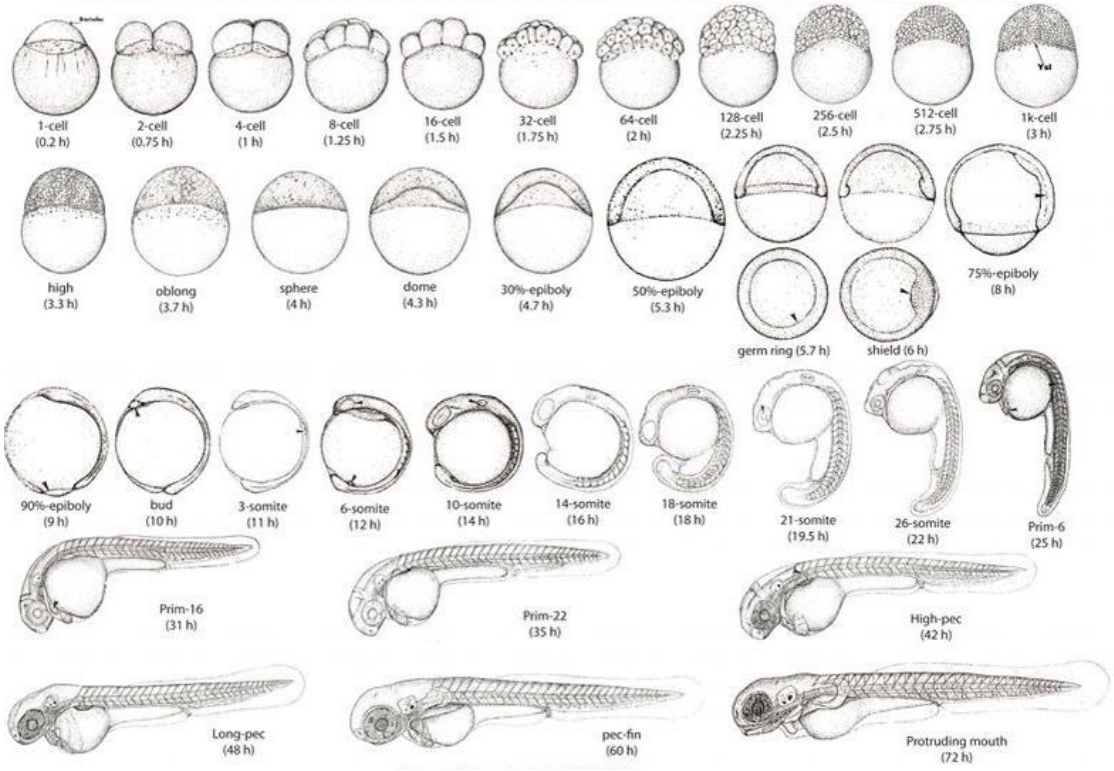


Fig.17 - Sequential morphological stages from early cleavage through blastula, gastrula, segmentation, pharyngula, and larval stages are shown, highlighting the major developmental transitions occurring during the first hours and days post-fertilization.

1.4.2.3 Experimental advantages and applications in ecotoxicology

The use of model species is based on the principle that many biological mechanisms are evolutionarily conserved across taxa. Model systems are therefore selected for traits that make them particularly suited to addressing specific scientific questions.

The teleost *Danio rerio* (zebrafish) has emerged as one of the most important vertebrate models in developmental and biomedical research. Unlike classical invertebrate genetic models such as *Drosophila melanogaster* or *Caenorhabditis elegans*, which are limited by their evolutionary distance from humans, zebrafish shares fundamental aspects of organogenesis, neurodevelopment, and endocrine regulation with mammals, making it highly relevant for translational studies (Howe et al., 2013; MacRae & Peterson, 2015; Lieschke & Currie, 2007).

Several biological features underlie its widespread use. Zebrafish are small (3–5 cm), inexpensive to maintain, reach sexual maturity within approximately three months, and produce large numbers of externally fertilized embryos year-round under controlled photoperiod and temperature conditions (28.5 °C; 14 h light:10 h dark).

External fertilization and optical transparency enable direct observation of embryogenesis and precise analysis of gene expression dynamics (Kimmel et al., 1995; Lawrence, 2007; Parichy et al., 2009).

High fecundity, short generation time, ease of genetic manipulation, and rapid development further enhance its experimental tractability (Easter & Nicola, 1996; Fishman, 1999; Parichy et al., 2009; Beliaeva et al., 2010; Santoriello & Zon, 2012).

Zebrafish is now widely used in toxicology and biomedical research at embryonic, larval, and adult stages.

Its genome shows strong conservation with humans despite approximately 450 million years of divergence, and many genes involved in human congenital diseases have identifiable orthologs in zebrafish (Bradford et al., 2017).

Major organ systems, including cardiovascular, digestive, and nervous systems, are functionally and morphologically comparable to those of mammals, reinforcing its value as a vertebrate disease and toxicity model (Easter & Nicola, 1996; Fishman, 1999; Parichy et al., 2009; Beliaeva et al., 2010; Gut et al., 2017).

In ecotoxicology, *Danio rerio* is extensively employed to evaluate the effects of chemical contaminants on survival, growth, development, and reproduction. Early-life-stage assays are well established for testing pesticides, pharmaceuticals, and industrial compounds (Dave et al., 1981; Bresch et al., 1990; Scholz et al., 2008; Hill et al., 2011).

The standardized developmental staging system established by Kimmel and colleagues ensures high reproducibility, particularly at 28.5 °C (Kimmel et al., 1995). Originally native to South Asian river systems and first introduced into genetic research by George Streisinger in the early 1980s, zebrafish has become a reference vertebrate model.

Its rapid embryogenesis (hatching within 48–72 hours), absence of parental care, and high reproductive output further facilitate experimental design (Talwar & Jhingran, 1991).

Collectively, its genetic conservation, physiological relevance, experimental accessibility, and established regulatory acceptance position *Danio rerio* as a “gold

standard" vertebrate model for investigating developmental toxicity and environmental stressors, including pesticides (Scholz et al., 2008; Spitsbergen & Kent, 2008; MacRae & Peterson, 2015; Bugel et al., 2014).

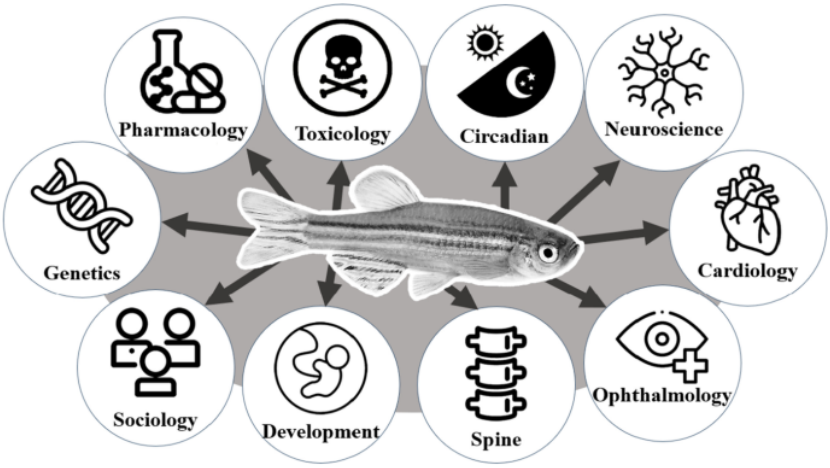


Fig.18 - Overview of zebrafish (Danio rerio) as a translational vertebrate model for toxicological and biomedical research.

1.5 The thyroid axis in embryonic development: A shared evolutionary pathway

Thyroid hormones (THs) are iodothyronines derived from tyrosine and represent one of the most ancient and evolutionarily conserved endocrine systems across the animal kingdom. In vertebrates, the principal forms are thyroxine (T4), predominantly secreted by the thyroid gland, and triiodothyronine (T3), the metabolically active form with high affinity for nuclear receptors (Leemans et al., 2019). THs constitute the peripheral output of the hypothalamic–pituitary–thyroid (HPT) axis, comprising hypothalamic TRH neurons, pituitary TSH-producing thyrotropes, and the thyroid gland, operating through negative feedback whereby THs suppress TRH and TSH secretion (Rousset et al., 2015; Rousseau et al., 2021). Within this axis, TRH stimulates TSH release, TSH activates thyrocytes via the TSH receptor (TSH-R), and T4 is converted to T3 in target tissues by deiodinases (Bellanger et al., 2015; Zoeller et al., 2007). TH biosynthesis depends on iodine uptake through the sodium/iodide symporter (NIS), iodination of thyroglobulin catalysed by thyroid peroxidase (TPO), and hormone release into circulation under HPT control (Cocurullo et al., 2023; Leemans et al., 2019).

In plasma, THs are largely protein-bound, with tissue uptake mediated by specific transporters (MCT, OATP, LAT) (Leemans et al., 2019). Intracellularly, iodothyronine deiodinases (DIO2, DIO3, DIO1) regulate local activation or inactivation of THs, enabling tissue-specific modulation largely independent of circulating levels (Bianco et al., 2002; Darras & Van Herck, 2012; Orozco et al., 2012; Steegborn & Schweizer, 2020). During embryogenesis, THs exert instructive roles beyond homeostasis, coordinating growth, differentiation, and developmental timing. Even before thyroid gland maturation, embryonic tissues express transporters,

deiodinases, and receptors, allowing precise spatiotemporal regulation (Leemans et al., 2019; Zwahlen et al., 2024). In this sense, THs function as endocrine regulators of developmental pace, particularly evident during metamorphic and post-embryonic transitions (Paris & Laudet, 2008; Rousseau et al., 2021).

These transitions differ across vertebrate lineages: amniotes exhibit direct development with earlier axis maturation, whereas many fishes and amphibians undergo indirect development with delayed HPT and stress axis maturation (Rousseau et al., 2021). Although THs are primary drivers of these processes, corticosteroids also contribute, integrating thyroid regulation with the hypothalamic–pituitary–adrenal/interrenal (HPA/HPI) stress axes (Paris & Laudet, 2008; Sachs & Buchholz, 2017; Zwahlen et al., 2024; Rousseau et al., 2021). Importantly, core components of thyroid signalling are present in several deuterostome invertebrates, including echinoderms and cephalochordates, despite the absence of a discrete thyroid gland. In these organisms, iodinated molecules modulate embryonic and larval processes such as Skeletogenesis and developmental transitions, indicating that thyroid-related signalling predates the emergence of the vertebrate thyroid organ (Cocurullo et al., 2023; Taylor & Heyland, 2017; Zwahlen et al., 2024).

Subsequent whole-genome duplications (1R/2R in early vertebrates, 3R in teleosts, 4R in selected lineages) promoted diversification of hormones, receptors, and deiodinases, increasing regulatory plasticity (Dehal & Boore, 2005; Meyer & Schartl, 1999; Maugars et al., 2014; Fleming et al., 2019). Examples of duplication and functional divergence include TSH, composed of a common α subunit and a hormone-specific TSHβ subunit paralogous to LHβ and FSHβ (Rousseau et al., 2021). In some basal vertebrates, a second TSHβ form exists, and teleost 3R duplication generated

tshβ1 paralogs with differentiated expression patterns, potentially linked to seasonal physiology (Maugars et al., 2014; Fleming et al., 2019; Yoshimura, 2013; Dardente et al., 2019). Similarly, TSH receptors (tshra, tshrb) in teleosts are expressed beyond the thyroid, including brain and gonads, enabling broader regulatory interactions (Maugars et al., 2014; Williams, 2011; Nakane & Yoshimura, 2019).

Thyroid hormone receptors (TRα, TRβ) also show lineage-specific duplications and isoform diversity via alternative splicing, further refining developmental regulation (Sap et al., 1986; Weinberger et al., 1986; Thompson et al., 1987; Brooks et al., 1989; Helbing et al., 2006; Kanaho et al., 2006; Lazcano & Orozco, 2018; Marchand et al., 2001). The multi-layered regulation of the HPT axis, integrating iodine-dependent synthesis, plasma transport, local metabolism, and receptor-mediated signalling, renders it highly sensitive to environmental perturbations during development.

Numerous contaminants and endocrine-disrupting chemicals interfere with one or more nodes of this system, altering TH bioavailability or signalling during critical windows with potentially irreversible outcomes (Leemans et al., 2019; Pesce et al., 2024). For this reason, the thyroid axis represents a central target in developmental ecotoxicology and a unifying framework for understanding how environmental stressors disrupt deeply conserved developmental programs (Vasamsetti et al., 2022; Pesce et al., 2024).

1.5.1 The thyroid system as a regulator of growth and development

In homeothermic and many poikilothermic species, thyroid hormones (THs) are essential regulators of somatic development, energy metabolism, and tissue differentiation (Bernal, 2007; Mullur et al., 2014). During embryonic and larval stages, precise temporal control of thyroid signalling governs key processes such as nervous system patterning, cardiovascular maturation, metamorphosis, and growth (Gilbert & Frieden, 2019; Tata, 2013; Tata, 2018). The hypothalamic–pituitary–thyroid (HPT) axis acts as a central integrative hub for endogenous and environmental cues, making it particularly vulnerable to disruption during critical developmental windows (Leemans et al., 2019; Rousseau et al., 2021).

In amphibians, metamorphosis is driven by increasing circulating T3 levels, which activate gene programs controlling tail resorption and limb development; insufficient thyroid signalling prevents metamorphic completion (Brown & Cai, 2007; Shi, 2013). These transitions depend on coordinated thyroid and corticosteroid signalling, highlighting cross-talk among neuroendocrine axes (Sterner et al., 2020). In mammals, maternal and fetal THs regulate cortical neuronal migration and myelination; congenital deficiency causes intellectual disability and growth impairment (Bernal, 2015; Korevaar et al., 2017).

Even subtle prenatal TH alterations induced by endocrine-disrupting chemicals have been associated with persistent neurocognitive deficits (Leemans et al., 2019). In fish, THs regulate pigmentation, craniofacial ossification, and allometric growth (Power et al., 2010; Campinho, 2019). In teleosts such as *Danio rerio*, thyroid development begins during the pharyngula stage and becomes functional a few days

post-hatching; by 4–5 days post-fertilization, larvae exhibit iodine-accumulating follicles capable of synthesizing T4 (Alt et al., 2006; Opitz et al., 2011). Thyroid progenitor specification depends on conserved transcription factors including pax2a, nkx2.4b, and hhex (Marelli et al., 2021), followed by activation of a functional HPT axis in which pituitary TSH stimulates thyroid hormone production (Liu & Chan, 2002; Chang et al., 2012).

Pharmacological inhibition of thyroid function (e.g., methimazole, perchlorate) induces developmental delay, impaired swim bladder inflation, and growth defects in zebrafish, confirming the enabling role of THs during the larval transition (Opitz et al., 2012; Thienpont et al., 2011; Hornung et al., 2018). These endpoints are now considered sensitive markers of thyroid-disrupting activity in ecotoxicology (Morthorst et al., 2022).

Conversely, excessive exogenous TH exposure accelerates development and induces metabolic imbalance (Chan & Yeung, 2009; Campinho et al., 2014). Thyroid hormone action operates through dual mechanisms. Genomically, T3 binds nuclear receptors (TRα, TRβ) to regulate transcription. Non-genomic pathways, mediated by membrane or cytosolic receptors, activate rapid intracellular cascades such as MAPK/ERK independently of transcription (Davis et al., 2016; Cheng et al., 2010).

These rapid pathways appear particularly relevant during early development, when cellular plasticity is high (Wang et al., 2019), and may operate even before widespread expression of classical nuclear receptors (Mendoza & Hollenberg, 2017). In sea urchin embryos, which lack a thyroid gland, T3 and T4 bind membrane sites on skeletogenic primary mesenchyme cells (PMCs), activating MAPK signaling and accelerating spicule formation (Heyland et al., 2006; Taylor & Heyland, 2017). This

supports the existence of alternative TH-responsive mechanisms, possibly involving integrin RGD-binding proteins, and suggests evolutionary conservation of thyroid-like signaling.

In vertebrates, genomic regulation predominates; in zebrafish gastrulation and organogenesis, TH levels modulate genes involved in somitogenesis and neural patterning, reinforcing the concept of an ancestral thyroid regulatory system conserved among deuterostomes and susceptible to environmental interference (Morthorst et al., 2022). Overall, the thyroid system functions as a master regulator of developmental timing, integrating metabolic and environmental inputs (Zoeller et al., 2017).

Its multi-level regulation makes it a critical vulnerability node: disruption during sensitive windows can result in malformations, developmental delay, or metamorphic failure (Gilbert, 2011; Diamanti-Kandarakis et al., 2020). For this reason, thyroid-specific endpoints are increasingly recognized as essential components of ecotoxicological risk assessment.

1.5.2 Evolutionary conservation of thyroid-related genes in invertebrates and vertebrates

The existence of endocrine systems analogous to those of vertebrates in invertebrate phyla is of major evolutionary interest (Paris & Laudet, 2008; Zoeller et al., 2017). The thyroid axis was long considered a chordate innovation, as only protochordates and vertebrates possess a thyroid gland or iodine-concentrating structures such as the tunicate endostyle (Canestro et al., 2008; Fredriksson et al., 1985a, 1988, 1989).

However, accumulating evidence indicates that key molecular components of the thyroid system predate the emergence of the thyroid gland and are distributed across deuterostome invertebrates, basal chordates, and vertebrates, supporting the existence of ancestral thyroid modules progressively refined during evolution (Cocurullo et al., 2023; Taylor & Heyland, 2018).

In this perspective, the vertebrate thyroid axis represents an incremental innovation rather than a de novo invention: iodine-dependent enzymatic pathways, nuclear receptors, and non-genomic signaling mechanisms were gradually integrated into a neuroendocrine feedback circuit, later stabilized by the evolution of a dedicated hormone-producing organ. In vertebrates, thyroid hormones regulate development, metabolism, metamorphosis, and regenerative processes such as fin regeneration, reflecting their pleiotropic integration within developmental programs (Bouzaffour et al., 2010; Sekimizu et al., 2007).

T4 and T3 synthesis occurs in thyroid follicles through NIS-mediated iodide uptake, TPO-dependent organification on thyroglobulin, and peripheral modulation by deiodinases, which regulate T3 availability and receptor activation in a tissue-specific

manner (Rousset et al., 2015; Mourouzis et al., 2020; Yaoita, 2019). This multi-layered regulation, combining systemic endocrine control with local modulation via transporters, metabolism, and receptor dynamics, creates multiple points of vulnerability to chemical interference (Kortenkamp et al., 2020; Paul-Friedman et al., 2019). From an evolutionary standpoint, this architectural complexity may have favored conservation: the ability to fine-tune hormone production, conversion, transport, and receptor responsiveness provides a versatile mechanism to coordinate growth, metamorphosis, and ecological adaptation.

Comparative analyses in aquatic invertebrates reveal, however, a non-uniform pattern of conservation. In ecdysozoan protostomes (e.g., arthropods and nematodes), the absence of THR genes in genomes such as *Drosophila* and *Caenorhabditis elegans,* together with limited evidence for functional thyroid-like pathways, suggests these taxa are generally unsuitable for thyroid-disruption assessment. In these groups, developmental regulation is instead mediated by distinct pathways such as the juvenile hormone system, based on bHLH-PAS receptors rather than nuclear TH receptors (Wu et al., 2007; Kostrouchova & Kostrouch, 2014; Flatt et al., 2006; LeBlanc et al., 2013; Li et al., 2011). Even in cases where THR-like receptors have been proposed (e.g., Daphnia magna), low sequence homology and comparative data question functional equivalence with vertebrate THR (Litoff et al., 2014; Holzer et al., 2017; Sainath et al., 2019).

Thus, hormonally regulated developmental phenotypes do not necessarily imply conservation of the vertebrate thyroid signaling cascade, and the suitability of a model species depends on conservation of specific molecular target nodes. In contrast, several lophotrochozoan protostomes, particularly mollusks, retain multiple thyroid-related

elements. THR homologs have been identified in gastropods and bivalves, and THR–RXR heterodimerization has been reported, paralleling vertebrate mechanisms (Kaur et al., 2015; Wang et al., 2019; Wu et al., 2007; Huang, Xu, Qu, Zhang, et al., 2015; Bouton et al., 2005; Bridgham et al., 2010; Carter et al., 2010).

In species such as Crassostrea gigas, T3 and T4 are detectable during embryonic and larval development, with peak levels at early stages, and homologs of DIO and TPO support endogenous synthesis and a role in metamorphosis (Huang, Xu, Qu, Zhang, et al., 2015; Huang, Xu, Qu, Li, et al., 2015). Functional studies show that THR knockdown reduces larval metamorphosis in Mytilus coruscus and Haliotis diversicolor, while T4/T3 administration stimulates metamorphosis in Aplysia californica (Li et al., 2020; Wang et al., 2019; Heyland, Price, et al., 2006a).

Interestingly, in some mollusks T4/T3 do not directly activate THR-mediated transcription, suggesting that THR may function in an unliganded or orphan-like state, with hormones modulating receptor expression or non-canonical pathways rather than acting through classical ligand-dependent activation (Huang, Xu, Qu, Zhang, et al., 2015; Harvey & Williams, 2004).

Overall, these findings support a mosaic evolutionary scenario: conservation may involve the presence of hormones, enzymes, and transcriptional regulators, whereas the mechanisms of receptor activation have diversified across lineages. This phylogenetic perspective is crucial for interpreting thyroid-disrupting effects in ecotoxicology and for selecting model organisms that truly reflect conserved endocrine targets.

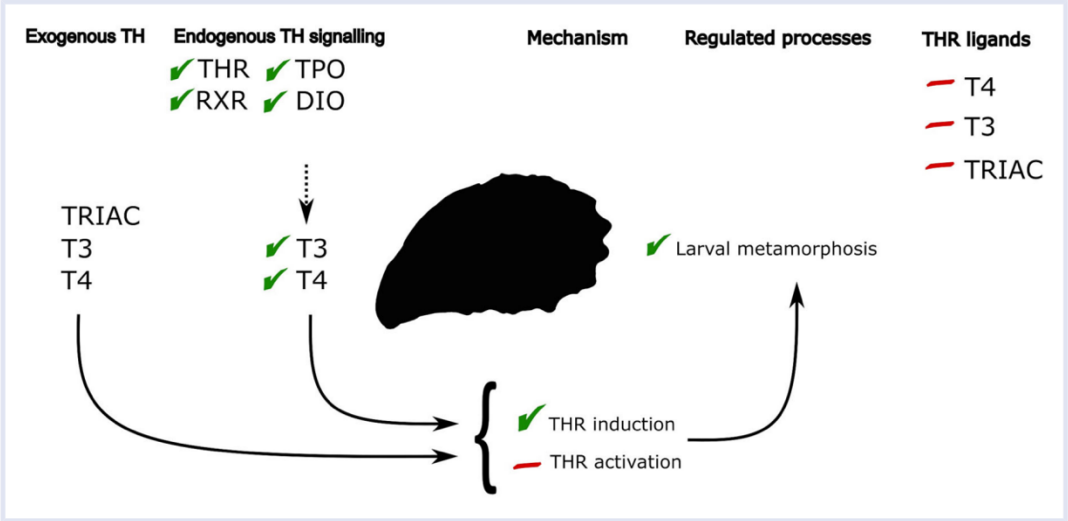


Fig.19 - Thyroid-like hormone signaling in mollusks. Tick marks denote the presence of the thyroid hormone signaling component or process. Minus signs denote the absence of the thyroid hormone signaling component or process. Black arrows indicate processes regulated by the pathway. Dotted arrow indicates the synthesis pathway is unknown

In deuterostome invertebrates, particularly echinoderms, conservation of thyroid-related mechanisms involves both enzymatic components and developmental responses to iodine and thyroid hormones (THs). Genome sequencing of *Strongylocentrotus purpuratus* has revealed homologs of vertebrate genes encoding key enzymes such as iodothyronine deiodinases, responsible for peripheral activation and inactivation of T_3 and T_4.

A deiodinase-like gene containing the characteristic selenocysteine domain has been identified, indicating that the capacity to metabolize iodinated compounds is an ancient deuterostome trait (Sodergren et al., 2006; Paris, Brunet, et al., 2008; Orozco et al., 2012). A THR gene has also been described in sea urchins, and RXR has been cloned in *S. purpuratus* and *Paracentrotus lividus*; however, current evidence suggests that echinoderm THR does not bind T4, T3, or TRIAC, supporting a possible orphan

function or the involvement of alternative, yet unidentified ligands (Howard-Ashby et al., 2006; Wu et al., 2007; Capitao et al., 2020; Rafiq et al., 2014; Paris et al., 2017).

Consistently, T4- and T3-like molecules have been detected in echinoderms, homologs of thyroid peroxidase (TPO) have been identified in several species, and iodine incorporation into T4 can be inhibited by peroxidase blockers, indicating functional capacities for iodinated compound synthesis or conversion (Chino et al., 1994; Heyland et al., 2004; Heyland, Price, et al., 2006a; Saito et al., 1998; Miller & Heyland, 2013; Heyland, Reitzel, et al., 2006b).

Functionally, exogenous T4 or T3 accelerates larval development and metamorphosis in sea urchins, sand dollars, and starfish, whereas inhibitors such as thiourea and perchlorate delay or block these transitions (Heyland & Hodin, 2004; Johnson, 1998; Johnson & Cartwright, 1996; Heyland, Reitzel, et al., 2006b; Saito et al., 1998).

Together, these findings indicate that, despite the absence of a morphologically defined thyroid gland and full ligand sensitivity of the nuclear receptor, echinoderms retain integrated modules of iodinated compound synthesis, metabolism, and cellular responsiveness that regulate developmental transitions.

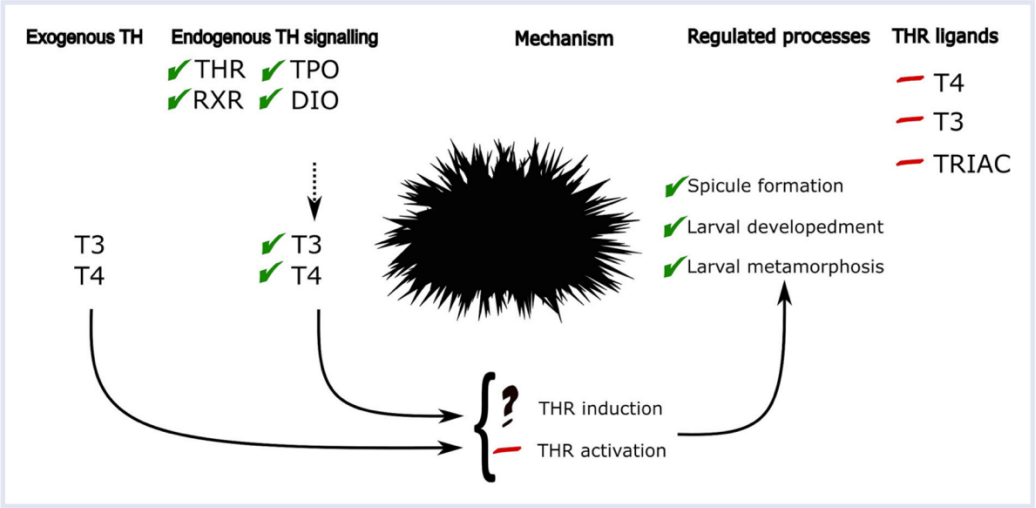


Fig.20 - Thyroid-like hormone signaling in echinoderms. Tick marks denote the presence of the thyroid hormone signaling component or process. Minus signs denote the absence of the thyroid hormone signaling component/process. Question mark denotes uncertainty about the thyroid hormone signaling component or process. Black arrows indicate processes regulated by the pathway. Dotted arrow indicates the synthesis pathway is unknown

An additional example of functional conservation, operating through a non-canonical pathway, is the ability of T4 to associate with primary mesenchyme cell (PMC) membranes via integrins, activate transcription factors such as Ets1, and accelerate skeletogenesis. This mechanism parallels non-genomic thyroid hormone actions described in vertebrates and demonstrates that membrane receptors can mediate thyroid-like responses even in the absence of classical nuclear receptor binding (Taylor & Heyland, 2018; Davis et al., 2011; Cao et al., 2009; Koga et al., 2010). In some echinoderms, an additional "exogenous" component has been proposed, whereby algal-derived T4 functions as an environmental cue triggering metamorphosis.

This suggests an ancient interaction between environmental iodinated signals and developmental decisions that may have preceded the full endocrinization of thyroid

regulation in vertebrates (Chino et al., 1994; Heyland et al., 2004). In this evolutionary framework, the high iodine availability in marine environments and the presence of biogenic iodinated compounds may have provided the chemical substrate for the emergence of iodine-dependent developmental circuits, later internalized and integrated into endocrine systems in chordates.

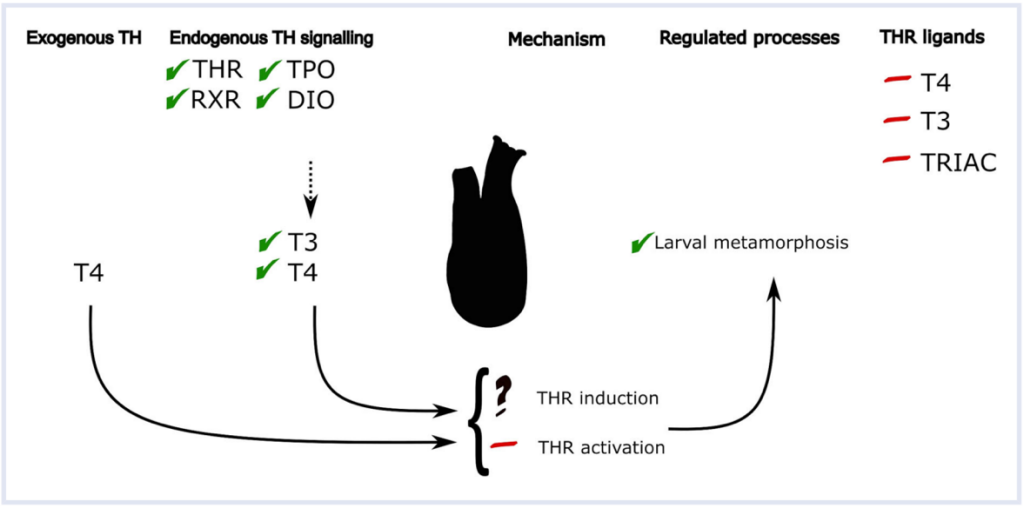


Figure 21 - Thyroid-like hormone signaling in tunicates. Tick marks denote the presence of thyroid hormone signaling component or process. Minus signs denote the absence of the thyroid hormone signaling component or process. Question mark denotes uncertainty about the thyroid hormone signaling component or process. Black arrows indicate processes regulated by the pathway. Dotted arrow indicates the synthesis pathway is unknown

In lower chordates such as *Branchiostoma* (amphioxus) and ascidians, conditions particularly informative for reconstructing the evolutionary "bridge" toward vertebrates can be observed. In tunicates, the endostyle concentrates iodine and produces iodinated compounds that function analogously to hormonal storage forms, while in amphioxus genes encoding deiodinases and thyroid hormone receptors (TRs) are present despite the absence of a morphologically organized thyroid gland (Paris & Laudet, 2008; Canestro et al., 2008). In tunicates, deuterostome invertebrates phylogenetically closest to vertebrates, this conservation is even more evident. THR

has been identified in *Styela clava* and *Ciona intestinalis* and is expressed during embryonic and larval development; in *S. clava*, expression peaks during tail regression (metamorphosis), whereas *Oikopleura dioica*, which retains a tadpole-like phenotype throughout life, lacks the THR gene, reinforcing the association between THR and metamorphosis (Carosa et al., 1998; Wei et al., 2020; Fenaux, 1998).

As in echinoderms, the DNA-binding domain is highly conserved, whereas the ligand-binding domain shows low homology and does not bind T4, T3, or TRIAC, suggesting unliganded regulatory modes and possible repressive functions, analogous to unliganded THR activity preventing premature metamorphosis in amphibians (Carosa et al., 1998; Fondell et al., 1993; Wen & Shi, 2015; Sachs et al., 2002). RXR is also present in several tunicates, and its pharmacological inhibition blocks metamorphosis, indicating a central role for the receptor complex (Wei et al., 2020; Blanchoud et al., 2018; Kawamura et al., 2013; Miglioli et al., 2021).

Biochemical evidence further supports a functional thyroid-like pathway: T4- and T3-like substances have been detected in ascidians; peroxidase activity and iodine binding occur in the endostyle; and homologs of TPO and deiodinases capable of converting T4 to T3 have been identified, consolidating the endostyle as an evolutionary precursor of the vertebrate thyroid gland (Patricolo et al., 1982; Roche et al., 1962; D'Agati & Cammarata, 2006; Ogasawara et al., 2002; Shepherdley et al., 2004; Canestro et al., 2008). Functionally, T4 exposure can stimulate metamorphosis, whereas inhibitors of hormone synthesis such as methimazole (via TPO inhibition) reduce larval metamorphosis; environmental factors like copper, an essential cofactor in vertebrate thyroid hormone synthesis, can induce precocious metamorphosis, underscoring the sensitivity of this regulatory system to environmental cues (Wei et

al., 2020; Lynch, 1961; Whittaker, 1964; Manisha et al., 2018). Collectively, these findings indicate that tunicates possess both the biochemical machinery for iodinated compound production and transformation and receptor-mediated circuits capable of translating these signals into developmental outcomes. They therefore represent a pivotal model for understanding the evolutionary transition from environmentally driven iodine-dependent regulation to the integrated endocrine control characteristic of vertebrates.

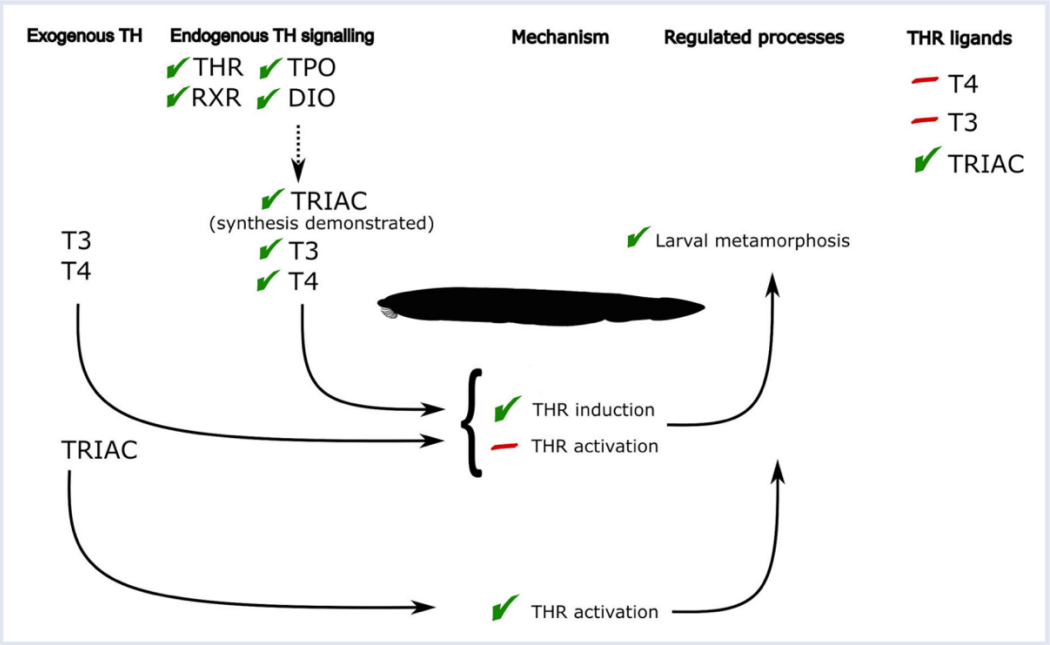


Fig.22 - Thyroid-like hormone signaling in cephalochordates. Tick marks denote the presence of the thyroid hormone signaling component or process. Minus signs denote the absence of the thyroid hormone signaling component or process. Black arrows indicate processes regulated by the pathway. Dotted arrow indicates the synthesis pathway is unknown

Cephalochordates, commonly known as amphioxus or lancelets, represent an additional invertebrate subphylum within Chordata. Although rarely used in ecotoxicology, their close evolutionary relationship with vertebrates makes them potentially informative models for detecting disruption of thyroid-like signaling,

similarly to tunicates. A thyroid hormone receptor (THR) has been identified in *Branchiostoma floridae*, and its cDNA reveals strong conservation of the DNA-binding domain relative to human THRα, whereas the ligand-binding domain is less conserved (Paris, Brunet, et al., 2008; Paris, Escriva, et al., 2008).

Consistently, *B. floridae* THR does not robustly bind T3 but is activated by the T3 derivative TRIAC, as shown by dose-dependent reporter activation, SRC1 recruitment, and NCOR release. Similar findings in *Branchiostoma belcheri* confirm strong TRIAC binding and only weak, likely non-physiological, T3 interaction (Paris, Escriva, et al., 2008; Wang et al., 2009). THR expression increases during larval development, peaking prior to metamorphosis, and is significantly upregulated by T3 treatment in both larvae and adults, paralleling hormone-induced receptor expression observed in mollusks (Paris, Escriva, et al., 2008). RXR has also been identified and cloned in *B. floridae*, and THR–RXR heterodimers bind DR4 response elements, reflecting a conserved receptor architecture (Paris, Brunet, et al., 2008; Paris, Escriva, et al., 2008; Laudet, 2011; Flamant, 2003). T4- and T3-like substances have been detected in *Branchiostoma*, particularly in the endostyle.

Radiolabeled TRIAC appears following administration of T4 or T3 precursors, indicating endogenous conversion capacity, although endogenous TRIAC is difficult to detect, possibly due to rapid turnover (Paris, Brunet, et al., 2008; Wang et al., 2009; Paris et al., 2010; Menegay et al., 1989; Rutgers et al., 1989). Homologs of thyroid peroxidase (TPO), peroxidase activity, and radioiodine incorporation demonstrate hormone synthesis in the endostyle, while multiple deiodinase genes are present in the genome. A unique non-selenoprotein deiodinase with high specificity for TRIAC, active on TRIAC but not T4 or T3, has been cloned, further supporting TRIAC as the

physiologically relevant ligand in amphioxus (Ogasawara, 2000; Ogasawara et al., 2002; Tsuneki et al., 1983; Fredriksson et al., 1985b; Monaco et al., 1981; Paris, Brunet, et al., 2008; Wang et al., 2009; Klootwijk et al., 2011). Developmentally, amphioxus represents an evolutionary transition between deuterostome invertebrates and vertebrates: early stages resemble other invertebrates, whereas later larval stages display vertebrate-like features, a shift mediated in part by thyroid signaling.

TRIAC exposure accelerates metamorphosis, an effect blocked by the THR inhibitor NH3; conversely, inhibition of thyroid hormone synthesis reduces metamorphosis, while T3 co-administration restores developmental progression. These findings indicate that metamorphosis in *B. floridae* is regulated by TRIAC through THR interaction (Bertrand & Escriva, 2011; Paris, Escriva, et al., 2008; Grover et al., 2007; Paris et al., 2010).

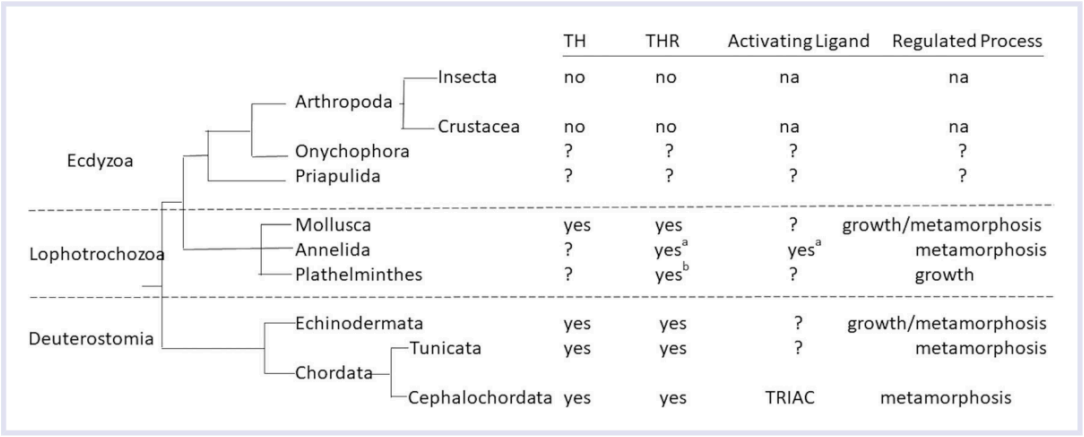


Fig. 23 - Evidence of thyroid hormone signaling among candidate surrogate lineages for the evaluation of endocrine disruption.

Collectively, these findings support a "mosaic" model of thyroid toolkit conservation. The presence of THR in lophotrochozoans and deuterostomes suggests a metazoan origin of the receptor, followed by secondary loss in ecdysozoans, while

the limited evidence for ligand-dependent activation in many invertebrates indicates that THR may have initially functioned as an orphan receptor, acquiring full ligand sensitivity only later in specific lineages (Escriva et al., 1997; Taylor & Heyland, 2018). Within this framework, non-classical metabolites such as TRIAC may have served as functional ligands in certain groups, supporting a gradual evolution of ligand specificity not universally centered on T3/T4 (Paris, Escriva, et al., 2008).

Thyroid-like signaling may also have been partially mediated by membrane receptors such as integrins, which are widespread in invertebrates, potentially inducing receptor isoform expression or THR nuclear translocation, consistent with non-genomic models and functional evidence (Burke, 1999; Davis et al., 2011; Sadow et al., 2003). Overall, the presence in echinoderms and basal chordates of a molecular toolkit closely related to the vertebrate thyroid system, including enzymes (TPO/DIO), receptors (THR/RXR), and signaling pathways (integrin–MAPK), reveals a shared evolutionary foundation. Long before the emergence of a specialized thyroid gland, pre-chordate marine organisms were already exploiting iodine and iodinated compounds, whether endogenous or environmental, to regulate development and metabolism. Vertebrate evolution likely internalized and integrated these modules into a highly specialized endocrine axis, optimizing the coordination of developmental transitions and ecological adaptation.

1.5.3 Chemical disruption and pesticide interference: The case of thiram

In light of the evolutionary conservation and multi-level regulatory complexity of thyroid-related signaling pathways described above, pesticides emerge as particularly relevant environmental stressors capable of perturbing this finely tuned system. A growing body of evidence indicates that numerous agrochemicals interfere with the hypothalamic–pituitary–thyroid (HPT) axis in non-target organisms, disrupting hormone synthesis, peripheral metabolism, transport, or receptor-mediated signaling, especially during sensitive developmental windows (Zoeller et al., 2007; Diamanti-Kandarakis et al., 2009; Gilbert, 2011). Rather than acting solely through direct receptor binding, many compounds impair upstream processes such as iodide uptake, thyroid peroxidase (TPO) activity, or hormone conversion, underscoring the intrinsic vulnerability of the thyroid axis at multiple regulatory nodes (Zoeller et al., 2017). Within this framework, dithiocarbamate fungicides, and particularly thiram (tetramethylthiuram disulfide), represent emblematic thyroid-disrupting pesticides.

Although relatively limited in environmental persistence, thiram can reach aquatic ecosystems through runoff and has been consistently associated with goitrogenic effects across vertebrate models (Goldner et al., 2010; Crofton et al., 2012). Mechanistically, thiram and its metabolites interfere with thiol-dependent enzymes and chelate essential metal cofactors, impairing key steps of thyroid hormone biosynthesis, including TPO-mediated iodide organification (Doerge & Chang, 2002; Hurley et al., 1998). Chronic exposure in mammals results in decreased circulating T_4 and compensatory TSH elevation, a pattern consistent with inhibition of thyroid hormone synthesis (Goldner et al., 2010; Crofton et al., 2012). In zebrafish (*Danio rerio*), whose embryonic transparency and rapid thyroid ontogeny provide a sensitive

developmental model, thiram exposure induces stage-dependent developmental delay, axial malformations, impaired hatching, and transcriptional dysregulation of thyroid-related genes (*tpo*, *dio2*, *dio3*, *thra*, *thrb*) (Opitz et al., 2005; Opitz et al., 2011; Thienpont et al., 2011; Hornung et al., 2018). The strong phenotypic resemblance between thiram-induced defects and those elicited by classical TPO inhibitors such as methimazole supports a shared mechanistic interference with thyroid hormone synthesis.

Importantly, when considered alongside the evolutionary conservation of thyroid-related signaling modules across deuterostomes, including marine invertebrates such as *Arbacia lixula*, these findings suggest that thiram-induced interference with iodinated developmental pathways may reflect a deeply conserved vulnerability. On this basis, the present thesis investigates the impact of thiram on embryonic development in phylogenetically distant aquatic models, integrating morphological, molecular, and endocrine endpoints, and evaluates the capacity of hydrothermal carbonization-derived hydrochar to mitigate its biological effects through reduction of contaminant bioavailability. This combined ecotoxicological and mitigation-oriented approach aims to provide both mechanistic insight into thyroid-related disruption and a sustainable strategy for environmental risk reduction (Morthorst et al., 2022).

References

Abbassy, M.S. Pesticide Residues in Selected Vegetables and Fruits in Alexandria City, Egypt, 1997–1998. Bull. Environ. Contam. Toxicol. 2001, 67, 0225–0232.

Adomako-Ankomah, A. and Ettensohn, C.A. (2013). Growth factor-mediated mesodermal cell guidance and skeletogenesis during sea urchin gastrulation. Development 140, 4214-4225.

Adomako-Ankomah, A. and Ettensohn, C.A. (2014). Growth Factors and Early Mesoderm Morphogenesis: Insights from the Sea Urchin Embryo. Genesis 52, 158–172.

Alt B, Reibe S, Feitosa NM, Elsalini OA, Wendl T, Rohr KB. Analysis of Origin and Growth of the Thyroid Gland in Zebrafish. Dev Dyn (2006) 235 (7):1872–83.

Álvarez-Ruiz, R., Picó, Y., & Campo, J. (2021). Bioaccumulation of emerging contaminants in mussel (Mytilus galloprovincialis): influence of microplastics. Science of the Total Environment, 796,149006.

Anand, U., Adelodun, B., Cabreros, C., Kumar, P., Suresh, S., Dey, A., ... & Bontempi, E. (2022). Occurrence, transformation, bioaccumulation, risk and analysis of pharmaceutical and personal care products from wastewater: a review. Environmental Chemistry Letters, 20(6), 3883-3904.

Andersen, J.H.; Poulsen, M.E. Results from the Monitoring of Pesticide Residues in Fruit and Vegetables on the Danish Market, 1998–1999. Food Addit. Contam. 2001, 18, 906–931.

Angerer, L. M., Angerer, R. C. (2000). Animal–Vegetal Axis Patterning Mechanisms in the Early Sea Urchin Embryo. Developmental Biology 218, 1– 12.

Angerer, L. M., Oleksyn, D. W., Levine, A. M., Li, X., Klein, W. H., Angerer, R. C. (2001). Sea urchin goosecoid function links fate specification along the animal-vegetal and oral-aboral embryonic axes. Development 128, 4393-4404.

Angerer, L. M., Oleksyn, D. W., Logan, C. Y., McClay, D. R., Dale, L., Angerer, R. C. (2000). A BMP pathway regulates cell fate allocation along the sea urchin animal-vegetal embryonic axis. Development 127, 1105-1114.

Anstrom, J.A., Chin, J.E., Leaf, D.S., Parks, A.L., Raff, R.A. (1987). Localization and expression of msp130, a primary mesenchyme lineage-specific cell surface protein in the sea urchin embryo. Development 101, 255-265.

Bacchetta, R., Santo, N., Fascio, U., Moschini, E., Freddi, S., Chirico, G., Camatini, M., Mantecca, P. (2012). Nano-sized CuO, TiO2 and ZnO affect Xenopus laevis development. Nanotoxicology 6, 381-398.

Bansal, O.P. 2022. Health Impacts of the Carbamate and Dithiocarbamate Pesticides: A Review. International Journal of Scientific and Research Publications.

Bargagli B., Cruscanti M., Leonzio C. e Bacci E. 1998. "I bioindicatori". In: Vighi M., Bacci E. Ecotossicologia. UTET, Torino, Italia, pp. 237.

Barman R.P. 1991. *"A taxonomic revision of the Indo-Burmese species of Danio Hamilton Buchanan (Pisces, Cyprinidae)".* Zoological Survey of India.

Baylis A.D. (2000) Why glyphosate is a global herbicide: strengths, weaknesses and prospects. Pest Management Science, 56, 299-308.

Belden J.B., and Lydy M.J. (2000) Impact of atrazine on organophosphate insecticide toxicity. Environmental Toxicology and Chemistry, 19, 2266-2274.

Beliaeva NF, Kashirtseva VN, Medvedeva NV, Khudoklinova I, Ipatova OM, Archakov AI. 2010. "*Zebrafish as a model organism for biomedical studies".* Biomed Khim. 56:120–31.

Bellanger M, Demeneix B, Grandjean P, Zoeller RT, Trasande L. Neurobehavioral deficits, diseases, and associated costs of exposure to endocrine-disrupting chemicals in the European Union. *J Clin Endocrinol Metab.* (2015) 100:1256–66

Bellisai, G.; Bernasconi, G.; Brancato, A.; Cabrera, L.C.; Castellan, I.; Del Aguila, M.; Ferreira, L.; Santonja, G.G.; Greco, L.; Jarrah, S.; et al. Review of the Existing Maximum Residue Levels for Dithiocarbamates according to Article 12 of Regulation (EC) No 396/2005. EFSA J. 2023, 21, 7987.

Benson, S., Sucov, H., Stephens, L., Davidson, E., Wilt, F. (1987). A lineage-specific gene encoding a major matrix protein of the sea urchin embryo spicule. I. Authentication of the cloned gene and its developmental expression. Developmental Biology 120, 499-506.

Bernal J. Thyroid hormone receptors in brain development and function. Nat Clin Pract Endocrinol Metab. (2007) 3:249–59. doi: 10.1038/ncpendmet0424

Bertrand, S., & Escriva, H. (2011). Evolutionary crossroads in developmental biology: Amphioxus. Development, 138, 4819–4830.

Blanchoud, S., Rutherford, K., Zondag, L., Gemmell, N. J., & Wilson, M. J. (2018). De novo draft assembly of the Botrylloides leachii genome provides further insight into tunicate evolution. Scientific Reports, 8, 5518.

Bouton, D., Escriva, H., de Mendonça, R. L., Glineur, C., Bertin, B., Noël, C., Robinson-Rechavi, M., de Groot, A., Cornette, J., Laudet, V., & Pierce, R. J. (2005). A conserved retinoid X receptor (RXR) from the mollusk Biomphalaria glabrata transactivates transcription in the presence of retinoids. Journal of Molecular Endocrinology, 34, 34–582.

Bouzaffour, M., Rampon, C., Ramaugé, M., Courtin, F., & Vriz, S. (2010). Implication of type 3 deiodinase induction in zebrafish fin regeneration. General and Comparative Endocrinology, 168, 88–94.

Bradbury S.P., and Coats J.R. (1989) Comparative toxicology of the pyrethroid insecticides. Reviews of Environmental Contamination and Toxicology, 108, 133-177.

Bradham, C. A., McClay, D. R. (2005). p38 MAPK is essential for secondary axis specification and patterning in sea urchin embryos. Development 133, 21- 32.

Bresch, H.; Beck, H.; Ehlermann, D.; Schlaszus, H.; Urbanek, M. 1990. *"A long-term toxicity test comprising reproduction and growth of zebrafish with 4-chloroaniline"*. Archives of Environmental Contamination and Toxicology 19(3):419-27.

Bridgham, J. T., Eick, G. N., Larroux, C., Deshpande, K., Harms, M. J., Gauthier, M. E., Ortlund, E. A., Degnan, B. M., & Thornton, J. W. (2010). Protein evolution by molecular tinkering: Diversification of the nuclear receptor superfamily from a ligand-dependent ancestor. PLoS Biology, 8, e1000497.

Bristow, J.T. Fungicidal Composition. Method and Use Thereof

C.J. Van Leeuwen, J.L. Maas-Diepeveen, G. Niebeek, W.H.A. Vergouw, P.S. Grif-Caldas, E.D.; Tressou, J.; Boon, P.E. Dietary Exposure of Brazilian Consumers to Dithiocarbamate Pesticides—A Probabilistic Approach. Food Chem. Toxicol. 2006, 44, 1562–1571.

Canestro, C., Bassham, S., & Postlethwait, J. H. (2008). Evolution of the thyroid: Anterior-posterior regionalization of the Oikopleura endostyle revealed by Otx, Pax2/5/8, and Hox 1 expression. Developmental Dynamics (Pembroke, Ont.), 237, 1490–1499

Cao, H. J., Lin, H.-Y., Luidens, M. K., Davis, F. B., & Davis, P. J. (2009). Cytoplasm-to-nucleus shuttling of thyroid hormone receptor-beta1 (Trbeta1) is directed from a plasma membrane integrin receptor by thyroid hormone. Endocrine Research, 34, 31–42.

Capitao, A., Lopes-Marques, M., Pascoa, I., Ruivo, R., Mendiratta, N., Fonseca, E., Castro, L. F. C., & Santos, M. M. (2020). The Echinodermata PPAR: Functional characterization and exploitation by the model lipid homeostasis regulator tributyltin. Environmental Pollution, 263, 114467.

Cappello T., Giannetto A., Parrino V., Maisano M., Oliva S., De Marco G., Guerriero G., Mauceri A., Fasulo S. 2018. Baseline levels of metabolites in different

tissues of mussel Mytilus galloprovincialis (Bivalvia: Mytilidae). Comp. Biochem. Physiol. D 26, 32–39.

Carballeira C., Ramos-Gòmez J., Martìn-Dìaz L., DelValls T.A. (2012). Identification of specific malformations of sea urchin larvae for toxicity assessment: Application to marine pisciculture effluents. Marine Environmental research 77, 12-22.

Carosa E., Fanelli, A., Ulisse, S., Di Lauro, R., Rall, J. E., & Jannini, E. A. (1998). Ciona intestinalis nuclear receptor 1: a member of steroid/thyroid hormone receptor family. Proceedings of the National Academy of Sciences of the United States of America, 95(19), 11152-11157.

Carter, C. J., Farrar, N., Carlone, R. L., & Spencer, G. E. (2010). Developmental expression of a molluscan RXR and evidence for its novel, nongenomic role in growth cone guidance. Developmental Biology, 343, 124–137.

Carvalho FP. Pesticides, environment, and food safety. Food Energy Secur. (2017) 6:48–60. doi: 10.1002/fes3.108

Cavalieri, V., Guarcello, R., Spinelli, G. (2011). Specific expression of a TRIM-containing factor in ectoderm cells affects the skeletal morphogenetic program of the sea urchin embryo. Development 138, 4279-4290.

Chen, J.; Akhtar, M.; Hardej, D. Exposure to Dithiocarbamate Fungicide Ziram Results in Hepatic and Renal Toxicity in Long Evan Rats. Environ. Toxicol. Pharmacol. 2023, 99, 104116.

Chino, Y., Saito, M., Yamasu, K., Suyemitsu, T., & Ishihara, K. (1994). Formation of the adult rudiment of sea urchins is influenced by thyroid hormones. Developmental Biology, 161(1), 1–11. https://doi.org/10.1006/ dbio.1994.1001

Chou, A.P.; Maidment, N.; Klintenberg, R.; Casida, J.E.; Li, S.; Fitzmaurice, A.G.; Fernagut, P.-O.; Mortazavi, F.; Chesselet, M.-F.; Bronstein, J.M. Ziram Causes

Dopaminergic Cell Damage by Inhibiting E1 Ligase of the Proteasome. J. Biol. Chem. 2008, 283, 34696–34703.

Chung, S.W.C.; Wong, W.W.K. Chromatographic Analysis of Dithiocarbamate Residues and Their Metabolites in Foods Employed in Dietary Exposure Studies—A Review. Food Addit. Contam. Part A 2022, 39, 1731–1743.

Ciacci, C., Barmo, C., Gallo, G., Maisano, M., Cappello, T., D'Agata, A., Leonzio, C., Mauceri, A., Fasulo, S., Canesi, L. (2012). Effects of sublethal, environmentally relevant concentrations of hexavalent chromium in the gills of Mytilus galloprovincialis. Aquat. Toxicol. 120-121, 109-118.

Coffman, J. A., McCarthy, J. J., Dickey-Sims, C., Robertson, A. J. (2004). Oral–aboral axis specification in the sea urchin embryo II. Mitochondrial distribution and redox state contribute to establishing polarity in Strongylocentrotus purpuratus. Developmental Biology 273, 160–171.

Cole D.J. (1985) Mode of action of glyphosate - a literature analysis, p. 48-74, In E. Grossbard and D. Atkinson, eds. The herbicide glyphosate. Butterworths, London.

Crofton KM, Foss JA, Hass U, Jensen KF, Levin ED, Parker SP. Undertaking positive control studies as part of developmental neurotoxicity testing A report from the ILSI Research Foundation /Risk Science Institute expert working group on neurodevelopmental endpoints. Neurotoxicol Teratol. (2008) 30:266–87. doi: 10.1016/j.ntt.2007.06.002

D'Agati, P., & Cammarata, M. (2006). Comparative analysis of thyroxine distribution in ascidian larvae. Cell and Tissue Research, 323, 529–535.

Dahm R. e Geisler R. 2006. *"Learning from small fry: the zebrafish as a genetic model organism for aquaculture fish species".* Marine Biotechnology, 8 (4), 329-45.

Dave G., Andersson K.; Berglind R.; Hasselrot B. 1968. *"Toxicity of eight solvent extraction chemicals and of cadmium to water fleas, Daphnia magna, rainbow trout,*

Davidson, E.H., Cameron, R.A., Ransick, A. (1998). Specification of cell fate in the sea urchin embryo: summary and some proposed mechanisms. Development 125(17), 3269-90.

Davidson, E.H., Rast, J.P., Oliveri, P., Ransick, A., Calestani, C., Yuh, C.H., Minokawa, T., Amore, G., Hinman, V., Arenas-Mena, C., Otim, O., Brown, C.T., Livi, C.B., Lee, P.Y., Revilla, R., Rust, A.G., Pan, Z.J., Schilstra, M.J., Clarke, P.J., Arnone, M.I., Rowen, L., Cameron, R.A., McClay, D.R., Hood, L., Bolouri, H. (2002). A genomic regulatory network for development. Science. 295(5560), 1669-78.

Davis, J. P., Davis, F. B., Mousa, S. A., Luidens, M. K., & Lin, H.-Y. (2011). Membrane receptor for thyroid hormone: Physiologic and pharmacologic implications. Annual Review of Pharmacology and Toxicology, 51, 99–115.

De Marco, G., Conti, G. O., Giannetto, A., Cappello, T., Galati, M., Iaria, C.,... & Maisano, M. (2022). Embryotoxicity of polystyrene microplastics in zebrafish Danio rerio. Environmental research, 208, 112552.

De Pomerai, D. I. (1996). Heat-shock proteins as biomarkers of pollution. Human &

De Rossetto, A.N.O.F., Pedroso Melegari, S., Ouriques, L.C., Gerson Matias, W. (2014). Comparative evaluation of acute and chronic toxicities of CuO nanoparticles and bulk using Daphnia magna and Vibrio fischeri. Sci. Total. Environ. 490, 807–814.

Della Torre, C., Bergami, E., Salvati, A., Faleri, C., Cirino, P., Dawson, K.A., Corsi, I. (2014). Accumulation and embryotoxicity of polystyrene nanoparticles at early stage of development of sea urchin embryos Paracentrotus lividus. Environ Sci Technol 48, 12302-12311.

Delmer D.P., Read S.M., and Cooper G. (1987) Identification of a receptor protein in cotton fibers for the herbicide 2,6-dichlorobenzonitrile. Plant Physiology, 84, 415-420.

DeLorenzo M.E., Scott G.I., and Ross P.E. (2001) Toxicity of pesticides to aquatic microorganisms: A review. Environmental Toxicology and Chemistry, 20, 84-98.

Diamanti-Kandarakis E, Bourguignon JP, Giudice LC, Hauser R, Prins GS, Soto AM, et al. Endocrine-disrupting chemicals: an Endocrine Society scientific statement. Endocr Rev. (2009) 30:293–342.

Dogheim, S.M.; Gad Alla, S.A.; El-Marsafy, A.M. Monitoring of Pesticide Residues in Egyptian Fruits and Vegetables during 1996. J. AOAC Int. 2001, 84, 519–531.

Duboc, V., Lapraz, F., Besnardeau, L., Lepage, T. (2008). Lefty acts as an essential modulator of Nodal activity during sea urchin oral–aboral axis formation. Developmental Biology 320, 49-59.

Duboc, V., Röttinger, E., Besnardeau, L., Lepage, T. (2004). Nodal and BMP2/4 Signaling Organizes the Oral-Aboral Axis of the Sea Urchin Embryo. Developmental Cell, 6, 397–410.

Duloquin, L., Lhomond, G., Gache, C. (2007). Localized VEGF signaling from ectoderm to mesenchyme cells controls morphogenesis of the sea urchin embryo skeleton. Development 134, 2293-2302.

Easter SS Jr, Nicola GN. 1996. "*The development of vision in the zebrafish (Danio rerio)".* Development Biology;180:646–63.

Ecobichon D.J. (1991) Toxic effects of pesticides, p. 565-622, In M. O. Amdur, et al., eds. Casarett and Doull's Toxicology- The basic science of poisons, 4th ed. McGraw-Hill, Inc., New York.

Edwards, I.R.; Ferry, D.G.; Temple, W.A. Fungicides & Related Compounds. In Handbook of Pesticide Toxicology; Volume 3: Classes of Pesticides; Academic Press, Inc.: New York, NY, USA, 1991; Chapter 21; pp. 1409–1470.

Elgueta, S.; Moyano, S.; Sepúlveda, P.; Quiroz, C.; Correa, A. Pesticide Residues in Leafy Vegetables and Human Health Risk Assessment in North Central Agricultural Areas of Chile. Food Addit. Contam. Part B Surveill. Commun. 2017, 10, 105–112.

Engeszer R.E.; Patterson L.B.; Roa A.A.; Parichy D.M. 2007. "*Zebrafish in the wild: a review of natural history and new notes from the field*". Zebrafish., 4(1): 21-40.

ENTOX/TIWET (The Faculty of the Department of Environmental Toxicology and The Institute of Wildlife and Environmental Toxicology, Clemson University). Aquatic and Terrestrial Ecotoxicology. In Casarett and Doull's Toxicology. The Basic Science of Poisons Klaassen CD (ed.). McGraw- Hill: New York, 1996; 883–905

Ettensohn, C. A. (2013). Encoding Anatomy: Developmental Gene Regulatory Networks and Morphogenesis. Genesis.

Ettensohn, C. A., Guss, K. A., Hodor, P. G., Malinda, K. M. (1997) The morphogenesis of the skeletal system of the sea urchin embryo. Progress in Developmental Biology 8 (Reproductive Biology of Invertebrates), John Wiley and Sons, New York, 225-265.

Ettensohn, C. A., Illies, M. R., Oliveri, P., De Jong, D. L. (2003). Alx1, a member of the Cart1/Alx3/Alx4 subfamily of Paired-class homeodomain proteins, is an essential component of the gene network controlling skeletogenic fate specification in the sea urchin embryo. Development 130, 2917-2928.

Ettensohn, C.A. (1999). Cell movements in the sea urchin embryo. Current Opinion in Genetics & Development 9, 461-465.

European Commission. Commission Implementing Regulation (EU) 2018/309 of 1 March 2018, Concerning the Non-Renewal of Approval of the Active Substance Propineb, in Accordance with Regulation (EC) No 1107/2009 of the European Parliament and of the Council Concerning the Placing of Plant Protection Products on

the Market, and Amending the Annex to Commission Implementing Regulation (EU) No 540/2011.

European Commission. Commission Implementing Regulation (EU) 2018/1500 of 9 October 2018 Concerning the Non-Renewal of Approval of the Active Substance Thiram, and Prohibiting the Use and Sale of Seeds Treated with Plant Protection Products Containing Thiram, in Accordance with Regulation (EC) No 1107/2009 of the European Parliament and of the Council Concerning the Placing of Plant Protection Products on the Market, and Amending the Annex to Commission Implementing Regulation (EU) No 540/2011

European Commission. Commission Implementing Regulation (EU) 2020/2087 of 14 December 2020 Concerning the NonRenewal of the Approval of the Active Substance Mancozeb, in Accordance with Regulation (EC) No 1107/2009 of the European Parliament and of the Council Concerning the Placing of Plant Protection Products on the Market, and Amending the Annex to Commission Implementing Regulation (EU) No 540/2011.

European Commission. Commission Implementing Regulation (EU) 2023/2455 of 7 November 2023 Concerning the NonRenewal of the Approval of the Active Substance Metiram, in Accordance with Regulation (EC) No 1107/2009 of the European Parliament and of the Council and Amending Commission Implementing Regulation (EU) No 540/2011.

European Commission. Regulation (EC) No 1107/2009 of the European Parliament and of the Council of 21 October 2009 Concerning the Placing of Plant Protection Products on the Market and Repealing Council Directives 79/117/EEC and 91/414/EEC.

European Food Safety Authority (EFSA). Peer Review of the Pesticide Risk Assessment of the Active Substance Propineb. EFSA J. 2016, 14, e04605

Fanjul-Bolado, P.; Fogel, R.; Limson, J.; Purcarea, C.; Vasilescu, A. Advances in the Detection of Dithiocarbamate Fungicides: Opportunities for Biosensors. Biosensors 2020, 11, 12

Fasulo, S., Mauceri, A., Maisano, M., Giannetto, A., Parrino, V., Gennuso, F., & D'Agata, A. (2010). Immunohistochemical and molecular biomarkers in Coris julis exposed to environmental contaminants. Ecotoxicology and Environmental Safety, 73(5), 873-882.

Fénaux, L., 1968. Maturation des gonades et cycle saisonnier des larveschez A. lixula, P. lividus et P. microtuberculatus à Villefranche-Sur-Mer. Vie et Milieu Série A Biologie Marine 19, 1–52.

Feng, Y.; Jiang, W.; Li, H.; Liang, X.; Tong, F.; Sheng, X.; Hou, R.; Wan, X.; Liu, Y. Detection of Dithiocarbamate Pesticide Residues in Tea by Colorimetric and Fluorescent Double-Mode Probe Regulated by Tyrosinase. Sens. Actuators B Chem. 2024, 426, 137026

Fioen And M.W. Luijken. Aquatic toxicological aspects of dithiocarbamates and related compounds. I. Short-term toxicity tests. Aquatic Tozicology, 7 (1985) 145-164

Fishman MC. 1999. "*Zebrafish genetics: the enigma of arrival*". Proceedings of the National Academy of Sciences USA.;96:10554–6.

Flamant F, Samarut J. Thyroid hormone receptors: lessons from knockout and knock-in mutant mice. Trends Endocrinol Metab. (2003) 14:85–90. doi: 10.1016/S1043-2760(02)00043-7

Flatt, T., Moroz, L. L., Tatar, M., & Heyland, A. (2006). Comparing thyroid and insect hormone signaling. Integrative and Comparative Biology, 46, 777–794.

Flowers, V. L., Courteau, G. R., Poustka, A. J., Weng, W., Venuti, J. M. (2004). Nodal/Activin Signaling Establishes Oral–Aboral Polarity in the Early Sea Urchin Embryo. Developmental Dynamics 231, 727–740.

Fondell, J. D., Roy, A. L., & Roeder, R. G. (1993). Unliganded thyroid hormone receptor inhibits formation of a functional preinitiation complex: Implications for active repression. Genes & Development, 7, 1400–1410.

Food and Agriculture Organization of the United Nations (FAO). FAOSTAT. (2019). Available online at: http://www.fao.org/faostat/en/#data/RF (accessed April 9, 2019).

Food and Agriculture Organization of the United Nations (FAO). Use Pattern, Registered Uses of Thiram.

Fossi, M.C. (1998). Biomarkers as diagnostic and prognostic tools for wildlife risk assessment: integrating endocrine-distrupting chemicals. Toxicol Ind Health 14(1-2), 291-309.

Fredriksson, G., Fenaux, R., & Ericson, L. E. (1989). Distribution of peroxidase and iodination activity in the endostyles of Oikopleura albicans and Oikopleura longicauda (Appendicularia, Chordata). Cell and Tissue Research, 255, 505–510.

Fredriksson, G., Fenaux, R., & Ericson, L. E. (1989). Distribution of peroxidase and iodination activity in the endostyles of Oikopleura albicans and Oikopleura longicauda (Appendicularia, Chordata). Cell and Tissue Research, 255, 505–510.

Fredriksson, G., Ofverholm, T., & Ericson, L. (1988). Iodine binding and peroxidase activity in the endostyle of Salpa fusiformis, Thalia democratica, Dolioletta gegenbauri and *Doliolum nationalis* (Tunicata, Thaliacea). Cell and Tissue Research, 253, 403–411.

Fredriksson, G., Ofverholm, T., & Ericson, L. E. (1985a). Ultrastructural demonstration of iodine binding and peroxidase activity in the endostyle of Oikopleura dioica (Appendicularia). General and Comparative Endocrinology, 58, 319–327.

Fredriksson, G., Öfverholm, T., & Ericson, L. E. (1985b). Electron-microscopic studies of iodine-binding and peroxidase activity in the endostyle of the larval amphioxus (*Branchiostoma lanceolatum*). Cell and Tissue Research, 241, 257–266.

Gambardella, C., Ferrando, S., Gatti, A.M., Cataldi, E., Ramoino, P., Aluigi, M.G., Faimali, M., Diaspro, A., Falugi, C. (2015). Review: Morphofunctional and Biochemical Markers of Stress in Sea Urchin Life Stages Exposed to Engineered Nanoparticles. Environ Toxicol. doi: 10.1002/tox.22159.

Gambardella, C., Ferrando, S., Morgana, S., Gallus, L., Ramoino, P., Ravera, S., Bramini, M., Diaspro, A., Faimali, M., Falugi, C. (2015). Exposure of Paracentrotus lividus male gametes to engineered nanoparticles affects skeletal bio-mineralization processes and larval plasticity. Aquat Toxicol 158, 181-191.

Ghoto, S.A.; Khuhawar, M.Y.; Jahangir, T.M. Silver Nanoparticles with Sodium Dodecyl Sulfate as a Colorimetric Probe for the Detection of Dithiocarbamate Pesticides in Environmental Samples. Anal. Sci. 2019, 35, 631–637.

Gianguzza, P., Visconti, G., Gianguzza, F., Vizzini, S., Sarà, G., Dupont S. (2014). Temperature modulates the response of the thermophilous sea urchin *Arbacia lixula* early life stages to CO2-driven acidification. Mar. Environ. Res. 93, 70-7.

Gil, F. and Pla, A. (2001). Biomarkers as Biological Indicators of Xenobiotic Exposure. J. Appl. Toxicol. 21, 245–255.

Goldner WS, Sandler DP, Yu F, Hoppin JA, Kamel F, Levan TD. Pesticide use and thyroid disease among women in the Agricultural Health Study. Am J Epidemiol. (2010) 171:455–64. doi: 10.1093/aje/kwp404

Goldner WS, Sandler DP, Yu F, Shostrom V, Hoppin JA, Kamel F, et al. Hypothyroidism and pesticide use among male private pesticide applicators in the agricultural health study. J Occup Environ Med. (2013) 55:1171–8. doi: 10.1097/JOM.0b013e31829b290b

González-Fernández, C., Albentosa, M., Campillo, J. A., Viñas, L., Fumega, J., Franco, A., ... & Bellas, J. (2015). Influence of mussel biological variability on pollution biomarkers. Environmental research, 137, 14-31.

Grossmann K. (2000) Mode of action of auxin herbicides: a new ending to a long, drawn out story. Trends in Plant Science, 5, 506-508.

Grover, G. H., Dunn, C., Nguyen, N.-H., Boulet, J., Dong, G., Domogauer, J., Barbounis, P., & Scanlan, T. S. (2007). Pharmacological profile of the thyroid hormone receptor antagonist NH3 in rats. Journal of Pharmacology and Experimental Therapeutics, 322, 385–390.

Guss, K.A. and Ettensohn, C.A. (1997). Skeletal morphogenesis in the sea urchin embryo: regulation of primary mesenchyme gene expression and skeletal rod growth by ectoderm-derived cues. Development 124, 1899-1908.

Gustafson, T., Wolpert, L., (1999). Studies on the cellular basis of morphogenesis in the sea urchin embryo. Directed movements of primary mesenchyme cells in normal and vegetalized larvae. Experimental Cell Research 253, 288-295.

Harkey, M. A., Whiteley, H. R., Whiteley, A. H. (1992). Differential expression of the msp130 gene among skeletal lineage cells in the sea urchin embryo: a three dimensional in situ hybridization analysis. Mechanisms of Development. 37, 173-184.

Harkey, M.A., Klueg, K., Sheppard, P., Raff, R.A. (1995). Structure, expression, and extracellular targeting of PM27, a skeletal protein associated specifically with growth of the sea urchin larval spicule. Developmental Biology 168, 549-566.

Harvey, C. B., & Williams, G. R. (2004). Mechanism of thyroid hormone action. Thyroid, 12, 441–446.

Heyland, A., & Hodin, J. (2004). Heterochronic developmental shift caused by thyroid hormone in larval sand dollars and its implications for phenotypic plasticity and the evolution of nonfeeding development. Evolution, 58, 524–53.

Heyland, A., & Hodin, J. (2004). Heterochronic developmental shift caused by thyroid hormone in larval sand dollars and its implications for phenotypic plasticity and the evolution of nonfeeding development. Evolution, 58, 524–53.

Heyland, A., Price, D. A., Bodnarova-buganova, M., & Moroz, L. L. (2006a). Thyroid hormone metabolism and peroxidase function in two non- chordate animals. Journal of Experimental Zoology-Part B, 306B, 551–566.

Heyland, A., Reitzel, A. M., & Hodin, J. (2004). Thyroid hormones determine developmental mode in sand dollars (Echinodermata: Echinoidea). Evolution & Development, 6, 382–392.

Hodor, P.G., Ettensohn, C.A. (1998). The dynamics and regulation of mesenchymal cell fusion in the sea urchin embryo. Developmental Biology 199, 111 –124.

Hodor, P.G., Illies, M.R., Broadley, S., Ettensohn, C.A. (2000). Cell-substrate interactions during sea urchin gastrulation: migrating primary mesenchyme cells interact with and align extracellular matrix fibers that contain ECM3, a molecule with NG2-like and multiple calcium-binding domains. Developmental Biology 222, 181-194.

Holzer, G., Roux, N., & Laudet, V. (2017). Evolution of ligands, receptors and metabolizing enzymes of thyroid signaling. Molecular and Cellular Endocrinology, 459, 5–13.

Howard-Ashby, M., Materna, S. C., Brown, C. T., Chen, L., Cameron, R. A., & Davidson, E. H. (2006). Gene families encoding transcription factors expressed in early development of Strongylocentrotus purpuratus. Developmental Biology, 300, 90–107.

Huang, W., Xu, F., Qu, T., Li, L., Que, H., & Zhang, G. (2015b). Iodothyronine deiodinase gene analysis of the Pacific oyster Crassostrea gigas reveals possible

conservation of thyroid hormone feedback regulation mechanism in mollusks. Chinese Journal of Oceanology and Limnology, 33, 997–1006.

Huang, W., Xu, F., Qu, T., Zhang, R., Li, L., Que, H., & Zhang, G. (2015a). Identification of thyroid hormones and functional characterization of thyroid hormone receptor in the pacific oyster Crassostrea gigas provide insight into evolution of the thyroid hormone system. PLoS One, 10, e0144991.

Hutter H, Moshammer H. Pesticides are an occupational and public health issue. Int J Environ Res Public Health. (2018) 15:1650. doi: 10.3390/ijerph15081650

International Agency for Research on Cancer (IARC). Overall Evaluations of Carcenogenicity. IARC Monographs on the Evaluation of Carcinogenic Risks to Humans, Suppl. 7; International Agency for Research on Cancer, Ethylene thiourea: Lyon, France, 1987; pp. 207–208.

Jespers A.B.K., and de Waard M.A. (1995) Effect of fenpiclonil on phosphorylation of glucose in Fusarium sulphureum. Pesticide Science, 44, 167-175.

Johnson, L. G. (1998). Stage-dependent thyroxine effects on sea urchin development. New Zealand Journal of Marine and Freshwater Research, 32, 531–536.

Johnson, L. G., & Cartwright, C. M. (1996). Thyroxine-accelerated larval development in the crown-of-throns starfish, Acanthaster planci. Biological Bulletin, 190, 299–301.

Jung, J.; Kiehs, K.; Zeeh, B.; Theobald, H. Salts of Phosphonic Acids. U.S. Patent 4135909 A, 29 December 1976.

Kadar, E., Dyson, O., Handy, R.D., Sherain, N., Al-Subiai, S.N. (2013). Are reproduction impairments of free spawning marine invertebrates exposed to zero-valent nano-iron associated with dissolution of nanoparticles? Nanotoxicology 7, 135-143.

Kane D.A., Warga R.M., Kimmel C.B. 1992. "*Mitotic domains in the early embryo of the zebrafish*". Nature 360, 735–737.

Karp, G.C., Solursh, M. (1985). Dynamic activity of the filopodia of sea urchin embryonic cells and their role in directed migration of the primary mesenchyme in vitro. Developmental Biology 112, 276-283.

Katow, H., Yazawa, S., Sofuku, S. (1990). A fibronectin-related synthetic peptide, Pro-Ala-Ser- Ser, inhibits fibronectin binding to the cell surface, fibronectin-promoted cell migration in vitro, and cell migration in vivo. Experimental Cell Research 190, 17-24.

Kaur, S., Jobling, S., Jones, C. S., Noble, L. R., Routledge, E. J., & Lockyer, A. E. (2015). The nuclear receptors of Biomphalaria glabrata and Lottia gigantea: Implications for developing new model organisms. PLoS One, 10, e0121259.

Kawamura, K., Shiohara, M., Kanda, M., & Fujiwara, S. (2013). Retinoid X receptor-medicated transdifferentiation cascade in budding tunicates. Developmental Biology, 384, 343–355.

Killian, C.E., Croker, L., Wilt, F.H. (2010). SpSM30 gene family expression patterns in embryonic and adult biomineralized tissues of the sea urchin, Strongylocentrotus purpuratus. Gene Expression Patterns : GEP 10, 135-139.

Killian, C.E., Wilt, F.H. (2008). Molecular aspects of biomineralization of the echinoderm endoskeleton. Chemical Reviews 108, 4463-4474.

Kimmel C.B., Ballard W.W., Kimmel S.R., Ullmann B. e Schilling T.F. 1995. "*Stages of embryonic development of the zebrafish*". Developmental Dynamics, 203 (3), 253-310.

Kimmel C.B., Warga R.M. 1987. "*Cell lineages generating axial muscle in the zebrafish embryo*". Nature 327, 234–237.

Klootwijk, W., Friesema, E. C. H., & Visser, T. V. (2011). A nonselenoprotein from Amphioxus deiodinates Triac but not T3: Is Triac the primordial bioactive thyroid hormone? Endocrinology, 152, 3259–3267. https://doi. org/10.1210/en.2010-1408

Köck-Schulmeyer, M., Ginebreda, A., Petrovic, M., Giulivo, M., Aznar-Alemany, Ò., Eljarrat, E., ... & Barceló, D. (2021). Priority and emerging organic microcontaminants in three Mediterranean river basins: Occurrence, spatial distribution, and identification of river basin specific pollutants. Science of the Total Environment, 754, 142344.

Koga, H., Matsubara, M., Fujitani, H., Miyamoto, N., Komatsu, M., Kiyomoto, M., Akasaka, K., & Wada, H. (2010). Functional evolution of Ets in echinoderms with focus on the evolution of echinoderm larval skeletons. Development Genes and Evolution, 220, 107–115.

Korevaar TIM, Muetzel R, Medici M, Chaker L, Jaddoe VWV, de Rijke YB, et al. Association of maternal thyroid function during early pregnancy with offspring IQ and brain morphology in childhood: A population-based prospective cohort study. Lancet Diabetes Endocrinol. (2017) 4:35–43. doi: 10.1016/S2213-8587(15)00327-7

Kortenkamp, A., Axelstad, M., Baig, A. H., Bergman, Å., Bornehag, C. G., Cenijn, P., Christiansen, S., Demeneix, B., Derakhshan, A., Fini, J. B., Frädrich, C., Hamers, T., Hellwig, L., Köhrle, J., Korevaar, T., Lindberg, J., Martin, O., Meima, M. E., Mergenthaler, P. … Zoeller, R. T. (2020). Removing critical gaps in chemical test methods by developing new assays for the identification of thyroid hormone system-disrupting chemicals— The ATHENA Project. International Journal of Molecular Sciences, 21(9), 3123.

Kostrouchova, M., & Kostrouch, Z. (2014). Nuclear receptors in nematode development: Natural experiments made by a phylum. Biochimica et Biophysica Acta—Gene Regulatory Mechanisms, 1849, 224–237.

Kumar, K.; Sabarwal, A.; Singh, R.P. Mancozeb Selectively Induces Mitochondrial-Mediated Apoptosis in Human Gastric Carcinoma Cells through ROS Generation. Mitochondrion 2019, 48, 1–10.

Kurokawa D., Kitajima T., Mitsunaga-Nakatsubo K., Amemiya S., Shimada H., Akasaka K. (1999). HpEts, an ets-related transcription factor implicated in primary mesenchyme cell differentiation in the sea urchin embryo. Mechanisms of Development 80, 41-52.

Lam, P. K., & Gray, J. S. (2003). The use of biomarkers in environmental monitoring programmes. Marine pollution bulletin, 46(2), 182–186.

Lamarck, J.B.P.M. (1816). Histoire Naturelle des Animaux sans Vertèbres, [...], Tome Troisième. Verdière (3&5).

Lapraz, F., Röttinger, E., Duboc, V., Range, R., Duloquin, L., Walton, K., Wu, S.-Y., Bradham, C., Loza, M. A., Hibino, T., Wilson, K., Poustka A., McClay, D., Angerer, L., Gache, C., Lepage, T. (2006). RTK and TGF-β signaling pathways genes in the sea urchin genome. Developmental Biology 300, 132–152.

Laudet, V. (2011). The origins and evolution of vertebrate metamorphosis. Current Biology, 21, R726–R737.

Lawrence C. 2007. "*The husbandry of zebrafish (Danio rerio*)". Aquaculture. 269(1-4):1- 20.

LeBlanc, G. A., Wang, Y. H., Homes, C. N., Kwon, G., & Medlock, E. K. (2013). A transgenerational endocrine signaling pathway in Crustacea. PLoS One, 8, e61715.

Lee, K.J., Browning, L.M., Nallathamby, P.D., Desai, T., Cherukuri, P.K., Xu, X.N. (2012). In vivo quantitative study of sized-dependent transport and toxicity of single silver nanoparticles using zebrafish embryos. Chem. Res. Toxicol. 25, 1029-1046.

Leemans, M., Couderq, S., Demeneix, B., & Fini, J. B. (2019). Pesticides with potential thyroid hormone-disrupting effects: a review of recent data. *Frontiers in endocrinology*, *10*, 743.

Legislative Decree, 1999. L.D. 11 May 1999, n. 152. Provisions on the protection of waters from pollution and implementation of Directive 91/271/EEC concerning the treatment of urban waste-water and Directive 91/676/EEC concerning the protection of waters from pollution caused by nitrates from agricultural sources.

Leroux P. (1996) Recent developments in the mode of action of fungicides. Pesticide Science, 47,191-197.

Li, E., Materna, S.C., Davidson, E.H. (2012). Direct and indirect control of oral ectoderm regulatory gene expression by Nodal signaling in the sea urchin embryo. Developmental Biology 369, 377-385.

Li, M., Mead, E. A., & Jhu, J. (2011). Heterodimer of two bHLH-PAS proteins mediates juvenile hormone-induced gene expression. Proceedings of the National Academy of Sciences of the United States of America, 108, 638–643.

Lin, C. Y., Viant, M. R., & Tjeerdema, R. S. (2006). Metabolomics: methodologies and applications in the environmental sciences. Journal of Pesticide Science, 31(3), 245-251.

Linnaeus, C. (1758). Systema naturae. Regnum animale: Editio decima.Laurentius Salvius, Holmiae (Stockholm).

Litoff, E. J., Garriott, T. E., Ginjupalli, G. K., Butler, L., Gay, C., Scott, K., & Baldwin, W. S. (2014). Annotation of the Daphnia magna nuclear receptors: Comparison to Daphnia pulex. Gene, 552, 116–125.

Liu, K.; Li, Y.; Iqbal, M.; Tang, Z.; Zhang, H. Thiram Exposure in Environment: A Critical Review on Cytotoxicity. Chemosphere 2022, 295, 133928.

Livingston B.T., Killian C.E., Wilt F., Cameron A., Landrum M.J., Ermolaeva O., Sapojnikov V., Maglott D.R., Buchanan A.M., Ettensohn C.A. (2006). A genome-wide analysis of biomineralization-related proteins in the sea urchin Strongylocentrotus purpuratus. Developmental Biology 300, 335–348.

Logan, C.Y., Miller, J.R., Ferkowicz, M.J., McClay, D.R. (1999). Nuclear beta-catenin is required to specify vegetal cell fates in the sea urchin embryo. Development 126, 345-357.

Lushchak VI, Matviishyn TM, Husak VV, Storey JM, Storey KB. Pesticide toxicity: a mechanistic approach. Excli J. (2018) 17:1101–36. doi: 10.17179/excli2018-1710

Lynch, W. F. (1961). Extrinsic factors influencing metamorphosis in bryozoan and ascidian larvae. American Zoologist, 1, 59–66.

Lyons, D.C., Kaltenbach, S.L., McClay, D.R. (2012). Morphogenesis in sea urchin embryos: linking cellular events to gene regulatory states. Wires Developmental Biology 1, 231-252.

Maisano, M., Cappello, T., Catanese, E., Vitale, V., Natalotto, A., Giannetto, A., Barreca, D., Brunelli, E., Mauceri, A., Fasulo, S. (2015). Developmental abnormalities and neurotoxicological effects of CuO NPs on the black sea urchin *Arbacia lixula* by embryotoxicity assay. Marine Environmental Research xxx 1- 7.

Malarvannan G., Dirinck E., Dirtu A.C., Pereira-Fernandes A., Neels H., Jorens P.G., Gaal L.V., Blust R., Covaci A. 2013. "Distribution of persistent organic pollutants in two different fat compartments from obese individuals". Environment International 55, 33–42.

Malik, A.K.; Faubel, W. Methods of Analysis of Dithiocarbamate Pesticides: A Review. Pestic. Sci. 1999, 55, 965–970.

Malinda, K. M., Fisher, G. W., Ettensohn, C. A. (1995). Four-Dimensional Microscopic Analysis of the Filopodial Behavior of Primary Mesenchyme Cells during Gastrulation in the Sea Urchin Embryo. Developmental Biology 172, 552–566.

Mallozzi, M., Bordi, G., Garo, C., & Caserta, D. (2016). The effect of maternal exposure to endocrine disrupting chemicals on fetal and neonatal development: A review on the major concerns. Birth Defects Research Part C: Embryo Today: Reviews, 108(3), 224-242.

Manisha, A., Roshan, K. M., Sudeep, K., Imran, M., & Sumesh, P. S. (2018). Study of trace elements in patients of hypothyroidism with special reference to zinc and copper. Biomedical Journal of Scientific & Technical Research, 6.

Manno, D., Carata, E., Tenuzzo, B.A., Panzarini, E., Buccolieri, A., Filippo, E., Rossi, M., Serra, A., Dini, L. (2012). High ordered biomineralization induced by carbon nanoparticles in the sea urchin Paracentrotus lividus. Nanotechnology 23, 495104.

Manzo, S., Miglietta, M.L., Rametta, G., Buono, S., Di Francia, G. (2013). Embryotoxicity and spermiotoxicity of nanosized ZnO for mediterranean sea urchin Paracentrotus lividus. J Hazard Mater 254-255,1-9.

Marelli, F., Rurale, G., & Persani, L. (2021). From endoderm to progenitors: an update on the early steps of thyroid morphogenesis in the Zebrafish. Frontiers in Endocrinology, 12, 664557.

Matsumura F. (1985) Toxicology of insecticides. 2nd ed. Plenum Press, New York, USA.

McCarty, L. S., & Munkittrick, K. R. (1996). Environmental biomarkers in aquatic toxicology: fiction, fantasy, or functional?

McClure M.M.; McIntyre P.B.; McCune A.R. 2006. "*Notes on the natural diet and habitat of eight danionin fishes, including the zebrafish Danio rerio".* Journal of Fish Biology 69:553–570.

Menegay, C., Juge, C., & Burger, A. G. (1989). Pharmacokinetics of 3,5,3'-triiodothyroacetic acid and its effects on serum TSH levels. Acta Endocrinologica, 121, 651–658.

Menezo, Y., Dale, B., & Elder, K. (2019). The negative impact of the environment on methylation/epigenetic marking in gametes and embryos: A plea for action to protect the fertility of future generations. Molecular Reproduction and Development, 86(10), 1273-1282.

Miglioli, A., Canesi, L., Gomes, I. D. L., Schubert, M., & Dumollard, R. (2021). Nuclear receptors and development of marine invertebrates. Genes, 12, 83.

Miller, A., & Heyland, A. (2013). Iodine accumulation in sea urchin larvae is dependent on peroxide. Journal of Experimental Biology, 216, 915–926.

Miller, J., Fraser S. E., McClay, D. (1995). Dynamics of thin filopodia during sea urchin gastrulation. Development 121, 2501-2511.

Miller, J.R., McClay, D.R. (1997). Characterization of the role of cadherin in regulating cell adhesion during sea urchin development. Developmental Biology 192, 323-339.

Missawi, O., Bousserrhine, N., Zitouni, N., Maisano, M., Boughattas, I., De Marco, G., ... & Banni, M. (2021). Uptake, accumulation and associated cellular alterations of environmental samples of microplastics in the seaworm Hediste diversicolor. Journal of Hazardous Materials, 406, 124287.

Mnif W, Ibn A, Hassine H, Bouaziz A, Bartegi A, Thomas O. Effect of endocrine disruptor pesticides: a review. Int J Environ Res Public Health. (2011) 8:2265–303. doi: 10.3390/ijerph8062265

Monaco, F., Dominici, R., Andreoli, M., De Pirro, R., & Roche, J. (1981). Thyroid hormone formation in the thyroglobulin synthesized in the Amphioxus (Branchiostoma lanceolatum pallas). Comparative Biochemistry and Physiology. B: Comparative Biochemistry, 70, 341–343.

Morthorst JE, Holbech H, De Crozé N, Matthiessen P, LeBlanc GA. Thyroid-like hormone signaling in invertebrates and its potential role in initial screening of thyroid hormone system disrupting chemicals. Integr Environ Assess Manag. 2023 Jan;19(1):63-82.

Mourouzis, I., Lavecchia, A. M., & Xinaris, C. (2020). Thyroid hormone signalling: From the dawn of life to the bedside. Journal of Molecular Evolution, 88, 88–103

Mulla M.S., and Mian L.S. (1981) Biological and environmental impacts of the insecticides malathion and parathion on nontarget biota in aquatic ecosystems. Residue Reviews, 78, 100-135.

Narahashi T. (1986) Nerve membrane ionic channels as the target of toxicants. Archives of Toxicology, Suppl., 9, 3-13.

Nasci C., Nesto N., Monteduro R.A., Da Ros L. 2002. “Field application of biochemical markers and a physiological index in the mussel Mytilus galloprovincialis: transplantation and biomonitoring studies in the lagoon of Venice (VE Italy)”. Marine Environmental Research 54:811–816.

National Pesticide Information Center (NPIC). EXTOXNET PIP—METIRAM. 2025.

National Pesticide Information Center (NPIC). EXTOXNET PIP—Thiram.

New Jersey Department of Health. Hazardous Substance Fact Sheet, Thiram; New Jersey Department of Health: Trenton, NJ, USA, 2010.

Nika, M. C., Ntaiou, K., Elytis, K., Thomaidi, V. S., Gatidou, G., Kalantzi, O. I., ... & Stasinakis, A. S. (2020). Wide-scope target analysis of emerging contaminants in landfill leachates and risk assessment using Risk Quotient methodology. Journal of Hazardous Materials, 394, 122493.

OECD, Busquet, F., Strecker, R., Rawlings, J.M., Belanger, S.E., Braunbeck, T., Carr, G.J., Cenijn, P., Fochtman, P., Gourmelon, A., Hübler, N., Kleensang, A., Kn€obel, M., Kussatz, C., Legler, J., Lillicrap, A., Martínez-Jer_onimo, F., Polleichtner, C., Rzodeczko, H., Salinasm, E., Schneiderm, K.E., Scholz, S., Van den Brandhof, E., van der Ven Leo, T.M., Walter-Rohde, S., Weigt, S., Witters, H., Halder, M. (2014). OECD validation study to assess intra- and inter- laboratory reproducibility of the zebrafish embryo toxicity test for acute aquatic toxicity testing. Regul. Toxicol. Pharmcol. 69, 496-511.

Ogasawara, M. (2000). Overlapping expression of amphioxus homologs of the thyroid transcription factor-1 gene and thyroid peroxidase gene in the endostyle: Insight into evolution of the thyroid gland. Development Genes and Evolution, 210, 231–242.

Ogasawara, M., Di Lauro, R., & Satoh, N. (2002). Ascidian homologs of mammalian thyroid peroxidase genes are expressed in the thyroid- equivalent region of the endostyle. Journal of Experimental Zoology, 285, 158–169.

Okazaki, K. (1965). Skeleton formation of sea urchin larvae. V. Continuous observation of the process of matrix formation. Experimental Cell Research 40, 585-596.

Okazaki, K. (1975). Normal development to metamorphosis. In: “The Sea Urchin Embryo” (G. Czihak, Ed.), Springer-Verlag, New York. 177-232.

Opitz R, Antonica F, Costagliola S. New Model Systems to Illuminate Thyroid Organogenesis. Part I: An Update on the Zebrafish Toolbox. Eur Thyroid J (2013) 2(4):229–42.

Opitz R, Maquet E, Huisken J, Antonica F, Trubiroha A, Pottier G, et al. Transgenic Zebrafish Illuminate the Dynamics of Thyroid Morphogenesis and its Relationship to Cardiovascular Development. Dev Biol (2012) 372 (2):203–16.

Opitz R, Maquet E, Zoenen M, Dadhich R, Costagliola S. TSH Receptor Function is Required for Normal Thyroid Differentiation in Zebrafish. Mol Endocrinol (2011) 25(9):1579–99.

Ortiz-Zarragoitia M. & Cajaraville M.P. 2006. "Biomarkers of exposure and reproduction related effects in mussels exposed to endocrine disruptors". Archives of Environmental Contamination and Toxicology 50: 361–369.

Parichy DM, Elizondo MR, Mills MG, Gordon TN, Engeszer RE. 2009. "*Normal table of post-embryonic zebrafish development: staging by externally visible anatomy of the living fish*". Developmental Dynamics.;238:2975–3015.

Paris, M., & Laudet, V. (2008). The history of a developmental stage: Metamorphosis in chordates. Genesis, 46, 657–672.

Paris, M., Brunet, F., Markov, G. V., Schubert, M., & Laudet, V. (2008a). The amphioxus genome enlightens the evolution of the thyroid hormone signaling pathway. Development Genes and Evolution, 218, 667–680.

Paris, M., Escriva, H., Schubert, M., Brunet, F., Brtko, J., Ciesielski, F., Roecklin, D., Vivat-Hannah, V., Jamin, E. L., Cravedi, J.-P., Scanlan, T. S., Renaud, J.-P., Holland, N., & Laudet, V. (2008b). Amphioxus postembryonic development reveals the homology of chordate metamorphosis. Current Biology, 18, 825–830.

Paris, M., Hillenweck, A., Bertrand, S., Delous, G., Escriva, H., Zalko, D., Cravedi, J.-P., & Laudet, V. (2010). Active metabolism of thyroid hormone during metamorphosis of amphioxus. Integrative and Comparative Biology, 50, 63–74.

Paris, M., Holzer, G., & Laudet, V. ((unpublished results) in Holzer G, Roux N, Laudet V (2017). Evolution of ligands, receptors and metabolizing enzymes of thyroid signaling. Molecular and Cellular Endocrinology, 459, 5–13.

Pastor Ciscato, C.H.; Bertoni Gebara, A.; Henrique Monteiro, S. Pesticide Residue Monitoring of Brazilian Fruit for Export 2006–2007. Food Addit. Contam. Part B-Surveill. 2009, 2, 140–145.

Patricolo, E., & Cammarata, M., D'Agati, P. (2001). Presence of thyroid hormones in ascidian larvae and their involvement in metamorphosis. Journal of Experimental Zoology, 290, 426–430.

Patricolo, E., Mansueto, C., D'Agati, P., & Pellerito, L. (2001). Organometallic complexes with biological molecules: XVI. Endocrine disruption effects of tributyltin (IV) chloride on metamorphosis of the ascidian larva. Applied Organometallic Chemistry, 15, 916–923.

Patricolo, E., Ortolani, G., & Cascop, A. (1982). The effect of L-thyroxine on the metamorphosis of Ascidia malaca. Cell and Tissue Research, 214, 289–301.

Paul-Friedman, K., Martin, M., Crofton, K. M., Hsu, C.-W., Sakamuru, S., Zhao, J., Xia, M., Huang, R., Stavreva, D. A., Soni, V., Vartikovski, L., Raziuddin, R., Hager, G. L., & Houck, K. A. (2019). Limited chemical structural diversity found to modulate thyroid hormone receptor in the tox21 chemical library. Environmental Health Perspectives, 127(9), 97009.

Pelegri F. 2003. "*Maternal factors in zebrafish development*". Developmental Dynamics. 228, 535-554.

Pinsino, A., Roccheri, M.C., Costa, C., Matranga, V. (2011). Manganese Interferes with Calcium, Perturbs ERK Signaling, and Produces Embryos with No Skeleton. Toxicological Sciences 123(1), 217-230.

Poulsen, M.E.; Andersen, J.H. Results from the Monitoring of Pesticide Residues in Fruit and Vegetables on the Danish Market, 2000–2001. Food Addit. Contam. 2003, 20, 742–757.

Rafiq, K., Shashikant, R., McManus, C. J., & Ettensohn, C. A. (2014). Genome-wide analysis of the skeletogenic gene regulatory network of sea urchins. Development, 141, 950–961.

Range, R., Lapraz, F., Quirin, M., Marro, S., Besnardeau, L., Lepage, T. (2007). Cis-regulatory analysis of nodal and maternal control of dorsal-ventral axis formation by Univin, a TGF-related to Vg1. Development 134, 3649-3664.

Rasgele, P.G.; Muranli, F.D.; Kekeçoˇglu, M. Assessment of the Genotoxicity of Propineb in Mice Bone Marrow Cells Using Micronucleus Assay. Tsitol. Genet. 2014, 48, 39–43.

Rho, H.K., McClay, D.R. (2011). The control of foxN2/3 expression in sea urchin embryos and its function in the skeletogenic gene regulatory network. Development 138, 937-945.

Roberts, J.R.; Reigart, J.R. Recognition and Management of Pesticide Poisonings; United States Environmental Protection Agency, Office of Pesticide Programs: Washington, DC, USA, 2013.

Roche, J., Salvatore, G., & Rametta, G. (1962). Presence and biosynthesis of thyroid hormones in a tunicate, Ciona intestinalis. Biochimica et Biophysica Acta/General Subjects, 63, 154–165.

Röttinger, E., Saudemont, A., Duboc, V., Besnardeau, L., McClay, D., Lepage, T. (2008). FGF signals guide migration of mesenchymal cells, control skeletal morphogenesis and regulate gastrulation during sea urchin development. Development 135, 353-365.

Rousset B, Dupuy C, Miot F, Dumont J. Chapter 2: thyroid hormone synthesis and secretion. In: Feingold KR, Anawalt B, Boyce A, et al., editors. Endotext. Dartmouth, MA: MDText.com, Inc. (2015).

Rout, P. R., Zhang, T. C., Bhunia, P., & Surampalli, R. Y. (2021). Treatment technologies for emerging contaminants in wastewater treatment plants: A review. Science of the Total Environment, 753, 141990.

Rutgers, M., Heusdens, F. A., Bonthuis, F., & Visser, T. J. (1989). Metabolism of triiodothyroacetic acid (TA3) in rat liver. II. Deiodination and conjugation of TA3 by rat hepatocytes and in rats in vivo. Endocrinology, 125, 433–443.

Sachs, L. M., Jones, P. L., Havis, E., Rouse, N., Demeneix, B. A., & Shi, Y. B. (2002). Nuclear receptor corepressor recruitment by unliganded thyroid hormone receptor in gene repression during Xenopus laevis development. Molecular and Cellular Biology, 22, 8527–8538.

Sainath, S. B., Andre, A., Castro, L. F. C., & Santos, M. M. (2019). The evolutionary road to invertebrate thyroid hormone signaling: Perspectives for endocrine disruption processes. Comparative Biochemistry and Physiology. C: Comparative Pharmacology and Toxicology, 223, 124–138.

Saito, M., Seki, M., Amemiya, S., Yamasu, K., Suyemitsu, T., & Ishihara, K. (1998). Induction of metamorphosis in the sand dollar Peronella japonica by thyroid hormones. Development, Growth and Differentiation, 40, 307–312.

Sarkar, A., Ray, D., Shrivastava, A. N., & Sarker, S. (2006). Molecular biomarkers: experimental toxicology, 15(4), 279-285

Schoenfuss, H. L. (2021). The effects of contaminants of emerging concern on water quality. Chemometrics and Cheminformatics in Aquatic Toxicology, 23- 44.

Scholz S.; Fischer S.; Gündel U.; Küster E.; Luckenbach T.; Voelker D. 2008. "*The zebrafish embryo model in environmental risk assessment - applications beyond acute toxicity testing".* Environmental Science and Pollution Research 15(5): 394-404.

Sekimizu, K., Tagawa, M., & Takeda, H. (2007). Defective fin regeneration in medaka fish (*Oryzias latipes*) with hypothyroidism. Zoological Science, 24(7), 693–699.

Selman K.; Wallace R.A.; Sarka A.; Qi X. 2005. "*Stages of oocyte development in the zebrafish BrachiDanio rerio"*. Journal of Morphology. 218(2): 203-224.

Shefali, Rahul Kumar, Mahipal Singh Sankhla,Rajeev Kumar, Swaroop S. Sonone. Impact of Pesticide Toxicity in Aquatic Environment.

Shepherdley, C. A., Klootwijk, W., Makabe, K. W., Visser, T. J., & Kuiper, G. G. (2004). An ascidian homolog of vertebrate iodothyronine deiodinases. Endocrinology, 145, 1255–1268.

Sikorski J.A., and Gruys K.J. (1997) Understanding Glyphosate's molecular mode of action with EPSP synthase: Evidence favoring an allosteric inhibitor model. Accounts of Chemical Research, 30, 2-8.

Spence R.; Gerlach, G.;Lawrence, C.; Smith, C. 2008. *"The behaviour and ecology of the zebrafish, Danio rerio"*. Biological Reviews of the Cambridge Philosophical Society 83(1):13-34.

Spitsbergen J.M.; Kent M.L. 2003. *"The sate of the art of the zebrafish model for toxicology and toxicologic pathology research- advantages and current limitations"*. Toxicologic Pathology 31: 62-87.

Stuke, S.; Wirkner, H.; Safferling, M.; Gorgulu, N.; Zupanc, C.; Ertz, K.; Steinbeck, M.; Haack, K.J.; Jasak, J.; Diot, R. Stabilized Dithiocarbamate Formulations. EP20733398 B1, 15 June 2020.

Sun, J., Fang, R., Wang, H., Xu, D. X., Yang, J., Huang, X., ... & Huang, Y. (2022). A review of environmental metabolism disrupting chemicals and effect biomarkers associating disease risks: Where exposomics meets metabolomics. Environment International, 158, 106941.

Talwar P.K.; Jhingran A.G. 1991. "*Inland fishes of India and adjacent countries"*. A.A. Balkema, Rotterdan, 1158pp.

Tang Fiona H. M., Manfred Lenzen, Alexander McBratney and Federico Maggi. 2021."Risk of pesticide pollution at the global scale". Nature Geoscience | VOL 14 |206–210.

Tang, X. W., Yu, R., Fan, M. H., Yang, Z., Liao, Z., Yang, Z. X., ... & Yan, X. J. (2022). Physiological and transcriptome analysis of Mytilus coruscus in response to Prorocentrum lima and microplastics. Frontiers in Marine Science, 9, 1087667.

Tata JR. The road to nuclear receptors of thyroid hormone. Biochim Biophys Acta Gen Subj. (2013) 1830:3860–66. doi: 10.1016/j.bbagen.2012.02.017

Taylor, E., & Heyland, A. (2018). Thyroid hormones accelerate initiation of skeletogenesis via MAPK (ERK1/2) in larval sea urchins (Strongylocentrotus purpuratus). Frontiers in Endocrinology, 9, 439. https://doi. org/10.3389/fendo.2018.00439

Thambirajah, A. A., Wade, M. G., Verreault, J., Buisine, N., Alves, V. A., Langlois, V. S., & Helbing, C. C. (2022). Disruption by stealth-Interference of endocrine disrupting chemicals on hormonal crosstalk with thyroid axis function in humans and other animals. Environmental Research, 203, 111906.

their significance and application in marine pollution monitoring. Ecotoxicology, 15(4), 333-340.

Thiruchelvam, M.; Brockel, B.J.; Richfield, E.K.; Baggs, R.B.; Cory-Slechta, D.A. Potentiated and Preferential Effects of Combined Paraquat and Maneb on Nigrostriatal Dopamine Systems: Environmental Risk Factors for Parkinson's Disease? Brain Res. 2000, 873, 225–234.

Tisdale, W.H.; Williams, I. Disinfectant and Fungicide. U.S. Patent 1972961A, 26 May 1931.

Tsen, C.-M.; Yu, C.-W.; Chen, S.-Y.; Lin, C.-L.; Chuang, C.-Y. Application of Surface-Enhanced Raman Scattering in Rapid Detection of Dithiocarbamate Pesticide Residues in Foods. Appl. Surf. Sci. 2021, 558, 149740.

Tsuneki, K., Kobayashi, H., & Ouji, M. (1983). Histochemical distribution of peroxidase in amphioxus and cyclostomes with special reference to the endostyle. General and Comparative Endocrinology, 50, 188–200.

Ullah Sana, Mohammad Jalil Zorriehzahra2. 2015. “Ecotoxicology: A Review of Pesticides Induced Toxicity in Fish”. Advances in Animal and Veterinary Sciences.

United States Environmental Protection Agency (EPA). Maneb-Developmental Toxicity Study in Rats; US EPA: Washington, DC, USA, 1993

United States Environmental Protection Agency (EPA). Prevention, Pesticides and Toxic Substances, EPA-738-F-05-002, Ferbam; US EPA: Washington, DC, USA, 2005.

Urry, L.A., Hamilton, P.C., Killian, C.E., Wilt, F.H. (2000). Expression of Spicule Matrix Proteins in the Sea Urchin Embryo during Normal and Experimentally Altered Spiculogenesis. Developmental Biology 225, 201-213.

Van der Krieken, W.M.; Mazzitelli, S. Dithiocarbamate Fungicide Macromolecular Complexes. EP20730112 B1, 28 May 2020.

Van der Krieken, W.M.; Stratmann, C. Aqueous Composition of Dithiocarbamate Fungicide. EP4156927 B1, 28 May 2021.

Vergova, M.; Jablonica, A.; Janota, S. Occupational Exposure to Mancozeb in Employees in the Production of Novozir Mn 80. Park. Lak 1988, 40, 425–430.

Vignet, C., Cappello, T., Fu, Q., Lajoie, K., De Marco, G., Clérandeau, C., ... & Cachot, J. (2019). Imidacloprid induces adverse effects on fish early life stages that are more severe in Japanese medaka (Oryzias latipes) than in zebrafish (Danio rerio). Chemosphere, 225, 470-478.

Wafford K.A., Sattelle D.B., Gant D.B., Eldefrawi A.T., and Eldefrawi M.E. (1989) Noncompetitive inhibition of GABA receptors in insect and vertebrate CNS by endrin and lindane. Pesticide Biochemistry and Physiology, 33, 213-219.

Wang, G., Zhang, L., Xu, J., Yin, C., Zhang, Z., & Wang, Y. (2019). The roles of thyroid hormone receptor and T3 in metamorphosis of Haliotis diversicolor. Journal of Oceanology and Limnology, 37, 745–758.

Wang, Z., Li, Y., Kong, F., Li, M., Xi, M., & Yu, Z. (2021). How do trophic magnification factors (TMFs) and biomagnification factors (BMFs) perform on toxic pollutant bioaccumulation estimation in coastal and marine food webs. Regional Studies in Marine Science, 44, 101797.

Wang, Z.; Yang, L.; Ye, X.; Huang, C.; Yang, W.; Zhang, L.; Wu, Z.; Fu, F. Multicolor Visual Screening of Total Dithiocarbamate Pesticides in Foods Based on Sulfydryl Mediated Growth of Gold Nanobipyramids. Anal. Chim. Acta 2020, 1139, 59–67.

Wei, J., Zhang, J., Lu, Q., Ren, P., Guo, X., Wang, J., Li, X., Chang, Y., Duan, S., Wang, S., Yu, H., Zhang, X., Yang, X., Gao, H., & Dong, B. (2020). Genomic basis of environmental adaptation in the leathery sea squirt (Styela clava). Molecular Ecology Resources, 20, 1414–1431.

Wei, Q.; Zhang, L.; Song, C.; Yuan, H.; Li, X. Quantitative Detection of Dithiocarbamate Pesticides by Surface-Enhanced Raman Spectroscopy Combined with an Exhaustive Peak-Seeking Method. Anal. Methods 2021, 13, 1479–1488.

Weitzel, H.E., Illies, M.R., Byrum, C.A., Xu, R., Wikramanayake, A.H., Ettensohn, C.A. (2004). Differential stability of beta-catenin along the animal- vegetal axis of the sea urchin embryo mediated by dishevelled. Development 131, 2947-2956.

Wen, L., & Shi, Y.-B. (2015). Unliganded thyroid hormone receptor α controls developmental timing in Xenopus tropicalis. Endocrinology, 156, 721–734.

Whittaker, J. R. (1964). Copper as a factor in the onset of ascidian metamorphosis. Nature, 202, 1024–1025.

World Health Organization (WHO). Dithiocarbamate Pesticides, Ethylenethiourea, and Propylenethiourea: A General Introduction/Published Under the Joint Sponsorship of the United Nations Environment Programme, the International Labour Organisation, and the World Health Organization; WHO: Geneva, Switzerland, 1988; ISBN 9789241542784

Wu, S.Y., McClay, D.R. (2007). The Snail repressor is required for PMC ingression in the sea urchin embryo. Development 134, 1061-1070.

Wu, W., Niles, E. G., & LoVerde, P. T. (2007). Thyroid hormone receptor orthologues from invertebrate species with emphasis on Schistosoma mansoni. BMC Evolutionary Biology, 7, 150. https://doi.org/10.1186/ 1471-2148-7-150

Yaguchi, S., Yaguchi, J., Burke, R.D. (2006). Specification of ectoderm restricts the size of the animal plate and patterns neurogenesis in sea urchin embryos. Development 133, 2337-2346.

Yaoita, Y. (2019). Tail resorption during metamorphosis in *Xenopus tadpoles*. Frontiers in Endocrinology, 10, 143.

Younis H.M., Abo-El-Saad M.M., Abdel-Razik R.K., and Abo-Seda S.A. (2002) Resolving the DDT target protein in insects as a subunit of the ATP synthase. Biotechnology and Applied Biochemistry, 35, 9-17.

Zhang, L. J., Qian, L., Ding, L. Y., Wang, L., Wong, M. H., & Tao, H. C. (2021). Ecological and toxicological assessments of anthropogenic contaminants based on environmental metabolomics. Environmental Science and Ecotechnology, 5, 100081.

Zito, F., Costa, C., Sciarrino, S., Cavalcante, C., Poma, V., Matranga, V. (2005). Cell adhesion and communication: a lesson from echinoderm embryos for the exploitation of new therapeutic tools. Prog Mol Subcell Biol 39, 7-44.

Zoratto, C.; Thais, D.; Aguera, R.G.; Sano Lini, R.; Pante, G.C.; Bueno, C.; Castro, J.C.; Aparecida, S.; Marchioni, C.; Machinski, M. Analytical and Toxicological Aspects of Dithiocarbamates: An Overview of the Last 10 Years. Toxicol. Mech. Methods 2022, 32, 637–649.

CHAPTER 2

Valorization of algal waste biomass for the mitigation of environmental contaminants within a Circular Economy framework

2.1 General introduction

In recent decades, the concept of the circular economy (CE) has emerged as an innovative paradigm to address global challenges related to the overexploitation of natural resources, waste generation, and the environmental impacts of anthropogenic activities. Unlike the traditional linear economic model, often summarized as “take, make, dispose”, the circular economy is based on principles of reuse, recycling, regeneration, and valorization of materials, with the aim of retaining the value of products and resources within the production system for as long as possible (Geissdoerfer et al., 2017). According to the definition provided by the Ellen MacArthur Foundation (2013), the circular economy is “an industrial system that is restorative and regenerative by intention and design,” in which technical and biological material flows are managed to minimize waste and transform by-products into new resources. This approach goes beyond end-of-life recycling and entails a comprehensive redesign of production and consumption chains, integrating technological, social, and policy innovations to foster long-term sustainability.

The current ecological and climate crisis has highlighted the unsustainability of the linear model, which relies on intensive raw material extraction and high levels of waste generation. It is estimated that by 2050 the global population will exceed 9 billion people, leading to an exponential increase in demand for food, energy, and materials (United Nations, 2019). Within this context, the circular economy offers an alternative perspective in which waste and residual biomasses are no longer regarded as liabilities to be disposed of, but rather as resources to be valorised.

In the agricultural and agro-industrial sectors, this paradigm is particularly relevant, as intensive production systems generate large amounts of organic residues and by-

products that are often underutilized. Their valorization through innovative biotechnological and physicochemical processes represents a concrete strategy to reduce environmental impacts while simultaneously generating high–value-added products, such as fertilizers, biostimulants, bioenergy, and functional materials (Dahiya et al., 2018). A closely related concept to the circular economy is the bioeconomy, defined as the sustainable use of renewable biological resources for the production of food, energy, and materials. In Europe, the link between these two paradigms has been reinforced through policy frameworks: both the Circular Economy Action Plan and the European Bioeconomy Strategy emphasize the need to reduce dependence on fossil resources while promoting the use of renewable biomasses and by-products (European Commission, 2020).

This integrated approach enables the alignment of environmental, economic, and social objectives, fostering the development of new value chains and stimulating technological innovation. Within this framework, the valorization of algal waste biomass represents a paradigmatic example of circular economy principles in action. Algal biomass is often regarded as a problematic by-product in coastal and lagoon ecosystems affected by dystrophic phenomena, where uncontrolled proliferation can negatively impact local economic activities such as fisheries, tourism, and aquaculture. However, these biomasses, commonly treated as waste, can be transformed into valuable resources through sustainable processes such as hydrothermal carbonization (HTC). Through HTC, algal waste biomass can be converted into two distinct yet complementary products. On the one hand, a solid material known as hydrochar is obtained, characterized by adsorptive properties that make it a promising candidate for use as a biofilter for environmental contaminant removal or as a soil amendment

capable of improving soil quality. On the other hand, the process generates a liquid fraction, referred to as aqueous HTC liquor (AHL), which is rich in nutrient compounds and can be reused as a natural biostimulant to enhance crop growth and increase resistance to abiotic and biotic stressors.

This dual valorization pathway not only mitigates the environmental impact associated with the accumulation of unused algal biomass but also provides innovative and sustainable solutions for agriculture and ecosystem remediation. The circular economy should not be viewed solely as a technological approach, but rather as a systemic vision that requires integration among scientific research, public policies, and business models. The success of circular strategies depends on the ability to develop resilient value chains and to actively engage diverse social and economic stakeholders. In this sense, the valorization of algal biomass represents a key component of a broader transition that encompasses energy sustainability, waste management, and the reduction of anthropogenic pressure on natural ecosystems.

2.4 Environmental burden of algal waste biomass and its ecotoxicological implications

The management of waste algal biomass represents one of the emerging challenges in coastal and lagoon systems, particularly in environments affected by eutrophication and dystrophic conditions. The uncontrolled proliferation of macroalgae is often associated with excessive inputs of anthropogenic nutrients and unfavorable hydrodynamic conditions, which promote the seasonal accumulation of large amounts of biomass along coastlines and in semi-enclosed basins (Nixon, 1995; Anderson et al., 2008; Glibert, 2017). These phenomena lead to negative impacts on water quality, biodiversity, and the overall functioning of aquatic ecosystems, while also impairing key local economic activities such as fisheries, aquaculture, and tourism (Valiela et al., 1997; Viaroli et al., 2008; Xiao et al., 2019).

Traditionally, accumulated algal biomass has been regarded as waste to be removed and disposed of through practices such as landfilling, uncontrolled composting, or temporary storage at dedicated sites. However, these approaches are associated with high management costs and additional environmental concerns, including anaerobic degradation, odour emissions, and the secondary release of nutrients and greenhouse gases (Chopin et al., 2012; Milledge et al., 2019). In light of these limitations, recent years have seen the emergence of an alternative perspective that considers waste algal biomass not as a management burden, but rather as a renewable biological resource to be valorized within a bioeconomy and circular economy framework (Zabaniotou et al., 2020; Thomsen et al., 2021; Cavali et al., 2025).

From a compositional standpoint, macroalgae exhibit distinctive features compared to terrestrial biomasses, including a high-water content, a matrix rich in structural and storage polysaccharides, proteins, mineral compounds, and bioactive molecules, as well as a substantial absence of lignin (Holdt & Kraan, 2011; Kraan, 2013).

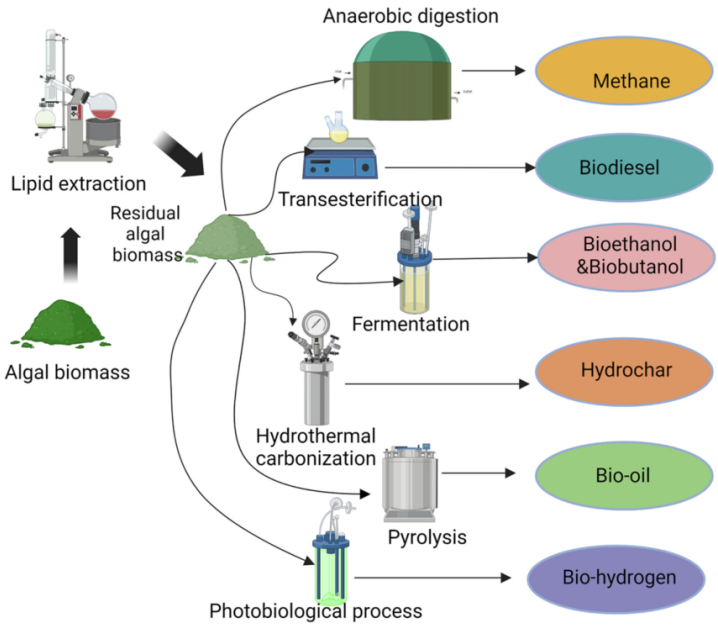


Fig. 24 - Schematic overview of the main biorefinery pathways for algal biomass valorization. Algal biomass can be processed through multiple conversion routes, including lipid extraction followed by transesterification for biodiesel production, anaerobic digestion for methane generation, fermentation for bioethanol and biobutanol, hydrothermal carbonization for hydrochar production, pyrolysis for bio-oil and bio-hydrogen, and photobiological processes. Residual algal biomass can be further exploited within integrated circular bioeconomy frameworks.

This composition makes algal biomass poorly suited for conventional thermochemical processes that require dry feedstocks, while rendering it particularly suitable for technologies capable of treating wet and heterogeneous matrices without energy-intensive pretreatments. Within this context, hydrothermal carbonization (HTC) emerges as a particularly promising technological strategy for the valorization of waste algal biomass. HTC enables the direct treatment of wet biomass in an aqueous

environment, thereby avoiding preliminary drying steps and significantly reducing the overall energy demand of the process (Stemann et al., 2023; Zhao et al., 2014; Funke & Ziegler, 2010; Libra et al., 2011; Patel et al., 2021; Calin et al., 2025). Operating typically under hot compressed water conditions (approximately 180–240 °C, autogenous pressure), algal biomass undergoes a series of hydrolysis, dehydration, and decarboxylation reactions, leading to the formation of a carbon-rich solid product (hydrochar) and a liquid fraction (Aqueous HTC Liquid, AHL) containing soluble organic compounds and nutrients (Shan et al., 2023; Reza et al., 2014; Heidari et al., 2019). Recent studies have demonstrated that HTC of algal biomass not only enhances carbon stability and increases the energy density of the solid product, but also reduces ash content and volatile compounds, thereby improving the functional properties of hydrochar for environmental and agricultural applications (Wang et al., 2022; Patel et al., 2021; Zhang et al., 2022).

In parallel, hydrochar derived from vegetal and algal residues have been shown to be further engineered or functionalized for advanced applications, such as contaminant adsorbents, chemical sensing materials, and functional electrodes, owing to the presence of oxygen-containing functional groups and a favourable porous microstructure (Espro et al., 2021; Wang et al., 2022). In light of this evidence, waste algal biomass assumes a key role as a feedstock for integrated valorization processes. The transformation of a problematic biomass into hydrochar and AHL not only mitigates the environmental impacts associated with algal proliferation but also enables the generation of value-added products suitable for environmental remediation, soil quality improvement, and the support of sustainable agricultural practices (Titirici et al., 2012; Thomsen et al., 2021; Lucian & Fiori, 2023).

2.5 Hydrothermal Carbonization (HTC) as a sustainable strategy for biomass valorization and pollutant mitigation

2.5.1 Hydrothermal Carbonization Process

Biomass comprises biological materials of plant or animal origin and their associated wastes and residues (Chew et al., 2011). In recent years, the valorization of waste biomass has been recognized as a concrete strategy to reduce greenhouse gas emissions and dependence on fossil resources, to the extent that near-zero emission balance scenarios may be envisaged when production and utilization are appropriately matched (Li et al., 2021; Hastings et al., 2009; Hillier et al., 2009; Akhtar, 2011). Within this framework, however, biomass presents several operational constraints that limit its direct use, including high moisture content, low energy density, heterogeneity, and the possible presence of contaminants.

For this reason, traditional approaches to energy and material valorization have relied on biochemical (fermentation, anaerobic digestion), physicochemical (densification), and thermochemical technologies (pyrolysis and hydrothermal processes) (Yu et al., 2012; You et al., 2017; Chew et al., 2011; Menon, 2012; Appels et al., 2008; Zhou et al., 2016; Wang et al., 2018; Zhao et al., 2018; Chandra et al., 2012). Although pyrolysis is a well-established technology, it is disadvantaged when dealing with highly wet biomass, as it requires substantial thermal input for water evaporation and often an energy-intensive pre-drying step (Yu et al., 2012; Zhao et al., 2014). Conversely, biological processes may be advantageous in terms of energy consumption, but they require longer processing times than thermal routes and can be sensitive to complex or inhibitory matrices (Masoumi et al., 2021; Moreno et al., 2014).

Consequently, increasing attention has been directed toward hydrothermal conversion processes, which are often considered more cost-effective than conventional drying, particularly for wet feedstocks (Zhao et al., 2014; Petrović et al., 2024). Within this group, Hydrothermal Carbonization (HTC), first described in the early twentieth century and traced back to the work of Bergius (1913), is now regarded as one of the most suitable options for the valorization of high-moisture biomasses such as sewage sludge, heterogeneous organic wastes, and aquatic residues, including algae and aquaculture by-products (Merzari et al., 2019; Du et al., 2014; Cavali et al., 2023;). Conceptually, HTC reproduces an accelerated form of "artificial coalification," converting raw biomass into a lignite-like solid ("hydrochar"), whose properties are strongly influenced by the reaction medium (D.W. vK, 1950). A key added value is that wet biomass does not require pre-drying, and water, besides being an inexpensive and relatively benign medium, acts directly as both solvent and reactive medium (Parshetti et al., 2014; Knez et al., 2015; Judy et al., 2011; Petrović et al., 2024). HTC typically operates at moderate temperatures (approximately 180–250 °C) under autogenous pressure, promoting dehydration and decarboxylation reactions that reduce the O/C and H/C ratios of the feedstock and increase the energy density of the solid product (Funke, 2010; Petrović et al., 2023).

Process severity is mainly governed by temperature and residence time, which control the extent of conversion and the degree of biomass "coalification" (Witrh et al., 2015; Wiedner et al., 2013; Xu et al., 2013). HTC takes place under subcritical conditions ($T < 374$ °C), where the properties of water change markedly: increasing temperature modifies the dielectric constant and hydrogen-bonding behavior, enhancing the ability of the medium to support ionic reactions and favoring

dissociation into acidic and basic species (H_3O^+ and OH^-) (Savage, 1999; Marcus, 1999; Kalinichev, 1997; Petrović et al., 2023; Fregolente et al., 2019). In practice, subcritical water can sustain acid-catalyzed reactions even in the absence of added acids, facilitating the decomposition and depolymerization of macromolecules and the formation of intermediates that may recombine and condense into the final solid (Savage, 1999; Ruiz et al., 2013).

From a product standpoint, HTC typically generates: (i) a solid fraction (hydrochar), (ii) an aqueous phase containing dissolved organic compounds (often referred to as "process water" or "bio-oil in water"), and (iii) a small gaseous fraction, commonly dominated by CO_2 (Cao et al., 2013; Sun et al., 2014; Petrović et al., 2023; Langone et al., 2020). Owing to its increased hydrophobicity and friability, hydrochar can be readily separated from the suspension and exhibits superior performance compared with raw biomass in terms of mass and energy density, dewaterability, and combustion behavior as a solid fuel (Kambo et al., 2015; Hoekman et al., 2012; Canencio et al., 2025).

At the laboratory scale, HTC is commonly conducted in a batch-type autoclave reactor, consisting of a hermetically sealed cylindrical stainless-steel vessel in which biomass and water are loaded and heated (via a heating jacket or furnace) and maintained at the desired conditions for a given residence time. Such systems typically include temperature and pressure sensors, safety valves, and, when required, stirring to homogenize the suspension.

Heating initiates the reactions in an environment devoid of atmospheric oxygen; internal pressure is generated by the system itself (autogenous pressure) and depends on operating conditions and reactor loading. At the end of the process, the reactor is

cooled and solid/liquid separation (by filtration or centrifugation) is performed to recover hydrochar and the liquid phase. At the industrial scale, the transition toward semi-continuous or continuous configurations aims to improve productivity but introduces engineering challenges related to feeding slurries against high pressure and managing both liquid and solid streams (Okajima et al., 2014; Petrović et al., 2023).

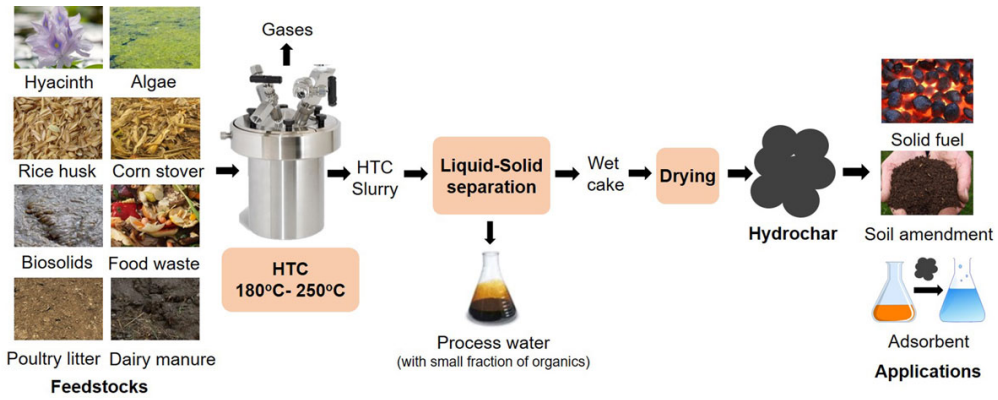


Fig. 25 - Process flow diagram of hydrothermal carbonization (HTC) applied to different organic feedstocks. Biomass sources such as algae, agricultural residues, food waste, and animal manure are subjected to HTC (180–250 °C) to produce a carbon-rich hydrochar. The process includes slurry formation, liquid–solid separation, and drying steps. The resulting hydrochar can be used as solid fuel, soil amendment, or adsorbent material, while the liquid phase contains process water rich in soluble organic compounds.

2.5.2 HTC-Derived materials in environmental remediation

The reason HTC is considered particularly attractive from a circular economy perspective is not limited to "waste-to-product" conversion but also lies in the possibility of obtaining functional materials with environmental applications. Hydrochar is a high-value carbonaceous material, enriched in carbon (with reduced relative H and O contents) and, in many cases, exhibiting properties that make it suitable not only as a fuel or soil amendment, but also as a sorbent for contaminant removal (Zhao et al., 2018; Funke, 2010; Saidur et al., 2011; Gautam et al., 2024; González et al., 2025).

Depending on feedstock type and process conditions, hydrochar may display favourable characteristics for adsorbing ions and molecules from aqueous effluents, making it a promising candidate for wastewater remediation and pollution mitigation (Saidur et al., 2011; Gautam et al., 2024; González et al., 2025).

This is also relevant from a climate perspective: converting biomass into a relatively stable carbonaceous solid can, under many conditions, represent a sustainable pathway to mitigate anthropogenic CO_2 by "immobilizing" part of the biogenic carbon in a more recalcitrant form (Titirici et al., 2012).

From a carbon cycle standpoint, carbon fixed by plants (or algae) through photosynthesis can be incorporated into the hydrochar structure; simultaneously, the products (hydrochar and valorised liquid fractions) may reduce dependence on fossil fuels, contributing to additional emission offsets (Titirici et al., 2012; Zhu et al., 2022).

An additional advantage, often decisive for overall sustainability, is the wide range of treatable feedstocks: beyond lignocellulosic materials, HTC has been applied to sewage sludge, municipal solid waste, food residues, and algal/aquaculture by-

products, matrices that require appropriate treatment to avoid environmental impacts and that are simultaneously available in large quantities (Parshetti et al., 2013; Alatalo et al., 2013; Du et al., 2012; Cao et al., 2013).

In the case of waste algal biomass, this aspect is strategic: such biomass is often extremely wet, voluminous, and seasonal, posing management challenges but also representing a resource for producing hydrochar aimed at carbon sequestration, soil improvement, and wastewater remediation (Saidur et al., 2011; Gautam et al., 2024).

This combination of feedstock flexibility and the absence of pre-drying requirements is one of the reasons behind the rapid increase in the literature on hydrochar production and applications since 2009, including reviews focused on climatic and technical aspects (Judy et al., 2011; Reza et al., 2014), properties as a clean solid fuel derived from waste biomass (Kambo et al., 2015), large-scale applications (Okajima et al., 2014), and formation mechanisms characterized by a high abundance of oxygenated functional groups (Jain et al., 2016).

Alongside the solid fraction, the liquid phase requires dedicated management and valorization: when intended for bio-oil production, it may require fractionation or extraction; however, several studies indicate that liquids from hydrothermal treatment can be biodegradable due to their high organic content, opening opportunities for biological treatment or process integration (Chandra et al., 2012; Tommaso et al., 2015).

From a “circular” perspective, therefore, HTC should not be viewed solely as a route for hydrochar production, but as a platform that enables: (i) the transformation of problematic biomass (such as waste algae) into high-value carbonaceous materials; (ii) the reduction of costs and energy associated with drying; (iii) the direct enabling

of environmental protection applications (adsorption, soil amelioration, carbon sequestration) (Titirici et al., 2012; González al., 2009); and (iv) the integrated management of the liquid phase, maximizing value recovery while minimizing environmental impact (Passos et al., 2015).

References

Akhtar J, Amin NAS. A review on process conditions for optimum bio-oil yield in hydrothermal liquefaction of biomass. Renew Sustain Energy Rev 2011;15:1615–24.

Alatalo S-M, Repo E, Mäkilä E, Salonen J, Vakkilainen E, Sillanpää M. Adsorption behavior of hydrothermally treated municipal sludge & pulp and paper industry sludge. Bioresour Technol 2013;147:71–6.

Appels L, Baeyens J, Degrève J, Dewil R. Principles and potential of the anaerobic digestion of waste-activated sludge. Prog. Energy Combust Sci 2008;34:755–81.

Cao X, Ro KS, Libra JA, Kammann CI, Lima I, Berge N, et al. Effects of biomass types and carbonization conditions on the chemical characteristics of hydrochars. J Agric Food Chem 2013;61:9401–11.

Cavali, M., Hennig, T. B., Libardi Junior, N., Kim, B., Garnier, V., Benbelkacem, H., ... & de Castilhos Junior, A. B. (2025). Co-hydrothermal carbonization of sawdust and sewage sludge: Assessing the potential of the hydrochar as an adsorbent and the ecotoxicity of the process water. *Applied Sciences*, *15*(3), 1052.

Cavali, M.; Libardi Junior, N.; de Sena, J.D.; Woiciechowski, A.L.; Soccol, C.R.; Belli Filho, P.; Bayard, R.; Benbelkacem, H.; de Castilhos Junior, A.B. A Review on Hydrothermal Carbonization of Potential Biomass Wastes,

Characterization and Environmental Applications of Hydrochar, and Biorefinery Perspectives of the Process. Sci. Total Environ. 2023, 857, 159627.

Chandra R, Takeuchi H, Hasegawa T. Methane production from lignocellulosic agricultural crop wastes: a review in context to second generation of biofuel production. Renew Sustain Energy Rev 2012;16:1462–76.

Chandra R, Takeuchi H, Hasegawa T. Methane production from lignocellulosic agricultural crop wastes: a review in context to second generation of biofuel production. Renew Sustain Energy Rev 2012;16:1462–76.

Chew JJ, Doshi V. Recent advances in biomass pretreatment – Torrefaction fundamentals and technology. Renew Sustain Energy Rev 2011;15:4212–22.

Colin, J., Sarrion, A., Diaz, E., de la Rubia, M. A., & Mohedano, A. F. (2025). Ecotoxicity assessment of hydrochar from hydrothermal carbonization of biomass waste. Sustainable Chemistry and Pharmacy, 44, 101909.

D.W vK. Graphical-statistical method for the study of structure and reaction processes of coal. Fuel 1950;29:25.

Du Z, Hu B, Shi A, Ma X, Cheng Y, Chen P, et al. Cultivation of a microalga Chlorella vulgaris using recycled aqueous phase nutrients from hydrothermal carbonization process. Bioresour Technol 2012;126:354–7.

Espro, C., Satira, A., Mauriello, F., Anajafi, Z., Moulaee, K., Iannazzo, D., & Neri, G. (2021). Orange peels-derived hydrochar for chemical sensing applications. *Sensors and Actuators B: Chemical*, *341*, 130016.

Fregolente, L.G.; Miguel, T.B.A.R.; de Castro Miguel, E.; de Almeida Melo, C.; Moreira, A.B.; Ferreira, O.P.; Bisinoti, M.C. Toxicity Evaluation of Process Water from Hydrothermal Carbonization of Sugarcane Industry By-Products. Environ. Sci. Pollut. Res. 2019, 26, 27579–27589.

Funke A, Ziegler F. Hydrothermal carbonization of biomass: a summary and discussion of chemical mechanisms for process engineering. Biofuels Bioprod Bioref 2010;4:160–77.

Funke A, Ziegler F. Hydrothermal carbonization of biomass: a summary and discussion of chemical mechanisms for process engineering. Biofuels Bioprod Bioref 2010;4:160–77.

González JF, Román S, Encinar JM, Martínez G. Pyrolysis of various biomass residues and char utilization for the production of activated carbons. J Anal Appl Pyrolysis 2009;85:134–41.

Hastings A, Clifton-Brown J, Wattenbach M, Mitchell CP, Stampfl P, Smith P. Future energy potential of Miscanthusin Europe. GCB Bioenergy 2009;1:180–96.

Hillier J, Whittaker C, Dailey G, Aylott M, Casella E, Richter GM, et al. Greenhouse gas emissions from four bioenergy crops in England and Wales:

integrating spatial estimates of yield and soil carbon balance in life cycle analyses. GCB Bioenergy 2009;1:267–81.

Hoekman SK, Broch A, Robbins C, Zielinska B, Felix L. Hydrothermal carbonization (HTC) of selected woody and herbaceous biomass feedstocks. BiomassConvers Biorefinery 2012;3:113–26.

Jain A, Balasubramanian R, Srinivasan MP. Hydrothermal conversion of biomass waste to activated carbon with high porosity: a review. Chem Eng J 2016;283:789–805.

Judy A, Libra KSR, Claudia Kammann, Axel Funke, Berge Nicole D, Neubauer York, Maria-Magdalena Titirici CF, Bens Oliver, Kern Jürgen, Emmerich KarlHeinz. Hydrothermal carbonization of biomass residuals: a comparative review of the chemistry, processes and applications of wet and dry pyrolysis. Biofuels 2011;2(1):89–124.

Kambo HS, Dutta A. A comparative review of biochar and hydrochar in terms of production, physico-chemical properties and applications. Renew Sustain Energy Rev 2015;45:359–78

Kambo, H.S.; Dutta, A. A Comparative Review of Biochar and Hydrochar in Terms of Production, Physico-Chemical Properties and Applications. Renew. Sustain. Energy Rev. 2015, 45, 359–378.

Knez Ž, Markočič E, Hrnčič MK, Ravber M, Škerget M. High pressure water reforming of biomass for energy and chemicals: a short review. J Supercrit Fluids 2015;96:46–52.

Langone, M.; Basso, D. Process Waters from Hydrothermal Carbonization of Sludge: Characteristics and Possible Valorization Pathways. Int. J. Environ. Res. Public. Health 2020, 17, 6618.

Li, H.Z.; Zhang, Y.N.; Guo, J.Z.; Lv, J.Q.; Huan, W.W.; Li, B. Preparation of Hydrochar with High Adsorption Performance for Methylene Blue by Co-Hydrothermal Carbonization of Polyvinyl Chloride and Bamboo. Bioresour. Technol. 2021, 337, 125442.

Masoumi, S.; Borugadda, V.B.; Nanda, S.; Dalai, A.K. Hydrochar: A Review on Its Production Technologies and Applications. Catalysts 2021, 11, 939.

Menon V, Rao M. Trends in bioconversion of lignocellulose: biofuels, platform chemicals & biorefinery concept. Prog Energy Combust Sci 2012;38:522–50.

Merzari, F.; Langone, M.; Andreottola, G.; Fiori, L. Methane Production from Process Water of Sewage Sludge Hydrothermal Carbonization. A Review. Valorising Sludge through Hydrothermal Carbonization. Crit. Rev. Environ. Sci. Technol. 2019, 49, 947–988.

Moreno AD, Ibarra D, Alvira P, Tomás-Pejó E, Ballesteros M. A review of biological delignification and detoxification methods for lignocellulosic bioethanol production. Crit Rev Biotechnol 2014;35:342–54

Okajima I, Sako T. Energy conversion of biomass with supercritical and subcritical water using large-scale plants. J Biosci Bioeng 2014;117:1–9.

Parshetti GK, Chowdhury S, Balasubramanian R. Hydrothermal conversion of urban food waste to chars for removal of textile dyes from contaminated waters. Bioresour Technol 2014;161:310–9.

Parshetti GK, Liu Z, Jain A, Srinivasan MP, Balasubramanian R. Hydrothermal carbonization of sewage sludge for energy production with coal. Fuel 2013;111:201–10.

Parshetti, G.K.; Chowdhury, S.; Balasubramanian, R. Hydrothermal Conversion of Urban Food Waste to Chars for Removal of Textile Dyes from Contaminated Waters. Bioresour. Technol. 2014, 161, 310–319.

Passos F, Ferrer I. Influence of hydrothermal pretreatment on microalgal biomass anaerobic digestion and bioenergy production. Water Res 2015;68:364–73.

Patel, N., Acharya, B., & Basu, P. (2021). Hydrothermal carbonization (HTC) of seaweed (macroalgae) for producing hydrochar. Energies, 14(7), 1805.

Petrovic, A.; Cencic Predikaka, T.; Škodic, L.; Vohl, S.; Cucek, L. Hydrothermal Co-Carbonization of Sewage Sludge and Whey:Enhancement of Product Properties and Potential Application in Agriculture. Fuel 2023, 350, 128807.

Reza MT, Andert J, Wirth B, Busch D, Pielert J, Lynam JG, et al. Hydrothermal carbonization of biomass for energy and crop production. Appl Bioenergy 2014;1.

Saidur R, Abdelaziz EA, Demirbas A, Hossain MS, Mekhilef S. A review on biomass as a fuel for boilers. Renew Sustain Energy Rev 2011;15:2262–89.

Saidur R, Abdelaziz EA, Demirbas A, Hossain MS, Mekhilef S. A review on biomass as a fuel for boilers. Renew Sustain Energy Rev 2011;15:2262–89.

Savage PE. Organic chemical reactions in supercritical water. Chem Rev 1999;99:603–22.

Shan, G.; Li, W.; Bao, S.; Li, Y.; Tan, W. Co-Hydrothermal Carbonization of Agricultural Waste and Sewage Sludge for Product Quality Improvement: Fuel Properties of Hydrochar and Fertilizer Quality of Aqueous Phase. J. Environ. Manage 2023, 326, 116781.

Sun Y, Gao B, Yao Y, Fang J, Zhang M, Zhou Y, et al. Effects of feedstock type, production method, and pyrolysis temperature on biochar and hydrochar properties. Chem Eng J 2014;240:574–8

Titirici M-M, White RJ, Falco C, Sevilla M. Black perspectives for a green future: hydrothermal carbons for environment protection and energy storage. Energy Environ Sci 2012;5:6796.

Tommaso G, Chen W-T, Li P, Schideman L, Zhang Y. Chemical characterization and anaerobic biodegradability of hydrothermal liquefaction aqueous products from mixed-culture wastewater algae. Bioresour Technol 2015;178:139–46.

Wang T, Zhai Y, Zhu Y, Peng C, Xu B, Wang T, et al. Influence of temperature on nitrogen fate during hydrothermal carbonization of food waste. Bioresour Technol 2018;247:182–9.

Wang, Q.; Wu, S.; Cui, D.; Zhou, H.; Wu, D.; Pan, S.; Xu, F.; Wang, Z. Co-Hydrothermal Carbonization of Organic Solid Wastes to Hydrochar as Potential Fuel: A Review. Sci. Total Environ. 2022, 850, 158034.

Wang, T., Zhai, Y., Zhu, Y., Li, C., & Zeng, G. (2018). A review of the hydrothermal carbonization of biomass waste for hydrochar formation: Process conditions, fundamentals, and physicochemical properties. Renewable and Sustainable Energy Reviews, 90, 223-247.

Wiedner K, Naisse C, Rumpel C, Pozzi A, Wieczorek P, Glaser B. Chemical modification of biomass residues during hydrothermal carbonization – What makes the difference, temperature or feedstock? Org Geochem 2013;54:91–100.

Wirth, B.; Reza, T.; Mumme, J. Influence of Digestion Temperature and Organic Loading Rate on the Continuous Anaerobic Treatment of Process Liquor from Hydrothermal Carbonization of Sewage Sludge. Bioresour. Technol. 2015, 198, 215–222.

Xu Q, Qian Q, Quek A, Ai N, Zeng G, Wang J. Hydrothermal carbonization of macroalgae and the effects of experimental parameters on the properties of hydrochars. ACS Sustain Chem Eng 2013;1:1092–101.

You, S.; Sik, Y.; Chen, S.S.; Tsang, D.C.W.; Kwon, E.E.; Lee, J.; Wang, C. A Critical Review on Sustainable Biochar System through Gasification: Energy and Environmental Applications. Bioresour. Technol. 2017, 246, 242–253.

Yu, C.; Chen, R.; Li, J.J.; Li, J.J.; Drahansky, M.; Paridah, M.; Moradbak, A.; Mohamed, A.Z.; Owolabi, F.H.; Abdulwahab, T.; Pyrolysis: A Sustainable Way to Generate Energy from Waste; Intech: Vienna, Austria, 2012; p. 13.

Zhao P, Shen Y, Ge S, Chen Z, Yoshikawa K. Clean solid biofuel production from high moisture content waste biomass employing hydrothermal treatment. Appl Energy 2014;131:345–67.

Zhao P, Shen Y, Ge S, Yoshikawa K. Energy recycling from sewage sludge by producing solid biofuel with hydrothermal carbonization. Energy Convers Manag 2014;78:815–21.

Zhao, K.; Li, Y.; Zhou, Y.; Guo, W.; Jiang, H.; Xu, Q. Characterization of Hydrothermal Carbonization Products (Hydrochars and Spent Liquor) and Their Biomethane Production Performance. Bioresour. Technol. 2018, 267, 9–16.

Zhou Y, Zhang Z, Zhang Y, Wang Y, Yu Y, Ji F, et al. A comprehensive review on densified solid biofuel industry in China. Renew Sustain Energy Rev 2016;54:1412–28.

Zhu, J.Y.; Pan, X. Efficient Sugar Production from Plant Biomass: Current Status, Challenges, and Future Directions. Renew. Sustain. Energy Rev. 2022, 164, 112583.

CHAPTER 3

Aims of the thesis

Aims of the thesis

The present research aims to address two interconnected environmental challenges within a unified and circular framework: (i) the ecotoxicological impact of the fungicide thiram, a widely used dithiocarbamate, and (ii) the sustainable valorization of waste algal biomass through hydrothermal carbonization (HTC) for environmental mitigation purposes.

The first objective of this study is to investigate the toxicological and ecotoxicological effects of thiram, with particular emphasis on its impact on non-target organisms and aquatic systems, using *Arbacia lixula* and zebrafish (*Danio rerio*) as model species. Given the extensive agricultural use of thiram, its environmental persistence, and the documented risks associated with chronic exposure, this work seeks to contribute to a deeper understanding of its biological effects, supporting the need for mitigation strategies capable of reducing its environmental footprint.

The second objective is to evaluate hydrothermal carbonization as a green and efficient technology for converting wet waste algal biomass into value-added products, avoiding energy-intensive pre-drying and enabling the recovery of both solid and liquid fractions. In this context, the study focuses on the production of algal-derived hydrochar and HTC process water, assessing their functional properties relevant to environmental applications.

A central aim of the research is to explore the potential of algal-derived hydrochar as a remediation material, specifically its suitability for the adsorption and mitigation of environmental contaminants, including pesticide-derived pollutants. In parallel, an additional objective of the thesis is to evaluate the potential of the HTC-derived aqueous liquid (AHL) as a sustainable fertilizer and biostimulant, investigating

its effects on plant growth, development, and stress tolerance. By coupling thiram toxicity assessment with the development of bio-based remediation materials, this study proposes an integrated "pollution–mitigation" approach, in which waste biomass is transformed into functional materials capable of contributing to environmental detoxification.

Overall, this work seeks to demonstrate that the integration of ecotoxicological evaluation and biomass valorization can provide innovative and sustainable solutions to environmental pollution. By linking the assessment of thiram-induced toxicity with HTC-based conversion of algal waste into remediation-oriented products, the study supports the development of circular, low-impact strategies aligned with current sustainability goals, environmental protection policies, and the transition toward a bio-based circular economy.

CHAPTER 4

The fungicide thiram alters the embryo-larval development of the black sea urchin *Arbacia lixula* by inducing multifactorial toxicological responses

4.1. Introduction

Thiram, a broad-spectrum dithiocarbamate fungicide, is widely used in agriculture to control fungal pathogens in crops such as fruits, vegetables, and ornamental plants (Lazo and Miller, 2014). Despite its agricultural benefits, the persistence of thiram in aquatic environments through runoff, leaching, or direct application poses significant risks to non-target aquatic organisms.

In recognition of these concerns, thiram has recently been re-evaluated by the European Food Safety Authority (EFSA, 2022) and the European Chemicals Agency (ECHA, 2023) due to its persistence, bioaccumulation potential, and suspected endocrine-disrupting effects. While regulatory frameworks often prioritize acute toxicity in target pests, growing evidence highlights that sublethal concentrations of thiram can disrupt critical physiological and developmental processes in aquatic species, particularly during embryonic stages (Chen et al., 2019; Vasamsetti et al., 2022). This underscores the urgent need to assess its ecotoxicological impacts on sensitive non-target organisms, such as sea urchins, which serve as keystone species in marine ecosystems and valuable models for developmental toxicity studies.

The embryonic stages of aquatic organisms are exceptionally vulnerable to chemical stress due to their rapid cell division, tissue differentiation, and limited detoxification capacity. In zebrafish *Danio rerio*, for example, exposure to thiram at low concentrations up to 0.1 μM induces delayed hatching, notochord curvature, and deformities such as yolk sac edema and spinal malformations, with dose-dependent responses observed even at environmentally relevant levels (Vasamsetti et al., 2022). Furthermore, thiram disrupts thyroid hormone synthesis by

modulating key enzymes such as deiodinase 3 and thyroid peroxidase (TPO), mechanisms that may impair metamorphosis and growth in aquatic taxa (Chen et al., 2019). Similar effects are likely to occur in marine invertebrates, such as sea urchins, whose embryonic development relies on conserved signalling pathways shared with vertebrates.

In this regard, an emerging aspect of research focuses on the role of phylogenetically conserved thyroid-related genes in sea urchins. These genes, essential for metamorphosis, may be sensitive to chemical pollutants like thiram, suggesting potential disruption of key molecular processes during embryonic development (Tian et al., 2016). Alteration of these pathways could have significant implications for the survival and life cycle of these organisms, as well as for the structure of marine communities (Lee et al., 2019). In other aquatic organisms, thiram toxicity extends to the induction of oxidative stress, depletion of glutathione (GSH), and lipid peroxidation, as previously documented in the water flea *Daphnia magna* (Belaid and Sbartai, 2021). These biochemical disruptions compromise cellular integrity, reproductive success, and survival, with cascading effects on population dynamics. Whole-transcriptome analyses in zebrafish reveal that thiram alters gene expression networks governing metabolism, reproduction, and stress responses, suggesting broad-spectrum molecular toxicity (Vasamsetti et al., 2023). However, data on marine invertebrates, particularly echinoderms like sea urchins, remain scarce despite their ecological relevance and sensitivity to environmental pollutants.

This study investigates the toxicity of thiram in embryo development of the black sea urchin *Arbacia lixula*, a model organism for ecotoxicological research

due to its sensitivity to pollutants, and suitable for embryotoxicity tests because of the large number of eggs available and their transparent envelope, which allow direct observation of developmental alterations (Eliso et al., 2025; Giannetto et al., 2018; Maisano et al. 2015; Martínez-Pita et al., 2017). By examining endpoints such as morphological abnormalities, oxidative stress biomarkers, molecular and metabolic alterations, we aim to quantify the impact of thiram on the early life stages of non-target aquatic organisms and elucidate the mechanisms underlying its toxicity.

4.2. Material and methods

4.2.1 Gamete collection and experimental design

To ensure an accurate assessment of the impact of this fungicide, a rigorous methodology was adopted involving the controlled administering thiram at multiple concentrations to developing sea urchin embryos. Specifically, a stock solution of thiram (Sigma Aldrich) was prepared by dissolving the powder in dimethyl sulfoxide (DMSO) and subsequently diluting it in filtered seawater (FSW) to achieve the desired concentrations. Adult organisms of *A. lixula* were collected along the Messina (Sicily, Italy) coastal shoreline and maintained in aerated aquaria filled with FSW. The animals were acclimated under controlled conditions (20 ± 1 °C and salinity 36 ppt). Spawning was induced by administering 0.5 M KCl at the level of the peristomial membrane, following the procedure described by Eliso et al. (2025). Gamete quality was assessed prior to fertilization: oocytes were selected based on the presence of an intact spherical morphology and a clearly visible nucleus, while sperm samples were considered suitable only if active motility was observed under light microscopy. To achieve a fertilization rate > 85%, eggs were collected following the method of Epel et al. (2004), with appropriate modifications. At fertilization, sperm was activated by performing a 1:1000 dilution in FSW and subsequently mixed with the eggs suspension at a standardized concentration of 100:1. The elevation of the fertilization envelope was visually monitored under an optical microscope. Fertilized eggs (500 per well) were dispensed into 24-well plates containing 2 mL of FSW, including a negative control condition consisting of eggs incubated in FSW with 0.01% DMSO. Fertilized eggs were then exposed to four different thiram concentrations: 0.24 µg/L, 1.2 µg/L, 6

µg/L, and 30 µg/L, to evaluate dose-dependent effects on morphology and key biochemical processes involved in embryonic development. Based on preliminary morphological observations, significant alterations were evident only at the two highest concentrations (6 and 30 µg/L). Therefore, these concentrations were selected for subsequent metabolomic and enzymatic analyses, aiming to better characterize the underlying mechanisms of toxicity of thiram. All treatments were conducted in quadruplicate, with two biological replicates. Embryonic development was monitored in an incubator at a controlled temperature of 20–22 °C until reaching the ampol-like stage at 72 hours post-fertilization (hpf).

4.2.2 Toxicological Dose-Response Modelling

To estimate toxicological thresholds, concentration–response curves were constructed using Generalized Linear Models (GLMs) with a binomial distribution and a logit link function (Ritz et al., 2015). LC_{50} (median lethal concentration) was calculated based on the proportion of dead embryos, whereas EC_{50} (median effective concentration for sublethal effects) was estimated considering both delayed developments alone and the combined proportion of delayed + dead embryos as response variables. Analyses were performed using GraphPad Prism (v10.0) and R (v4.3.2). For each tested concentration (0, 0.24, 1.2, 6, and 30 µg/L thiram), embryo counts from three replicates were aggregated to derive proportion data. Confidence intervals (95%) for LC_{50} and EC_{50} were obtained using profile-likelihood estimation. The Teratogenic Index (TI) was calculated as the ratio between LC_{50} and EC_{50}, providing an estimate of the relative potency of thiram to induce malformations versus lethality. To estimate toxicological thresholds,

concentration–response curves were constructed using Generalized Linear Models (GLMs) with a binomial distribution and a logit link function (Ritz et al., 2015). LC_{50} (median lethal concentration) was calculated based on the proportion of dead embryos, whereas EC_{50} (median effective concentration for sublethal effects) was estimated considering both delayed developments alone and the combined proportion of delayed + dead embryos as response variables. Analyses were performed using GraphPad Prism (v10.0) and R (v4.3.2). For each tested concentration (0, 0.24, 1.2, 6, and 30 µg/L thiram), embryo counts from three replicates were aggregated to derive proportion data. Confidence intervals (95%) for LC_{50} and EC_{50} were obtained using profile-likelihood estimation. The Teratogenic Index (TI) was calculated as the ratio between LC_{50} and EC_{50}, providing an estimate of the relative potency of thiram to induce malformations versus lethality.

4.2.3 Morphological observations

At 48 and 72 hpf, *A. lixula* embryos at the pluteus and ampol-like stages in free-swimming phase were obtained from control and thiram-exposed groups to assess developmental morphology. The progression of early developmental stages was arrested using cold 100% methanol (MeOH), followed by a wash in FSW after 10 minutes (Giudice 1973; Maisano et al., 2015). Samples were analysed under an inverted light microscope equipped with a Nikon high-definition digital imaging system to compare morphological characteristics across experimental conditions.

4.2.4 Biochemical analysis

In parallel, to better understand the biochemical effects of thiram, plutei and ampol-like larvae at 48 and 72 hpf, respectively, were disrupted in ice-cold Tris-HCl buffer (pH 7.6) through ultrasonic homogenization using a Micoson Ultrasonic Cell Disruptor XL. The sonication process was carried out for 2 minutes with intermittent pulses, keeping samples on ice prevent thermal defradation of enzymatic activity. Homogenates were then clarified by centrifugation at 9000 x g for 20 minutes at 4 °C, and the resulting supernatant were collected for enxymatic assay. Enzymatic activities were evaluated spectrophotometrically using established colorimetric protocols.

4.2.4.1 Neurotoxicity

Acetylcholinesterase (AChE) activity was quantified spectrophotometrically at 412 nm for 5 minutes, in accordance with the classic method described by Ellman et al. (1961), and normalized to total protein concentration, which was determined using the Pierce BCA Protein Assay Kit (Thermo Scientific).

4.2.4.2 Antioxidant activity

The activity of Glutathione *S*-transferase (GST) was determined by measuring the conjugation rate of reduced glutathione to CDNB (1-chloro-2,4-dinitrobenzene), following absorbance changes at 340 nm for 5 minutes (Habig et al., 1974), while catalase (CAT) activity was estimated by evaluating the decomposition rate of hydrogen peroxide at 240 nm over a 90 seconds interval, based on the method developed by Aebi(1974). Activity values were normalized to

total protein content and expressed as nmol or μmol of product for minute for mg of protein, with each measurement repeated three times.

4.2.5 Metabolomic observations

4.2.5.1 Metabolite extraction from sea urchin embryos

Metabolomic analyses were carried out at 48- and 72-hours post-fertilization using pools of embryos from three wells for experimental group, including both controls and thiram-exposed samples. To isolate polar metabolites, a biphasic solvent extraction method based on methanol, chloroform, and water was used, following an optimized version of the protocol described by Wu et al. (2008) and Cappello et al. (2017). Embryos were initially lysed in cold methanol (8 mL/g) and distilled water (2.5 mL/g) using an immersion sonicator set at 50% amplitude, applying three one-minute cycles. The homogenized mixtures were then transferred into chemically resistant polypropylene centrifuge tubes, where chloroform (8 mL/g) and additional water (4 mL/g) were added to facilitate phase separation. After vigorous mixing and stabilization on ice for 8 minutes, samples were centrifuged at 2000 × g for 5 minutes at 4 °C to separate the organic and aqueous layers. The methanol-rich upper phase, containing the targeted polar compounds, was carefully aspirated (300 μL), dried using a vacuum concentrator (Eppendorf 5301), and stored at −80 °C until NMR analysis.

4.2.5.2 Metabolomics based on ^{1}H NMR

For spectral acquisition, each dried extracts were reconstituted in 500 μL of deuterium oxide (D_2O) (Armar AG, Döttingen, Switzerland) containing 0.1 M sodium phosphate buffer (pH 7.0) and supplemented with 1 mM DSS (2,2-

dimethyl-2-silapentane-5-sulfonate) (Sigma-Aldrich Co) as a chemical shift reference standard. Samples were transferred into 5 mm NMR tubes and analyzed using a Varian-500 spectrometer (operating at 499.74 MHz) Spectral acquisition was performed at 25°C using a 1D NOESY pulse sequence with water suppression. collecting 256 transients across a spectralwidth of 11.6808 ppm and 32,768 data points. Spectra were processed (phasing, baseline correction, and calibration) with Chenomx NMR Suite (v11.1, Chenomx Inc., Edmonton, Canada). Metabolite identification and quantification were achieved through comparison with validated libraries and databases (Cappello et al., 2017).

4.2.5.3 Metabolic Pathway and Enrichment Analysis

To support the biological interpretation of the metabolomic profile alterations observed in thiram-exposed *Arbacia lixula* embryos, a functional metabolic analysis was performed using MetaboAnalyst 6.0 (https://www.metaboanalyst.ca) (Chong et al., 2019). The list of significantly altered polar metabolites ($p < 0.05$) identified through ^{1}H-NMR spectroscopy at 48- and 72-hours post-fertilization (hpf), was submitted to the Pathway Analysis module for both enrichment and topology-based interpretation. To increase biological relevance and pathway specificity, two organism-specific libraries were used in parallel. For the enrichment analysis, the KEGG pathway library for *Homo sapiens* was selected, as it provided the most comprehensive annotation set for metabolite identifiers used in the experimental dataset. For the topological analysis, the KEGG reference library of *Strongylocentrotus purpuratus* was selected as the phylogenetically closest echinoderm model to *A. lixula*, allowing for a more accurate representation

of sea urchin-specific metabolic networks. Over-representation analysis (ORA) was based on hypergeometric testing, while pathway topology analysis considered node centrality (degree and betweenness) as measures of impact. Pathways were ranked according to combined evidence from statistical significance and network position of altered metabolites. Data were visualized using MetaboAnalyst's native plotting tools, with statistical significance expressed as $-\log_{10}(p)$ and impact as pathway perturbation scores.

4.2.6 Gene Expression Analysis (RT-qPCR)

To investigate the molecular response to thiram exposure, gene expression levels of five target genes (MSP130, SM30, DIO1, SOD Cu/Zn and CAT) were assessed in *Arbacia lixula* embryos collected at 72 hpf from control and thiram-treated groups (6 µg/L and 30 µg/L). RNA extraction was performed using Direct-zol RNA Microprep Kit (Zymo Research) according to the manufacturer's instructions. RNA concentration and purity were determined using a NanoDrop ultra spectrophotometer (Thermo Scientific), and RNA integrity was verified by agarose gel electrophoresis. Complementary DNA (cDNA) was synthesized from 1 µg of total RNA using the RevertAid RT Kit (Thermo Scientific) with random hexamer primers. Quantitative real-time PCR (qPCR) was performed on a QIAquant 72 2plex Real-Time PCR System (QIAGEN), using DyNAmo HS SYBR Green qPCR Master Mix (Thermo Scientific) in 72-well BioPlates sealed with Optical BioFilm Covers (Biogenerica). Specific primers for each target gene were designed based on conserved sequences from echinoid databases or adapted from previously published studies. Each sample was analyzed in technical triplicates and

included at least three biological replicates per condition. Gene expression levels were normalized using β-actin as the housekeeping gene. The relative expression of each gene was calculated using the ΔΔCt method (Livak and Schmittgen, 2001). Statistical analysis was performed using one-way ANOVA followed by Dunnett's post hoc test, with $p < 0.05$ considered statistically significant.

Table 1. Sequences of primers for the genes used.

GENE- ID	Forward primer	Reverse primer
CAT	CCACACGCAGAAGAGGAAC	CGGTCAGAGAACAGGAAGG
SOD Cu/Zn	GCAGGAGCCATCTACACCAT	ATTGTTGGTGTGGGATCCAT
DIO 1	AAGTGGTGGATCTGCCAATTGTA	ACACCTCTGGGCAATCATGG
SM30	GACAGTGGGGCTTTCTTGAG	AACACATCGGTTTCCCTACG
MSP130	ATGGACAGGAAGTCAGGTGG	GGTGTGCTGTTTCCAGGGGC
Act	TCAGAGCAAGAGGGGTATCC	TGTAGAAGGTGTGATGCCAGA

4.2.7 Statistical analysis

Statistical analyses for morphological, enzymatic, metabolomic, and molecular endpoints were performed using GraphPad Prism (Version 10, GraphPad Software, La Jolla, CA, USA). Data are reported as mean ± standard deviation (SD). Data from the embryotoxicity assay were analysed using the non-parametric Kruskal-Wallis test followed by Dunn's post hoc test. Group comparisons were conducted using one-way ANOVA followed by Dunnett's post hoc test (*$p < 0.05$; **$p < 0.001$). LC_{50} and EC_{50} values were estimated in R (version 4.4.1) using generalized linear models (GLMs) with a binomial distribution and logit link. The Teratogenic Index (TI) was calculated as the LC_{50}/EC_{50} ratio. Metabolomic data were log-transformed and z-score normalized prior to statistical analysis. Significant

metabolites were selected based on ANOVA with Dunnett's test and visualized via heatmaps (z-score per row). Pathway and enrichment analyses were performed using MetaboAnalyst 6.0. Hypergeometric testing was applied for enrichment analysis using the human KEGG library, while pathway topology was assessed using relative-betweenness centrality based on the *Strongylocentrotus purpuratus* KEGG database. Multiple testing correction was applied using the false discovery rate (FDR) method.

4.3.Results

4.3.1 Mortality and Developmental Effects

The GLM analysis revealed that thiram exposure caused a dose-dependent increase in both mortality and sublethal developmental alterations in *A. lixula* embryos at 72 hpf (Figure 1). The estimated LC_{50}, based on the proportion of dead embryos, was 26.42 µg/L. In contrast, the EC_{50}, calculated from the combined proportion of delayed and dead embryos, was substantially lower at 2.76 µg/L, indicating a higher sensitivity of embryos to sublethal effects. These findings highlight that developmental toxicity occurs at thiram concentrations well below those required to induce lethality. Consequently, the TI was calculated as:

$$TI = LC_{50} / EC_{50} = 26.42/2.76 \approx 9.57$$

This value exceeds the threshold of 1, suggesting a clear teratogenic potential of thiram in the species under examination. The use of GLM models provided a statistically robust framework for assessing these toxicological endpoints, reinforcing the relevance of early developmental disruption as a sensitive marker of environmental risk. Additionally, statistical analysis using one-way ANOVA followed by Dunnett's test indicated that the lowest tested thiram concentration (0.24 µg/L) induced early signs of developmental alterations compared to the control group ($p < 0.05$). Thus, the Lowest Observed Effect Concentration (LOEC) for thiram was identified as 0.24 µg/L, while a No Observed Effect Concentration (NOEC) could not be established within the range tested.

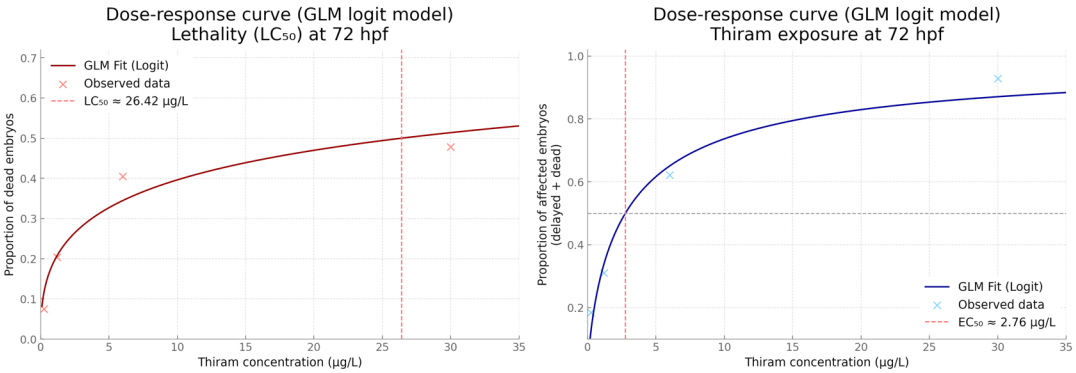


Figure 1. *At 48 hpf, a dose-dependent reduction in the percentage of normally developed A. lixula embryos and a corresponding increase in their malformations were observed in thiram-exposed groups than control. At 72 hpf, the proportion of normally developed embryos remained stable in the control group but decreased in all treated groups, with a parallel increase in the number of delayed developmental stages, indicating persistent sublethal effects over time.*

4.3.2 Morphological analysis

At 48 and 72 hpf, *A. lixula* embryos at pluteus and ampol-like stages, respectively, were collected from control and thiram-treated wells for morphological assessment. At 48 hpf, control embryos showed a regular development, with approximately 80 % reaching a fully formed larval stage, displaying proper arm elongation and dermal deposition (Figure 1). In contrast, thiram-exposed embryos exhibited a dose-dependent decrease in normal development than control, with a higher frequency of malformations observed at increased concentrations of thiram (from 0.24 to 30 µg/L). Malformed embryos showed deformed arms due to soft tissue retraction, and in severe cases, only the exoskeleton was visible, indicating embryo mortality (Figure 1).

At 72 hpf, the control group maintained a stable 80 % rate of normal developed embryos. In treated groups, however, the proportion of normally developed embryos decreased, while the number of embryos at delayed developmental stages increased. Unlike controls, where embryos reached the typical ampol-like morphology, embryos

exposed to thiram, even at the lower tested doses, often remained at the pluteus stage with elongated arms. However, this delay was most evident at 6 and 30 µg/L of thiram exposure, where the transition to the ampol-like form was impaired, suggesting developmental arrest or delay (Figure 2).

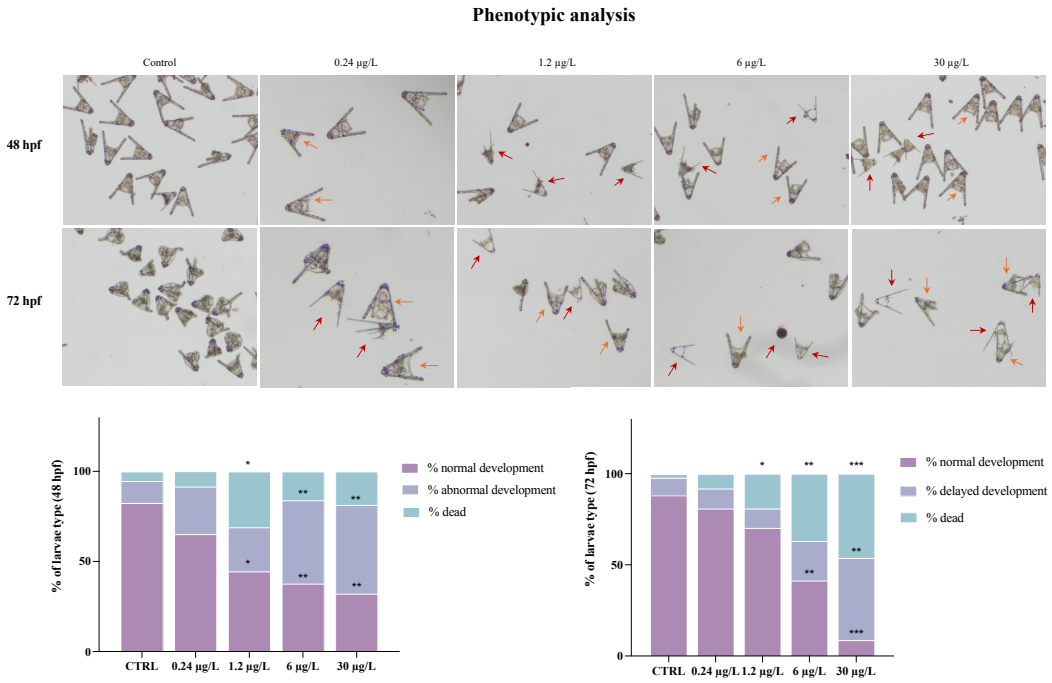


Figure 2. *(A) At 48 hours post-fertilization (hpf), a dose-dependent reduction in the percentage of normally developed A. lixula larvae and a corresponding increase in malformations were observed in thiram-exposed groups. (B) At 72 hpf, the proportion of normally developed embryos remained stable in the control group but decreased in all treated groups, with a parallel increase in delayed developmental stages, indicating persistent sublethal effects over time.*

4.3.3 Biochemical assays

4. 3.3.1 Neurotoxicity

AChE activity, involved in synaptic transmission, exhibited a biphasic response to thiram exposure (Figure 3). At 48 hpf, a slight not significant increase was detected at both 6 µg/L and 30 µg/L compared to the control. At 72 hpf, AChE activity showed a

mild reduction at 6 µg/L and a more pronounced significant decrease at 30 µg/L (Figure 3).

4.3.3.2 Antioxidant activity

Exposure to thiram induced oxidative stress in *A. lixula* embryos, as demonstrated by significant alterations in the antioxidant enzymes activities at 48 and 72 hpf (Figure 3). GST activity remained unchanged at 6 µg/L after 48 hpf compared to the control but showed a significant increase at the higher concentration of 30 µg/L ($p < 0.05$). At 72 hpf, GST levels were significantly and markedly elevated at both concentrations relative to the control (Figure 3).

In contrast, CAT activity significantly decreased at 6 µg/L at 48 hpf, with a more pronounced reduction at 30 µg/L. A similar decreasing trend in CAT activity was observed at 72 hpf at both exposure concentrations (Figure 3).

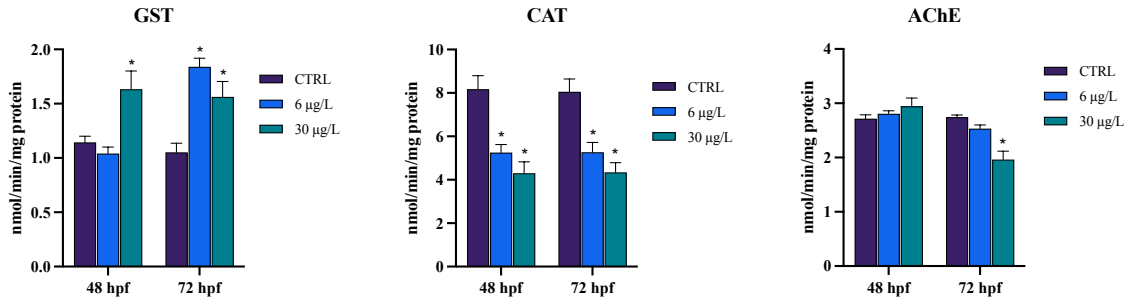


***Figure 3**. Enzymatic responses in A. lixula embryos exposed to thiram at 48 and 72 hpf. GST, CAT, and AChE activities were measured in embryos treated with 6 and 30 µg/L thiram. Data are expressed as mean ± SD. Significant differences vs. control: *p < 0.05 (Dunnett's test).*

4.3.4 Metabolomic evaluation

Figure illustrates the typical [1]H-NMR spectral profile obtained from control samples of *Arbacia lixula* embryos. The analysis revealed a set of roughly 20 metabolite signals. Among the compounds identified were amino acids like glycine; substances involved in energy metabolism, such as lactate and glucose; neuromodulatory molecules including choline, acetylcholine, and N-acetyl serotonin; and solutes related to redox and osmotic balance, such as gluthatione, betaine and trimethylamine-N-oxide.

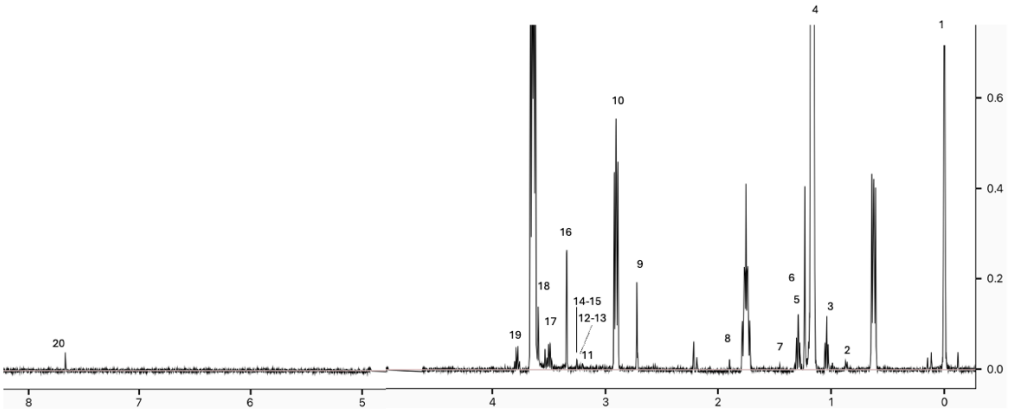


Figure 4. *A representative 1-D 500 MHz [1]H NMR spectrum of sea urchin A. lixula embryos from the negative control plates. Keys: (1) DSS, (2) BCAA, (3) 2-oxobutyrate, (4) ethanol, (5) lactate, (6) threonine, (7) alanine, (8) acetate, (9) sarcosine, (10) N-acetilserotonin, (11) arginine, (12) choline, (13) acetylcholine, (14) betaine, (15) trimethylamine-N-oxide (TMAO), (16) methanol, (17) glucose, (18) glycine, (19) glutathione, and (20) methylhistidine.*

4.3.4.1 Effects on metabolites

The [1]H NMR metabolomic analysis identified several concentration- and time-dependent variations in metabolite levels in embryos exposed to thiram. In

particular, significant increases ($p < 0.05$) were observed in metabolites involved in energy metabolism, neurotransmission, biomineralization, oxidative stress, and osmoregulation in thiram-exposed embryos compared with controls. Specifically, glycine concentrations were found to increase at both 48 and 72 hpf in samples treated with 6 μg/L and 30 μg/L, compared with the control group. Likewise, betaine levels were higher in treated embryos at both time points. Notable alterations were also detected in metabolites associated with energy metabolism. In particular, lactate levels decreased at 48 hpf in thiram-exposed samples, whereas they increased at 72 hpf compared with controls. Acetate concentrations were also elevated in treated groups relative to controls. Conversely, alanine levels were reduced at 48 hpf and elevated at 72 hpf in exposed embryos. Glucose concentrations, instead, increased in all treated groups at both time points. Significant changes were also observed in metabolites related to neurotransmission; notably, acetylcholine and choline levels decreased at 48 hpf in exposed embryos, whereas both metabolites increased at 72 hpf. Furthermore, N-acetylserotonin concentrations were higher in the group treated with 30 μg/L at both exposure times.

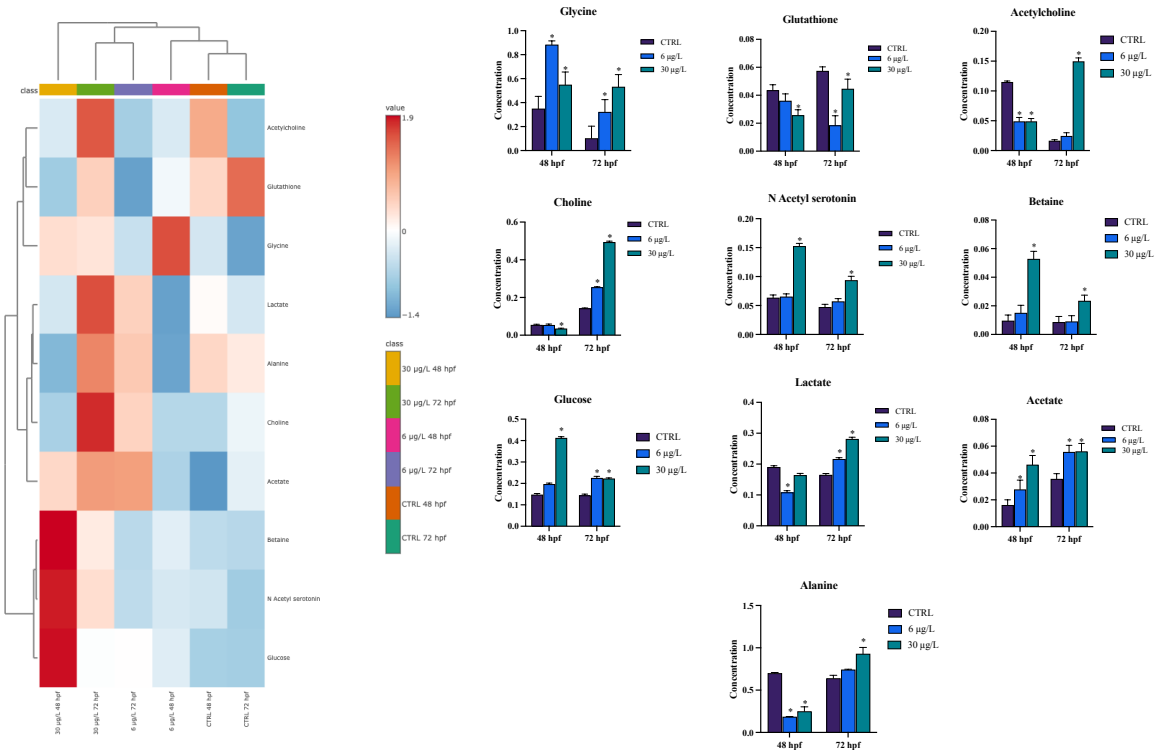


Figure 5. *Heatmap showing z-score normalized concentrations of of significantly altered metabolites across control and thiram-treated groups (6 and 30 µg/L) at 48 and 72 hpf. Each row was scaled by subtracting the mean and dividing by the standard deviation, allowing inter-metabolite comparison. Metabolites were selected based on ANOVA ($p < 0.05$). Color scale indicates relative abundance: red = above-average, blue = below-average, white = near mean. Data processed via MetaboAnalyst 6.0. Bar plots representing absolute ^{1}H NMR concentrations (mM, mean ± SD) of key metabolites significantly altered after thiram exposure. Significant differences from control are indicated (*$p < 0.05$; Dunnett's test).*

4.3.4.2 Pathway and enrichment analysis

The integration of enrichment and pathway topology analysis provided strong evidence that thiram exposure causes a broad disruption of core metabolic networks in *Arbacia lixula* embryos. The pathway impact plot (node-based topology analysis) highlighted several biological pathways as significantly perturbed, with a clear

separation of high-impact and high-significance nodes. Among these, glycine, serine and threonine metabolism, glutathione metabolism, pyruvate metabolism, and glycolysis/gluconeogenesis emerged with both high topological centrality and strong statistical significance, indicating their key involvement in the organism's metabolic response to thiram. These results were further supported by the bubble enrichment diagram, where several of the same pathways ranked among the most significantly enriched based on the adjusted p-values. Pathways related to neurotransmission, one-carbon metabolism (including the folate pool), and osmotic balance also appeared prominently, suggesting a systemic response affecting not only energetic and redox balance but also signaling and developmental processes.

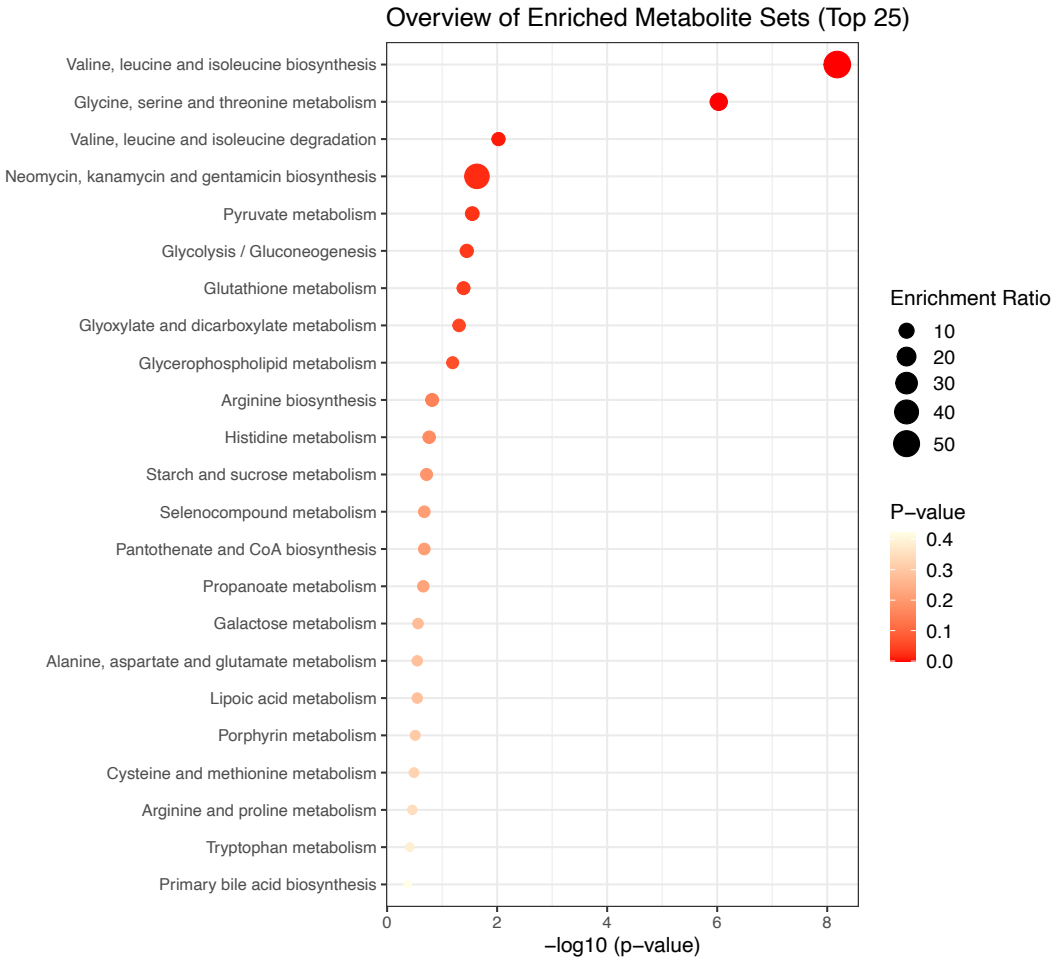


Figure 6. *Enrichment analysis of altered metabolites in thiram-exposed A. lixula embryos. Over-representation analysis performed with MetaboAnalyst using the human KEGG database identified significant enrichment of pathways related to energy metabolism, redox balance, and neurotransmission. Significance was determined using the hypergeometric test ($p < 0.05$).*

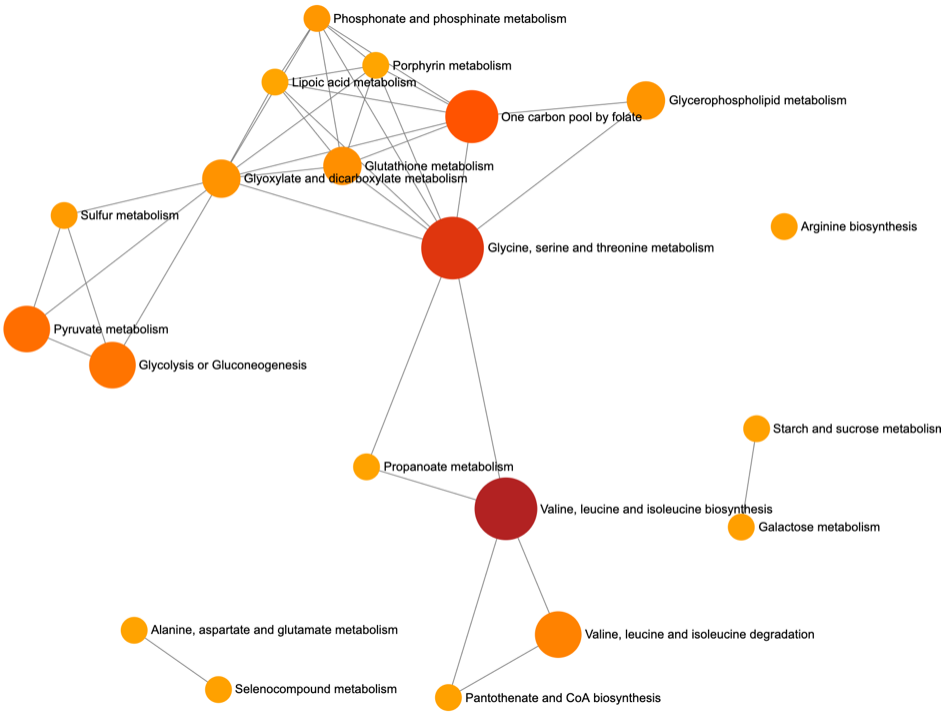


Figure 7. *Pathway topology analysis of metabolomic alterations in thiram-exposed A. lixula embryos. Topological mapping (Strongylocentrotus purpuratus KEGG reference) revealed key affected pathways based on betweenness centrality. Bubble size reflects pathway impact, and color gradient indicates statistical significance ($p < 0.05$ after FDR correction).*

4.3.5 Up-Regulation of developmental and stress-related genes

RT-qPCR analysis revealed a significant up-regulation of all tested genes in *Arbacia lixula* embryos exposed to thiram at both 6 µg/L and 30 µg/L compared to the control group. Specifically, the skeletal markers MSP130 and SM30 showed a pronounced increase in transcript levels in both exposure conditions. The DIO gene, encoding iodothyronine deiodinase and involved in thyroid hormone metabolism, was significantly overexpressed. Genes associated with oxidative stress response, namely SOD and CAT, also exhibited elevated mRNA expression.

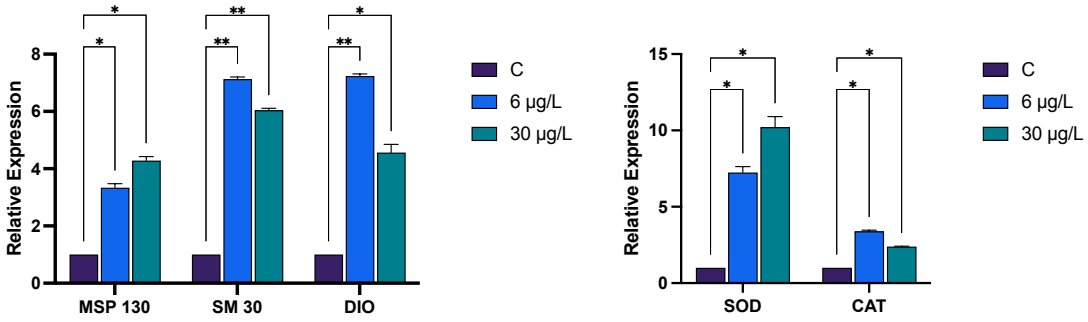


Figure 8. *Relative expression of sod, cat, msp130, sm30 and dio genes in Arbacia lixula embryos at 72 hpf after thiram exposure (6 and 30 µg/L). Expression levels were normalized to actin and calculated using the ΔΔCt method. Data represent mean ± SD. Asterisks indicate significant differences vs. control (*p < 0.05; **p < 0.001; one-way ANOVA with Dunnett's test).*

4.4 Discussions

The results of the present study demonstrated, for the first time to our knowledge, that thiram, a dithiocarbamate fungicide, is capable of inducing developmental delay or arrest and multifactorial toxicological effects in the early life stages of *Arbacia lixula*, which was revealed to be a good model species to determining the influence of thiram on aquatic ecosystem health.

Similar to other xenobiotics, organosulfur compounds can infiltrate the food chain and pose risks to animal and human health through toxicity from chronic low dose exposure (Bjørge et al., 1996; Regoli and Giuliani, 2014). However to date, only a limited number of studies have examined the toxicity of thiram, with mostly focusing primarily on evaluating its LC_{50} (Vasamsetti et al., 2022; Salam et al., 2020). In light of this, we therefore conducted embryotoxicity tests on sea urchin *A. lixula* embryos at 48 and 72 hpf, covering respectively the pluteus stage, characterized by elongated arms and a developing skeletal structure, and the subsequent ampol-like stage, representing an advanced phase toward metamorphosis, in order to assess any developmental effects due to exposure of thiram at concentrations from 0.24 to 30 µg/L (Cameron et al., 1978; Formery et al., 2022). Morphological observations allowed comparison of fungicide-exposed embryos with those grown under control conditions, revealing at 48 hpf a 80 % of embryos from the control group reaching a fully developed larval stage, exhibiting normal arm growth and proper deposition of the dermis, whereas treated-embryos displayed a dose-dependent increase in malformed embryos with evident alterations in arm morphology, which appeared deformed due to soft tissue retraction, leaving only the exoskeleton visible. At 72 hpf the percentage of normal development in the control group remained stable with most

embryos showing a typical ampol-like morphology, characterized by retracted and rotated arms resembling the adult sea urchin form. However, in the treated groups, even at low thiram concentrations, plutei with elongated arms were observed, indicating a significant developmental delay. This phenomenon was observed across all tested concentrations, but it was particularly evident at 6 µg/L and 30 µg/L, where most treated embryos failed to reach the ampol-like form, indicative of a block or slowdown in the developmental process. Additionally, in some extreme cases proportionally to the administered fungicide dose, dead embryos were noticed, characterized by the presence of only the exoskeleton. Therefore, 6 and 30 µg/L thiram were selected as the two doses of the fungicide to be further investigated.

Consistently, toxicological modeling performed on the same embryonic stages at 72 hpf further confirmed a strong developmental sensitivity to thiram. In fact, dose–response analysis based on a GLM indicated an EC_{50} of 2.76 µg/L for sublethal developmental alterations, and a LC_{50} of 26.42 µg/L. The resulting TI was 9.57, clearly above the threshold of 1, suggesting a high teratogenic potential of thiram, while the LOEC was identified at 0.24 µg/L, confirming that significant developmental impairments arise even at low environmental concentrations. These results reinforce the sensitivity of *A. lixula* embryos to thiram and validate the use of sublethal endpoints as early and informative indicators of toxicity.

The morphological abnormalities observed at 72 hpf suggest that thiram may exert its toxic effect through molecular mechanisms potentially involving the inhibition of genes responsible for thyroid hormone (TH) synthesis, known to be phylogenetically conserved in *A. lixula* (Morthorst et al., 2022). These hormones, essential for regulating energy balance, cellular differentiation, and larval development, especially

the metamorphosis process (Chino et al., 1994; Heyland et al., 2006; Johnson, 1998) appear crucial in sea urchins for transitioning from the pluteus stage to the amphol-like stage. Therefore, the gene expression of DIO, encoding iodothyronine deiodinase and involved in TH metabolism (Cocurullo et al., 2023), was evaluated in thiram-treated sea urchin embryos, and found to be markedly elevated than control. This suggests a possible interference with the TH signaling pathways, in line with the observed developmental delay and failure of metamorphic transition. Evidences are reported in the literature regarding the inhibitory effects of xenobiotic substances on TH synthesis in marine organisms such as echinoderms (Leemans et al., 2019; Morthorst et al., 2022), highlighting that the observed toxic effect may result from interference with the endocrine system, preventing proper activation of metamorphic processes. Recent -omics and functional studies further support conserved TH-like pathways in echinoderms (Cocurullo et al., 2023). Morphological abnormalities and alterations in thyroid-related genes have also been observed in initial developmental stages of zebrafish exposed to 0.1 and 1 μM thiram (Brown, 1997; Chen et al., 2019). Similarly, Vasamsetti et al. (2022) observed significant abnormalities in zebrafish embryos/larvae treated with thiram (Vasamsetti et al., 2022). Notochord distortions were also reported in zebrafish following exposure to the dithiocarbamate sodium metam (NaM) (Tilton et al., 2006).

Consistently, recent studies have demonstrated that skeletal formation and larval development in echinoderms are influenced by TH–like pathways, supporting the hypothesis that endocrine regulation contributes to the control of biomineralization and morphogenesis (Taylor et al., 2024). Indeed, gene expression analysis revealed also a significant up-regulation of msp130 and sm30 in 72 hpf embryos exposed to 6

and 30 µg/L thiram. The transcriptional increase of msp130, a primary mesenchyme cell (PMC)-specific surface glycoprotein (Anstrom et al., 1987; Cappello et al., 2017; Vidavsky et al., 2016), and sm30, a spicule matrix protein (Cappello et al., 2017; Wilt, 1999; Wilt et al., 2008, 2013), both involved in the formation of the sea urchin skeleton, exhibiting dynamic and spatially regulated expression patterns within the PMC syncytium (Guss and Ettensohn, 1997), is consistent with the morphological alterations seen in the skeletonized arms of malformed plutei (Cappello et al., 2017; Guss and Ettensohn, 1997). These findings are further supported by the NMR metabolomic profiling that highlighted a marked alteration in glycine concentration, an amino acid essential for the production of matrix proteins associated with the biomineralization process (Benson et al., 1986; Cappello et al., 2017). Increased glycine concentrations were observed at both 48 hpf and 72 hpf, at both thiram tested concentrations, compared to the control. In general, variations in this amino acid suggest disrupted skeletogenesis in sea urchin embryos. These metabolite alterations are further supported by pathway enrichment and network topology analyses, which revealed a coordinated disruption of interconnected metabolic pathways, particularly those related to amino acid turnover, redox balance, and energy metabolism, highlighting a system-level response to thiram exposure.

As previously reported on the non-target organism *Daphnia magna* (Belaid and Sbartai, 2021), one of the main effects of thiram is the induction of oxidative stress. Similarly, Lee et al. (2020) reported that the dithiocarbamate compound orbencarb caused embryotoxic effects during zebrafish development, including intestinal apoptosis and elevated levels of reactive oxygen species (ROS). Consistent with these studies, exposure to thiram induced notable dose- and time-dependent alterations in

the antioxidant system of *A. lixula* embryos. The observed increase in GST activity likely reflects an attempt by cells to neutralize the toxic compounds and ROS generated by thiram. Indeed, after thiram enters cells, it results in the formation of toxic byproducts such as dimethyldithiocarbamate, carbon disulfide (CS_2), and dimethylamine (Elskens and Penninckx, 1997; Pocsi et al., 2004). In addition, due to its high reactivity, thiram can bind to both protein bound and free thiol groups, potentially disrupting protein functionality. This interference may be further exacerbated by its ability to chelate metal ions, thereby altering metal dependent enzymatic process (Cereser et al., 2001; Elskens and Penninckx, 1995; Grosicka et al., 2005; Grosicka-Maciag et al., 2008; Kaul et al., 2021; Mathieu et al., 2015; Pocsi et al., 2004; Viquez et al., 2012).

Regarding CAT, a significant decrease in its enzymatic activity was observed at both 48 and 72 hpf embryos after exposure to the two thiram doses. The decrease in CAT activity indicates an inhibition of mitochondrial antioxidant defenses, leading to an accumulation of ROS. Indeed, CAT is widely recognized as a highly responsive enzymatic indicator of oxidative stress caused by chemical contaminants in aquatic systems (Livingstone, 2001; Regoli et al., 2003). The results of this study align with those of Salam et al. (2020), who reported that thiram exposure in human erythrocytes led to elevated levels of ROS and malondialdehyde (MDA).

The occurrence of oxidative stress is further supported by the NMR metabolomic data. Indeed glycine, besides being involved in the biomineralization process, is also a precursor in the synthesis of glutathione (GSH), a tripeptide that plays a fundamental role in cellular defence mechanisms against oxidative stress (Lushchak, 2011). Specifically, the increase in glycine, correlated with reduced glutathione levels under

all experimental conditions compared to the control, provides clear evidence of the pro-oxidant effect induced by thiram in sea urchin embryos. These changes, consistent with the increased GST activity observed by biochemical analyses, suggest an attempt by cells to neutralize ROS and toxic compounds generated by thiram. Moreover, the decrease in CAT activity further indicates an inhibition of mitochondrial antioxidant defenses, leading to ROS accumulation. This could explain why protective metabolites such as glycine and betaine increased to compensate for the depletion of traditional antioxidant defenses (Craig, 2004; Eklund et al., 2005; Grădinariu et al., 2025; Ratriyanto et al., 2009).

The enzymatic function of AChE, known for its pivotal role in regulating synaptic transmission, showed a complex pattern in sea urchin embryos in response to thiram exposure. This enzyme plays a role in embryonic patterning, being implicated in the coordination of morphogenetic movements during the gastrulation phase of development (Maisano et al., 2015), and successive larval behaviour and substrate search. Surprisingly, AChE demonstrated to be particularly resistant to the impact of thiram since its activity remained unchanged in all the developmental stages of sea urchins, except for the 72 hpf embryos exposed to the higher thiram dose, solely in which a significant decline in AChE activity was observed, in line with morphological observations.

Metabolomic analysis also highlighted significant perturbations in neurotransmission pathways induced by thiram. Specifically, the decrease in acetylcholine and choline at 48 hpf reflects initial inhibition of synaptic transmission or damage to cellular membranes, while their increase at 72 hpf suggests a compensatory attempt to restore neuronal functionality. Furthermore, samples treated

with the highest thiram concentration (30 µg/L) exhibited a marked elevation in N-acetyl serotonin levels at both time points, suggesting disruption of normal neuronal signaling mechanisms (Bishop et al., 2013; Squires et al., 2010). Collectively, these neurochemical and enzymatic alterations likely impair neuromotor development and larval behaviour, contributing to the developmental arrest observed in 72 hpf embryos exposed to the higher thiram dosage, and further supported by data of increased malformations and mortality.

Additionally, betaine, an osmolyte that plays a role in osmotic pressure regulation (Simon, 1999), increased in treated samples compared to the control. Betaine, involved in homocysteine remethylation (Ganu et al., 2015) and the synthesis of S-adenosylmethionine, critical for neurotransmitters, reflects a response to thiram-induced cellular damage.

Exposure to thiram also caused significant alterations in the energy metabolism of *A. lixula* embryos. Interestingly, the level of glucose increased in all developmental stages, particularly at 48 hpf, and then it seems to be compensated by other energy sources to support the development of sea urchins. At 48 hpf, the decrease in lactate levels in treated samples suggests a partial utilization of oxidative phosphorylation, likely as an initial compensatory response to stress. However, at 72 hpf, the increase in lactate indicates a shift to anaerobic glycolysis, caused by mitochondrial damage or compromised oxidative phosphorylation. Additionally, acetate, a key metabolite in energy and lipid metabolism, was altered. Its increase in treated samples compared to the control may reflect reduced mitochondrial activity or impaired lipid metabolism, a critical essential metabolic pathway that transforms nutrients into key intermediates required for membrane formation, energy reservoir development, and the synthesis of

signaling molecules (DeBose-Boyd, 2018; Röhrig and Schulze, 2016). Thiram may interfere with fatty acid oxidation, leading to the accumulation of acetate as an intermediate product. Alanine, involved in energy metabolism and gluconeogenesis, also showed temporal dynamics; indeed, its decrease at 48 hpf in treated samples may reflect interference with pyruvate metabolism or increased consumption to support gluconeogenesis. Conversely, at 72 hpf, the increase in alanine indicates an accumulation of glycolytic intermediates, consistent with enhanced anaerobic glycolytic activity induced by metabolic stress. The increase in free amino acids, such as alanine, has been associated with thiram-induced protein catabolism, which facilitates the generation of ROS (Juan et al., 2021). This metabolic adaptation is typical of organisms under stress conditions and suggests that thiram exposure induces a compromise in energy metabolism, leading to ATP deficiency, which is essential for processes such as skeletal calcification and cellular differentiation, contributing to developmental inhibition.

4.5. Conclusions

Thiram, like other dithiocarbamate pesticides, appears to represent a threat to aquatic organisms, particularly when it comes into contact with coastal waters through surface runoff or agricultural discharge. Its potential to disrupt endocrine signaling pathways and induce oxidative stress makes it a particularly concerning compound for the health of marine ecosystems. Specifically, our results suggest that thiram acts as a multifactorial stress agent, affecting various biological pathways in *A. lixula* embryos including normal development, skeletogenesis, endocrine regulation, antioxidant system, neurotransmission, and energy metabolism. In this context, dose - response modelling confirmed a strong sublethal sensitivity to thiram, with an EC_{50} of 2.76 µg/L and a much higher LC_{50} of 26.42 µg/L. The resulting TI of 9.57 indicates a clear teratogenic potential, and the identification of a LOEC as low as 0.24 µg/L highlights the occurrence of significant effects even at environmentally relevant concentrations. Although in this study thyroid hormone levels were not directly assessed, the observed metabolic and developmental impairments are consistent with a possible interference with the thyroid endocrine system, indicating a direction for future scientific inquiry. Supporting this hypothesis, the significant up-regulation of dio observed in thiram-treated embryos suggests an early disruption of thyroid-like signaling pathways. The up-regulation of msp130 and sm30, involved in biomineralization, further supports the link between skeletal abnormalities and gene-level alterations. Furthermore, the occurrence of oxidative stress, neurotoxicity and disorders in the energy metabolism lead to a slowdown or blockage in the developmental process of *A. lixula*, with an increased mortality at 72 hpf embryos exposed at the higher tested thiram dose, thus suggesting that thiram may have long-term effects on sea urchin populations,

compromising their ability to complete growth. In conclusion, our findings highlight the need for further studies to assess the impact and toxicity of thiram and other pesticides on the health of aquatic non-target species.

4.6 References

Aebi, H., Mörikofer-Zwez, S., & von Wartburg, J. P. (1972). Alternative molecular forms of erythrocyte catalase. In Structure and Function of Oxidation–Reduction Enzymes (pp. 345-351). Pergamon.

Anstrom, J. A., Chin, J. E., Leaf, D. S., Parks, A. L., & Raff, R. A. (1987). Localization and expression of msp130, a primary mesenchyme lineagespecific cell surface protein of the sea urchin embryo. *Development*, *101*(2), 255-265.

Belaid, C., & Sbartai, I. (2021). Assessing the effects of Thiram to oxidative stress responses in a freshwater bioindicator cladoceran (Daphnia magna). *Chemosphere*, *268*, 128808.

Benedetti, M., Giuliani, M. E., Mezzelani, M., Nardi, A., Pittura, L., Gorbi, S., & Regoli, F. (2022). Emerging environmental stressors and oxidative pathways in marine organisms: Current knowledge on regulation mechanisms and functional effects. *Biocell*, *46*(1), 37.

Benedetti, M., Giuliani, M. E., & Regoli, F. (2015). Oxidative metabolism of chemical pollutants in marine organisms: molecular and biochemical biomarkers in environmental toxicology. *Annals of the New York Academy of Sciences*, *1340*, 8–19.

Benson, S. C., Benson, N. C., & Wilt, F. (1986). The organic matrix of the skeletal spicule of sea urchin embryos. *The Journal of cell biology*, *102*(5), 1878-1886.

Bishop, C. D., MacNeil, K. E., Patel, D., Taylor, V. J., & Burke, R. D. (2013). Neural development in Eucidaris tribuloides and the evolutionary history of the echinoid larval nervous system. *Developmental biology*, *377*(1), 236-244.

Brown, D. D. (1997). The role of thyroid hormone in zebrafish and axolotl development. *Proceedings of the National Academy of Sciences*, *94*(24), 13011-13016.

Cameron, R.A., and Hinegardner, R.T. (1974). Initiation of metamorphosis in sea urchins, description and analysis. J. Morphol. 157, 21-32.

Cappello, T., Vitale, V., Oliva, S., Villari, V., Mauceri, A., Fasulo, S., & Maisano, M. (2017). Alteration of neurotransmission and skeletogenesis in sea urchin *Arbacia lixula* embryos exposed to copper oxide nanoparticles. Comparative Biochemistry and Physiology Part C: Toxicology & Pharmacology, 199, 20-27.

Cereser, C., Boget, S., Parvaz, P., & Revol, A. (2001). Thiram-induced cytotoxicity is accompanied by a rapid and drastic oxidation of reduced glutathione with consecutive lipid peroxidation and cell death. *Toxicology*, *163*(2-3), 153-162.

Chen, X., Fang, M., Chernick, M., Wang, F., Yang, J., Yu, Y., ... & Dong, W. (2019). The case for thyroid disruption in early life stage exposures to thiram in zebrafish (Danio rerio). *General and comparative endocrinology*, *271*, 73-81.

Chino, Y., Saito, M., Yamasu, K., Suyemitsu, T., & Ishihara, K. (1994). Formation of the adult rudiment of sea urchins is influenced by thyroid hormones. *Developmental biology*, *161*(1), 1-11.

Cocurullo, M., Paganos, P., Wood, N. J., Arnone, M. I., & Oliveri, P. (2023). Molecular and cellular characterization of the TH pathway in the Sea urchin Strongylocentrotus purpuratus. *Cells*, *12*(2), 272.

Craig, S. A. (2004). Betaine in human nutrition. *The American journal of clinical nutrition*, *80*(3), 539-549.

Drews, U. (1975). Cholinesterase in embryonic development. *Progress in histochemistry and cytochemistry*, *7*(3), 1-52.

EFSA Panel on Additives and Products or Substances used in Animal Feed (FEEDAP), Bampidis, V., Azimonti, G., Bastos, M. D. L., Christensen, H., Dusemund, B., ... & Pizzo, F. (2022). Safety and efficacy of a feed additive consisting of sepiolite for all animal species (Sepiol SA and Tolsa, SA). *EFSA Journal*, *20*(4), e07250.

European Chemicals Agency (ECHA). *Thiram – Substance Evaluation Conclusion and Justification Document.* Helsinki: ECHA; 2023.

Eklund, M., Bauer, E., Wamatu, J., & Mosenthin, R. (2005). Potential nutritional and physiological functions of betaine in livestock. *Nutrition research reviews*, *18*(1), 31-48.

Eliso, M.C., Billè, B., De Marco, G., Pulvirenti, E., Dal Bello, F., Rapisarda, P., Pereira, P., Galati, M., Oliveri Conti, G., Ferrante, M., Bovolin, P., Maisano, M., Cappello, T., (2025). Embryotoxicity of polystyrene microplastics, alone and conjugated with bisphenol A, in the black sea urchin Arbacia lixula: A multi-biomarker approach. *Journal of Hazardous Materials*, 499 140139.

Ellman, G. L., Courtney, K. D., Andres Jr, V., & Featherstone, R. M. (1961). A new and rapid colorimetric determination of acetylcholinesterase activity. *Biochemical pharmacology*, *7*(2), 88-95.

El-SiKaily, A., & Shabaka, S. (2024). Biomarkers in aquatic systems: advancements, applications and future directions. *Egyptian Journal of Aquatic Research*, *50*(2), 169-182.

Elskens, M. T., & Penninckx, M. J. (1995). Enhanced sensitivity of a glutathione-deficient yeast strain to thiram and dimethyldithiocarbamic acid. *Zeitschrift für Pflanzenernährung und Bodenkunde*, *158*(1), 79-81.

Elskens, M. T., & Penninckx, M. J. (1997). Thiram and dimethyldithiocarbamic acid interconversion in Saccharomyces cerevisiae: a possible metabolic pathway under the control of the glutathione redox cycle. *Applied and environmental microbiology*, *63*(7), 2857-2862.

Formery, L., Wakefield, A., Gesson, M., Toisoul, L., Lhomond, G., Gilletta, L., Lasbleiz, R., Schubert, M., Croce, J. C. (2022). Developmental atlas of the indirect-developing sea urchin Paracentrotus lividus: From fertilization to juvenile stages. *Frontiers in Cell and Developmental Biology, section Morphogenesis and Patterning*, *10*. https://doi.org/10.3389/fcell.2022.966408

Giannetto, A., Cappello, T., Oliva, S., Parrino, V., De Marco, G., Fasulo, S., ... & Maisano, M. (2018). Copper oxide nanoparticles induce the transcriptional modulation of oxidative stress-related genes in *Arbacia lixula* embryos. Aquatic Toxicology, 201, 187-197.

Gil, F., & Pla, A. (2001). Biomarkers as biological indicators of xenobiotic exposure. *Journal of Applied Toxicology: An International Journal*, *21*(4), 245-255.

Grădinariu, L., Crețu, M., Vizireanu, C., & Dediu, L. (2025). Oxidative Stress Biomarkers in Fish Exposed to Environmental Concentrations of Pharmaceutical Pollutants: A Review. *Biology*, *14*(5), 472.

Grosicka-Maciąg, E., Kurpios, D., Czeczot, H., Szumiło, M., Skrzycki, M., Suchocki, P., & Rahden-Staroń, I. (2008). Changes in antioxidant defense systems

induced by thiram in V79 Chinese hamster fibroblasts. *Toxicology in Vitro*, *22*(1), 28-35.

Giudice, G. (1973). Developmental Biology of the Sea Urchin Embryo. Academic Press.

Grosicka, E., Sadurska, B., Szumiło, M., Grzela, T., Łazarczyk, P., Niderla-Bielińska, J., & Rahden-Staroń, I. (2005). Effect of glutathione depletion on apoptosis induced by thiram in Chinese hamster fibroblasts. *International immunopharmacology*, *5*(13-14), 1945-1956.

Guss, K. A., & Ettensohn, C. A. (1997). Skeletal morphogenesis in the sea urchin embryo: regulation of primary mesenchyme gene expression and skeletal rod growth by ectoderm-derived cues. *Development*, *124*(10), 1899-1908.

Habig, W. H., Pabst, M. J., & Jakoby, W. B. (1974). Glutathione S-transferases: the first enzymatic step in mercapturic acid formation. *Journal of biological Chemistry, 249*(22), 7130-7139.

Hafed-Khatiri, S., Salinas-Torres, D., & Montilla, F. (2025). Assessing acetylcholinesterase catalytic activity in the marine environment. *Electrochimica Acta*, *521*, 145930.

Heyland, A., Price, D. A., Bodnarova-buganova, M., & Moroz, L. L. (2006). Thyroid hormone metabolism and peroxidase function in two non-chordate animals. *Journal of Experimental Zoology Part B: Molecular and Developmental Evolution, 306*(6), 551-566.

Johnson, L. G. (1998). Stage-dependent thyroxine effects on sea urchin development.

Juan, C. A., Pérez de la Lastra, J. M., Plou, F. J., & Pérez-Lebeña, E. (2021). The chemistry of reactive oxygen species (ROS) revisited: outlining their role in biological macromolecules (DNA, lipids and proteins) and induced pathologies. *International journal of molecular sciences*, *22*(9), 4642.

Killian, C. E., & Wilt, F. H. (2008). Molecular aspects of biomineralization of the echinoderm endoskeleton. *Chemical reviews*, *108*(11), 4463-4474.

Kovačević, T. B., Borković, S. S., Pavlović, S. Z., Despotović, S. G., & Saičić, Z. S. (2008). Glutathione as a suitable biomarker in hepatopancreas, gills and muscle of three freshwater crayfish species. *Archives of Biological Sciences*, *60*(1), 59-66.

Lee, J. Y., Park, S., Lim, W., & Song, G. (2020). Orbencarb induces lethality and organ malformation in zebrafish embryos during development. *Comparative Biochemistry and Physiology Part C: Toxicology & Pharmacology*, *233*, 108771.

Leemans, M., Couderq, S., Demeneix, B., & Fini, J. B. (2019). Pesticides with potential thyroid hormone-disrupting effects: a review of recent data. *Frontiers in endocrinology*, *10*, 743.

Li, Y., Yin, W., Zhan, Y., Jia, Y., Cui, D., Zhang, W., & Chang, Y. (2020). Comparative metabolome analysis provides new insights into increased larval mortality under seawater acidification in the sea urchin Strongylocentrotus intermedius. *Science of the Total Environment*, *747*, 141206.

Li, Z. H., Zlabek, V., Grabic, R., Li, P., & Randak, T. (2010). Modulation of glutathione-related antioxidant defense system of fish chronically treated by the fungicide propiconazole. *Comparative Biochemistry and Physiology Part C: Toxicology & Pharmacology*, *152*(3), 392-398.

Livingstone, D. R. (2001). Contaminant-stimulated reactive oxygen species production and oxidative damage in aquatic organisms. *Marine pollution bulletin*, *42*(8), 656-666.

Lushchak, V. I. (2011). Environmentally induced oxidative stress in aquatic animals. *Aquatic toxicology*, *101*(1), 13-30.

Lushchak, V. I. (2016). Contaminant-induced oxidative stress in fish: a mechanistic approach. *Fish physiology and biochemistry*, *42*, 711-747.

Maisano, M., Cappello, T., Catanese, E., Vitale, V., Natalotto, A., Giannetto, A., ... & Fasulo, S. (2015). Developmental abnormalities and neurotoxicological effects of CuO NPs on the black sea urchin *Arbacia lixula* by embryotoxicity assay. Marine environmental research, 111, 121-127.

Mathieu, C., Duval, R., Xu, X., Rodrigues-Lima, F., & Dupret, J. M. (2015). Effects of pesticide chemicals on the activity of metabolic enzymes: focus on thiocarbamates. *Expert opinion on drug metabolism & toxicology*, *11*(1), 81-94.

Morthorst, J. E., Holbech, H., De Crozé, N., Matthiessen, P., & LeBlanc, G. A. (2022). Thyroid-like hormone signaling in invertebrates and its potential role in initial screening of thyroid hormone system disrupting chemicals. *Integrated Environmental Assessment and Management, 19*(1), 63-82.

Pocsi, I., Prade, R. A., & Penninckx, M. J. (2004). Glutathione, altruistic metabolite in fungi. *Advances in microbial physiology*, *49*(1), 1-76.

Polak, M. (2014). Human fetal thyroid function. *Endocr Dev*, *26*, 17-25.

Ratriyanto, A., Mosenthin, R., Bauer, E., & Eklund, M. (2009). Metabolic, osmoregulatory and nutritional functions of betaine in monogastric animals. *Asian-Australasian Journal of Animal Sciences*, *22*(10), 1461-1476.

Regoli, F., Winston, G. W., Gorbi, S., Frenzilli, G., Nigro, M., Corsi, I., & Focardi, S. (2003). Integrating enzymatic responses to organic chemical exposure with total oxyradical absorbing capacity and DNA damage in the European eel Anguilla anguilla. *Environmental Toxicology and Chemistry*, *22*(9), 2120-2129.

Regoli, F., & Giuliani, M. E. (2014). Oxidative pathways of chemical toxicity and oxidative stress biomarkers in marine organisms. *Marine environmental research*, *93*, 106-117.

Ritz, C., Baty, F., Streibig, J. C., & Gerhard, D. (2015). Dose–response analysis using R. PLoS ONE, 10(12), e0146021.

Salam, S., Arif, A., & Mahmood, R. (2020). Thiram-induced cytotoxicity and oxidative stress in human erythrocytes: an in vitro study. Pesticide biochemistry and physiology, 164, 14-25.

Squires, L. N., Rubakhin, S. S., Wadhams, A. A., Talbot, K. N., Nakano, H., Moroz, L. L., & Sweedler, J. V. (2010). Serotonin and its metabolism in basal deuterostomes: insights from Strongylocentrotus purpuratus and Xenoturbella bocki. *Journal of Experimental Biology*, *213*(15), 2647-2654.

Taylor, E., & Heyland, A. (2017). Evolution of thyroid hormone signaling in animals: Non-genomic and genomic modes of action. *Molecular and cellular endocrinology, 459*, 14-20.

Taylor, E., Corsini, M., & Heyland, A. (2024). Shared regulatory function of non-genomic thyroid hormone signaling in echinoderm skeletogenesis. *EvoDevo*, *15*(1), 10.

Tilton, F., La Du, J. K., Vue, M., Alzarban, N., & Tanguay, R. L. (2006). Dithiocarbamates have a common toxic effect on zebrafish body axis formation. *Toxicology and applied pharmacology*, *216*(1), 55-68.

Urry, L. A., Hamilton, P. C., Killian, C. E., & Wilt, F. H. (2000). Expression of spicule matrix proteins in the sea urchin embryo during normal and experimentally altered spiculogenesis. *Developmental biology*, *225*(1), 201-213.

Valavanidis, A., Vlahogianni, T., Dassenakis, M., & Scoullos, M. (2006). Molecular biomarkers of oxidative stress in aquatic organisms in relation to toxic environmental pollutants. *Ecotoxicology and environmental safety*, *64*(2), 178-189.

Van Leeuwen, C. J., Espeldoorn, A., & Mol, F. (1986). Aquatic toxicological aspects of dithiocarbamates and related compounds. III. Embryolarval studies with rainbow trout (Salmo gairdneri). *Aquatic toxicology*, *9*(2-3), 129-145.

Vasamsetti, B. M. K., Chon, K., Kim, J., Oh, J. A., Yoon, C. Y., & Park, H. H. (2022). Developmental toxic effects of thiram on developing zebrafish (Danio rerio) embryos. *Toxics*, *10*(7), 369.

Vidavsky, N., Addadi, S., Schertel, A., Ben-Ezra, D., Shpigel, M., Addadi, L., & Weiner, S. (2016). Calcium transport into the cells of the sea urchin larva in relation to spicule formation. *Proceedings of the National Academy of Sciences*, *113*(45), 12637-12642.

Vignet, C., Cappello, T., Fu, Q., Lajoie, K., De Marco, G., Clérandeau, C., ... & Cachot, J. (2019). Imidacloprid induces adverse effects on fish early life stages that are more severe in Japanese medaka (Oryzias latipes) than in zebrafish (Danio rerio). Chemosphere, 225, 470-478.

Viquez, O. M., Caito, S. W., McDonald, W. H., Friedman, D. B., & Valentine, W. M. (2012). Electrophilic adduction of ubiquitin activating enzyme E1 by N, N-diethyldithiocarbamate inhibits ubiquitin activation and is accompanied by striatal injury in the rat. *Chemical research in toxicology*, *25*(11), 2310-2321.

Wilt, F. H. (1999). Matrix and mineral in the sea urchin larval skeleton. *Journal of Structural Biology*, *126*(3), 216-226.

Wilt, F. H., Killian, C. E., Hamilton, P., & Croker, L. (2008). The dynamics of secretion during sea urchin embryonic skeleton formation. *Experimental cell research*, *314*(8), 1744-1752.

Wilt, F., Killian, C. E., Croker, L., & Hamilton, P. (2013). SM30 protein function during sea urchin larval spicule formation. *Journal of structural biology*, *183*(2), 199–204.

Wu, H., Southam, A. D., Hines, A., & Viant, M. R. (2008). High-throughput tissue extraction protocol for NMR-and MS-based metabolomics. *Analytical biochemistry*, *372*(2), 204-212.

Zhang, X. J., Yang, L., Zhao, Q., Caen, J. P., He, H. Y., Jin, Q. H., ... & Shi, Y. F. (2002). Induction of acetylcholinesterase expression during apoptosis in various cell types. *Cell Death & Differentiation*, *9*(8), 790-800.

Zhu, B. K., Wang, P., Zhang, X. D., Jiang, C. C., Chen, L. H., Avery-Kiejda, K. A., ... & Hersey, P. (2008). Activation of Jun N-terminal kinase is a mediator of vincristine-induced apoptosis of melanoma cells. *Anti-cancer drugs*, *19*(2), 189-200.

CHAPTER 5

Macroalgae-Derived Hydrochar as an Eco-Sustainable Biofilter: Adsorption Properties and Protective Potential against Thiram Toxicity

5.1 Introduction

Pesticides represent one of the major classes of environmental contaminants, with pervasive effects on aquatic ecosystems due to their persistence, bioaccumulative potential, and toxicity toward non-target species (Regoli & Giuliani, 2014; Salam et al., 2020). Among them, *tetramethylthiuram disulfide* (thiram), a dithiocarbamate fungicide widely used for seed protection and crop treatment, has raised particular concern because of its ability to induce oxidative stress, endocrine disruption, and neurotoxicity in aquatic organisms (Vasamsetti et al., 2022; Kim et al., 2021; Zhang et al., 2023). Dithiocarbamates disrupt redox homeostasis and thyroid signalling, causing developmental impairments across vertebrate and invertebrate models (Bjørge et al., 1996; Zhou et al., 2019; Yang et al., 2020). Their frequent detection in surface waters near agricultural areas highlights the risk of chronic exposure to sublethal concentrations in coastal ecosystems. Our previous research demonstrated that thiram exerts marked developmental toxicity in the sea urchin *Arbacia lixula*, causing dose-dependent delay and arrest of embryogenesis and revealing a high teratogenic potential even at environmentally relevant concentrations. Molecular evidence revealed that thiram acts as a multifactorial stressor, activating oxidative stress pathways (sod, cat), disrupting thyroid-like regulation (dio), and altering biomineralization processes (msp130, sm30). These findings emphasize the ecological risk posed by thiram to early life stages of marine organisms and underscore the urgent need for sustainable remediation strategies capable of reducing its bioavailability and toxicity in aquatic environments. Conventional techniques for pesticide removal, such as coagulation, advanced oxidation, and membrane filtration, often present limitations related to high costs, incomplete mineralization, or generation of toxic by-products (Gao et al., 2022;

Liu et al., 2021). In contrast, adsorption-based methods have emerged as versatile, low-impact, and energy-efficient alternatives, particularly when using carbonaceous sorbents derived from renewable biomasses (Hayoun et al., 2022; Nguyen et al., 2021). Among these, hydrothermal carbonization (HTC) has gained growing attention as a sustainable thermochemical route for converting wet biomass into functional sorbents known as hydrochars (Fang et al., 2018; Leong et al., 2021). This process enables direct conversion of high-moisture feedstocks without the need for drying or chemical activation. The resulting hydrochar is a carbon-rich material characterized by high porosity, surface heterogeneity, and abundant oxygenated functional groups (–COOH, –OH, –C=O), which promote strong interactions with organic and inorganic contaminants (Lucian & Fiori, 2017; Baccile et al., 2020). Among the various potential precursors, algal biomass has emerged as a particularly promising feedstock for hydrochar production due to its rapid growth rate, high photosynthetic efficiency, and intrinsic ability to sequester nutrients and CO_2 from wastewater (Shahid et al., 2020; Khan et al., 2018; Wang et al., 2024). Algae constitute a phylogenetically diverse group of photosynthetic organisms ranging from cyanobacteria to macroalgae, rich in proteins, polysaccharides, and lipids that enhance the reactivity and surface chemistry of derived carbon materials. In eutrophic environments, excessive algal proliferation often results in the accumulation of biomass that disrupts aquaculture and tourism activities. However, within a circular bioeconomy perspective, this waste biomass can be valorised as a renewable source for producing high-value materials through HTC, transforming an ecological problem into a technological opportunity (Yap et al., 2021; Vishwakarma et al., 2022; Sun et al., 2023). Hydrochars obtained from algal feedstocks exhibit high sorptive and catalytic performance, as demonstrated in several

studies involving the removal of dyes (Hong et al., 2020), pharmaceuticals (Hayoun et al., 2022), antibiotics (Li et al., 2021), and heavy metals (Zhao et al., 2022). The presence of nitrogen- and sulfur-containing moieties in algal biomass enhances doping during carbonization, resulting in increased surface activity and adsorption capacity (Benavente et al., 2022; Jansson et al., 2022). Furthermore, the HTC process operates under mild conditions, generating minimal emissions and enabling the recovery of liquid fractions enriched in nutrients, suitable for secondary valorization (Bevan et al., 2020; Masek et al., 2019). These features make algal hydrochars particularly attractive for sustainable water treatment and pollution control, consistent with the principles of circular economy and low-carbon technologies (Buss et al., 2021; Wurzer & Masek, 2021). From an ecological standpoint, the conversion of waste algal biomass into reactive sorbents provides a dual environmental benefit: mitigation of eutrophication and removal of organic pollutants from water bodies. However, despite the increasing number of studies on algal hydrochars, their application to pesticide remediation remains limited, and few investigations have assessed their ecotoxicological performance, a critical step in verifying real detoxification beyond chemical removal (Gallego-Ramírez et al., 2025; Rubio-Clemente et al., 2023). Bridging this gap is essential to validate hydrochar-based technologies as effective and safe tools for environmental recovery. In this framework, the present study aims to evaluate the adsorption capacity and detoxification potential of algal-derived hydrochar toward the fungicide thiram, integrating physicochemical assays with biological assessment using *Arbacia lixula* embryos. This research aims to elucidate both the mechanistic aspects of pollutant–adsorbent interaction and the potential of algal hydrochar as an eco-friendly material for coastal bioremediation. This work integrates principles of circular

bioeconomy and environmental recovery, proposing algal hydrochar as an innovative bio-based material to mitigate pesticide contamination in marine ecosystems.

5.2 Material and methods

5.2.1. Hydrothermal carbonization (HTC) process

The green macroalga *Chaetomorpha aerea* (Chlorophyta) was collected from Lake Ganzirri (Messina, Italy; 38°15'47.6″ N, 15°37'34.2″ E). The biomass was thoroughly rinsed with tap and distilled water to remove sediments and salts, air-dried at room temperature, and subsequently oven-dried at 60 °C until constant weight. The dried material was ground to a fine powder (< 1 mm) and used as feedstock for hydrothermal carbonization (HTC). HTC experiments were carried out in a 300 mL stainless-steel autoclave (Parr Instrument Company, IL, USA) equipped with a Teflon-lined reactor. Approximately 5 g of algal powder and 150 mL of deionized water (solid-to-liquid ratio ≈ 1:30) were loaded into the vessel, which was then tightly sealed. The reactor was heated to 240 °C under autogenous pressure and maintained at that temperature for 3 h, with continuous internal stirring at 600 rpm. Temperature was monitored by a thermocouple connected to the reactor controller. After the residence time, the system was allowed to cool to room temperature. The solid and liquid fractions were separated by vacuum filtration using a Büchner funnel and Whatman No. 1 filter paper. The solid product (hydrochar) was washed several times with warm distilled water until neutral pH, oven-dried at 60 °C overnight, and weighed, yielding 0.9764 g of dried hydrochar. The corresponding aqueous phase (154 mL) was collected and stored at 4 °C for possible further analyses.

5.2.2. Morpho-chemical analyses of hydrochar

Morpho-chemical analyses of the hydrochar before and after thiram adsorption were performed using a Nicolet™ RaptIR+ Micro-FTIR system (Thermo Fisher Scientific), which integrates an infrared spectrophotometer with a microscopy platform. The instrument is equipped with a high-speed motorized stage and a liquid-nitrogen-cooled MCT (mercury cadmium telluride) detector. Measurements were acquired using 164 sample scans and a spectral resolution of 8 cm^{-1}, with a 14× optical zoom. The system is coupled with a Nicolet iS50 FT-IR equipped with an ATR detector. FT-IR analyses were conducted in a wavelength range from 4000 to 500 cm^{-1}, with a spectral resolution of 4 cm^{-1}, 64 accumulation scans. Spectra were processed using Omnic Paradigm Software.

5.2.3. Preparation of thiram solutions and exposure conditions

A stock solution of thiram (analytical grade, Sigma-Aldrich) was prepared in dimethyl sulfoxide (DMSO) and diluted in artificial seawater to obtain a final nominal concentration of 30 μg L^{-1}, selected based on previous findings showing significant sublethal and teratogenic effects in *Arbacia lixula* embryos. Control treatments contained equivalent volumes of solvent (< 0.01% v/v DMSO). The hydrochar was dispersed in the thiram solution under continuous stirring to evaluate its adsorption efficiency and the resulting detoxification potential. Adsorption assays were conducted at room temperature (22 ± 1 °C) for 90 min, followed by filtration to remove the solid phase. The treated and untreated thiram solutions were then used for comparative toxicological assessments.

5.2.4 Biological assays and experimental setup using the sea urchin *Arbacia lixula*

Adult specimens of the sea urchin *Arbacia lixula* were collected from the coastal waters of Messina (Sicily, Italy) and maintained in aerated aquaria containing filtered seawater (FSW) under controlled conditions (20 ± 1 °C; salinity 36 ppt). Spawning was induced by gently injecting 0.5 M KCl into the peristomial membrane to stimulate gamete release (Eliso et al., 2025). Eggs and sperm were collected separately, and their quality was verified under optical microscopy. Oocytes displaying intact spherical morphology and a clearly visible germinal vesicle were selected, while sperm samples were used only if high motility was observed. Fertilization was achieved by adding freshly diluted sperm (1:1000 in FSW) to egg suspensions at a standardized ratio of 100:1, ensuring a fertilization success rate exceeding 85%. The formation of the fertilization envelope was used as a visual indicator of successful activation. Approximately 500 fertilized eggs were transferred into each well of sterile 24-well culture plates containing 2 mL of FSW. A stock solution of thiram (Sigma-Aldrich, analytical grade) was prepared by dissolving the powder in dimethyl sulfoxide (DMSO) and diluting it in FSW to the required concentrations. The final solvent concentration was maintained below 0.01% (v/v) in all treatments, including the negative control. Based on previous toxicological data, embryos were exposed to a nominal concentration of 30 μg L^{-1}, corresponding to the level that previously induced the most pronounced sublethal effects. Exposure assays were conducted under static conditions in a temperature-controlled incubator (20–22 °C) until the pluteus/ampol-like stage (72 h post-fertilization, hpf). Each experimental group (Control: CTRL, Thiram 30 μg L^{-1} : THR and Thiram + hydrochar: THR-HC)

was performed in quadruplicate with three independent biological replicates. Morphological endpoints included the rate of normal development, occurrence of skeletal abnormalities, and delay or arrest in embryogenesis, assessed under a Nikon Eclipse optical microscope. The experimental design also included parallel collections of embryos for subsequent metabolomic and molecular analyses, aimed at linking morphological alterations with changes in metabolic pathways and gene expression related to oxidative stress (*sod*, *cat, mt*), endocrine regulation (*dio*), and biomineralization (*msp130*, *sm30*).

5.2.5 Developmental assessment

At 72 hours post-fertilization (hpf), *Arbacia lixula* embryos at the ampol-like stages were collected from both control and exposed groups to assess developmental morphology. The swimming embryos were fixed by immersion in cold 100% methanol for 10 minutes to halt developmental progression, followed by two washes in filtered seawater (Maisano et al., 2015; Eliso et al., 2025). Fixed samples were transferred onto glass slides and examined under an inverted light microscope (Nikon Eclipse) equipped with a high-definition digital imaging system (Nikon DS-Fi3). Morphological endpoints were evaluated by comparing the structural integrity and symmetry of larval arms, body proportions, and spicule organization across treatments. For each condition, at least 300 embryos were analyzed from three independent replicates. The proportion of normally developed larvae (PNL) was calculated as the percentage of embryos reaching the expected developmental stage with correct morphology relative to the total observed. Representative micrographs were captured

and processed using NIS-Elements software (Nikon) for image standardization and documentation.

5.2.6 Metabolomic investigation

5.2.6.1 Metabolite extraction from sea urchin embryos

Metabolomic profiling was conducted on *Arbacia lixula* embryos collected at 72 hours post-fertilization (hpf) from both control and treated groups. For each condition, pools of embryos from three replicate wells were combined to obtain sufficient biomass for analysis. Extraction of polar metabolites was performed using a modified methanol/chloroform/water biphasic protocol adapted from Wu et al. (2008) and Eliso et al. (2025). Briefly, frozen embryo pellets were lysed in cold methanol (8 mL g^{-1}) and distilled water (2.5 mL g^{-1}) using an ultrasonic probe (50% amplitude, three cycles of 1 min each, on ice). After homogenization, chloroform (8 mL g^{-1}) and additional water (4 mL g^{-1}) were added to promote phase separation. The mixtures were vortexed for 30 s and kept on ice for 8 min, followed by centrifugation at 2000 × g for 5 min at 4 °C. The upper aqueous–methanolic phase, enriched in polar metabolites, was carefully collected, transferred into clean polypropylene tubes, and evaporated to dryness under vacuum (Eppendorf Concentrator 5301). The dried extracts were stored at −80 °C until analysis. The lower chloroform phase containing lipophilic components was discarded. All procedures were performed under chilled conditions to minimize metabolite degradation.

5.2.6.2 NMR-based metabolomic profiling

Before spectral acquisition, the lyophilized extracts were dissolved in 500 µL of deuterium oxide (D_2O) (Armar AG, Döttingen, Switzerland) prepared with 0.1 M sodium phosphate buffer adjusted to pH 7.0 and supplemented with 1 mM 2,2-dimethyl-2-silapentane-5-sulfonate (DSS) as the chemical-shift standard. The reconstituted solutions were transferred into 5-mm NMR tubes and analyzed on a Varian spectrometer operating at 500 MHz (^1H resonance = 499.74 MHz) and maintained at 25 °C. Spectra were acquired using a standard 1D NOESY presaturation pulse sequence for water suppression, with 256 scans, a spectral width of 11.7 ppm, and 32,768 data points. Free induction decays (FIDs) were zero-filled and Fourier-transformed to 65,536 points. All spectra were manually phase- and baseline-corrected and referenced to the DSS signal at 0.00 ppm. Spectral processing and metabolite identification were carried out using Chenomx NMR Suite (v12.0, Chenomx Inc., Edmonton, Canada). Metabolite quantification was performed by spectral fitting against the Chenomx library and confirmed through comparison with publicly available reference databases (Cappello et al., 2017). Identified metabolites were grouped according to their involvement in key biochemical pathways, including energy metabolism, amino acid turnover, and osmolyte regulation, to support biological interpretation of thiram-induced alterations.

5.2.7 Trascriptional analysis of stress-related genes

To evaluate the transcriptional effects of thiram exposure and the potential mitigating action of the algal hydrochar, gene expression profiling was performed on *Arbacia lixula* embryos collected at 72 hours post-fertilization (hpf) from the

experimental conditions (CTRL , THR, THR – HC). Total RNA was extracted from pooled embryos using the RNeasy Plus Micro Kit (Qiagen, Germany, cat. no. 74034) following the manufacturer's protocol. RNA quantity and purity were determined spectrophotometrically with a NanoDrop 2000 (Thermo Fisher Scientific), while RNA integrity was verified by electrophoresis on 1% agarose gel. Complementary DNA (cDNA) was synthesized from 1 µg of total RNA using the QuantiTec Reverse Transcription Kit (Qiagen, Germany, cat. nos. 205310) which includes genomic DNA elimination and random hexamer primers steps to ensure high quality cDNA synthesis. Quantitative real-time PCR (qPCR) assays were carried out using a QIAquant 72 2plex Real-Time PCR System (QIAGEN) and DyNAmo HS SYBR Green Master Mix (Thermo Scientific). Reactions were performed in 20 µL final volume under the following cycling conditions: 95 °C for 10 min, followed by 40 cycles of 95 °C for 15 s and 60 °C for 1 min. Each amplification included a melt-curve analysis to verify product specificity. The transcriptional levels of five target genes, msp130 and sm30 (biomineralization), dio (thyroid hormone metabolism), sod Cu/Zn and cat (oxidative stress response), were quantified. Primer sequences were either adapted from published echinoid datasets or designed de novo using Primer-BLAST based on *A. lixula* transcriptome data. Each biological condition was analyzed in triplicate, including three independent biological replicates and three technical replicates per sample. β-actin (actb) was used as reference genes for normalization. Relative expression levels were calculated using the $2^{-\Delta\Delta Ct}$ method (Livak and Schmittgen, 2001), with the control group as the calibrator. Statistical comparisons among groups were performed using one-way ANOVA followed by Dunnett's post-hoc test, with $p <$

0.05 considered statistically significant. The analysis was aimed at determining whether hydrochar treatment modulated the transcriptional alterations induced by thiram exposure, particularly those related to oxidative defense, endocrine regulation, and skeletogenic pathways.

Table 1. *Sequences of primers for the genes used.*

GENE- ID	Forward primer	Reverse primer
CAT	CCACACGCAGAAGAGGAAC	CGGTCAGAGAACAGGAAGG
SOD Cu/Zn	GCAGGAGCCATCTACACCAT	ATTGTTGGTGTGGGATCCAT
DIO 1	AAGTGGTGGATCTGCCAATTGTA	ACACCTCTGGGCAATCATGG
SM30	GACAGTGGGGCTTTCTTGAG	AACACATCGGTTTCCCTACG
MSP130	ATGGACAGGAAGTCAGGTGG	GGTGTGCTGTTTCCAGGGGC
Mt	CAAAGCCTGCCAGAAGAATG	CCGCATTTGAACACTGGATA
Act	TCAGAGCAAGAGGGGTATCC	TGTAGAAGGTGTGATGCCAGA

5.2.8 Statistical evaluation

All quantitative data are expressed as mean ± standard deviation (SD) and derive from at least three independent biological replicates. Statistical analyses were carried out to evaluate differences among experimental conditions (CTRL, THR, THR-HC). For morphological endpoints, including the percentage of normally developed larvae, statistical comparisons were conducted using one-way analysis of variance (ANOVA) followed by Tukey's post hoc test to identify significant pairwise differences ($p < 0.05$). For gene expression data, differences relative to the control condition were evaluated by one-way ANOVA followed by Dunnett's post hoc test, using the Control group as reference. A significance threshold of $p < 0.05$ was applied. Metabolomic data analysis was carried out using MetaboAnalyst 6.0 (https://www.metaboanalyst.ca). Prior to statistical analysis, data were normalized,

log-transformed, and autoscaled. Principal Component Analysis (PCA) was used as an unsupervised method to explore global metabolic patterns and sample clustering, while Partial Least Squares–Discriminant Analysis (PLS-DA) was applied as a supervised approach to support group discrimination and identify metabolites contributing to treatment-related separation. Hierarchical clustering analysis combined with heatmap visualization was performed using Euclidean distance and Ward's linkage method. Univariate statistical analysis of individual metabolites was conducted using one-way ANOVA, with $p < 0.05$ considered statistically significant. All statistical analyses were also performed using GraphPad Prism 10.0 (GraphPad Software, USA), unless otherwise specified.

5.3 Results

5.3.1 Morpho-chemical observations

Optical microscopy (Figures 1 - 2) reveals distinct morphological differences between the hydrochar before adsorption (Hydrochar-pre) and the hydrochar after exposure to thiram (Hydrochar-post). In the pre-use sample, the carbonaceous matrix appears relatively homogeneous, with smooth lignocellulosic domains and only limited surface fissuring. Darker inclusions show sharp boundaries that likely correspond to carbon-rich condensed aromatic regions formed during hydrothermal carbonization. In contrast, the post-adsorption hydrochar exhibits more irregular and enlarged dark domains, partially swollen or softened surface microregions, and the formation of discrete reaction zones around P-points (P1–P6), which were later analysed by FTIR. These morphological modifications suggest surface reactivity and micro-environmental rearrangements associated with the adsorption of thiram or its

possible degradation products. The apparition of new darkened areas in the post-sample could indicate sulfur-rich or nitrogen-containing deposits. FTIR microspectroscopy performed on multiple points of the hydrochar surface pre and post use revealed clear chemical differences between the material before and after exposure to thiram. The Hydrochar-pre spectrum is dominated by a broad O–H stretching band at ~3340 cm^{-1} and typical lignocellulosic features, including C–N/C=C vibrations at ~1638 cm^{-1}. After adsorption, the Hydrochar-post sample exhibits a noticeable enhancement of the aliphatic C–H stretching region (2800–3000 cm^{-1}), consistent with the introduction of methyl groups. The most significant change is the appearance of a strong and well-defined band in the 1200–1000 cm^{-1} region, absent or poorly expressed in the pristine material. This band is characteristic of C=S and C–S stretching modes of thiocarbamate structures and aligns with the known infrared fingerprint of thiram. The increased intensity in the 1500–1650 cm^{-1} region at selected points further suggests interactions involving thiram's C–N functionalities. Together, these spectral modifications provide direct evidence of thiram adsorption and/or deposition of its degradation products on the hydrochar surface.

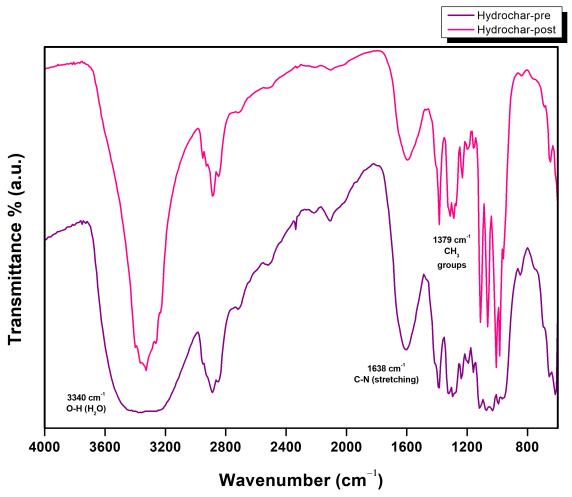


Figure 1. *FTIR microspectroscopy spectra collected from multiple points of Hydrochar-pre and Hydrochar-post.*

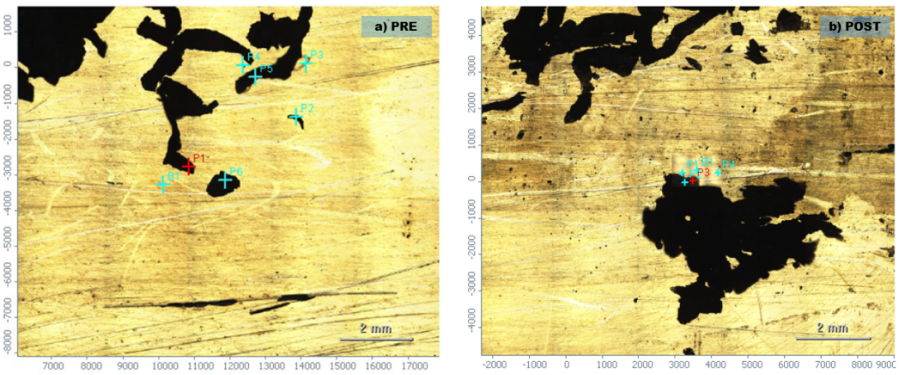


Figure 2. *Optical microscopy image of the* ***a)*** *pristine hydrochar (hydrochar-pre), and* ***b)*** *of the hydrochar after exposure to tiram (hydrochar-post). Measurement points indicate the locations selected for FTIR microspectroscopy.*

5.3.2 Developmental outcomes

At 72 hours post-fertilization (hpf), *Arbacia lixula* embryos showed distinct developmental patterns across treatments (Fig. 3). In the control group, over 85% of embryos completed normal morphogenesis, progressing to the fully developed ampol-like stages. These larvae displayed a typical bilaterally symmetrical morphology with correctly formed skeletal arms and a well-defined apical structure, confirming normal development. In contrast, exposure to thiram (30 µg L^{-1}) caused a marked deterioration in development. The percentage of normally developed larvae decreased dramatically, accompanied by a significant increase in malformed, retarded, and dead embryos. Morphological observations revealed that the most severe developmental arrest occurred at the pluteus stage, where the larvae failed to transition to the ampol-like form typical of the control group. Affected embryos often had shortened or asymmetrical arms, altered spicule organization, and

irregular skeletal calcification. The combined treatment with thiram and hydrochar significantly attenuated these effects. Embryos exposed to the hydrochar-conditioned thiram solution showed a substantial recovery in developmental progression, with most individuals reaching the pluteus or early ampol-like stage. The percentage of malformed or retarded larvae decreased considerably compared to the thiram-only group, although normal development remained slightly lower than in controls.

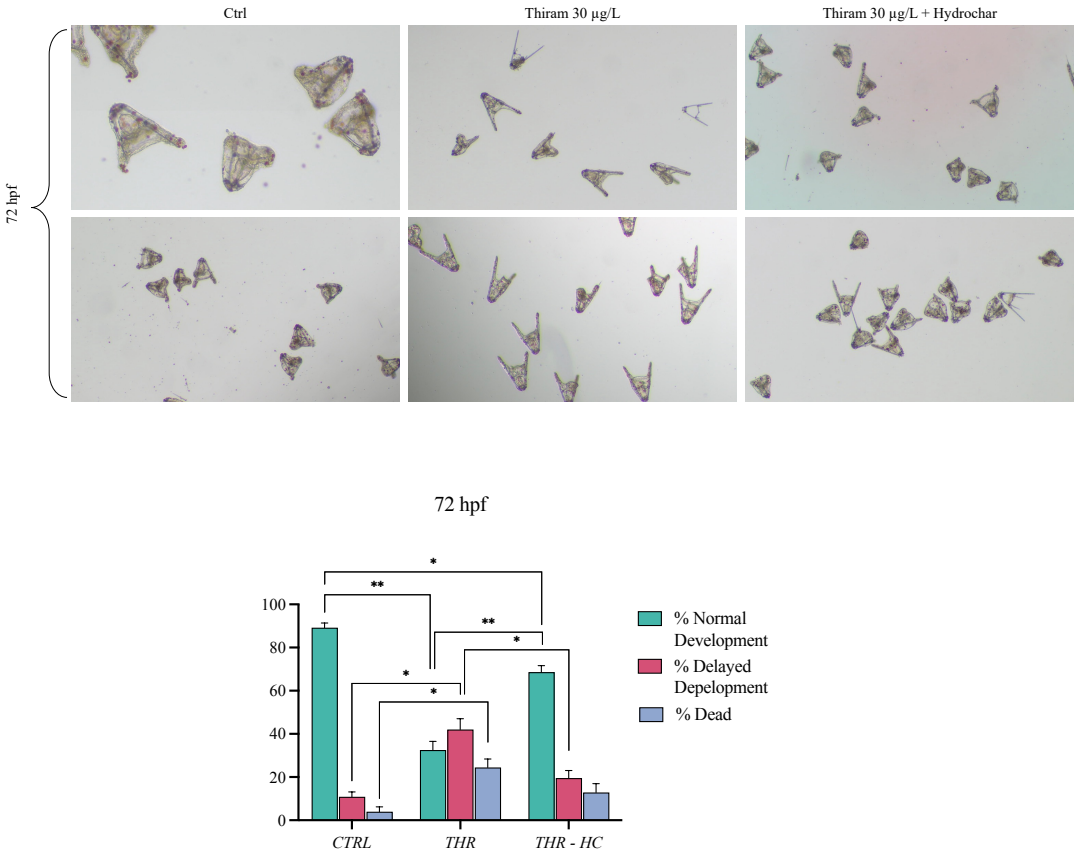


Figure 3. *Representative light microscopy images show normal larval development in control embryos, developmental arrest and skeletal abnormalities following thiram exposure (30 µg L⁻¹), and partial recovery in embryos exposed to thiram in the presence of algal-derived hydrochar. The bar graph summarizes the percentage of normally developed, developmentally delayed, and dead embryos*

*at 72 hpf. Data are presented as mean ± SD from at least three independent biological replicates. Statistical significance was assessed by one-way ANOVA followed by Tukey's post-hoc test ($p < 0.05$; *$p < 0.01$).*

5.3.3 Metabolomic response

Figure illustrates the typical ^{1}H-NMR spectral profile obtained from control samples of *Arbacia lixula* embryos. The analysis revealed a set of roughly 20 metabolite signals. Among the compounds identified were amino acids like glycine; substances involved in energy metabolism, such as lactate and glucose; neuromodulatory molecules including choline, acetylcholine, and N-acetyl serotonin; and solutes related to redox and osmotic balance, such as gluthatione, betaine and trimethylamine-N-oxide.

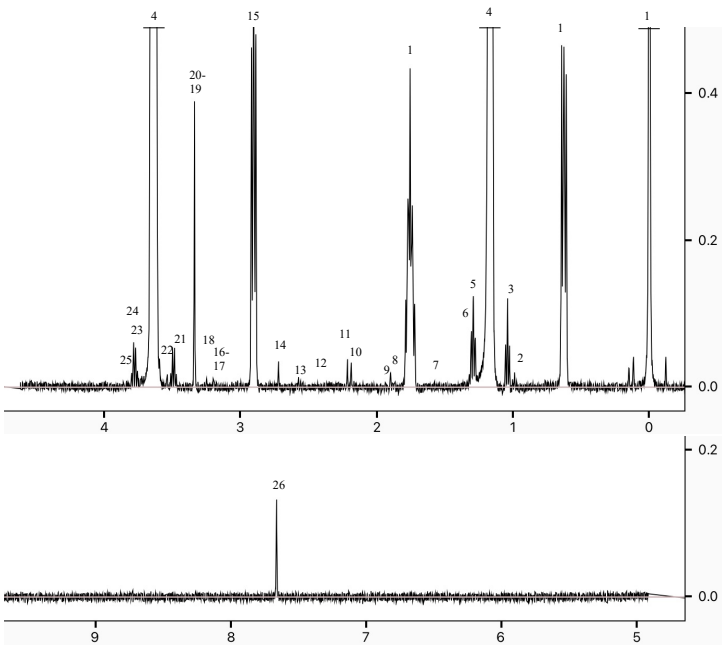


Figure 4. *Representative ^{1}H NMR spectrum acquired from embryo extracts at 72 hours post-fertilization (hpf), spectra were recorded in D_2O with DSS as internal chemical shift reference. Keys:*

(1) DSS, (2) BCAA, (3) 2-oxobutyrate, (4) ethanol, (5) lactate, (6) threonine, (7) alanine, (8) acetate, (9) arginine, (10) glutamate, (11) glutamine, (12) succinate, (13) malate, (14) citrate, (15) N-acetilserotonin, (16) choline, (17) acetylcholine, (18) tyrosine, (19) betaine, (20) trimethylamine-N-oxide (TMAO), (21) taurine, (22) glycine, (23) glucose, (24) glutathione, (25) aspartate and (26) methylhistidine.

5.3.3.1 Effects on metabolites

^{1}H NMR–based metabolomic analysis revealed significant treatment-dependent alterations in the metabolic profile of *Arbacia lixula* embryos at 72 hours post-fertilization (hpf) (Fig. 5). Clear differences were observed among control embryos, those exposed to thiram (30 μg L^{-1}), and embryos treated with thiram in the presence of algal-derived hydrochar. In embryos exposed to thiram, a generalized reduction in the levels of several polar metabolites was detected compared with controls. Metabolites associated with energy metabolism showed marked decreases, indicating impaired metabolic activity. In particular, glucose and lactate concentrations were significantly reduced in thiram-exposed embryos. Likewise, alanine and glycine, which are closely linked to energy metabolism and nitrogen turnover, exhibited lower levels relative to controls, pointing to a global metabolic downshift. Significant alterations were also observed in metabolites involved in osmotic regulation and membrane metabolism. Specifically, betaine and choline levels were reduced in thiram-treated embryos, reflecting altered osmoregulatory balance and membrane phospholipid turnover under stress conditions. In contrast, embryos exposed to thiram in the presence of algal-derived hydrochar displayed a metabolomic profile markedly different from that of the thiram-only group. For most detected metabolites, concentrations were restored toward control levels, indicating a

substantial recovery of metabolic homeostasis. Glucose, lactate, alanine, and glycine levels in the combined treatment were comparable to those measured in control embryos, while betaine and choline also showed a pronounced recovery relative to thiram exposure alone. Although minor deviations from control values persisted for selected metabolites, the overall pattern indicated a strong attenuation of thiram-induced metabolic perturbations.

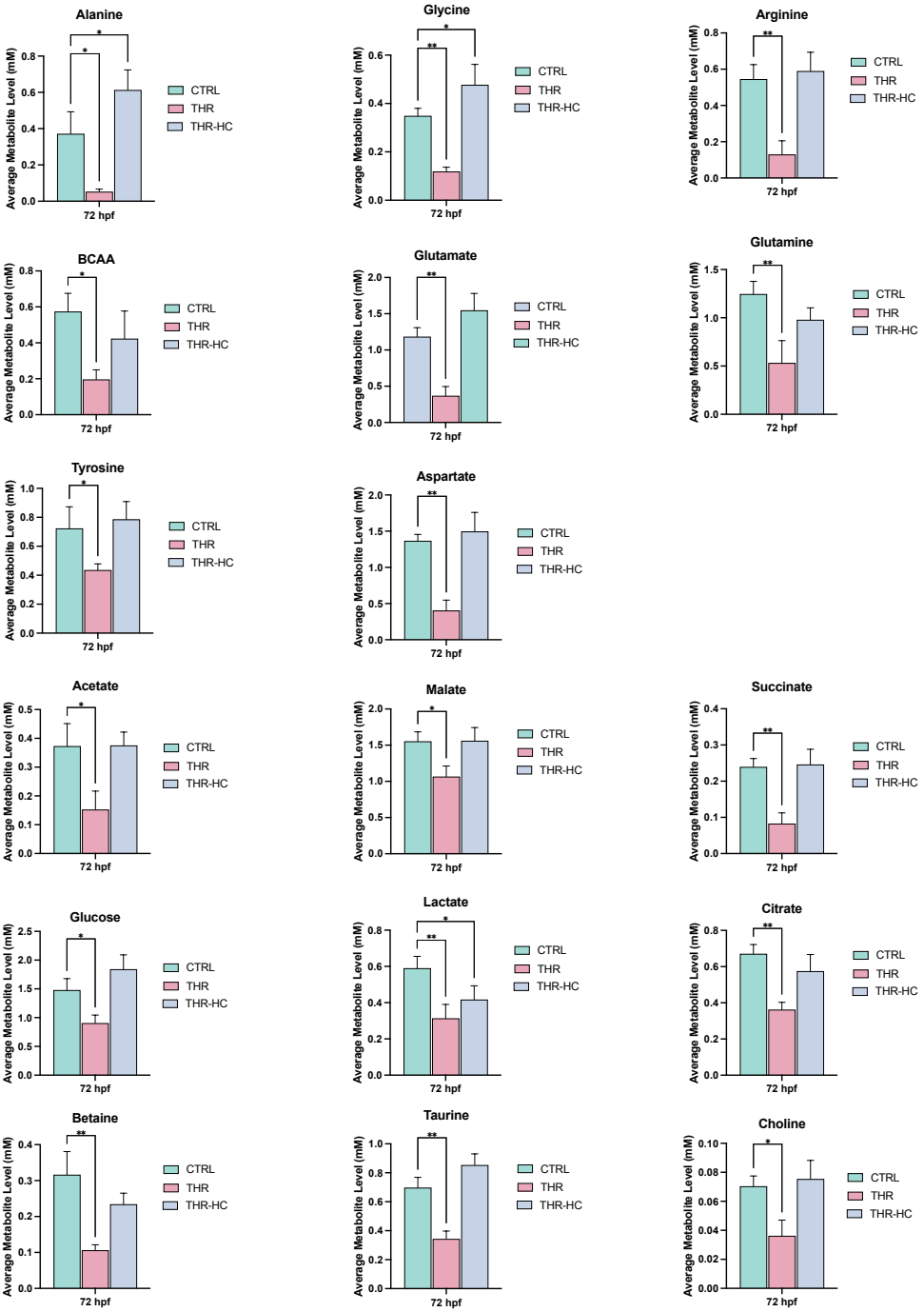


Figure 5. *Bar plots showing relative concentrations of selected polar metabolites quantified by ^{1}H NMR in Arbacia lixula embryos at 72 hours post-fertilization (hpf) under Control, Thiram (30 µg L^{-1}), and Thiram + Hydrochar conditions. Metabolites include compounds involved in energy metabolism, amino acid turnover, and osmotic regulation. Data are expressed as mean ± standard deviation (SD) from at least three independent biological replicates. Statistical differences among groups were assessed by*

one-way ANOVA followed by Dunnett's post-hoc tests; asterisks indicate significant differences compared with the control group ($p < 0.05$*).*

5.3.3.2 Multivariate metabolomic analysis

Multivariate statistical analyses were applied to the ^{1}H NMR metabolomic dataset to explore global metabolic differences among experimental groups at 72 hours post-fertilization (hpf). The unsupervised Principal Component Analysis (PCA) revealed a clear separation among control, thiram-exposed, and thiram + hydrochar embryos (Fig. 6). The first principal component (PC1) accounted for the majority of the total variance, indicating that thiram exposure represented the main source of metabolic variability. Embryos exposed to thiram clustered distinctly from controls, whereas samples from the thiram + hydrochar group were positioned closer to the control cluster, suggesting a substantial recovery of the overall metabolic profile. Hierarchical clustering analysis coupled with heatmap visualization further supported these findings (Fig. 7). The heatmap showed a consistent pattern of reduced metabolite abundance in thiram-exposed embryos, affecting metabolites involved in energy metabolism, amino acid turnover, and osmotic regulation. In contrast, embryos exposed to thiram in the presence of hydrochar displayed metabolite levels largely comparable to those of controls, with most metabolites showing a clear trend toward normalization. Hierarchical clustering grouped thiram-treated samples separately from both control and hydrochar-treated embryos, while the latter clustered closer to the control condition, confirming the mitigating effect of hydrochar at the metabolic level. To further identify the metabolites contributing most strongly to group discrimination, a supervised Partial Least Squares–Discriminant Analysis (PLS-DA) was performed

(Fig. 8). The PLS-DA biplot confirmed the separation observed in the PCA, with thiram-exposed samples clearly discriminated from controls along the first latent component, while thiram + hydrochar samples showed an intermediate-to-control-like positioning. The loading distribution highlighted energy-related metabolites (e.g., glucose, lactate, malate), amino acids involved in carbon and nitrogen metabolism (alanine, glutamate, glutamine, aspartate, arginine, branched-chain amino acids), and osmolytes (such as taurine) as the main contributors to the observed separation. These metabolites were negatively associated with thiram exposure and positively correlated with control and hydrochar-treated embryos.

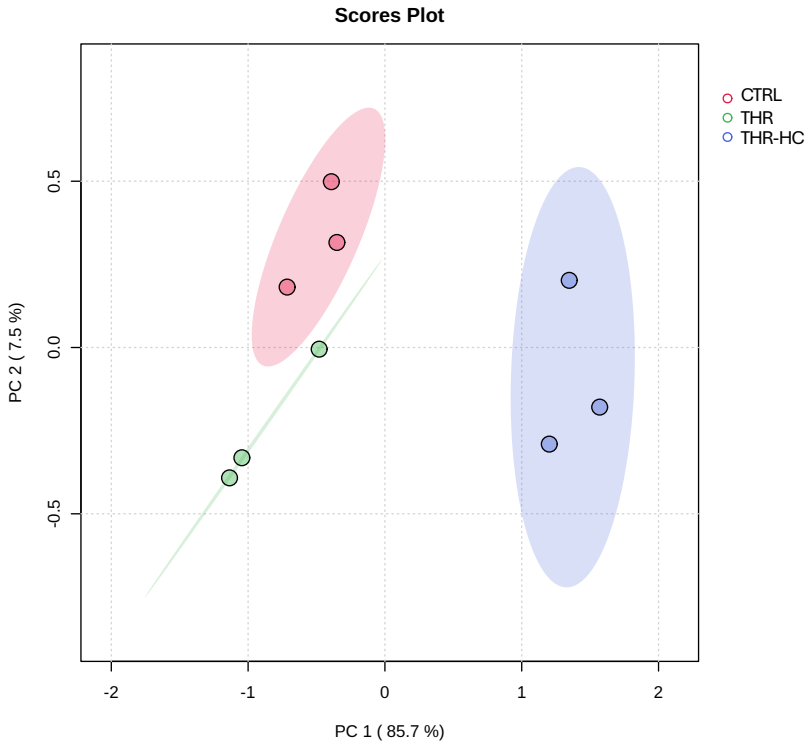


Figure 6. *Principal Component Analysis (PCA) of metabolomic profiles. PCA score plot based on ^{1}H NMR metabolomic data of Arbacia lixula embryos at 72 h post-fertilization under Control, Thiram (30 µg L^{-1}), and Thiram + Hydrochar conditions. PC1 and PC2 explain 85.7% and 7.5% of the total*

variance, respectively. Thiram-exposed samples cluster separately from controls, while hydrochar-treated samples show a clear shift toward the control metabolic profile.

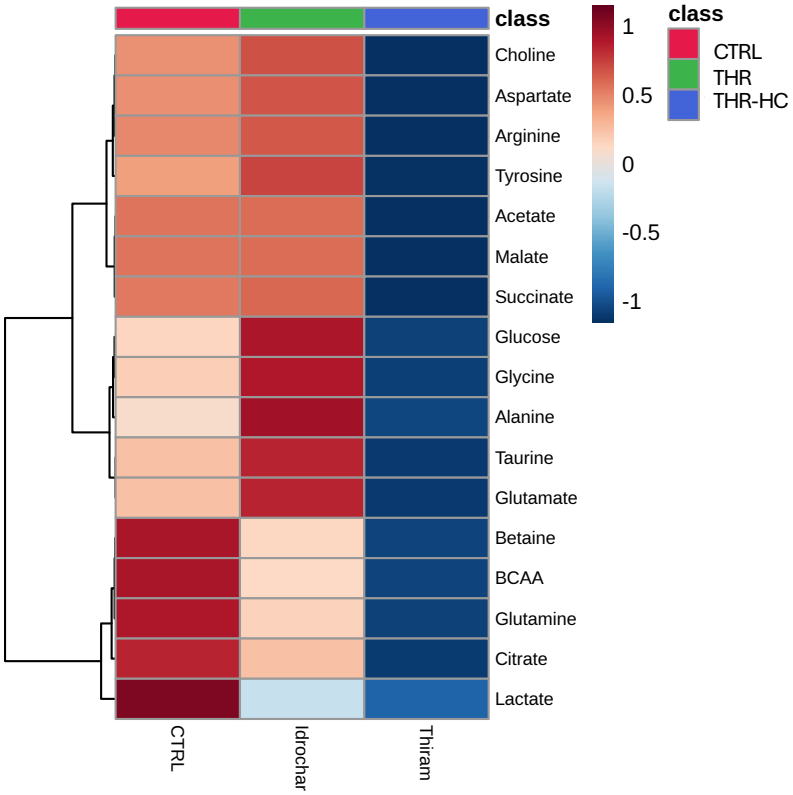


Figure 7. *Heatmap and hierarchical clustering of differential metabolites. Heatmap representing relative levels of selected polar metabolites detected by ^{1}H NMR in A. lixula embryos at 72 hpf.*

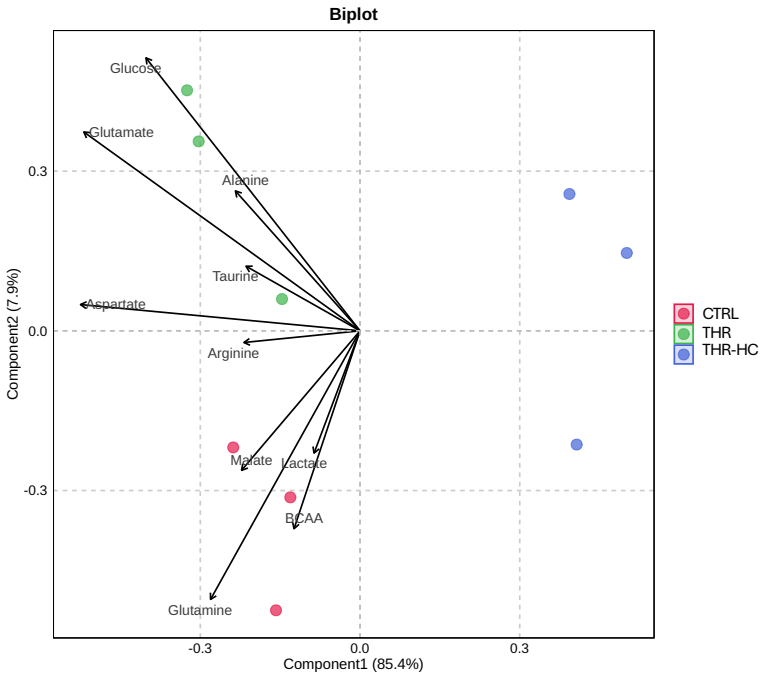


Figure 8. *PLS-DA biplot of metabolomic profiles. PLS-DA biplot based on ¹H NMR metabolomic data of Arbacia lixula embryos at 72 h post-fertilization under Control, Thiram (30 µg L⁻¹), and Thiram + Hydrochar conditions. Component 1 (85.4%) and Component 2 (7.9%) describe the main sources of variance. Vectors represent metabolites contributing to group discrimination, including energy-related metabolites, amino acids, and osmolytes.*

5.3.4 Gene expression patterns

Quantitative RT-PCR analysis revealed distinct transcriptional profiles among the experimental groups (Fig. 9). Exposure to thiram (30 µg L^{-1}) caused a significant alteration in the expression of all investigated genes compared with controls. In particular, antioxidant defence genes (sod, cat) were strongly up-regulated. Similarly, the thyroid-related deiodinase gene (dio) showed a marked increase. A comparable up-regulation trend was observed for skeletogenic genes (msp130, sm30), which are involved in spicule formation and larval arm elongation.

In parallel, metallothionein (mt) transcripts were significantly induced. In contrast, embryos exposed to the Thiram + Hydrochar treatment exhibited a clear reduction in the expression of all target genes compared with the thiram group. Levels of sod, cat, and mt decreased markedly, approaching or slightly below those of controls. Expression of dio also declined toward baseline values. Likewise, msp130 and sm30 showed a partial down-regulation relative to thiram exposure.

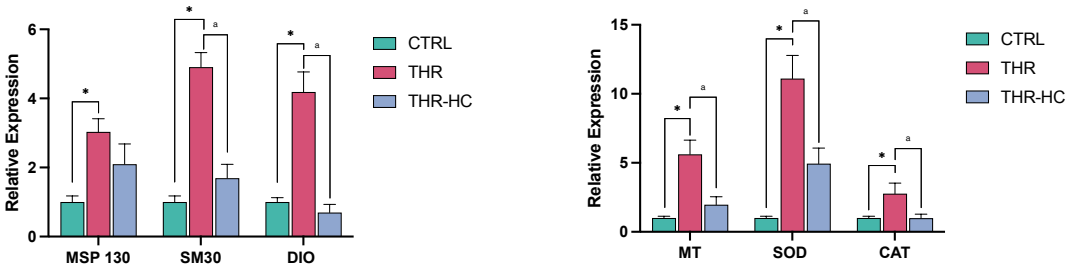


***Figure 9**. Gene expression of markers involved in oxidative stress response (*sod*, *cat*), detoxification (*mt*), thyroid hormone metabolism (*dio*), and skeletogenesis (*msp130*, *sm30*) in Arbacia lixula embryos at 72 hours post-fertilization (hpf) under Control, Thiram (30 µg L^{-1}), and Thiram + Hydrochar conditions. Data are presented as mean ± standard deviation (SD) from at least three independent biological replicates. Statistical differences among groups were evaluated by one-way ANOVA followed by Tukey's post-hoc tests; asterisks indicate statistically significant differences (*$p < 0.05$).*

5.4 Discussions

The integrated evaluation of morphological, metabolomic, and molecular endpoints provides a robust and coherent framework for elucidating both the embryotoxic effects of thiram and the mitigating role of algal-derived hydrochar in *Arbacia lixula*. By combining physicochemical characterization of the adsorbent with multi-level biological responses, this study establishes a direct link between pollutant adsorption processes and biologically meaningful detoxification. Exposure to thiram at 30 μg L^{-1} resulted in pronounced developmental impairment, as evidenced by the marked reduction in normally developed larvae and the increased incidence of delayed, malformed, or non-viable embryos. Morphological analyses identified the pluteus stage as a critical developmental bottleneck, with exposed larvae failing to progress toward the ampol-like form typical of healthy development. Similar developmental arrest at late larval stages has been reported in sea urchins and other marine invertebrates exposed to dithiocarbamates and related pesticides, highlighting the sensitivity of skeletogenesis and late morphogenetic remodelling to chemical stress (Pesando et al., 2003; Pinsino et al., 2015). The teratogenic profile observed here is consistent with previous evidence indicating that thiram and other dithiocarbamate fungicides interfere with energy-demanding developmental processes and calcium-dependent biomineralization. In particular, thiram has been shown to disrupt endocrine and metabolic pathways critical for embryonic development, leading to impaired energy homeostasis (Chen et al., 2019). Moreover, the chelating properties of dithiocarbamates toward essential metal ions, together with the high sensitivity of sea urchin skeletogenesis to chemical stress, provide a mechanistic basis for the observed defects in larval skeletal formation (Pagano et al., 1986; Bonaventura et al., 2006;

Morroni et al., 2016; Harischandra et al., 2019). At the molecular level, thiram exposure elicited a multifactorial stress response involving oxidative, endocrine, and skeletogenic pathways. The strong up-regulation of *sod* and *cat* confirms activation of antioxidant defences in response to increased reactive oxygen species (ROS), in line with the well-documented redox-disrupting properties of dithiocarbamates (Schroder et al., 2005; Ragusa et al., 2017; Belaid et al., 2020). The concomitant induction of *metallothionein (mt)* further supports the involvement of thiol-reactive and metal-binding detoxification mechanisms, as MTs are known to play a central role in buffering oxidative stress and maintaining metal homeostasis under xenobiotic exposure (Nemer et al., 1984; Russo et al., 2003; Hwang et al., 2012; Ragusa et al., 2017). In parallel, the significant increase in *dio* expression suggests disruption of thyroid-like signaling pathways, which are increasingly recognized as targets of dithiocarbamate toxicity across taxa. Altered deiodinase activity has been linked to impaired energy metabolism, developmental timing, and morphogenesis in both vertebrate and invertebrate models (Taylor et al., 2018; Masullo et al., 2021; Taylor et al., 2023; Taylor et al., 2024). Moreover, the up-regulation of the skeletogenic markers *msp130* and *sm30* likely reflects a compensatory transcriptional response to impaired spicule formation rather than effective skeletal maturation, as previously reported in sea urchin embryos exposed to metals and organic pollutants (Manzo et al., 2006; Mantranga et al., 2010; Sharma et al., 2010). Together, these transcriptional signatures portray thiram as a stressor capable of simultaneously perturbing redox balance, endocrine regulation, and biomineralization. These molecular alterations are closely mirrored by the metabolomic signatures observed under thiram exposure. The generalized depletion of polar metabolites involved in energy metabolism (e.g.,

glucose, lactate), amino acid turnover (e.g., alanine, glycine), and osmotic regulation (e.g., betaine, choline) indicates a global metabolic downshift. Similar metabolomic patterns, characterized by reduced energetic metabolites and altered osmolyte balance, have been described in marine embryos exposed to oxidative and endocrine-disrupting chemicals, reflecting mitochondrial dysfunction and altered carbon fluxes (Marsh et al., 1999; Cappello et al., 2017; Wang et al., 2019; Wang et al., 2020; Isaac et al., 2025). The clear separation of thiram-exposed embryos from controls in PCA and PLS-DA analyses further confirms that thiram profoundly reshapes the metabolic landscape during early development. A central finding of the present study is that algal-derived hydrochar significantly attenuates thiram toxicity. Physicochemical analyses revealed distinct morphological and chemical modifications of the hydrochar surface following exposure to thiram, including the appearance of FTIR bands attributable to thiocarbamate-related functional groups. These observations are consistent with previous studies demonstrating the strong affinity of hydrochars for sulfur- and nitrogen-containing organic contaminants, mediated by hydrogen bonding, π–π interactions, and surface complexation (Lucian & Fiori, 2017; Lin et al., 2023; Zhang et al., 2024; Vu et al., 2025). Importantly, this adsorption translated into a clear biological benefit. Embryos exposed to hydrochar-treated thiram solutions exhibited improved developmental outcomes, with a substantial recovery in the proportion of normally developing larvae and a reduction in skeletal abnormalities. At the molecular level, hydrochar treatment markedly attenuated the thiram-induced transcriptional stress signature, with the expression of sod, cat, mt, and dio shifting toward control levels. While direct evidence of transcriptional normalization in aquatic organisms following adsorption-based remediation remains limited, previous studies have

demonstrated that biochar- and hydrochar-based materials effectively reduce the bioavailability and biological impact of organic contaminants, thereby attenuating toxic responses in exposed biota (Haider et al., 2022; Mukherjee et al., 2022; Dong et al., 2023; Sharma et al., 2024). The metabolomic data further corroborate this protective effect. In the presence of hydrochar, metabolite levels were largely shifted toward control values, and multivariate analyses consistently positioned hydrochar-treated samples closer to controls than to thiram-exposed embryos. Although direct evidence of sorbent-mediated metabolomic normalization remains limited, previous metabolomic studies in zebrafish embryos and benthic invertebrates have shown that reduced chemical stress or contaminant removal is associated with a partial restoration of metabolic homeostasis (Huang et al., 2016; Kim et al., 2021; Ortiz-Villanueva et al., 2017; Ortiz-Villanueva et al., 2018). In parallel, adsorption-based remediation using carbonaceous materials has been demonstrated to decrease contaminant bioavailability and attenuate biological toxicity in aquatic organisms (Shirani et al., 2024), supporting the concept that chemical adsorption can effectively translate into reduced biological stress. From an ecological and applied perspective, these findings highlight the dual value of algal-derived hydrochar. Beyond acting as an efficient adsorbent for organic pollutants, algal hydrochar represents a sustainable strategy for the valorization of excess algal biomass within a circular bioeconomy framework, transforming an abundant and often problematic biological resource into a high-value material for environmental remediation (Ye et al., 2020; Arora et al., 2024). The ability of hydrochar to mitigate pesticide toxicity in early developmental stages of a sentinel marine species underscores its potential as a nature-based solution for coastal bioremediation, particularly in environments impacted by agricultural runoff.

5.5 Conclusion

This study demonstrates that thiram acts as a multifactorial embryotoxic agent, disrupting redox balance, endocrine signaling, and skeletogenesis, while algal-derived hydrochar provides an effective and environmentally compatible strategy to mitigate its impact. By integrating chemical, metabolomic, and molecular evidence, this work highlights the importance of coupling adsorption studies with ecotoxicological validation to assess real detoxification outcomes and supports the further development of hydrochar-based materials for sustainable remediation of pesticide-contaminated aquatic ecosystems.

5.6 References

Arora, N., Tripathi, S., Bhatnagar, P., Gururani, P., Philippidis, G. P., Kumar, V., Poluri, K. M., & Nanda, M. (2024). Algal-based biochar and hydrochar: A holistic and sustainable approach to wastewater treatment. *Chemical Engineering Journal, 153953*.

Belaid, C., & Sbartai, I. (2021). Assessing the effects of thiram to oxidative stress responses in a freshwater bioindicator cladoceran (*Daphnia magna*). *Chemosphere, 268*, 128808.

Bocșa, M., et al. (2023). Biochar-Based Adsorbents for Pesticides, Drugs and Other Emerging Contaminants—A Review. *Separations, 10*(10), 533.

Bonaventura, R., Poma, V., Russo, R., Zito, F., & Matranga, V. (2006). Effects of UV-B radiation on development and hsp70 expression in sea urchin cleavage embryos. Marine Biology, 149(1), 79-86.

Huang, S. S., Benskin, J. P., Chandramouli, B., Butler, H., Helbing, C. C., & Cosgrove, J. R. (2016). Xenobiotics produce distinct metabolomic responses in zebrafish larvae (Danio rerio). Environmental science & technology, 50(12), 6526-6535.

Kim, H. M., & Kang, J. S. (2021). Metabolomic studies for the evaluation of toxicity induced by environmental toxicants on model organisms. Metabolites, 11(8), 485.

Ortiz-Villanueva, E., Jaumot, J., Martínez, R., Navarro-Martín, L., Piña, B., & Tauler, R. (2018). Assessment of endocrine disruptors effects on zebrafish (Danio rerio) embryos by untargeted LC-HRMS metabolomic analysis. Science of the Total Environment, 635, 156-166.

Ortiz-Villanueva, E., Navarro-Martín, L., Jaumot, J., Benavente, F., Sanz-Nebot, V., Piña, B., & Tauler, R. (2017). Metabolic disruption of zebrafish (Danio rerio) embryos by bisphenol A. An integrated metabolomic and transcriptomic approach. Environmental pollution, 231, 22-36.

Cappello, T., Vitale, V., Oliva, S., Villari, V., Mauceri, A., Fasulo, S., & Maisano, M. (2017). Alteration of neurotransmission and skeletogenesis in sea urchin *Arbacia lixula* embryos exposed to copper oxide nanoparticles. *Comparative Biochemistry and Physiology Part C: Toxicology & Pharmacology, 199*, 20–27.

Chen, X., Fang, M., Chernick, M., Wang, F., Yang, J., Yu, Y., Zheng, N., Teraoka, H., Nanba, S., Hiraga, T., Hinton, D. E., & Dong, W. (2019). The case for thyroid disruption in early life stage exposures to thiram in zebrafish (*Danio rerio*). *General and Comparative Endocrinology, 271*, 73–81.

Cui, S., et al. (2024). Recent advances and prospects of neonicotinoid insecticides remediation in aquatic environments: occurrence, fate, and removal technologies (include biochar adsorption mechanisms). *Science of the Total Environment*.

de Souza, T. F., et al. (2024). Biochars as Adsorbents of Pesticides: Laboratory-Scale Insights and Research Needs. *ACS ES&T Water*.

Dong, M., He, L., Jiang, M., Zhu, Y., Wang, J., Gustave, W., Wang, S., & Zhang, X. (2023). Biochar for the Removal of Emerging Pollutants from Aquatic Systems: A Review. International Journal of Environmental Research and Public Health.

Haider, F. U., Hussain, A., & Tanveer, M. (2022).Biochar application for remediation of organic toxic contaminants in polluted systems. Journal of Environmental Management.

Harischandra, D. S., Ghaisas, S., Zenitsky, G., Jin, H., Kanthasamy, A., Anantharam, V., & Kanthasamy, A. G. (2019). Manganese-induced neurotoxicity: new insights into the triad of protein misfolding, mitochondrial impairment, and neuroinflammation. Frontiers in neuroscience, 13, 654.

Hwang, U. K., Park, J. S., Kwon, J. N., Heo, S., Oshima, Y., & Kang, H. S. (2012). Effect of nickel on embryo development and expression of metallothionein gene in the sea urchin (Hemicentrotus pulcherrimus).

Isaac, S., Dubosky, D., Waldron, A., Emura, N., Furze, A., Rao, K., ... & Yajima, M. (2025). Unique metabolic regulation of micromeres contributes to gastrulation in the sea urchin embryo. Nature Communications, 16(1), 7410.

Lin, Z., Wang, R., Tan, S., Zhang, K., Yin, Q., Zhao, Z., & Gao, P. (2023). Nitrogen-doped hydrochar prepared by biomass and nitrogen-containing wastewater for dye adsorption: effect of nitrogen source in wastewater on the adsorption performance of hydrochar. Journal of Environmental Management, 334, 117503.

Lucian, M., & Fiori, L. (2017). Hydrothermal Carbonization of Waste Biomass: Process Design, Modeling, Energy Efficiency and Cost Analysis. *Energies, 10*(2), 211.

Maisano, M., Cappello, T., Natalotto, A., Vitale, V., Parrino, V., Giannetto, A., ... & Fasulo, S. (2017). Effects of petrochemical contamination on caged marine mussels using a multi-biomarker approach: Histological changes, neurotoxicity and hypoxic stress. *Marine environmental research*, *128*, 114-123.

Marsh, A. G., Leong, P. K., & Manahan, D. T. (1999). Energy metabolism during embryonic development and larval growth of an Antarctic sea urchin. Journal of Experimental Biology, 202(15), 2041-2050.

Masullo, T., Biondo, G., Natale, M. D., Tagliavia, M., Bennici, C. D., Musco, M., ... & Nicosia, A. (2021). Gene expression changes after parental exposure to metals in the sea urchin affect timing of genetic programme of embryo development. Biology, 10(2), 103.

Matranga, V., Zito, F., Costa, C., Bonaventura, R., Giarrusso, S., & Celi, F. (2010). Embryonic development and skeletogenic gene expression affected by X-rays in the Mediterranean sea urchin Paracentrotus lividus. Ecotoxicology, 19(3), 530-537.

Morroni, L. (2016). Toxicological effects of metals on embryo development in sea urchin: applicative perspectives for ecotoxicological assessment criteria in harbor areas.

Mukherjee, S., Lal, R., Zimmerman, A. R., & Harris, W. (2022). Biochar–microorganism interactions for organic pollutant removal and toxicity reduction. Environmental Pollution, 304(Pt A), 119609.

Nemer, M., Travaglini, E. C., Rondinelli, E., & D'Alonzo, J. (1984). Developmental regulation, induction, and embryonic tissue specificity of sea urchin metallothionein gene expression. Developmental biology, 102(2), 471-482.

Pagano, G., Cipollaro, M., Corsale, G., Esposito, A., Ragucci, E., Giordano, G. G., & Trieff, N. M. (1986). The Sea Urchin: Bioassay for the Assessment of Damage from. In Community Toxicity Testing: A Symposium (No. 920, p. 66). ASTM International.

Pesando, D., Huitorel, P., Dolcini, V., Angelini, C., Guidetti, P., & Falugi, C. (2003). Biological targets of neurotoxic pesticides analysed by alteration of developmental events in the Mediterranean sea urchin, Paracentrotus lividus. Marine environmental research, 55(1), 39-57.

Pinsino, A., & Matranga, V. (2015). Sea urchin immune cells as sentinels of environmental stress. Developmental & Comparative Immunology, 49(1), 198-205.

Ragusa, M. A., Costa, S., Cuttitta, A., Gianguzza, F., & Nicosia, A. (2017). Coexposure to sulfamethoxazole and cadmium impairs development and attenuates transcriptional response in sea urchin embryo. Chemosphere, 180, 275-284.

Ragusa, M. A., Nicosia, A., Costa, S., Cuttitta, A., & Gianguzza, F. (2017). Metallothionein gene family in the sea urchin Paracentrotus lividus: gene structure, differential expression and phylogenetic analysis. International journal of molecular sciences, 18(4), 812.

Regoli, F., & Giuliani, M. E. (2014). Oxidative pathways of chemical toxicity and oxidative stress biomarkers in marine organisms. *Marine Environmental Research, 93*, 106–117.

Russo, R., Bonaventura, R., Zito, F., Schröder, H. C., Müller, I., Müller, W. E., & Matranga, V. (2003). Stress to cadmium monitored by metallothionein gene induction in Paracentrotus lividus embryos. Cell Stress & Chaperones, 8(3), 232.

Schröder, H. C., Janipour, N., Müller, W. E. G., Di Bella, G., Bonaventura, R., Russo, R., & Matranga, V. (2005). DNA damage and developmental defects after exposure to UV and heavy metals in sea urchin cells and embryos compared to other invertebrates. Echinodermata, 111-137.

Sharma, T., & Ettensohn, C. A. (2010). Activation of the skeletogenic gene regulatory network in the early sea urchin embryo. Development, 137(7), 1149-1157.

Sharma, H. B., Vanapalli, K. R., Bhatia, D., Singh, S., Arora, G., Panigrahi, S., ... & Mohanty, B. (2024). Engineered biochar/hydrochar derived from organic wastes for energy, environmental, and agricultural applications. Clean Technologies and Environmental Policy, 26(12), 4059-4093.

Shirani, Z., Carrasco-Navarro, V., Majlesi, S., Yli-Pirilä, P., Kukkonen, J. V. K., & Akkanen, J. (2024). Efficiency and ecotoxicity of activated biochar in the treatment of wastewater contaminated by pharmaceuticals. Journal of Environmental Management, 371, 123224.

Taylor, E. (2024). Thyroid hormones regulate skeletogenesis and metamorphosis in diverse echinoderms (sea urchins, sea stars, and brittle stars) (Doctoral dissertation, University of Guelph).

Taylor, E., & Heyland, A. (2018). Thyroid hormones accelerate initiation of skeletogenesis via MAPK (ERK1/2) in larval sea urchins (Strongylocentrotus purpuratus). Frontiers in Endocrinology, 9, 439.

Taylor, E., Wynen, H., & Heyland, A. (2023). Thyroid hormone membrane receptor binding and transcriptional regulation in the sea urchin Strongylocentrotus purpuratus. Frontiers in Endocrinology, 14, 1195733.

Vu, T. M., Nguyen, T. M. P., Van, H. T., Le, N. T., & Tran, D. T. (2025). Biomass-derived hydrochar and activated carbon in pharmaceutical pollution mitigation: a comprehensive overview. RSC advances, 15(50), 43053-43084.

Wang, H., Ding, J., Ding, S., & Chang, Y. (2019). Metabolomic changes and polyunsaturated fatty acid biosynthesis during gonadal growth and development in the

sea urchin Strongylocentrotus intermedius. Comparative Biochemistry and Physiology Part D: Genomics and Proteomics, 32, 100611.

Wang, H., Ding, J., Ding, S., & Chang, Y. (2020). Integrated metabolomic and transcriptomic analyses identify critical genes in eicosapentaenoic acid biosynthesis and metabolism in the sea urchin Strongylocentrotus intermedius. Scientific Reports, 10(1), 1697.

Xiang, L., et al. (2022). Integrating Biochar, Bacteria, and Plants for Sustainable Soil Remediation: Mechanisms and Applications. Environmental Science & Technology, 56(1), 239–257.

Ye, H., He, Y., Xie, Y., Sen, B., & Wang, G. (2020). Fed-batch fermentation of mixed carbon source significantly enhances the production of docosahexaenoic acid in Thraustochytriidae sp. PKU# Mn16 by differentially regulating fatty acids biosynthetic pathways. Bioresource technology, 297, 122402.

Zhang, Y., Wan, Y., Zheng, Y., Yang, Y., Huang, J., Chen, H., ... & Gao, B. (2024). Hydrochar loaded with nitrogen-containing functional groups for versatile removal of cationic and anionic dyes and aqueous heavy metals. Water, 16(23), 3387.

CHAPTER 6

Hydrochar-Mediated rescue of thiram-induced developmental, metabolic, and thyroid disorders in Zebrafish (Danio rerio)

6.1 Introduction

Hydrothermal carbonization (HTC) has emerged in recent years as a promising and sustainable thermochemical strategy for the conversion of wet biomass into value-added carbonaceous materials. Operating in aqueous media under moderate temperatures and autogenous pressure, HTC enables the direct processing of high-moisture feedstocks without the need for energy-intensive drying or chemical activation steps (Fang et al., 2018; Leong et al., 2021; Leng et al., 2020). Through a sequence of hydrolysis, dehydration, decarboxylation, and condensation reactions, raw biomass is transformed into a carbon-rich solid product, referred to as hydrochar, alongside a liquid fraction enriched in soluble organic compounds and nutrients (Lucian & Fiori, 2017; Baccile et al., 2020). Hydrochars produced via HTC typically exhibit heterogeneous surfaces, high porosity, and a high density of oxygen-containing functional groups (e.g., –COOH, –OH, –C=O), which collectively promote strong physicochemical interactions with a wide range of organic and inorganic contaminants (Lucian & Fiori, 2017; Baccile et al., 2020). These properties make hydrochars attractive candidates for applications in environmental remediation, particularly as low-cost and renewable adsorbents. Compared with conventional activated carbons, HTC-derived materials offer additional advantages in terms of feedstock flexibility, reduced processing energy, and compatibility with circular economy principles. Among the various biomass sources suitable for HTC, algal biomass has attracted growing attention. Algae are characterized by rapid growth rates, high photosynthetic efficiency, and an intrinsic ability to assimilate nutrients and CO_2 from aquatic environments, including wastewater streams (Shahid et al., 2020; Khan et al., 2018; Wang et al., 2024). Algal biomass encompasses a phylogenetically diverse group of

photosynthetic organisms, ranging from microalgae to macroalgae, and is typically rich in proteins, polysaccharides, lipids, and heteroatoms such as nitrogen and sulfur. These compositional features favor heteroatom doping during carbonization, enhancing surface reactivity and adsorption capacity in the resulting hydrochars (Benavente et al., 2022; Jansson et al., 2022). In eutrophic and dystrophic aquatic environments, excessive algal proliferation often leads to the seasonal accumulation of large quantities of biomass, which negatively impacts water quality, biodiversity, aquaculture, and tourism. While traditionally regarded as waste requiring costly removal and disposal, this surplus biomass can be reinterpreted as a renewable resource within a circular bioeconomy framework (Yap et al., 2021; Vishwakarma et al., 2022; Sun et al., 2023). Several studies have demonstrated that hydrochars derived from algal feedstocks are effective in removing dyes (Hong et al., 2020), pharmaceuticals (Petrovic et al., 2024; Hayoun et al., 2022), antibiotics (Li et al., 2021), and heavy metals (Zhao et al., 2022) from aqueous matrices. Moreover, the HTC process operates under relatively mild conditions, generates limited emissions, and allows for the potential valorization of the liquid fraction, further strengthening its sustainability profile (Bevan et al., 2020; Masek et al., 2019; Buss et al., 2021). Within this context of sustainable materials development, the application of algal-derived hydrochars to the remediation of pesticide-contaminated waters represents a particularly relevant yet still underexplored opportunity. Pesticides constitute one of the most widespread classes of anthropogenic contaminants, exerting persistent pressure on aquatic ecosystems due to their chemical stability, potential for bioaccumulation, and toxicity toward non-target organisms (Regoli & Giuliani, 2014; Salam et al., 2020). Agricultural runoff and diffuse pollution frequently result in the

presence of pesticide residues in surface waters, creating scenarios of chronic exposure for aquatic biota. Among pesticide classes, dithiocarbamate fungicides have raised increasing concern. Tetramethylthiuram disulfide (thiram), widely used for seed treatment and crop protection, is of particular interest due to its documented ability to interfere with redox balance, endocrine signaling, and neural function in aquatic organisms (Vasamsetti et al., 2022; Kim et al., 2021; Tang et al., 2023; Zhang et al., 2023, 2024). Dithiocarbamates are known to disrupt oxidative homeostasis and thyroid-related pathways, leading to developmental impairments across vertebrate and invertebrate models (Bjørge et al., 1996; Zhou et al., 2019; Yang et al., 2020). Their frequent detection in surface waters near agricultural areas highlights the ecological relevance of long-term exposure to sublethal concentrations. Early life stages are particularly vulnerable to such contaminants. Thiram has been shown to act as a multifactorial toxicant, inducing oxidative stress, endocrine disruption, and developmental abnormalities even at environmentally realistic concentrations. These effects underscore the limitations of conventional water treatment strategies, such as coagulation–flocculation, advanced oxidation, and membrane filtration, which are often associated with high operational costs, incomplete removal, or the formation of secondary toxic by-products (Gao et al., 2022; Liu et al., 2021). In contrast, adsorption-based approaches using renewable, biomass-derived carbonaceous materials have emerged as energy-efficient and low-impact alternatives (Hayoun et al., 2022; Nguyen et al., 2021). However, despite the growing body of literature on algal hydrochars, their application to pesticide remediation remains limited, and few studies have coupled chemical removal with ecotoxicological validation. This represents a critical gap, as effective remediation should not only reduce contaminant concentrations but

also demonstrably mitigate biological toxicity (Gallego-Ramírez et al., 2025; Rubio-Clemente et al., 2023). In this framework, the present study investigates the potential of hydrochar derived from waste algal biomass as a sustainable adsorbent for the fungicide thiram. The work integrates physicochemical characterization with biological assessment using zebrafish (*Danio rerio*) embryos, a well-established vertebrate model in aquatic toxicology. Owing to its rapid development, optical transparency, and sensitivity to chemical stressors, zebrafish provides a robust platform to evaluate developmental and sublethal toxicity. By combining adsorption performance with biological endpoints, this study aims to assess not only contaminant removal but also effective detoxification, supporting the use of algal-derived hydrochar as an eco-friendly material for pesticide mitigation within a circular bioeconomy perspective.

6.2 Material and methods

6.2.1. Preparation of hydrochar-based systems

Biomass of the green macroalga Chaetomorpha aerea (Chlorophyta) was sampled from the coastal lagoon of Lake Ganzirri (Messina, Italy; 38°15′47.6″ N, 15°37′34.2″ E). After collection, the algal material was repeatedly washed with tap water followed by distilled water to eliminate adhering sediments, epiphytes, and residual salts. The cleaned biomass was first air-dried at ambient conditions and subsequently dried in a ventilated oven at 60 °C until a stable mass was achieved. The dehydrated material was then mechanically milled and sieved to obtain a homogeneous powder with particle size below 1 mm, which was used as precursor for hydrothermal carbonization. Hydrothermal carbonization was performed in a laboratory-scale batch reactor

consisting of a 300 mL stainless-steel autoclave (Parr Instrument Company, IL, USA) fitted with a Teflon-lined internal vessel. For each experiment, approximately 1 g of algal powder was dispersed in 150 mL of deionized water, corresponding to a solid-to-liquid ratio of about 1:150. The reactor was hermetically closed and heated to 240 °C, allowing pressure to build up autogenously. The system was maintained at the target temperature for 3 h, while continuous stirring (600 rpm) ensured adequate mixing of the biomass slurry. The internal temperature was continuously monitored via a thermocouple connected to the reactor control unit. Upon completion of the reaction time, the autoclave was left to cool naturally to room temperature. The resulting suspension was then processed to separate the solid and liquid phases by vacuum filtration using a Büchner apparatus equipped with Whatman No. 1 filter paper. The recovered solid fraction, corresponding to the hydrochar, was repeatedly rinsed with warm distilled water until neutral pH was reached, in order to remove residual soluble compounds. The hydrochar used in this study was previously characterized in terms of morphology and surface chemistry. The washed hydrochar was subsequently dried at 60 °C overnight and weighed, resulting in a final dry mass of 0.9764 g.

6.2.2 Preparation of thiram solutions and exposure conditions

Thiram exposure solutions were freshly prepared starting from a concentrated stock of tetramethylthiuram disulfide (analytical grade, Sigma-Aldrich), dissolved in dimethyl sulfoxide (DMSO) to ensure complete solubilization. The stock solution was subsequently diluted with embryo medium to obtain a nominal thiram concentration of 5 μg L^{-1}. This concentration was selected based on previous ecotoxicological

studies reporting measurable sublethal and developmental effects in aquatic organisms at low microgram-per-liter levels, thereby representing an environmentally relevant exposure scenario. Solvent controls were prepared in parallel, containing the same final DMSO concentration as treated samples, which never exceeded 0.01% (v/v). To investigate the ability of the hydrochar to reduce thiram bioavailability and toxicity, a known amount of hydrochar was added to the thiram-containing medium and maintained under constant magnetic agitation to promote contact between the sorbent and the pesticide. The adsorption step was performed at room temperature (22 ± 1 °C) for 90 minutes. At the end of the incubation period, the suspension was filtered to remove the solid phase, yielding a clarified aqueous solution. Both the hydrochar-treated thiram solution and the untreated thiram solution were subsequently employed for exposure experiments on *Danio rerio* embryos, allowing a direct comparison of developmental and toxicological outcomes and providing an integrated assessment of chemical removal efficiency and biological detoxification.

6.2.3 Zebrafish husbandry and breeding conditions

Adult wild-type *Danio rerio* (approximately 6 months of age) were maintained at the Zebrafish facility of the Institute for Experimental, Comparative, Forensic and Aquatic Pathology “Slavko Bambir”, Department of Chemical, Biological, Pharmaceutical and Environmental Sciences, University of Messina. Fish were housed in an automated Stand-Alone recirculating system (Zebtec Multilinking System, Tecniplast, Buguggiate, VA, Italy) under controlled environmental conditions, including a 14:10 h light/dark photoperiod. Water parameters were maintained at 28 °C, pH 7.2, conductivity of 700 µS/cm, and dissolved oxygen concentration of 6.00 ppm. Animals

were fed twice daily with a combination of commercial dry feed and live Artemia salina, administered at 3% of body weight.

6.2.4 Embryo collection and exposure protocol

Zebrafish embryos were collected the day after breeding and selected under a stereomicroscope (Leica M205C, Leica Microsystems Srl, Buccinasco, Italy). Exposure solutions were prepared using standard embryo medium (E3), composed of 15 mM NaCl, 0.5 mM KCl, 1 mM $CaCl_2$, 1 mM $MgSO_4$, 0.15 mM KH_2PO_4, 0.05 mM Na_2HPO_4, and 0.7 mM $NaHCO_3$, adjusted to pH 7.3. Viable embryos were exposed to thiram (5 μg L^{-1}), hydrochar alone, thiram adsorbed onto hydrochar, and incubated at 28 °C under a 14:10 h light/dark photoperiod until 120 hpf. All experiments involving zebrafish embryos and larvae were conducted without ethical authorization, as zebrafish up to 120 hpf are not classified as protected animals according to Directive 2010/63/EU and its transposition into Italian law (D.lgs. 26/2014). Breeding was performed by pairing sexually mature adults in a 2 female:1 male ratio to promote successful reproduction. Spawning occurred naturally following the onset of the light phase. For all experimental analyses performed at 24, 72, 96, and 120 hpf, one-third of the exposure medium was replaced daily. Fresh exposure solutions were prepared prior to each renewal to ensure consistent experimental conditions throughout the exposure period.

6.2.5 Zebrafish Embryo Acute Toxicity Test (ZFET)

The Zebrafish Embryo Acute Toxicity Test (ZFET) was conducted following OECD guideline No. 236 (OECD, 2013) to evaluate the acute and developmental toxicity of thiram. All validity criteria required by the guideline were satisfied. Fertilized embryos were individually placed into 96-well plates (one embryo per well) containing the

respective exposure media (THR: thiram at 5 μg L^{-1}, HC: hydrochar alone, and THR-HC: thiram adsorbed onto hydrochar). Each experimental condition consisted of 20 embryos per plate, performed in triplicate. Control embryos were maintained in E3 medium only. Embryos were incubated at 26 °C under a 14:10 h light/dark photoperiod. According to OECD recommendations, embryos were inspected every 24 h to assess apical lethal endpoints, including embryo coagulation, absence of somite formation, failure of tail detachment, and lack of heartbeat (Capparucci et al., 2022).

6.2.6 Analysis of developmental phenotypes

Morphological evaluations were performed to assess developmental alterations induced by thiram exposure and to determine the potential mitigation effects of hydrochar-treated solutions. Embryos and larvae were examined at defined developmental stages (24, 48, 72, and 96 h post-fertilization, hpf) using an inverted light microscope equipped with a digital imaging system. Observations were conducted on live specimens maintained in embryo medium under controlled temperature conditions (26 ± 1 °C). A standardized set of morphological endpoints was recorded following internationally accepted criteria for zebrafish developmental toxicity testing (De Marco et al., 2022; Missawi et al 2021; Vignet et al 2019). These endpoints included overall growth delay, abnormal body axis curvature, craniofacial malformations, yolk sac and pericardial edema, tail deformities, impaired somite development, and alterations in pigmentation patterns. Hatching success and timing were also documented as indicators of developmental progression. Quantitative morphometric measurements were performed on digital images using ImageJ software. Total body length, yolk sac area, and pericardial area were measured to provide objective indicators of growth and edema severity. All measurements were

carried out on at least 10 embryos or larvae per replicate and per treatment group, ensuring adequate statistical robustness. Morphological abnormalities were classified and scored based on their severity, and results were expressed as the percentage of affected individuals per treatment group. Embryos exhibiting coagulation, lack of heartbeat, or complete developmental arrest were excluded from morphometric analyses and recorded separately as lethal endpoints. All morphological assessments were performed in a blinded manner to minimize observer bias. The collected data provided an integrated evaluation of both lethal and sublethal developmental effects, allowing comparison between untreated thiram-exposed groups and embryos exposed to hydrochar-treated solutions, thereby supporting the assessment of detoxification efficacy.

6.2.7 Metabolomic investigation

6.2.7.1 Extraction of polar metabolites

Metabolomic analyses were performed on *Danio rerio* embryos collected at 96 hours post-fertilization (hpf) from control, thiram-exposed, and hydrochar-treated groups. For each experimental condition, embryos from three independent replicate wells were pooled to obtain a sufficient amount of biological material and to reduce intra-group variability. Embryos were briefly rinsed with ice-cold embryo medium to remove residual exposure solutions, excess liquid was carefully removed, and samples were immediately snap-frozen in liquid nitrogen. Frozen samples were stored at −80 °C until extraction. For metabolite extraction, pooled embryo samples were transferred into pre-chilled 2 mL polypropylene tubes. Polar metabolites were extracted using a cold biphasic solvent system based on methanol, chloroform, and water, optimized for small aquatic embryos. Initially, 800 µL of ice-cold methanol were added to each

frozen sample, followed by 250 µL of ultrapure water. Samples were vortex-mixed for 30 s to ensure complete solvent penetration and protein precipitation. Cell disruption was achieved by probe sonication using an ultrasonic homogenizer set at 50% amplitude. Sonication was performed on ice in three cycles of 40 s each, with 30 s cooling intervals between cycles, to prevent sample overheating and metabolite degradation. After homogenization, 800 µL of chloroform were added to each tube, followed by an additional 400 µL of ultrapure water to promote phase separation. Samples were vortexed vigorously for 30 s and incubated on ice for 10 min. Phase separation was obtained by centrifugation at 2,000 × g for 5 min at 4 °C (Eliso et al., 2025). This procedure resulted in the formation of three distinct layers: an upper aqueous–methanolic phase containing polar metabolites, a lower organic phase enriched in lipophilic compounds, and an interfacial proteinaceous layer. The upper phase was carefully collected using glass Pasteur pipettes, transferred into clean tubes, and immediately subjected to solvent removal. Drying was performed under reduced pressure using a vacuum concentrator operated at ambient temperature until complete solvent evaporation. The resulting dried metabolite extracts were sealed and stored at −80 °C until further analysis. The organic phase and protein interphase were discarded, as the present study focused exclusively on polar metabolites related to energy metabolism, amino acid turnover, osmotic regulation, and stress-responsive pathways. All extraction steps were carried out under chilled conditions, and samples were processed in randomized order to minimize batch effects and preserve metabolite integrity (Vignet et al 2019).

6.2.7.2 ^{1}H NMR metabolic profiling

Prior to nuclear magnetic resonance (NMR) analysis, dried polar metabolite extracts were re-dissolved in 500 µL of deuterated aqueous solution prepared with deuterium oxide (D_2O; Armar AG, Döttingen, Switzerland). The reconstitution medium was supplemented with 0.1 M sodium phosphate buffer to stabilize the pH at 7.0 and with 1 mM 2,2-dimethyl-2-silapentane-5-sulfonate (DSS), used as both a chemical shift reference and quantitative internal standard. Samples were gently vortexed until complete dissolution and then centrifuged briefly to remove any insoluble particles. The clarified solutions were transferred into standard 5 mm NMR tubes and analyzed using a 500 MHz Varian NMR spectrometer operating at a proton resonance frequency of 499.74 MHz. All measurements were carried out at a controlled temperature of 25 °C. One-dimensional ^{1}H-NMR spectra were acquired using a NOESY-based presaturation pulse sequence to efficiently suppress the residual water signal. Acquisition parameters included 256 transients, a spectral window of 11.7 ppm, and a data size of 32,768 points. Following acquisition, free induction decays were zero-filled to 65,536 points prior to Fourier transformation. Spectra were subsequently subjected to manual phase adjustment and baseline correction to ensure optimal signal quality. Chemical shift calibration was performed by setting the DSS singlet to 0.00 ppm. Spectral interpretation, metabolite identification, and quantification were conducted using Chenomx NMR Suite software (version 11.1; Chenomx Inc., Edmonton, Canada). Metabolites were identified by matching experimental signals with reference spectral libraries and further verified through comparison with publicly available NMR databases. Quantification was achieved through targeted spectral deconvolution relative to the DSS internal standard. Identified metabolites were

subsequently classified into major biochemical categories, including energy metabolism, amino acid metabolism, and osmolyte regulation, to facilitate biological interpretation of metabolic alterations associated with thiram exposure and hydrochar-mediated mitigation.

6.2.7.3 Pathway and network analysis

Pathway enrichment analysis was performed to identify metabolic pathways significantly affected by the experimental treatments based on the ^{1}H-NMR–derived polar metabolomic data. Metabolites showing significant alterations among experimental conditions were selected and annotated according to zebrafish-specific metabolic pathways using the Kyoto Encyclopedia of Genes and Genomes (KEGG) database. Enrichment and pathway analyses were carried out using MetaboAnalyst (web-based platform), employing the zebrafish (*Danio rerio)* pathway library. An over-representation analysis (ORA) approach was applied to evaluate whether specific metabolic pathways were represented more frequently than expected by chance within the list of altered metabolites. Statistical significance was assessed using the appropriate enrichment test implemented in MetaboAnalyst, and pathways with $p < 0.05$ were considered significantly enriched. For visualization, enriched pathways were ranked according to their statistical significance and enrichment ratio and displayed using a bubble plot, in which the x-axis represents the −log10(p-value), bubble size reflects the enrichment ratio, and color intensity indicates statistical significance. In addition, a network-based pathway visualization was generated in MetaboAnalyst to explore functional relationships among enriched pathways. In this network, nodes represent individual metabolic pathways, while edges indicate shared

metabolites between pathways, highlighting pathway interconnectivity and coordinated metabolic perturbations. All enrichment and network analyses were performed using zebrafish-specific KEGG annotations to ensure biological relevance to the experimental model.

6.2.8 Gene Expression analysis of endocrine and stress markes

To characterize the transcriptional effects induced by thiram exposure and to evaluate the potential modulatory role of algal-derived hydrochar, gene expression analyses were performed on *Danio rerio* embryos collected at 96 hours post-fertilization (hpf). Embryos were sampled from three experimental conditions: untreated controls, thiram-exposed embryos (5 μg L^{-1}), and embryos exposed to thiram after hydrochar treatment. For each condition, embryos from independent replicates were pooled to obtain sufficient material for molecular analyses and to reduce inter-sample variability. Total RNA was extracted using the RNeasy Plus Micro Kit (Qiagen, Germany, cat. no. 74034), which includes a genomic DNA eliminator column to prevent DNA contamination. The extraction procedure was carried out following the manufacturer's instructions, ensuring high RNA purity from small biological samples. RNA concentration and purity were assessed spectrophotometrically by measuring absorbance ratios at 260/280 nm and 260/230 nm using a NanoDrop™ system, while RNA integrity was verified by electrophoretic separation on 1% agarose gels. Complementary DNA (cDNA) synthesis was performed starting from 1 μg of total RNA using the QuantiTect Reverse Transcription Kit (Qiagen, Germany, cat. no. 205310). This system includes an optimized genomic DNA removal step followed by reverse transcription using a mixture of random hexamer primers, allowing efficient

and unbiased conversion of RNA into high-quality cDNA. The resulting cDNA samples were diluted appropriately and stored at −20 °C until further analysis. Quantitative real-time PCR (qPCR) analyses were carried out using a QIAquant 72 2plex Real-Time PCR System (QIAGEN) and DyNAmo™ HS SYBR Green Master Mix (Thermo Scientific). Amplification reactions were prepared in a final volume of 20 µL, containing SYBR Green master mix, gene-specific primers, and diluted cDNA template. Thermal cycling conditions consisted of an initial denaturation step at 95 °C, followed by 40 amplification cycles with denaturation at 95 °C and annealing/extension at 60 °C. At the end of each run, melt curve analysis was performed to confirm amplification specificity and exclude the presence of non-specific products or primer dimers. The transcriptional profiling focused on genes involved in oxidative stress response and detoxification (nrf2, sod, cat, gstp), apoptosis and cell survival regulation (bax, bcl2), neurodevelopmental and thyroid-related pathways (pax, trb, dio1, dio2), and thyroid hormone transport and synthesis (ttr, tpo, tg). Primer pairs were selected from validated zebrafish studies or designed de novo based on *Danio rerio* reference sequences, ensuring specificity and optimal amplification efficiency. Each experimental condition was analyzed using three independent biological replicates, with each sample measured in technical triplicate. Gene expression data were normalized using stable housekeeping genes (e.g., β-actin and ef1α), previously validated for zebrafish embryos under similar experimental conditions. Relative changes in gene expression were calculated using the $2^{-}\Delta\Delta Ct$ method, with the control group used as the calibrator. Statistical evaluation of transcriptional data was performed using one-way analysis of variance (ANOVA),

followed by appropriate post hoc comparisons to identify significant differences between control and treated groups. A significance threshold of $p < 0.05$ was applied.

Table 1. *Sequences of primers for the genes used.*

GENE- ID	Forward primer (from 5′ to 3′)	Reverse primer
TG	CCAGCCGAAAGGATAGAGTTG	ATGCTGCCGTGGAATAGGA
TPO	GCGCTTGGAACACAGTATCA	CTTCAGCACCAAACCCAAAT
TTR	CGGGTGGAGTTTGACACTTT	GCTCAGAAGGAGAGCCAGTG
DIO1	GTTCAAACAGCTTGTCAAGGACT	AGCAAGCCTCTCCTCCAAGTT
DIO2	GCATAGGCAGTCGCTCATTT	TGTGGTCTCTCATCCAACCA
TRB	TGGGAGATGATACGGGTTGT	ATAGGTGCCGATCCAATGTC
PAX6B	GCCAGGACAACCAAATCAAGACG	GTGAAGGACGTTCTGTTTCTCTGC
EF1A	GAATCGACAAGAGAACCATCG	CCGTTCTTGGAGATACCAGC
CAT	AGGGCAACTGGGATCTTACA	TTTATGGGACCAGACCTTGG
SOD	GGCCAACCGATAGTGTTAGA	CCAGCGTTGCCAGTTTTTAG
CYP3A	ACATGGACTCTGCTGGCGTTCTTAGTGGCG	CGTGGAGATCTTGCAGAGGTTCGACGTCTC
BCL2	TCACTCGTTCAGACCCTCAT	ACGCTTTCCACGCACAT
BAX	GGCTATTTCAACCAGGGTTCC	TGCGAATCACCAATGCTGT
NRF2	GACAAAATCGGCGACAAAAT	TTAGGCCATGTCCACACGTA
GSTP2	CACAGACCTCGCTTTTCACAC	GAGAGAAGCCTCACAGTCGT
CASP3	CCGCTGCCCATCACTA	ATCCTTTCACGACCATCT

6.2.9 Statistical analysis

All experimental data were expressed as mean ± standard deviation (SD), unless otherwise specified. Prior to statistical testing, data distribution was evaluated for normality using the Shapiro–Wilk test, and homogeneity of variances was assessed using Levene's test. When these assumptions were satisfied, differences among experimental groups were analysed using one-way analysis of variance (ANOVA). In the presence of significant overall effects, post hoc comparisons were performed using Dunnett's multiple comparison tests, with the control group used as the reference. For

datasets that did not meet parametric assumptions, non-parametric alternatives were applied, including the Kruskal–Wallis test followed by Dunnt's post hoc test for multiple comparisons. Embryotoxicity endpoints (e.g., survival rate, hatching success, and incidence of developmental abnormalities) were analysed as proportions and compared among groups using χ^2 tests or Fisher's exact test, depending on sample size. Gene expression results obtained by quantitative real-time PCR were analysed using ΔCt values prior to statistical testing. Relative expression levels were calculated using the $2^{-}\Delta\Delta Ct$ method, and statistical comparisons were conducted on normalized data to avoid bias due to logarithmic transformation. Metabolomic data derived from NMR spectroscopy were subjected to multivariate statistical analysis, including principal component analysis (PCA), to explore global metabolic differences among treatments. When appropriate, univariate analyses were also performed on individual metabolites using ANOVA or non-parametric tests, with correction for multiple comparisons applied where necessary. All statistical analyses were performed using dedicated software packages (GraphPad Prism). A p-value < 0.05 was considered statistically significant for all tests. This statistical framework allowed robust evaluation of thiram-induced toxic effects and the potential mitigating role of algal-derived hydrochar across morphological, molecular, and metabolic endpoints.

6.3 Results

6.3.1 Developmental toxicity and rescue effects

Embryos of *Danio rerio* were exposed to 5 µg/mL THR, HC, and their combination (THR-HC), while the control group (Fig. 1) was maintained in embryo medium only. At 24 hours post-fertilization (hpf), no mortality was observed in any experimental

group. However, at this early developmental stage, embryos exposed to thiram already exhibited morphological alterations in the caudal region compared with controls (Fig. 2a). At 48 hpf, thiram exposure induced a clearly pathological condition, characterized by complete depigmentation and marked notochord deformation in 100% of the examined embryos (Figs. 2b and 2c). In contrast, embryos exposed to hydrochar alone and to the thiram/hydro mixture did not display detectable morphological abnormalities, either at the level of the notochord (Figs. 3a and 3c) or in the melanization process (Figs. 3b and 3d), and appeared comparable to the control group. Thiram-induced morpho-functional alterations became more pronounced at 72 hpf. Embryos in this group showed severe tail curvature, structural distortion of the notochord, pericardial edema, and reduced pigmentation relative to controls. Moreover, 100% of thiram-exposed embryos exhibited delayed hatching (Figs. 4a and 4b). No developmental abnormalities or hatching delays were observed in embryos treated with hydrochar alone or with the thiram/hydro combination (Figs. 5a and 5b). The toxicological profile associated with thiram persisted up to 96 hpf. At this time point, only 20% of exposed embryos had successfully completed hatching (Fig. 6), indicating a significant and prolonged delay in embryonic development. Despite the pronounced morphological and developmental alterations observed, no mortality was recorded in any experimental group at the end of the exposure period.

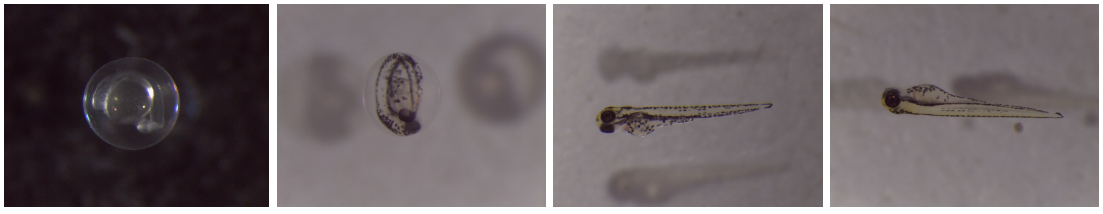


Figure 1. *Representative brightfield micrographs of Danio rerio embryos/larvae under control*

conditions at 24, 48, 72, and 96 hours post-fertilization (hpf). Images illustrate normal developmental progression, including intact chorion and early embryonic structures at 24 hpf, proper axis formation and organogenesis at 48 hpf, elongated body axis with developing pigmentation at 72 hpf, and fully formed larvae with normal morphology and successful hatching at 96 hpf.

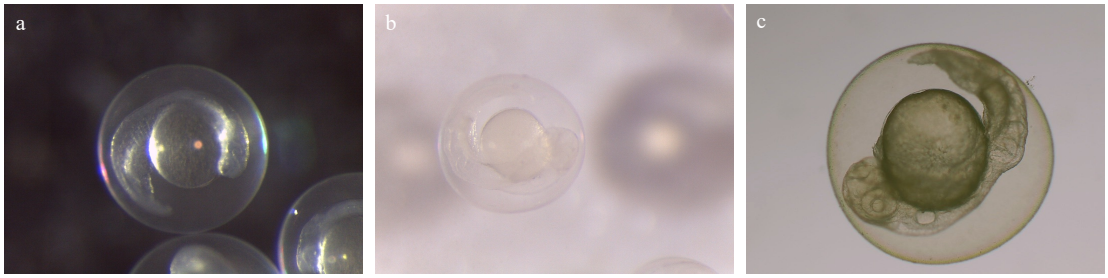


Figure 2. *Representative brightfield micrographs of Danio rerio embryos exposed to thiram during early development. (a) At 24 hours post-fertilization (hpf), embryos show early morphological alterations in the caudal region compared with control embryos, despite the absence of mortality. (b–c) At 48 hpf, thiram exposure induces a pronounced pathological phenotype, characterized by severe depigmentation and marked deformation of the notochord, observed consistently in all examined embryos.*

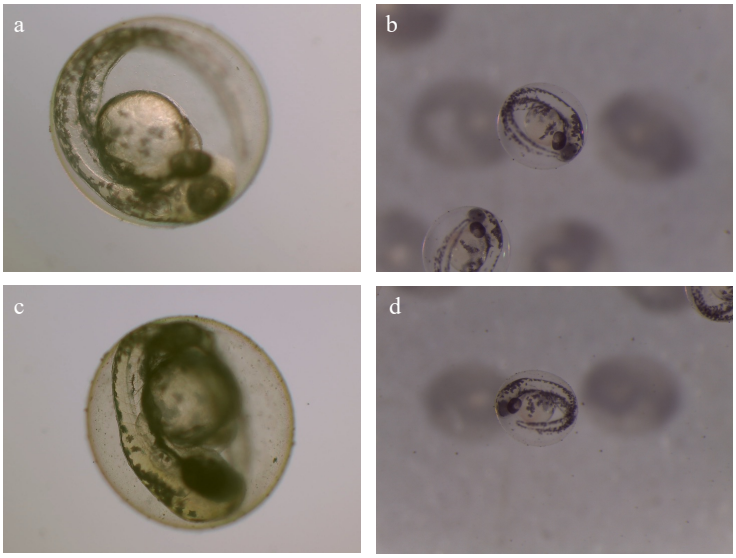


Figure 3. *Representative brightfield micrographs of Danio rerio embryos exposed to hydrochar alone and to the thiram–hydrochar combination. (a, c) Embryos exposed to hydrochar alone (a) and to thiram adsorbed onto hydrochar (c) show normal notochord development and body axis organization, comparable to control embryos. (b, d) No alterations in the melanization process were observed in embryos exposed to hydrochar alone (b) or to the thiram–hydrochar mixture (d).*

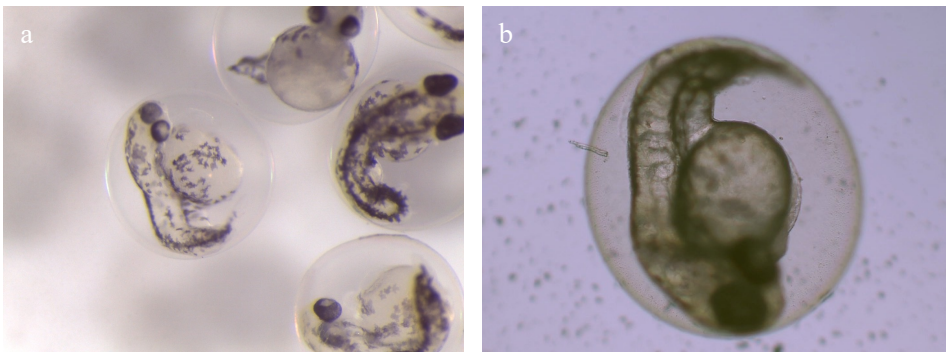


Figure 4. *Representative brightfield micrographs of Danio rerio embryos exposed to thiram at 72 hours post-fertilization (hpf). (a, b) Thiram-treated embryos exhibit severe morpho-functional alterations, including pronounced tail curvature, structural distortion of the notochord, pericardial edema, and reduced pigmentation compared with control embryos.*

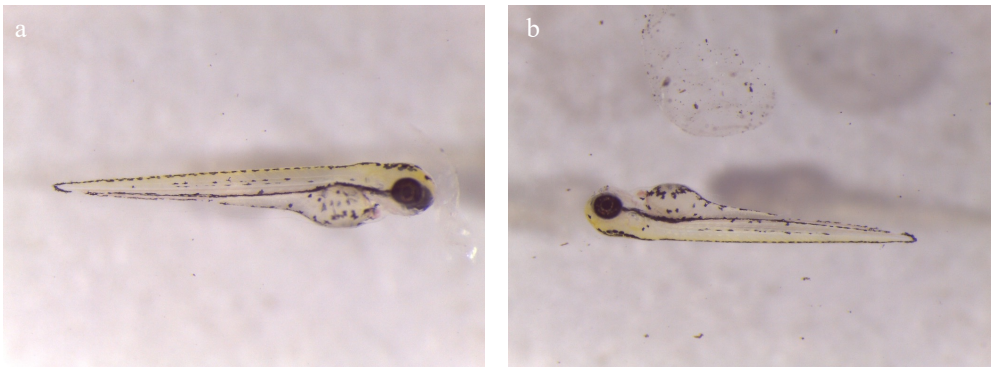


Figure 5. *Representative brightfield micrographs of Danio rerio larvae exposed to hydrochar alone and to the thiram–hydrochar combination at advanced developmental stages. (a, b) Larvae exposed to hydrochar alone (a) or to thiram adsorbed onto hydrochar (b) show normal body morphology, proper axial alignment, regular pigmentation, and successful hatching, comparable to control larvae.*



Figure 6. *Representative brightfield micrograph of Danio rerio embryos exposed to thiram at 96 hours post-fertilization (hpf). Thiram-treated embryos exhibit a persistent toxicological phenotype, characterized by a marked delay in hatching. At this time point, only approximately 20% of embryos had successfully hatched, indicating a sustained impairment of embryonic development induced by thiram exposure.*

6.3.2 Metabolomic reprogramming and mitigation

Figure 7 illustrates the representative ^{1}H-NMR spectral profile obtained from zebrafish larvae at 96 hpf. The analysis enabled the identification of a broad panel of polar metabolites, encompassing compounds involved in energy metabolism, amino acid turnover, neurotransmission, redox balance, and osmotic regulation. Among the detected metabolites were energy-related molecules such as lactate, glucose, pyruvate, acetate, creatine, phosphocreatine, and tricarboxylic acid cycle intermediates including malate, fumarate, and citrate. The spectrum also revealed several amino acids and amino acid–derived compounds, including glycine, serine, alanine, arginine, threonine, lysine, tyrosine, phenylalanine, tryptophan, methylhistidine, and branched-chain amino acids (BCAA). Neuromodulatory and choline-related metabolites, such as choline, acetylcholine, and serotonin, were also identified. In addition, metabolites associated with redox status and osmotic balance, including glutathione, betaine,

taurine, and myo-inositol, were detected. Finally, signals corresponding to nitrogen- and purine-related metabolites, such as inosine monophosphate (IMP), oxypurinol, imidazole, and formate, were observed, completing the metabolic fingerprint of the analyzed samples.

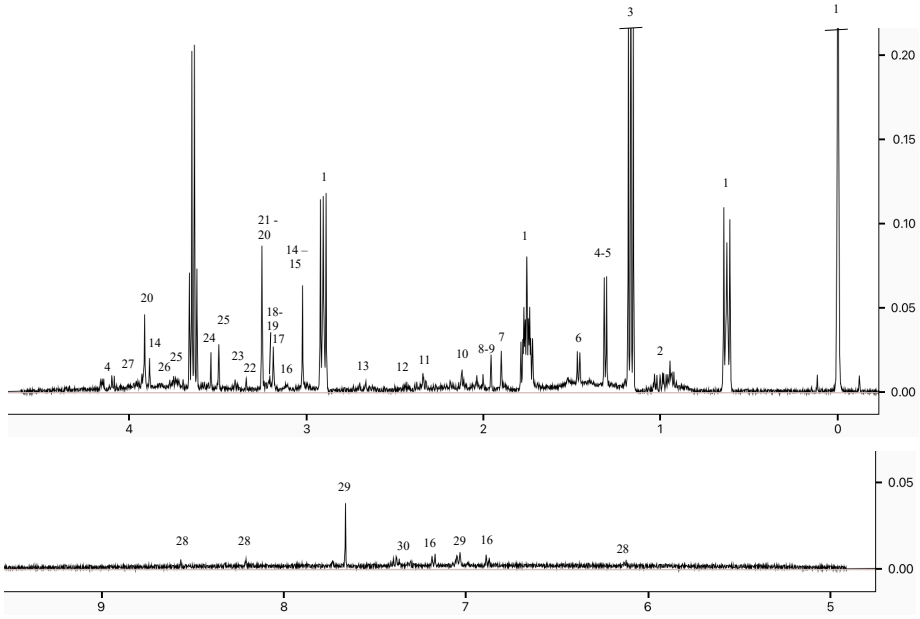


Figure 7. *Representative 1-D 500 MHz ^{1}H-NMR reference spectrum of polar extracts obtained from Danio rerio larvae under control conditions at 96 hours post-fertilization (hpf). Keys: (1) DSS, (2) BCAA, (3) ethanol, (4) lactate, (5) threonine, (6) alanine, (7) acetate, (8) arginine, (9) lysine, (10) glutamate, (11) malate, (12) pyruvate, (13) citrate, (14) creatine, (15) phosphocreatine, (16) tyrosine, (17) choline, (18) acetylcholine, (19) phosphocholine (20) betaine, (21) trimethylamine-N-oxide (TMAO), (22) methanol, (23) taurine, (24) glycine, (25) glucose, (26) glutathione, (27) serine, (28) inosine monophosphate (IMP), (29) methylhistidine and (30) imidazole.*

6.3.2.1 Differential metabolite signatures

At 96 hpf, the polar metabolomic profile differed markedly among experimental groups (Control, Hydrochar, Thiram, and Thiram/Hydrochar), revealing condition-specific alterations in energy-related metabolites, osmolytes, amino acids, and

nitrogen-containing compounds (Figure 8). Larvae exposed to thiram showed a clear increase in glycolysis-related metabolites, with lactate and alanine levels markedly elevated compared to the control group, together with a significant increase in glucose. In parallel, alterations in tricarboxylic acid (TCA) cycle–related metabolites were observed, with malate levels significantly affected relative to controls, indicating a shift in central carbon metabolism. Energy-buffering metabolites were also significantly modulated, as reflected by altered levels of creatine and phosphocreatine, resulting in a decreased phosphocreatine/creatine ratio. In the same group, several osmoprotective and redox-associated metabolites were significantly altered. Specifically, taurine and betaine levels were reduced in thiram-exposed larvae compared to the control condition, together with a significant decrease in glutathione. Metabolites associated with membrane turnover and cholinergic metabolism, including choline and phosphocholine, were also significantly altered in the thiram group. Amino acid profiling revealed significant changes in multiple amino acids, with decreased levels of glycine and tyrosine, while glutamate and arginine levels were increased relative to controls. Additionally, pyruvate levels were significantly altered in thiram-exposed larvae. Among energy-related nitrogen-containing metabolites, acetate levels were significantly increased in the thiram group. In contrast, larvae exposed to hydrochar alone exhibited a polar metabolomic profile largely comparable to that of the control group. Most metabolites involved in energy metabolism, osmoprotection, amino acid balance, and membrane-related pathways showed no significant differences relative to controls, with only minor fluctuations that did not follow a consistent directional trend. In the thiram/hydrochar condition, the metabolomic alterations observed in the thiram-only group were largely absent. Levels

of lactate, glucose, alanine, malate, creatine, phosphocreatine, and pyruvate were comparable to those of control larvae. Similarly, taurine, betaine, glutathione, and choline-related metabolites (choline, phosphocholine, acetylcholine) were restored to values close to control levels. Amino acid profiles, including glycine, glutamate, arginine, threonine, tyrosine, and lysine, also overlapped with those of control embryos, without evidence of a stress-associated metabolic signature. Overall, the polar metabolomic data at 96 hpf highlight a distinct metabolic signature associated with thiram exposure, characterized by pronounced alterations in energy metabolism, osmotic balance, amino acid homeostasis, and redox status, whereas both hydrochar and thiram–hydrochar treatments exhibited metabolite profiles comparable to those of control larvae.

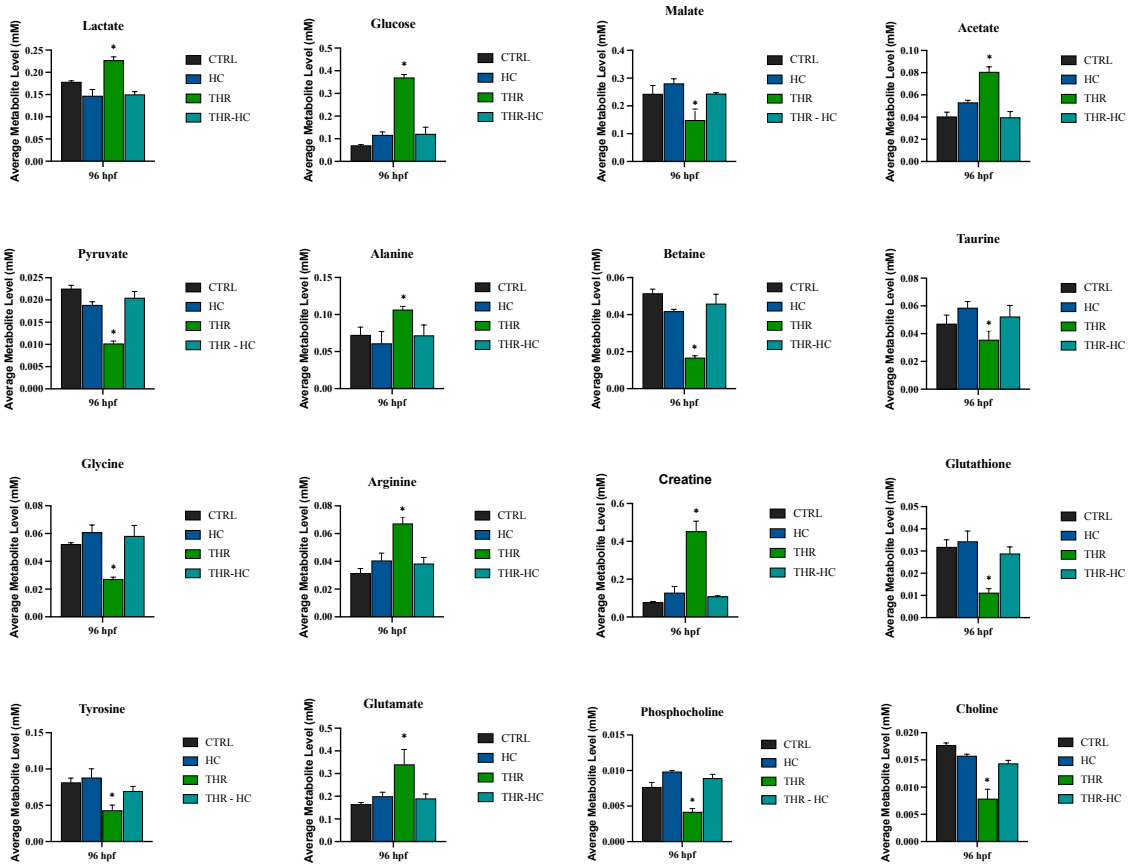


Figure 8. *Bar plots showing the relative levels of selected significantly altered polar metabolites identified by* ^{1}*H-NMR analysis in zebrafish larvae at 96 hpf under the different experimental conditions (CTRL, HC, THR, and THR–HC). Metabolites are grouped according to their involvement in energy metabolism, amino acid metabolism, osmotic balance, redox status, and membrane-related pathways. Data are expressed as mean ± SD of biological replicates and are reported relative to the control condition. Statistical significance was assessed by one-way ANOVA followed by appropriate post hoc testing; significant differences compared to the control group are indicated (*$p < 0.05$*).*

6.3.2.2 Multivariate statistical analysis of the polar metabolomic data

Multivariate statistical analysis was applied to the ^{1}H-NMR polar metabolomic dataset to investigate global metabolic differences among experimental groups

(Control, Hydrochar, Thiram, and Thiram/Hydrochar). Principal component analysis (PCA) revealed a clear separation of samples according to treatment condition (Figure 9). The first principal component (PC1), accounting for 82.6% of the total variance, primarily discriminated larvae exposed to thiram from all other groups, while the second principal component (PC2) explained an additional 6.8% of the variance. The PCA score plot (Figure 10) showed that thiram-exposed larvae formed a distinct and well-separated cluster, clearly distant from control samples along PC1. In contrast, control, hydrochar, and thiram/hydrochar samples clustered closely together, showing substantial overlap and indicating similar overall metabolomic profiles. Notably, the thiram/hydrochar group clustered near the control and hydrochar-only groups, suggesting an attenuation of the metabolic alterations induced by thiram. The corresponding PCA biplot highlighted the metabolites contributing most strongly to group separation. Positive loadings along PC1 were primarily associated with lactate, glucose, glutamate, and arginine, which were aligned with the thiram-exposed samples. Conversely, metabolites such as glutathione, taurine, betaine, choline, phosphocholine, glycine, and tyrosine loaded in the opposite direction, contributing to the clustering of control, hydrochar, and thiram/hydrochar samples. Hierarchical clustering analysis combined with heatmap visualization further supported the PCA results, revealing a distinct metabolic signature associated with thiram exposure. The heatmap (Figure 11) showed increased relative levels of lactate, glucose, alanine, acetate, creatine, arginine, and glutamate in thiram-exposed larvae, accompanied by decreased levels of glutathione, malate, taurine, betaine, choline, phosphocholine, glycine, and pyruvate. In contrast, the hydrochar and thiram/hydrochar groups displayed metabolite profiles largely comparable to those of control larvae, with no

evident stress-associated clustering pattern. Overall, multivariate analysis consistently identified thiram exposure as the main factor driving metabolic divergence, while hydrochar alone did not induce significant metabolic shifts. Importantly, the co-exposure to thiram and hydrochar resulted in a metabolomic profile closely resembling that of the control condition, corroborating the mitigation of thiram-induced metabolic alterations.

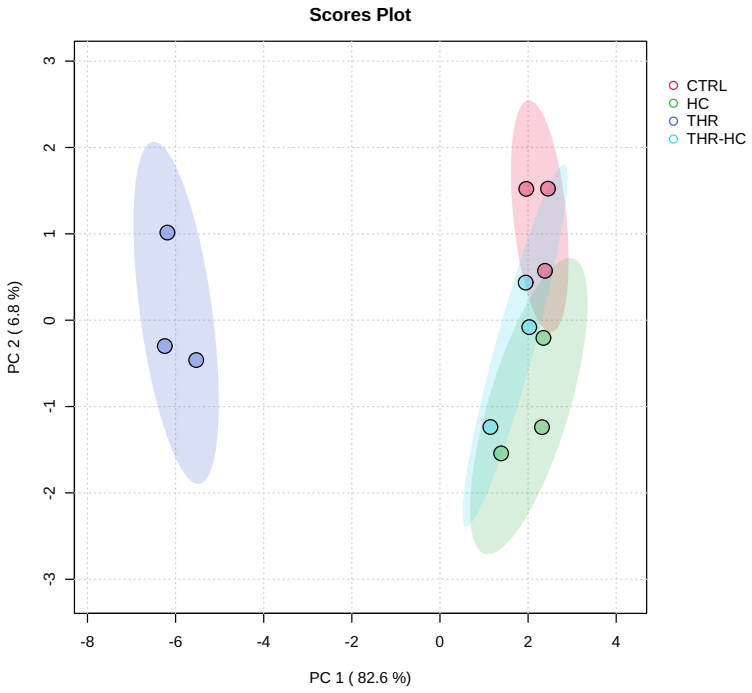


Figure 9. *Principal component analysis (PCA) score plot of the ^{1}H-NMR–based polar metabolomic profiles of zebrafish larvae at 96 hpf under the different experimental conditions (CTRL, HC, THR, and THR–HC). The first principal component (PC1) explains 82.6% of the total variance, while the second principal component (PC2) accounts for 6.8%. Each point represents an individual biological replicate, and shaded ellipses indicate the 95% confidence interval for each experimental group.*

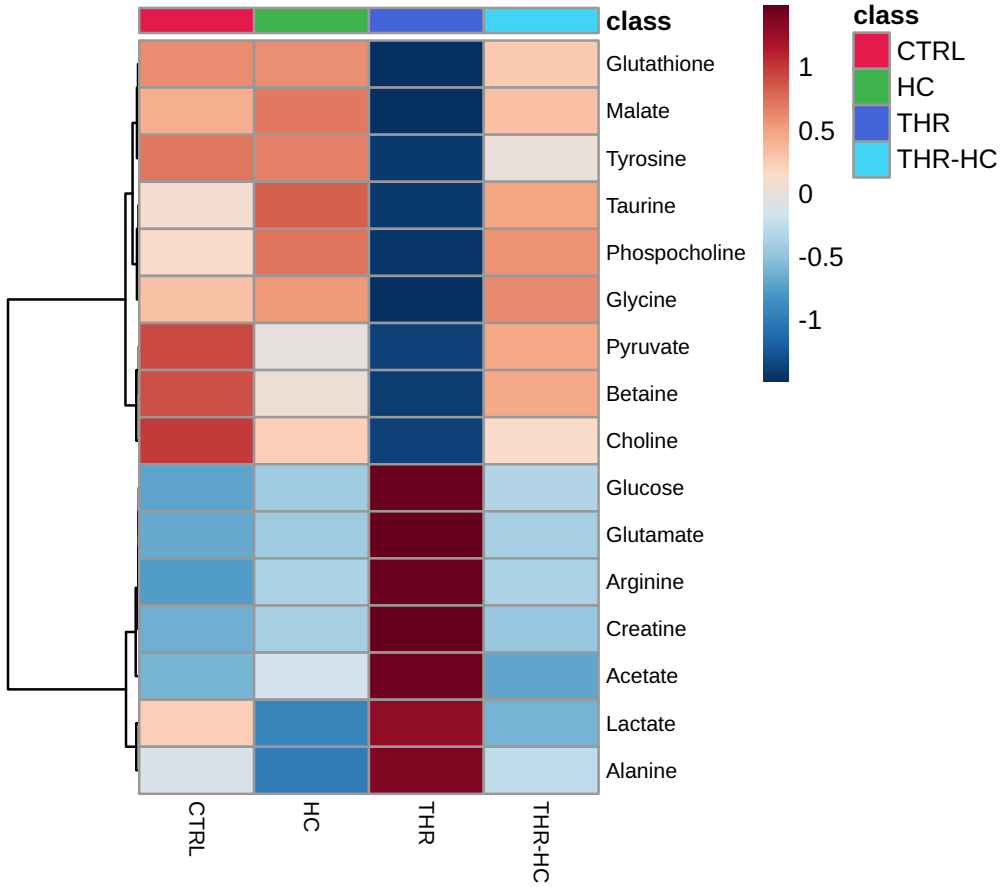


Figure 10. *Heatmap representation and hierarchical clustering analysis of significantly altered polar metabolites identified by* ^{1}*H-NMR analysis in zebrafish larvae at 96 hpf across experimental conditions (CTRL, HC, THR, and THR–HC). Metabolite levels are normalized and displayed as Z-scores, with color intensity indicating relative abundance (blue, lower levels; red, higher levels). Hierarchical clustering was performed using Euclidean distance and complete linkage, highlighting condition-dependent metabolic patterns.*

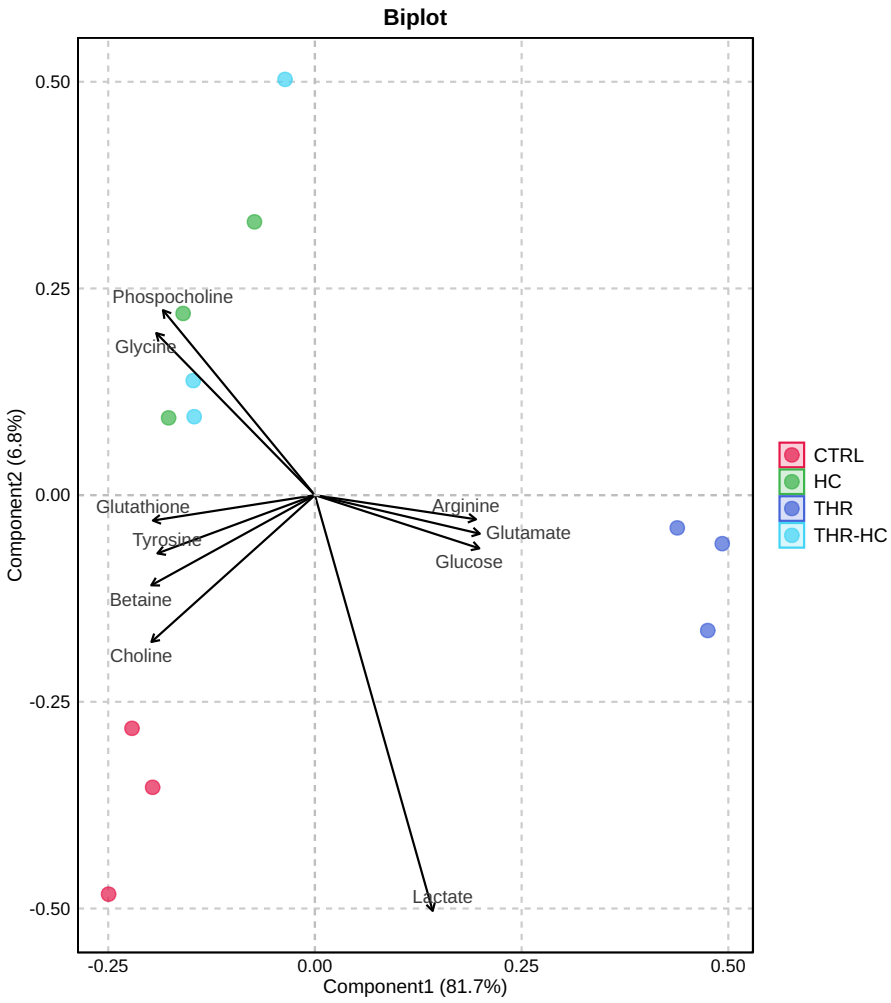


Figure 11. *PCA biplot showing the distribution of samples and the relative contribution of selected polar metabolites to group separation. Arrows represent metabolite loadings, indicating the direction and magnitude of their contribution to the principal components. Metabolites associated with energy metabolism, amino acid turnover, redox balance, and membrane-related pathways contribute differentially to the separation of thiram-exposed samples from control, hydrochar, and thiram/hydrochar groups.*

6.3.2.3 Pathway-level metabolic responses

Pathway enrichment analysis of the significantly altered polar metabolites revealed a broad and coordinated perturbation of multiple metabolic pathways in zebrafish larvae exposed to thiram at 96 hpf (Figure 12). The enrichment overview highlighted a strong over-representation of pathways involved in central carbon and energy metabolism, with glycolysis/gluconeogenesis, pyruvate metabolism, and the citrate cycle (TCA cycle) among the most significantly enriched pathways. These pathways showed high enrichment ratios and low p-values, indicating a major contribution to the metabolic divergence observed in thiram-exposed larvae. Amino acid–related pathways were also prominently enriched. In particular, glycine, serine and threonine metabolism, alanine, aspartate and glutamate metabolism, arginine biosynthesis, and arginine and proline metabolism emerged as significantly affected pathways. Additionally, pathways related to branched-chain amino acid (valine, leucine and isoleucine) biosynthesis and degradation were enriched, indicating widespread alterations in amino acid homeostasis. Several pathways associated with redox balance and cellular stress responses were significantly represented, including glutathione metabolism, taurine and hypotaurine metabolism, and nitrogen metabolism, consistent with the observed alterations in redox-related metabolites. Pathways linked to one-carbon metabolism, such as the one carbon pool by folate, were also enriched, suggesting perturbations in methyl group metabolism and biosynthetic capacity. Metabolic pathways related to aromatic amino acids, including phenylalanine metabolism, tyrosine metabolism, and phenylalanine, tyrosine and tryptophan biosynthesis, were significantly enriched, together with tryptophan metabolism, indicating alterations in pathways connected to neurotransmitter

precursors and neurodevelopmental processes. In addition, enrichment of glycerophospholipid metabolism was observed, reflecting changes in membrane-associated metabolic pathways. Network-based pathway analysis further illustrated (Figure 13) the extensive interconnectivity among the enriched pathways, with glycolysis/gluconeogenesis, pyruvate metabolism, TCA cycle, and glycine–serine–threonine metabolism occupying central positions within the metabolic network. These pathways showed strong connectivity with amino acid, redox, and nitrogen-related metabolic routes, highlighting a coordinated metabolic reprogramming rather than isolated pathway-specific effects. Overall, pathway enrichment and network analyses consistently identified energy metabolism, amino acid metabolism, redox homeostasis, and nitrogen-related pathways as major targets of thiram exposure. In contrast, samples from the hydrochar-only and thiram/hydrochar conditions did not exhibit a comparable enrichment pattern, supporting the attenuation of thiram-induced metabolic disruptions when hydrochar was present.

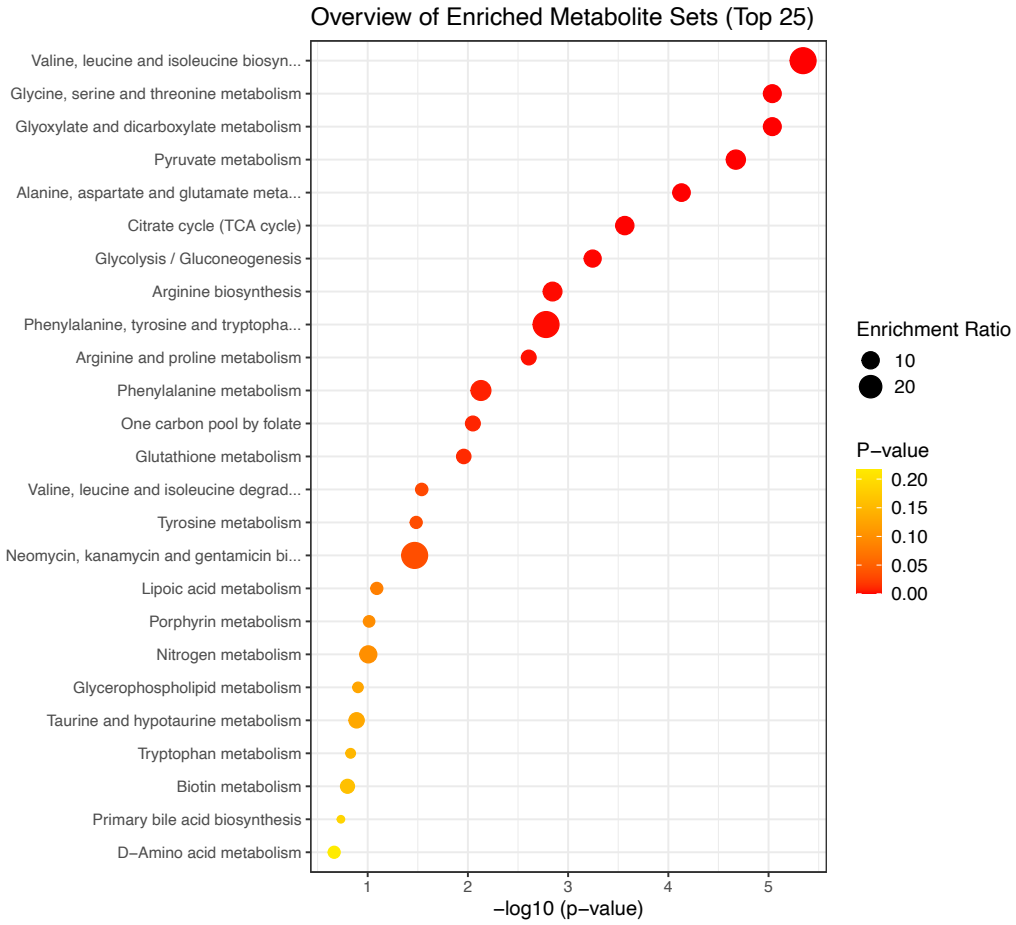


Figure 12. *Bubble plot showing the top enriched metabolic pathways identified by pathway enrichment analysis based on significantly altered polar metabolites detected by* ^{1}*H-NMR in zebrafish larvae at 96 hpf. The x-axis represents the statistical significance expressed as* $-log10$*(*p*-value), while the y-axis lists the enriched metabolic pathways. Bubble size corresponds to the enrichment ratio, and color intensity reflects the associated* p*-value, with darker colors indicating higher statistical significance.*

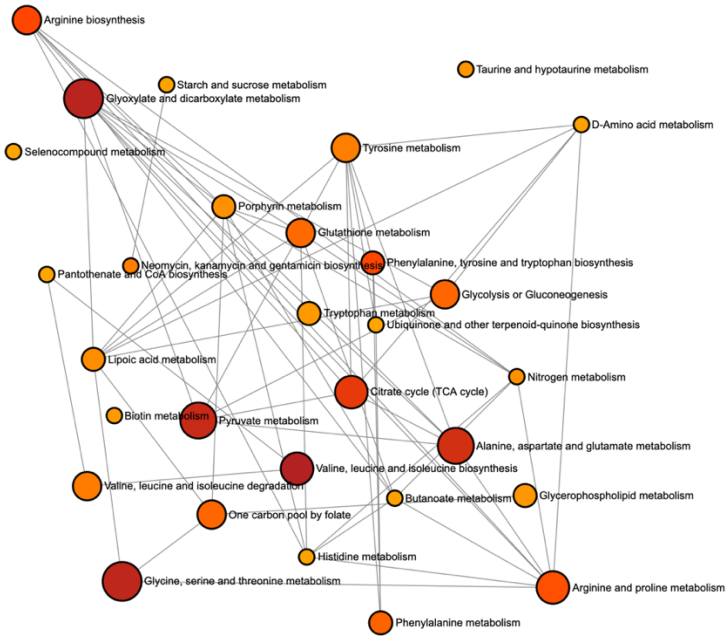


Figure 13. *Network representation of enriched metabolic pathways derived from pathway enrichment analysis of polar metabolomic data in zebrafish larvae at 96 hpf. Nodes represent individual metabolic pathways, with node size proportional to the enrichment ratio and node color indicating the level of statistical significance. Edges denote shared metabolites between pathways, highlighting the degree of interconnectivity and coordinated perturbation among energy metabolism, amino acid metabolism, redox balance, and nitrogen-related pathways.*

6.3.3 Endocrine and stress-related transcriptional alterations

At 96 hpf, the expression of antioxidant, apoptotic, neurodevelopmental, and thyroid-related genes differed markedly among the experimental conditions (Control, Hydrochar, Thiram, and Thiram/Hydrochar) (Figure 14). For the antioxidant enzymes gstp, sod, and cat, larvae exposed to thiram showed a pronounced and statistically significant reduction in transcript levels compared to the control group. In contrast, embryos exposed to hydrochar alone displayed expression values close to those of the control, with a slight decrease for gstp and cat. In the thiram/hydrochar condition, gstp expression was restored to values comparable to the control, while sod and cat showed

expression levels similar to or higher than those observed in control embryos. A similar trend was observed for nrf2, whose expression was significantly down-regulated in the thiram group relative to all other conditions. Both hydrochar and thiram/hydrochar treatments resulted in expression levels close to the control, although a mild reduction was observed in the hydrochar-only group. Regarding apoptotic markers, bcl2 expression was markedly reduced in larvae exposed to thiram, whereas control and hydrochar-treated embryos showed comparable expression levels. In the thiram/hydrochar group, bcl2 expression returned to values similar to those of the control. Conversely, bax expression was significantly increased in the thiram group compared to all other conditions, while control, hydrochar, and thiram + hydrochar groups displayed comparable levels. The expression of casp3 was significantly increased in thiram-exposed larvae, whereas control and hydrochar groups showed similar basal levels; in the thiram/hydrochar condition, casp3 expression was comparable to the control. Analysis of the neurodevelopmental marker pax6a revealed a strong and significant down-regulation in the thiram group. Control and hydrochar-exposed larvae exhibited similar expression levels, while the thiram/hydrochar group showed expression values close to the control. Concerning xenobiotic metabolism, cyp3a expression was significantly reduced in the thiram group compared to the control. In contrast, larvae exposed to hydrochar alone showed expression levels comparable to the control, and the thiram/hydrochar condition exhibited a clear restoration of cyp3a expression to control values. Thyroid-related genes showed a distinct modulation pattern following thiram exposure. tpo expression was significantly increased in the thiram group relative to the control, whereas control, hydrochar, and thiram/hydrochar groups displayed similar expression levels. In

contrast, tg expression was strongly down-regulated in thiram-exposed larvae, while control embryos showed higher transcript levels. In the thiram/hydrochar group, tg expression was restored to values comparable to the control, whereas hydrochar alone showed intermediate levels. The expression of dio1 was significantly reduced in the thiram group compared to the control, while hydrochar and thiram/hydrochar treatments resulted in expression levels similar to those of control embryos. Conversely, dio2 expression was markedly increased in thiram-exposed larvae, whereas control and hydrochar groups showed comparable basal expression. In the thiram/hydrochar condition, dio2 expression was intermediate between control and thiram. Finally, trb expression was significantly down-regulated in the thiram group, while control, hydrochar, and thiram + hydrochar groups exhibited similar transcript levels. Similarly, ttr expression was markedly reduced following thiram exposure, whereas hydrochar and thiram/hydrochar treatments restored expression to levels comparable to those observed in control embryos.

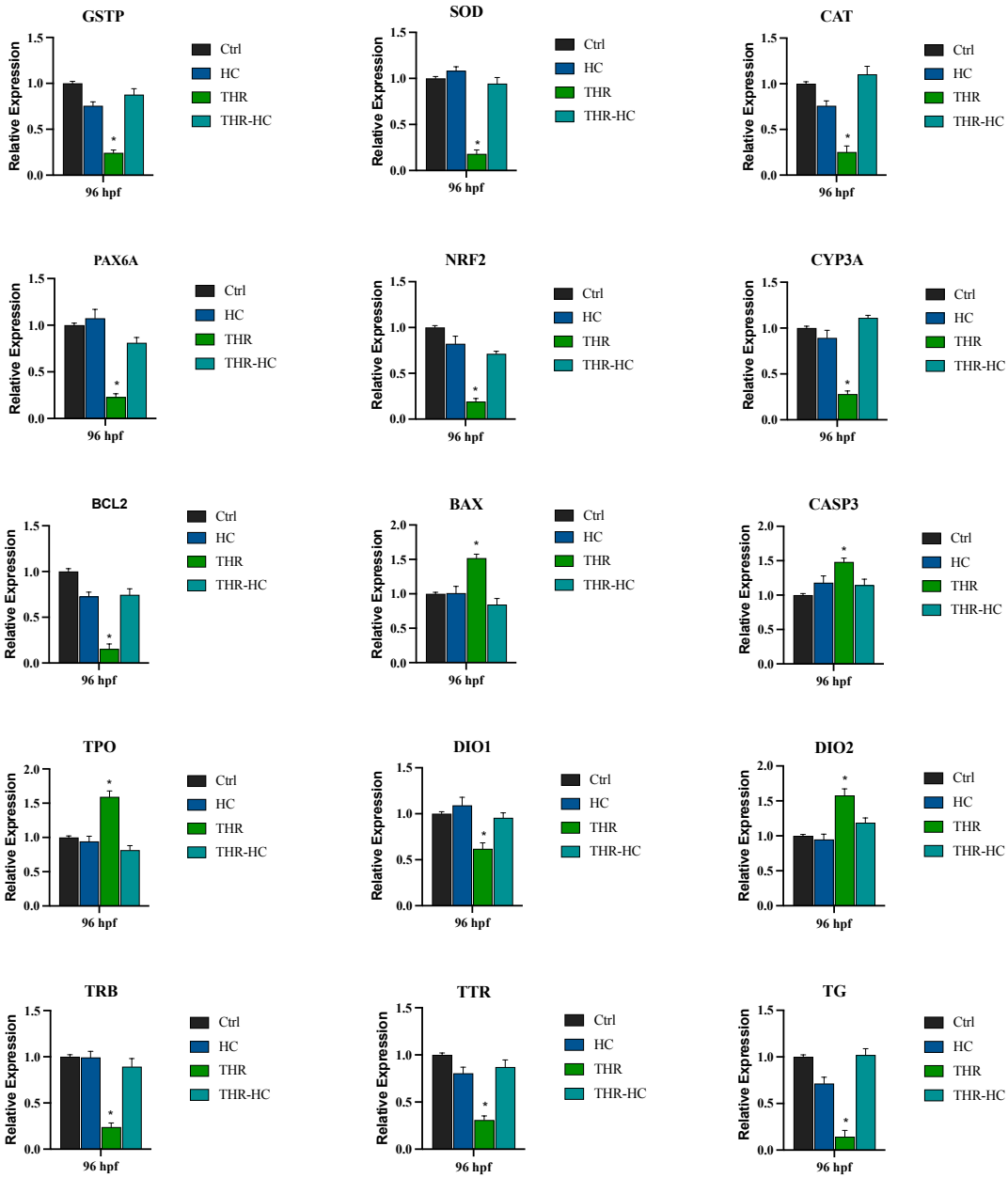


Figure 14. *Ctrl, control embryos; HC, embryos exposed to hydrochar; THR, embryos exposed to thiram (5 µg L⁻¹); THR–HC, embryos exposed to thiram adsorbed onto hydrochar.*

6.4 Discussions

The present study provides an integrated multi-level characterization of thiram-induced toxicity in zebrafish larvae and demonstrates the effectiveness of hydrochar in mitigating its adverse effects. Morphological analyses revealed a clear time-dependent progression of thiram-induced developmental toxicity. Although no mortality was observed at 24 hpf, embryos exposed to thiram already exhibited early morphological alterations in the caudal region compared with controls, indicating a prompt interference with axial patterning processes. At 48 hpf, thiram exposure induced a clearly pathological phenotype, characterized by complete depigmentation and marked notochord deformation in 100% of the examined embryos. These developmental impairments became more pronounced at 72 hpf, when thiram-exposed embryos displayed severe tail curvature, structural distortion of the notochord, pericardial edema, and reduced pigmentation, together with a complete delay in hatching. The toxicological profile associated with thiram persisted up to 96 hpf, with only a minor fraction of embryos completing hatching, indicating a significant and prolonged delay in embryonic development. Despite the pronounced morphological and developmental alterations observed, no mortality was recorded at the end of the exposure period. Overall, these alterations are consistent with previous studies reporting developmental toxicity of dithiocarbamate fungicides in zebrafish and other aquatic models, where similar phenotypes have been associated with disrupted axial development, cardiovascular dysfunction, and neurodevelopmental impairment (Zhang et al., 2013; Wang et al., 2016; Zhou et al., 2019). Importantly, many of these developmental endpoints are tightly regulated by thyroid hormones during early embryogenesis, as TH signaling plays a pivotal role in somitogenesis, hatching,

pigmentation, neurogenesis, and cardiovascular maturation in teleosts (Porazzi et al., 2009; Alt et al., 2006; Wendl et al., 2007). In contrast, embryos exposed to hydrochar alone developed normally, confirming the biocompatibility of the material, while the complete rescue of normal morphology and hatching success observed in the thiram/hydrochar condition strongly suggests that hydrochar effectively reduces thiram bioavailability and prevents its interaction with developing tissues. Metabolomic profiling further revealed that thiram exposure induces a profound metabolic reprogramming, characterized by marked alterations in central carbon metabolism, energy buffering, redox balance, and amino acid homeostasis. The significant increase in glycolysis-related metabolites such as lactate, glucose, and alanine, together with alterations in pyruvate and malate levels, indicates a shift toward inefficient energy production and reduced mitochondrial flux. Similar metabolic signatures have been described in zebrafish embryos exposed to compounds that impair mitochondrial function or induce oxidative stress, reflecting a metabolic adaptation to compromised oxidative phosphorylation (van der Ven et al., 2013; Pallocca et al., 2016). Notably, thyroid hormones are key regulators of mitochondrial biogenesis and oxidative metabolism during early development, and disruption of TH signaling has been repeatedly associated with metabolic inflexibility, reduced aerobic capacity, and altered carbohydrate utilization in fish embryos (Schmidt & Braunbeck, 2011; van der Ven et al., 2006). The concomitant modulation of creatine and phosphocreatine levels, resulting in a reduced phosphocreatine/creatine ratio, further supports the presence of an impaired energy-buffering system, which is critical during highly energy-demanding developmental stages such as somitogenesis and hatching. Increased acetate levels are also indicative of disrupted central metabolism and altered

carbon flux, a feature commonly observed under conditions of metabolic stress. In parallel, thiram exposure was associated with a pronounced depletion of metabolites involved in redox homeostasis and osmotic regulation, including glutathione, taurine, and betaine. Glutathione depletion is a well-recognized hallmark of oxidative stress and has been widely reported in association with dithiocarbamate toxicity, given their capacity to interfere with redox-sensitive pathways and metal homeostasis (Fitsanakis et al., 2002; Regoli & Giuliani, 2014). Reduced levels of taurine and betaine further suggest impaired osmotic balance and membrane stabilization, which may contribute to the development of pericardial edema and cellular dysfunction observed at the morphological level. Oxidative stress has also been shown to directly impair thyroid hormone synthesis and deiodination processes, further exacerbating thyroid axis dysfunction during embryogenesis (Rehberger et al., 2018; Di Jeso & Arvan, 2016). These metabolomic alterations are fully consistent with the transcriptional down-regulation of key antioxidant genes, including nrf2, sod, cat, and gstp, indicating that thiram overwhelms endogenous antioxidant defenses rather than eliciting an effective compensatory response, as reported for other oxidative stress–inducing xenobiotics (Kobayashi et al., 2016; Li et al., 2021). The molecular data also revealed a clear activation of pro-apoptotic signaling in thiram-exposed larvae, as shown by the up-regulation of bax and casp3 and the concomitant down-regulation of bcl2, a transcriptional pattern consistent with activation of the intrinsic apoptotic pathway. This finding aligns with previous evidence of thiram-induced apoptosis in neuronal and embryonic systems and provides a mechanistic link between metabolic collapse, oxidative stress, and tissue damage (Zhang et al., 2017; Kim et al., 2021). Thyroid hormone deficiency during early development has been shown to sensitize embryonic

tissues to apoptosis, particularly in neural and sensory structures, further supporting a causal link between thyroid axis disruption and the observed neurodevelopmental defects (Tonyushkina et al., 2014; Zhu et al., 2018).The strong down-regulation of the neurodevelopmental marker pax6a further supports the presence of neurodevelopmental disruption, coherently explaining the ocular malformations observed at the morphological level, as PAX6 is a key regulator of eye and central nervous system development in vertebrates. Additionally, thiram exposure induced a marked dysregulation of thyroid-related genes, including altered expression of tg, tpo, dio1, dio2, trb, and ttr, indicating disruption of thyroid hormone synthesis, transport, and peripheral metabolism. Dithiocarbamates are well-established thyroid-disrupting chemicals, acting through multiple mechanisms including inhibition of thyroid peroxidase activity, interference with iodination of thyroglobulin, and alteration of deiodinase-mediated T4–T3 conversion (Chen et al., 2019; Bjørge et al., 1996; Elsalini & Rohr, 2003; Rehberger et al., 2018). In zebrafish and medaka models, disruption of tg, tpo, dio1/2, and ttr expression has been directly linked to delayed hatching, impaired growth, abnormal pigmentation, and altered energy metabolism, highlighting the central role of thyroid signaling in coordinating embryonic development (Porazzi et al., 2009; Spaan et al., 2019; Pesce et al., 2024). The observed thyroid axis imbalance likely contributes to the global developmental delay and metabolic alterations detected in thiram-exposed larvae. Multivariate statistical analysis, pathway enrichment, and metabolic network reconstruction provided an integrated view of these alterations, clearly identifying thiram exposure as the main driver of metabolic divergence. The strong separation of thiram-exposed samples from all other conditions in PCA and hierarchical clustering analyses, together with the enrichment

of pathways related to glycolysis, the TCA cycle, amino acid metabolism, redox balance, and nitrogen metabolism, highlights a coordinated metabolic reprogramming rather than isolated pathway-specific effects. Importantly, the absence of a comparable multivariate or pathway-level signature in the hydrochar and thiram + hydrochar conditions confirms that hydrochar alone does not perturb larval metabolism and that co-exposure effectively prevents thiram-induced metabolic disruption. Taken together, these findings demonstrate that thiram induces a tightly interconnected cascade of developmental, metabolic, oxidative, apoptotic, and endocrine alterations in zebrafish larvae, ultimately leading to severe morphological defects and reduced survival. By specifically targeting the thyroid axis during a critical window of embryonic development, thiram disrupts the hormonal control of growth, metabolism, and tissue differentiation, providing a mechanistic explanation for the multi-systemic toxicity observed. Crucially, the adsorption of thiram onto hydrochar fully mitigates these effects across all investigated levels, restoring normal morphology, metabolic homeostasis, and gene expression profiles. This study therefore provides strong experimental evidence supporting the use of hydrochar as an environmentally compatible material for reducing pesticide bioavailability and toxicity in aquatic ecosystems, in line with previous reports on the protective role of carbon-based materials in contaminant remediation (Beesley et al., 2011; Ahmad et al., 2014; Regoli et al., 2022).

6.5 Conclusion

This study shows that thiram exposure during early zebrafish development induces a marked, time-dependent impairment of embryonic and larval development, characterized by delayed hatching and axial, pigmentation, and cardiovascular abnormalities. Integrated morphological, metabolomic, and gene expression analyses indicate that these effects are primarily driven by disruption of the thyroid axis, leading to altered metabolic homeostasis and developmental timing. Hydrochar alone did not induce adverse effects, while co-exposure to thiram and hydrochar effectively prevented thiram-induced morphological, metabolic, and transcriptional alterations, restoring profiles comparable to control conditions. These findings identify hydrochar as an effective and environmentally compatible material for mitigating thiram bioavailability and toxicity and highlight thyroid hormone disruption as a key mechanistic link between pesticide exposure and developmental toxicity in aquatic organisms.

6.6 References

Benavente, V., Lage, S., Gentili, F. G., & Jansson, S. (2022). Influence of lipid extraction and processing conditions on hydrothermal conversion of microalgae feedstocks–Effect on hydrochar composition, secondary char formation and phytotoxicity. *Chemical engineering journal*, *428*, 129559.

Bevan, E., Santori, G., & Luberti, M. (2023). Kinetic modelling of the hydrothermal carbonisation of the macromolecular components in lignocellulosic biomass. *Bioresource Technology Reports*, *24*, 101643.

Capparucci, F., De Benedetto, G., Natale, S., Pecoraro, R., Iaria, C., & Marino, F. (2022). Evaluation of anaesthetic effect of commercial basil Ocimum basilicum on zebrafish (*Danio rerio*) embryos. *Fishes*, *7*(6), 318.

Chen, X., Fang, M., Chernick, M., Wang, F., Yang, J., Yu, Y., ... & Dong, W. (2019). The case for thyroid disruption in early life stage exposures to thiram in zebrafish (*Danio rerio*). *General and comparative endocrinology*, *271*, 73-81.

De Marco, G., Conti, G. O., Giannetto, A., Cappello, T., Galati, M., Iaria, C., ... & Maisano, M. (2022). Embryotoxicity of polystyrene microplastics in zebrafish Danio rerio. *Environmental research*, *208*, 112552.

Eliso, M. C., Billè, B., De Marco, G., Pulvirenti, E., Dal Bello, F., Rapisarda, P., ... & Cappello, T. (2025). Embryotoxicity of polystyrene microplastics, alone and conjugated with bisphenol A, in the black sea urchin *Arbacia lixula*: A multi-biomarker approach. *Journal of Hazardous Materials*, 140139.

Fang, J., Zhan, L., Ok, Y. S., & Gao, B. (2018). Minireview of potential applications of hydrochar derived from hydrothermal carbonization of biomass. *Journal of Industrial and Engineering Chemistry*, *57*, 15-21.

Gallego-Ramírez, C., García-Zapata, Y., Aguirre, N., Chica, E., & Rubio-Clemente, A. (2025). Acute Toxicity Assessment of Textile Wastewater Treated with Pinus patula Biochar Using Daphnia pulex. *Water*, *17*(8), 1143.

Gao, W., Zhang, Y., Mo, A., Jiang, J., Liang, Y., Cao, X., & He, D. (2022). Removal of microplastics in water: Technology progress and green strategies. *Green Analytical Chemistry*, *3*, 100042.

Giuliani, M. E., & Regoli, F. (2014). Identification of the Nrf2–Keap1 pathway in the European eel Anguilla anguilla: role for a transcriptional regulation of antioxidant genes in aquatic organisms. *Aquatic Toxicology*, *150*, 117-123.

Hong, J. W., Jo, S. W., & Yoon, H. S. (2015). Research and development for algae-based technologies in Korea: a review of algae biofuel production. *Photosynthesis research*, *123*(3), 297-303.

Jansson, E., Kjell, M., & Ålund, K. (2024). The Important Role of Pyrolysis and Hydrothermal Carbonization in a Sustainable Circular Bioeconomy: A Brief Literature Review. *Studia Ecologiae et Bioethicae*, *22*(2), 101-114.

Khan, S. A., Sharma, G. K., Malla, F. A., Kumar, A., & Gupta, N. (2019). Microalgae based biofertilizers: a biorefinery approach to phycoremediate wastewater and harvest biodiesel and manure. *Journal of Cleaner production*, *211*, 1412-1419.

Kim, D., Kim, S. A., Nam, S. H., Kwak, J. I., Kim, L., Lee, T. Y., ... & An, Y. J. (2024). Microplastic ingestion in aquatic and soil biota: A comprehensive review of laboratory studies on edible size and intake pattern. *Marine Pollution Bulletin*, *200*, 116056.

Leng, L., Zhang, W., Leng, S., Chen, J., Yang, L., Li, H., ... & Huang, H. (2020). Bioenergy recovery from wastewater produced by hydrothermal processing biomass: progress, challenges, and opportunities. *Science of the Total Environment*, *748*, 142383.

Li, H. Z., Zhang, Y. N., Guo, J. Z., Lv, J. Q., Huan, W. W., & Li, B. (2021). Preparation of hydrochar with high adsorption performance for methylene blue by co-hydrothermal carbonization of polyvinyl chloride and bamboo. *Bioresource technology*, *337*, 125442.

Liu, Y., Liu, H., & Shen, Z. (2021). Nanocellulose based filtration membrane in industrial waste water treatment: a review. *Materials*, *14*(18), 5398.

Lucian, M., & Fiori, L. (2017). Hydrothermal carbonization of waste biomass: Process design, modeling, energy efficiency and cost analysis. *Energies*, *10*(2), 211.

Nguyen, N. T., Le, P. A., & Phung, V. B. T. (2021). Biomass-derived carbon hooks on Ni foam with free binder for high performance supercapacitor electrode. *Chemical Engineering Science*, *229*, 116053.

Petrović, J., Ercegović, M., Simić, M., Koprivica, M., Dimitrijević, J., Jovanović, A., & Janković Pantić, J. (2024). Hydrothermal carbonization of waste

biomass: a review of hydrochar preparation and environmental application. *Processes*, *12*(1), 207.

Regoli, F., & Giuliani, M. E. (2014). Oxidative pathways of chemical toxicity and oxidative stress biomarkers in marine organisms. *Marine environmental research*, *93*, 106-117.

Rubio-Clemente, A., Gutiérrez, J., Henao, H., Melo, A. M., Pérez, J. F., & Chica, E. (2023). Adsorption capacity of the biochar obtained from Pinus patula wood micro-gasification for the treatment of polluted water containing malachite green dye. *Journal of King Saud University-Engineering Sciences*, *35*(7), 431-441.

Salam, M. A., Paul, S. C., Zain, R. A. M. M., Bhowmik, S., Nath, M. R., Siddiqua, S. A., ... & Amin, M. F. M. (2020). Trace metals contamination potential and health risk assessment of commonly consumed fish of Perak River, Malaysia. *Plos one*, *15*(10), e0241320.

Shahid, A., Malik, S., Zhu, H., Xu, J., Nawaz, M. Z., Nawaz, S., ... & Mehmood, M. A. (2020). Cultivating microalgae in wastewater for biomass production, pollutant removal, and atmospheric carbon mitigation; a review. *Science of the Total Environment*, *704*, 135303.

Sun, J., Benavente, V., Jansson, S., & Mašek, O. (2023). Comparative characterisation and phytotoxicity assessment of biochar and hydrochar derived from municipal wastewater microalgae biomass. Bioresource technology, 386, 129567.

Sun, L., Bai, Z., Wei, Y., Liang, J., Al-Dhabi, N. A., Tang, W., ... & Zhang, R. (2025). Biofilm-mediated algal-bacterial consortia for enhanced nitrogen removal: Exploring the dynamics of symbiotic interactions in membrane aerated reactors. *Journal of Membrane Science*, *733*, 124356.

Tang, Z., Liu, X., Niu, X., Yin, H., Liu, M., Zhang, D., & Guo, H. (2023). Ecological risk assessment of aquatic organisms induced by heavy metals in the estuarine waters of the Pearl River. *Scientific Reports*, *13*(1), 9145.

Vasamsetti, B. M. K., Chon, K., Kim, J., Oh, J. A., Yoon, C. Y., & Park, H. H. (2022). Developmental toxic effects of thiram on developing zebrafish (Danio rerio) embryos. *Toxics*, *10*(7), 369.

Vignet, C., Cappello, T., Fu, Q., Lajoie, K., De Marco, G., Clérandeau, C., ... & Cachot, J. (2019). Imidacloprid induces adverse effects on fish early life stages that are more severe in Japanese medaka (Oryzias latipes) than in zebrafish (Danio rerio). *Chemosphere*, *225*, 470-478.

Vishwakarma, P., Pal, V., Nagar, J., & Rai, R. (2024). Biofertilizers and soil amendments from algae: production and agronomic benefits. In *Value Added Products From Bioalgae Based Biorefineries: Opportunities and Challenges* (pp. 343-363). Singapore: Springer Nature Singapore.

Wang, J., Yang, S., Tian, Y., Liang, E., Zhao, X., & Li, B. (2024). Intensified anthropogenic disturbances impair planktonic algae in an urban river. *Journal of Cleaner Production*, *468*, 143091.

Zhang, Y., Qiu, Y., Liu, K., Zhong, W., Yang, J., Altermatt, F., & Zhang, X. (2024). Evaluating eDNA and eRNA metabarcoding for aquatic biodiversity assessment: From bacteria to vertebrates. *Environmental science and ecotechnology*, *21*, 100441.

Zhao, P., Lin, C., Li, Y., Zhang, J., Huang, N., Cui, X., ... & Guo, Q. (2022). Combustion and slagging characteristics of hydrochar derived from the co-hydrothermal carbonization of PVC and alkali coal. *Energy*, *244*, 122653.

CHAPTER 7

AHL-Derived Liquid as a Natural Biostimulant: Effects on *Phaseolus vulgaris* under Stress Conditions

7.1 Introduction

Climate change is increasingly exposing agricultural crops to combinations of abiotic stresses, particularly heat and water stress, which often occur simultaneously and severely impair plant productivity at the global scale (IPCC, 2014; FAO, 2020). Elevated temperatures increase evaporative demand and accelerate soil water depletion, while drought directly limits water availability to plants, inducing stomatal closure, reduced carbon assimilation, hydraulic dysfunction, and ultimately marked growth inhibition or crop failure (Blum, 2017; Rodríguez-Domínguez & Brodribb, 2020). In this context, improving plant resilience to combined heat and water stress represents a major objective of both fundamental plant physiology and applied agronomic research. Seed priming has emerged as an effective and low-cost strategy to enhance plant performance under adverse environmental conditions. Through controlled seed hydration in the presence of chemical or biological agents, seed priming induces a form of "physiological memory" that can persist throughout plant development, resulting in enhanced stress tolerance without the need for genetic modification (Paparella et al., 2015; Chen & Arora, 2013). Priming treatments have been shown to modulate germination dynamics, metabolic readiness, antioxidant capacity, and plant water relations, thereby improving plant survival and recovery following stress events (Waqas et al., 2019; Srivastava et al., 2021). However, the identification of sustainable, biologically derived priming agents capable of effectively increasing tolerance to abiotic stress remains an open challenge. In recent years, growing attention has been devoted to the valorization of biomass-derived products within the framework of circular economy and sustainable agriculture. Hydrothermal carbonization (HTC) is a thermochemical process that enables the conversion of wet

biomass into a carbon-rich solid fraction (hydrochar) and an aqueous phase containing nutrients and organic compounds, commonly referred to as aqueous HTC liquid (AHL) (Stemann et al., 2013; Maniscalco et al., 2020). While hydrochar has been extensively investigated for energy and environmental applications, the aqueous phase is often regarded as a waste by-product, raising concerns related to disposal and potential environmental impact (Langone & Basso, 2020). Nevertheless, AHL contains a complex mixture of organic compounds, minerals, and bioactive molecules that may represent a valuable resource for agronomic applications (Celletti et al., 2021; Leng et al., 2020). Recent evidence indicates that AHL obtained from algal biomass can act as an effective seed-priming agent, improving plant growth and physiological performance under optimal conditions. In particular, seed priming with AHL derived from the hydrothermal carbonization of macroalgae has been shown to increase photosynthetic rate, water use efficiency, stomatal density, and biomass accumulation in *Phaseolus vulgaris L.,* with effects not attributable to a simple osmotic stimulus (Spagnuolo et al., 2023). These findings support the hypothesis that AHL functions as a genuine biostimulant rather than merely as a nutrient source or an osmotic priming agent, in line with observations reported for other algal extracts and naturally derived biostimulants (Khan et al., 2009; Deolu-Ajayi et al., 2022).

Despite these promising results, a major knowledge gap remains. It is still unclear whether the physiological advantages conferred by AHL seed priming under well-watered conditions translate into enhanced tolerance to abiotic stress, particularly under combined heat and drought scenarios. Plant resistance to drought and heat stress is tightly linked to the coordination among leaf traits (such as leaf density, leaf mass area, leaf thickness, as some examples) and hydraulics. (Blum, 2017; Nardini, 2022;

Wang et al., 2025). Furthermore, the ability to maintain hydraulic functionality during stress and to rapidly recover gas exchange and water transport following rehydration represents a fundamental component of plant resilience (Trifilò et al., 2004; Abate et al., 2021).

Plant tolerance to elevated temperature depends on the capacity to maintain carbon assimilation, regulate transpiration, preserve leaf water status, and limit oxidative damage. Heat stress typically accelerates metabolic processes and increases reactive oxygen species (ROS) production, leading to membrane destabilization and impairment of photosynthetic machinery. The ability to sustain gas exchange and activate antioxidant systems therefore represents a central component of plant thermotolerance.

In this study, we investigated whether seed priming with an algal-derived aqueous phase (AHL), obtained from the hydrothermal carbonization of *Chaetomorpha aerea*, enhances plant performance under elevated temperature and improves tolerance to subsequent water deficit in *Phaseolus vulgaris* L. Plants were grown under two contrasting temperature regimes (optimal and elevated) to assess the effects of AHL priming on growth and physiological performance under heat conditions. Thereafter, irrigation was withheld until plants reached the turgor loss point ($Y_t$lp), followed by re-irrigation to evaluate post-stress recovery capacity.

We analysed plant growth, gas exchange, leaf structural traits, plant water relations, antioxidant responses, and recovery dynamics after rehydration. By integrating physiological and biochemical parameters, we aimed to determine whether AHL priming enhances (i) growth and functional stability under elevated temperature and

(ii) the ability to tolerate dehydration and rapidly restore physiological function following water stress.

We hypothesize that AHL seed priming acts as a physiological pre-conditioning strategy that induces persistent functional reprogramming, improving performance under high temperature and strengthening both drought tolerance and post-stress recovery capacity. Through this dual effect on thermal performance and dehydration resilience, AHL priming may enhance plant resistance to heat-amplified water stress.

7.2 Materials and Methods

7.2.1. Obtaining AHL Solutions

The aqueous phase derived from hydrothermal carbonization (AHL) employed in this study was produced from algal biomass subjected to HTC treatment. Samples of the green macroalga *Chaetomorpha aerea* (Chlorophyta) were collected from the coastal lagoon of Lake Ganzirri (Messina, Italy; 38°15′47.6″ N, 15°37′34.2″ E). After sampling, the biomass was thoroughly cleaned through successive washing steps with tap water followed by distilled water to remove sediments, epiphytic material, and residual salts. The washed algal material was air-dried at room temperature and subsequently dried in a ventilated oven at 60 °C until constant mass was reached. The dried biomass was then ground and sieved to obtain a fine and homogeneous powder with particle size below 1 mm, which was used as precursor for the HTC process. Hydrothermal carbonization was performed in a laboratory-scale batch system consisting of a 300 mL stainless-steel autoclave (Parr Instrument Company, IL, USA) equipped with a Teflon-lined inner vessel. For each run, approximately 1 g of algal powder was suspended in 150 mL of deionized water, corresponding to a solid-to-

liquid ratio of about 1:150 (w/v). The reactor was sealed and heated to 240 °C, allowing pressure to develop autogenously. After reaching the set temperature, the reaction was maintained for 3 h under isothermal conditions. Throughout the process, continuous agitation at 600 rpm was applied to ensure adequate dispersion of the biomass within the aqueous medium. The internal temperature was continuously monitored using a thermocouple connected to the reactor control unit. At the end of the treatment, the reactor was allowed to cool spontaneously to ambient temperature. Following the HTC process, the resulting slurry was subjected to vacuum filtration using a Büchner apparatus fitted with Whatman No. 1 filter paper to separate the liquid phase from the solid residue. The solid fraction was rinsed repeatedly with warm distilled water until neutral pH was achieved, then dried overnight at 60 °C and weighed, yielding a final dry mass of 0.9764 g. The liquid fraction, corresponding to the aqueous HTC liquid (AHL; approximately 154 mL), was collected separately and stored at 4 °C in the dark until further characterization and application in seed-priming experiments.

7.2.2. NMR-Based Metabolomic Characterization of the AHL

Prior to nuclear magnetic resonance (NMR) analysis, aliquots of the aqueous HTC liquid (AHL) were centrifuged to remove residual suspended particles and subsequently filtered through 0.22 μm membrane filters. A defined volume of the clarified AHL was then mixed with deuterium oxide (D_2O; Armar AG, Döttingen, Switzerland) containing sodium phosphate buffer (0.1 M, pH 7.0) to ensure pH stability during spectral acquisition. Sodium 2,2-dimethyl-2-silapentane-5-sulfonate (DSS, 1 mM) was added as both a chemical shift reference and a quantitative internal

standard. Samples were gently vortexed to ensure homogeneity and briefly centrifuged to eliminate any remaining insoluble material. The resulting solutions were transferred into standard 5 mm NMR tubes and analyzed using a 500 MHz Varian NMR spectrometer operating at a proton resonance frequency of 499.74 MHz. All measurements were performed at a controlled temperature of 25 °C. One-dimensional ^{1}H NMR spectra were acquired using a NOESY-based presaturation pulse sequence for efficient suppression of the residual water signal. Acquisition parameters included 256 scans, a spectral width of 11.7 ppm, and a data size of 32,768 points. Free induction decays were zero-filled to 65,536 points prior to Fourier transformation. Spectra were manually phase-corrected and baseline-adjusted to optimize signal quality. Chemical shift calibration was performed by setting the DSS singlet to 0.00 ppm. Metabolite identification and quantification were carried out using Chenomx NMR Suite software (version 11.1; Chenomx Inc., Edmonton, Canada). Resonances were assigned by comparison with reference spectral libraries and further validated against publicly available NMR databases. Quantification was achieved through targeted spectral deconvolution relative to the DSS internal standard. Identified metabolites were subsequently grouped into major biochemical classes, such as organic acids, carbohydrates, amino acids, and other low-molecular-weight compounds, to facilitate interpretation of the chemical composition of the AHL.

7.2.2.1 Pathway mapping and enrichment analysis of AHL metabolites

To gain functional insight into the biochemical composition of the hydrothermal carbonization (HTC) aqueous liquid (AHL) produced from the green macroalga *Chaetomorpha aerea*, the list of metabolites identified by ^{1}H NMR was

subjected to pathway mapping and enrichment analysis using MetaboAnalyst (version 6). Metabolites were annotated against the KEGG database and processed using over-representation analysis (ORA) based on the hypergeometric test. Pathway topology analysis was performed to compute pathway impact scores (relative-betweenness centrality). Multiple-testing correction was applied using the false discovery rate (FDR), and pathways were considered significantly enriched at adjusted $p < 0.05$. Because AHL originates from an algal feedstock but is applied to a higher-plant system, enrichment analyses were performed using two complementary KEGG reference libraries: (i) Chlamydomonas reinhardtii to provide a feedstock-oriented functional annotation reflecting algal metabolic context; and (ii) Arabidopsis thaliana to provide a plant-oriented mapping aimed at identifying pathways that are plant-relevant and potentially modulated upon application. In both cases, results were interpreted as putative pathway associations based on the metabolites detected in AHL, rather than as direct evidence of in vivo pathway activation in plant tissues.

7.2.3. Seed Priming Procedure and Experimental Design

Seeds of common bean (*Phaseolus vulgaris* L. cv. 'Borlotto'), a widely cultivated commercial variety in Italy, were used in all experiments. Prior to priming, seeds were visually inspected to exclude damaged or malformed individuals. Seed priming was carried out by soaking seeds for 24 h either in distilled water (control treatment) or in the aqueous HTC liquid (AHL treatment), at room temperature and in the dark to prevent premature germination. After priming, seeds were gently blotted dry with absorbent paper and immediately transferred to germination conditions. Primed seeds were germinated under controlled conditions until root emergence. Once

the primary roots were sufficiently developed, seedlings were transplanted into individual pots filled with a standardized growth substrate (Comodo, Tercomposti, S.P.A., Italy),and allowed to establish under well-watered conditions. Plants were grown in the greenhouse facilities of the Department of Chemical, Biological, Pharmaceutical and Environmental Sciences (ChiBioFarAm), University of Messina. The greenhouse was illuminated by LED lamps (Led Spectrum Grow 6, I-GROW s.r.l., Italy), ensuring a 12 h light/12 h dark photoperiod (Spagnuolo et al., 2023). To evaluate the effects of AHL seed priming under different thermal regimes, plants were divided between two greenhouses, each equipped with the same LED lamps subjected to two temperature conditions: optimal temperature (25 °C) and heat stress conditions (32 °C). For each temperature regime, both control (water-primed) and AHL-primed plants were included, resulting in four experimental groups: Control–Optimal, AHL–Optimal, Control–Heat, and AHL–Heat. All plants were maintained under well-watered conditions for approximately one month to allow full vegetative development. Thereafter, irrigation was withheld across all experimental groups to impose a controlled water deficit until plants reached the turgor loss point. Following the stress phase, plants were re-irrigated to restore well-watered conditions and to assess post-stress recovery prior to subsequent physiological measurements.

7.2.4. Plant growth and anatomical traits

Plant growth was monitored throughout the experimental period. Morphological parameters, including plant height, number of leaves, and basal stem diameter, were recorded weekly over a nine-week period on five plants per experimental group. Measurements were performed on the same individuals to track

growth dynamics over time. Leaf anatomical traits were assessed on fully expanded leaves collected from eight-week-old plants. At the end of the experimental period, all leaves from each plant were excised and scanned using a flatbed scanner (HP Scanjet G4050, USA). Digital images were analyzed with ImageJ software to determine total leaf area (A_L) for each individual plant. Moreover, five leaves per experimental group were collected to estimate leaf thickness (TL), measured at the base, middle, and tip of each leaf with a digital caliper (±0.01 mm); leaf mass per area (LMA), calculated as dry weight divided by leaf area after drying samples at 70°C for 3 days. At the end of the experimental period, plants were carefully removed from the pots, and the root system was gently washed with water to remove adhering soil. Roots, stems, and leaves were separated and oven-dried at 70 °C for three days to obtain dry weight (DW). Dry biomass was determined separately for each organ in order to evaluate biomass allocation patterns among roots, stems, and leaves.

7.2.5. Plant Water Relations

Gas exchange was measured on fully expanded leaves using a portable photosynthesis system (Ciras 4, Amesbury, MA, USA; CO_2 set at 400 μmol m^{-2} s^{-1}). Measurements were taken at midday on three plants per experimental group before drought imposition (irrigation withheld for one week) and for five days following re-irrigation, during the recovery phase. In order to check if AHL seed priming and/or growth temperature may cause differences in turgor loss point in C vs AHL samples, leaf water potential at the turgor loss point (Ψ_{tlp}) and osmotic potential at full turgor (π_0) were quantified on five leaves collected from five individual plants, following the methodology described by Petruzzellis et al. 2019. Fully expanded leaves were

sampled in the early morning, prior to the onset of the light period, from well-watered plants. Immediately after excision, leaves were wrapped in plastic film and immersed in liquid nitrogen for 2 min to rapidly arrest metabolic activity. The frozen samples were then ground while still enclosed in the plastic film and stored in sealed plastic containers at −20 °C until analysis. Prior to measurements, samples were thawed at room temperature and osmotic potential was determined using a dew point hygrometer (WP4, Decagon Devices Inc.). According to Petruzzellis et al. 2019, osmotic potential at full turgor (π_0) was estimated using the following equation:

$\pi_0 = (0.5303 \times \pi_{WP4}) + (0.0019 \times \text{LDMC})$Where π_{WP4} represents the osmotic potential measured with the dew point hygrometer and LDMC is the leaf dry matter content. Leaf water potential at the turgor loss point (Ψ_{tlp}) was subsequently calculated using the following relationship:

$$\Psi_{tlp} = (1.31 \times \pi_0) - 0.03$$

7.2.6. Enzymatic Antioxidant Activities and Lipid Peroxidation

Leaf samples for biochemical analyses were collected from all experimental groups before the imposition of water stress and at the end of the recovery period (i.e. five days after re-irrigation). Fully expanded leaves were excised, immediately frozen in liquid nitrogen, and stored at −80 °C until analysis. Enzymatic assays were performed exclusively on leaf tissues, as stem samples were not suitable for reliable homogenization. Frozen leaf material was finely ground under liquid nitrogen using a mortar and pestle and homogenized in an extraction buffer consisting of 50 mM sodium phosphate buffer (pH 7.6), supplemented with 0.1 mM Na-EDTA, 1% (w/v)

polyvinylpyrrolidone (PVP), 0.1 mM phenylmethylsulfonyl fluoride (PMSF), and 1 mM dithiothreitol (DTT), freshly added prior to extraction. The ratio of plant material to extraction buffer was 0.100 g fresh weight per 1.6 mL buffer. Homogenates were centrifuged at 14,000 × g for 20 min at 4 °C, and the resulting supernatants were collected and stored at −80 °C until enzymatic determinations (Pereira et al., 2024). Catalase (CAT) activity was assayed spectrophotometrically by monitoring the decrease in absorbance at 240 nm associated with hydrogen peroxide decomposition (Teranishi et al., 1974). The reaction mixture contained 50 mM sodium phosphate buffer (pH 7.6), 0.1 mM Na-EDTA, and 100 mM H_2O_2. The reaction was initiated by adding 10 µL of enzyme extract to 200 µL of reaction mixture, and CAT activity was expressed as µmol H_2O_2 decomposed min^{-1} mg $protein^{-1}$. Ascorbate peroxidase (APX) activity was determined by following the oxidation of ascorbate, measured as a decrease in absorbance at 290 nm (Tiryakioglu et al., 2006). The reaction mixture consisted of 50 mM sodium phosphate buffer (pH 7.6), 12 mM H_2O_2, and 0.25 mM L-ascorbate. The reaction was initiated by the addition of 10 µL of enzyme extract to 200 µL of reaction mixture, and APX activity was expressed as µmol ascorbate oxidized min^{-1} mg $protein^{-1}$. Lipid peroxidation (LPO) was estimated by quantifying thiobarbituric acid reactive substances (TBARS) (Dhindsa et al., 1981; Anjum et al., 2013; Duarte et al., 2015). Approximately 0.10 g of frozen leaf tissue was homogenized under liquid nitrogen and mixed with a solution containing 0.5% (w/v) thiobarbituric acid (TBA) and 20% (w/v) trichloroacetic acid (TCA). The homogenates were incubated at 95 °C for 30 min and immediately cooled on ice to stop the reaction. Samples were then centrifuged at 3000 × g for 5 min at 4 °C, and the absorbance of the supernatant was measured at 532 nm and corrected for nonspecific

turbidity at 600 nm. Lipid peroxidation was expressed as nmol TBARS g^{-1} fresh weight using a molar extinction coefficient of 1.55×10^5 M^{-1} cm^{-1}. Total soluble protein content was determined according to the Bradford method using a commercial assay kit, with bovine serum albumin (BSA) as the protein standard (Bradford, 1976). All enzymatic activities were normalized to protein concentration.

7.2.7 Statistical analysis

All data were tested for normality and homogeneity of variances prior to statistical analyses. Normality was assessed using the Shapiro–Wilk test, while homoscedasticity was evaluated using Levene's test. Differences among treatments were analysed using two-way analysis of variance (ANOVA), with seed priming treatment (Control vs. AHL) and growth temperature (optimal vs. heat stress) as fixed factors, including their interaction term. When significant main effects or interactions were detected, post hoc comparisons were performed using Tukey's honestly significant difference (HSD) test. For variables assessed before and after water stress (e.g., enzymatic activities and lipid peroxidation), samples collected at the two time points were analysed separately using two-way ANOVA, given that measurements were obtained from different leaves, albeit from the same plant. Statistical significance was set at $p < 0.05$, and significance levels are reported in the figures as $p < 0.05$ (*) and $p < 0.001$ (**). Data are presented as mean ± SD. Statistical analyses were performed using GraphPad Prism (version 10).

7.3 Result

7.3.1 NMR-Based Metabolomic Profile of the AHL

^{1}H NMR analysis revealed that the aqueous HTC liquid (AHL) contained a complex mixture of low-molecular-weight metabolites. The metabolomic profile was dominated by organic acids, carbohydrates, amino acids, and other soluble organic compounds typically associated with biomass-derived aqueous phases. The presence of multiple metabolite classes suggests that the biostimulant effect of AHL cannot be attributed to a single compound but rather to the combined action of diverse bioactive molecules. This complex chemical composition provides a plausible basis for the observed physiological, anatomical, and biochemical responses induced by AHL seed priming (see below).

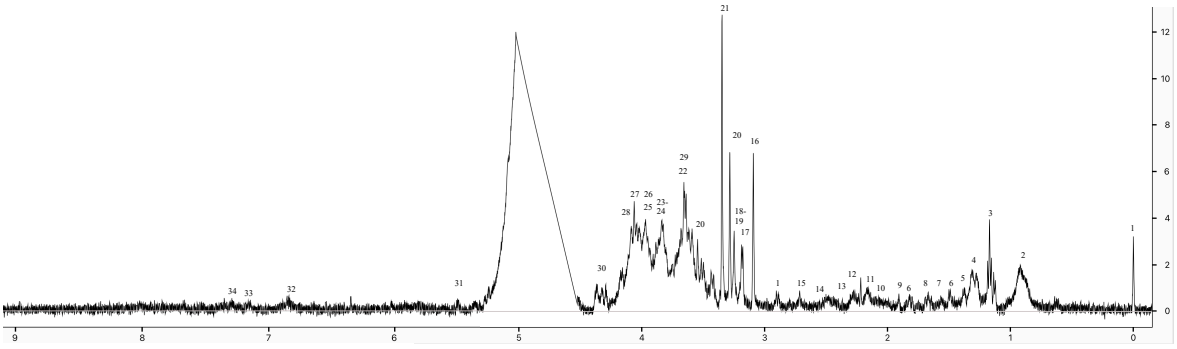


Figure 1 - Representative one-dimensional ^{1}H NMR spectrum of the algal-derived aqueous HTC liquid (AHL) acquired at 500 MHz. The spectrum reveals a complex mixture of low-molecular-weight metabolites, including organic acids, carbohydrates, amino acids, and other soluble compounds. DSS was used as internal standard and chemical shift reference (0.00 ppm). The chemical complexity of the AHL supports its role as a multifunctional biostimulant rather than a single-compound effector. Keys: (1) DSS, (2) BCAA, (3) ethanol, (4) lactate, (5) alanine, (6) lysine, (7) butyrate, (8) valerate, (9) acetate, (10) glutamate, (11) proline, (12) malate, (13) pyruvate, (14) citrate, (15) dimethylamine, (16) 1,3-

diaminopropane, (17) choline, (18) betaine, (19) trimethylamine-N-oxide (TMAO), (20) glycine, (21) methanol, (22) glucose, (23) erythritol, (24) lactose, (25) ribose, (26) fructose, (27) galactonate, (28) gluconate, (29) xylose, (30) AMP/ADP, (31) UDP-N-Acetylglucosamine, (32) N-Acetyl tyrosine, (33) imidazole, (34) N-acetyl serotonin.

7.3.1.1 Pathway enrichment analysis

Network-based pathway enrichment performed using the *Chlamydomonas reinhardtii* KEGG library (feedstock-oriented mapping) indicated that metabolites detected in the HTC-derived AHL were primarily associated with central carbon metabolism and nitrogen-related pathways. Highly connected nodes included glyoxylate and dicarboxylate metabolism, alanine/aspartate/glutamate metabolism, glycolysis/gluconeogenesis, the TCA cycle, and amino sugar and nucleotide sugar metabolism, together with pathways linked to sulphur and nitrogen metabolism. The prominence of these routes is consistent with a complex algal-derived mixture enriched in small polar metabolites generated and/or released during HTC processing and supports the interpretation of AHL as a chemically active process liquid rather than an inert by-product. When the same metabolite list was mapped against the *Arabidopsis thaliana* KEGG library (plant-oriented mapping), enrichment similarly emphasized core energetic and redox-related processes that are directly relevant to plant stress physiology. In particular, pathways such as glycolysis/gluconeogenesis, pyruvate metabolism, TCA cycle, pentose phosphate pathway, glutathione metabolism, and one-carbon metabolism by folate were highlighted as major network hubs. Amino acid pathways (e.g., glycine/serine/threonine; alanine/aspartate/glutamate; branched-chain amino acid biosynthesis and degradation; arginine and proline metabolism) were also strongly represented, consistent with the

presence of metabolites potentially acting as metabolic precursors, osmolyte-related compounds, and redox modulators. Taken together, the dual-reference enrichment strategy provides a coherent two-level interpretation: (i) a feedstock-consistent functional annotation of AHL composition in an algal metabolic context; and (ii) a plant-relevant mapping indicating that AHL contains metabolites linked to pathways that are central to energy supply, redox homeostasis, and stress-response metabolism in higher plants. This framework supports downstream mechanistic discussion connecting AHL chemical complexity with the observed improvements in antioxidant capacity, post-stress physiological recovery, and biomass maintenance in AHL-primed *Phaseolus vulgaris.*

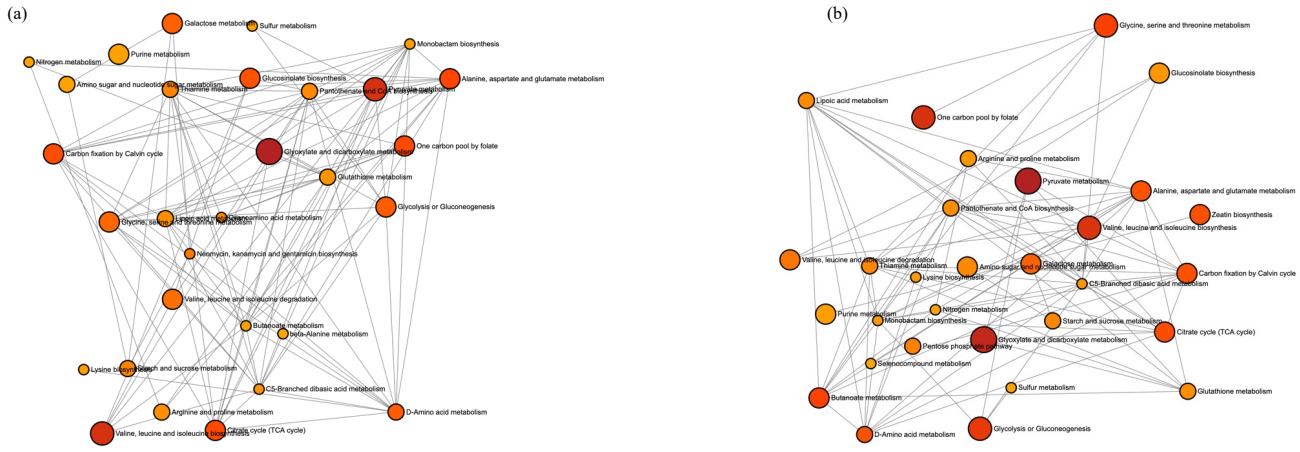


Figure 2 - Pathway enrichment analysis of metabolites identified in the HTC-derived AHL. Network-based enrichment analysis performed in MetaboAnalyst using KEGG libraries. (a) Enrichment against Chlamydomonas reinhardtii pathways, reflecting the algal origin of the HTC liquid. (b) Enrichment against Arabidopsis thaliana pathways, highlighting plant-related metabolic processes potentially modulated by AHL. Node size indicates pathway impact, and color intensity reflects statistical significance (FDR-adjusted $p < 0.05$). Edges represent shared metabolites among pathways.

7.3.2 Effects of AHL Seed Priming on Plant Morphology

Seed germination was similar (i.e. about 80%) in both AHL-primed and control seeds (Figure 3, Figure 5a). Despite seed priming with algal-derived AHL didn't impact on germinabiliyty, it significantly influenced plant growth and biomass production under both optimal and heat stress conditions (Figure 4).

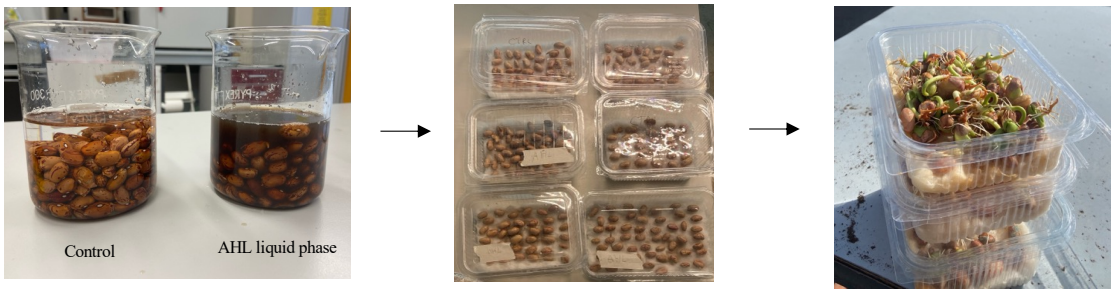


Figure 3- Representative images illustrating the seed priming procedure and subsequent germination of Phaseolus vulgaris seeds. Seeds were primed either in distilled water (Control) or in algal-derived aqueous HTC liquid (AHL) for 24 h prior to germination. Images show seeds during the priming phase, immediately after priming, and following germination, highlighting the absence of visible phytotoxic effects and the high germination success in both treatments.

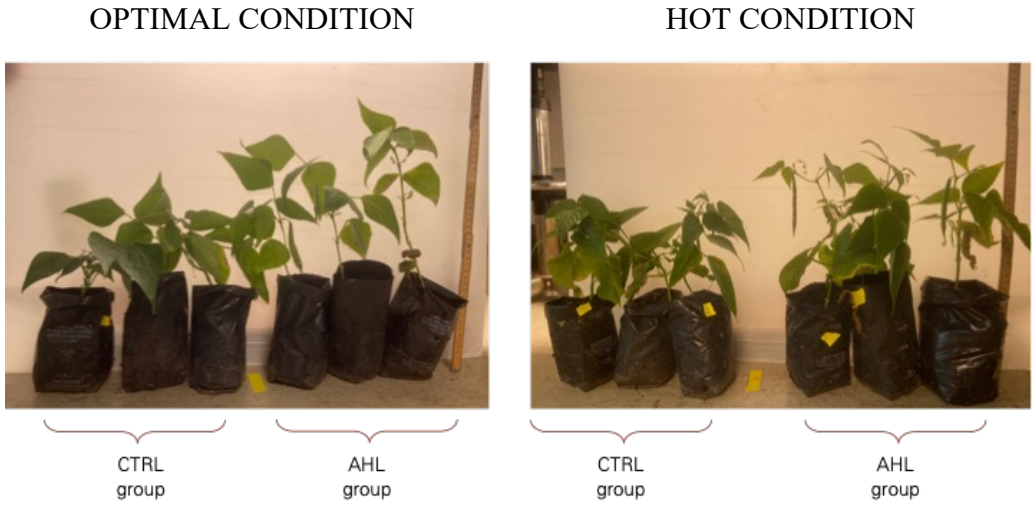


Figure 4 - Representative images of Phaseolus vulgaris *plants grown from control and AHL-primed seeds under optimal temperature (OPT) and heat stress (HOT) conditions at the end of the experimental*

period. AHL-primed plants exhibit enhanced growth performance, with increased stem height and overall vigor compared to control plants, particularly under heat stress conditions.

At the end of the experimental period, AHL-primed plants exhibited a significantly higher basal stem diameter, greater plant height, and increased number and surface area of leaves compared to control plants under both temperature regimes (Figure 5b-c-d, Figure 6e). Moreover, higher biomass occurred in AHL-treated plants compared to control samples, both under optimal and high temperature (Figure 5e-f-g-h). Specifically, exposure to elevated temperature markedly reduced growth performance in control plants, resulting in shorter stems, reduced basal diameter, and decreased leaf area respect samples growing under optimal temperature and the same occurred in AHL-plants. However, AHL-primed plants subjected to heat stress showed a partial to substantial mitigation of these negative effects, maintaining significantly higher values for all morphological parameters. Regarding plant water relations, heat stress induced more negative values of osmotic potential at full turgor (π_0) and turgor loss point (Ψtlp) in control plants, indicating enhanced osmotic adjustment under stress. AHL-primed plants showed a similar trend but maintained slightly less negative π_0 and Ψtlp values under heat stress, suggesting improved water status regulation (Figure 6c-d). LMA was higher in AHL-primed plants under optimal conditions and decreased under heat stress in both treatments; however, AHL plants maintained significantly greater LMA than controls under heat, with values comparable to or exceeding those of control plants grown at optimal temperature (Figure 6b). In contrast, LDMC showed a slight decrease under heat stress, particularly in control plants, whereas AHL-treated plants maintained values comparable to or slightly higher than those of controls, indicating a more stable leaf structural integrity under stress (Figure 6a).

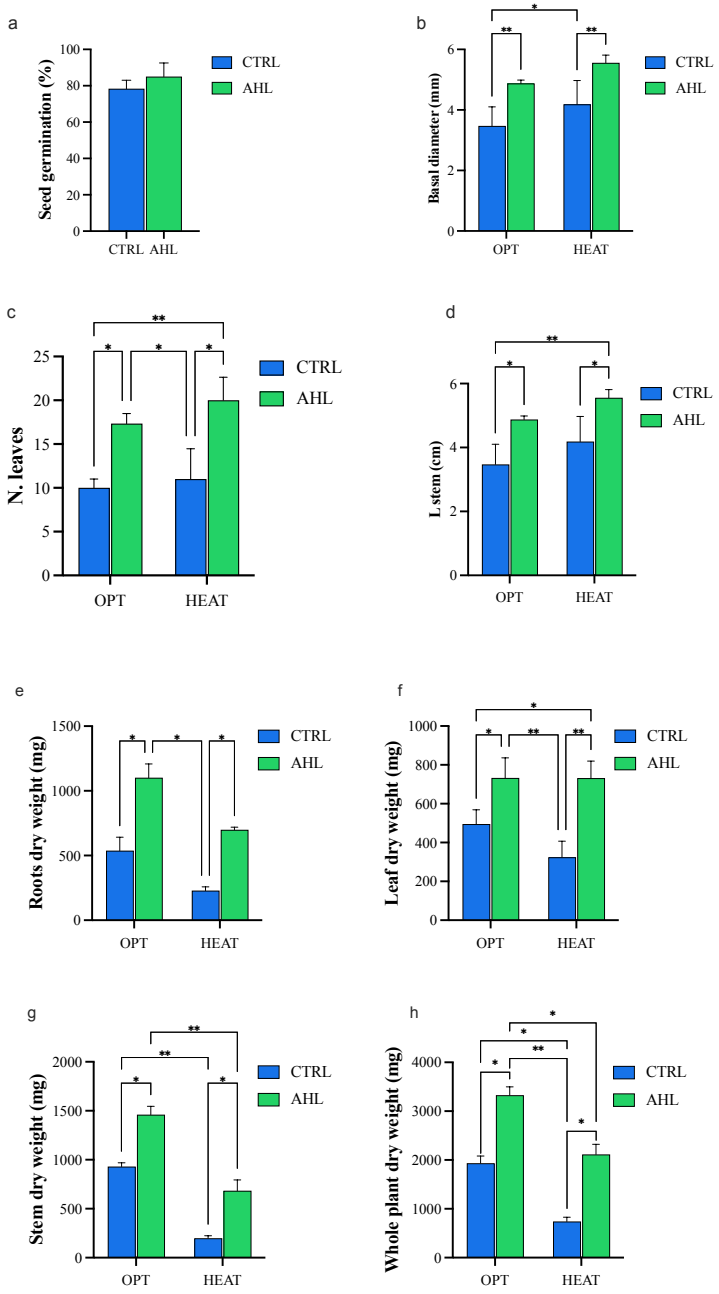


Figure 5 – (a) Seed germination percentage of Phaseolus vulgaris following seed priming with distilled water (Control) or aqueous HTC liquid (AHL). (b-c-d) Morphological parameters of Phaseolus vulgaris plants grown from control and AHL-primed seeds under optimal (OPT) and heat stress (HOT) conditions. Dry weight (DW) of roots (e), stems (g), leaf (f) and whole plant (h) in Phaseolus vulgaris plants grown from control and AHL-primed seeds under optimal and heat stress conditions. Data are

*expressed as mean ± SD (n = 5). Asterisks indicate significant differences between different treatments (*p < 0.05, **p<0.001).*

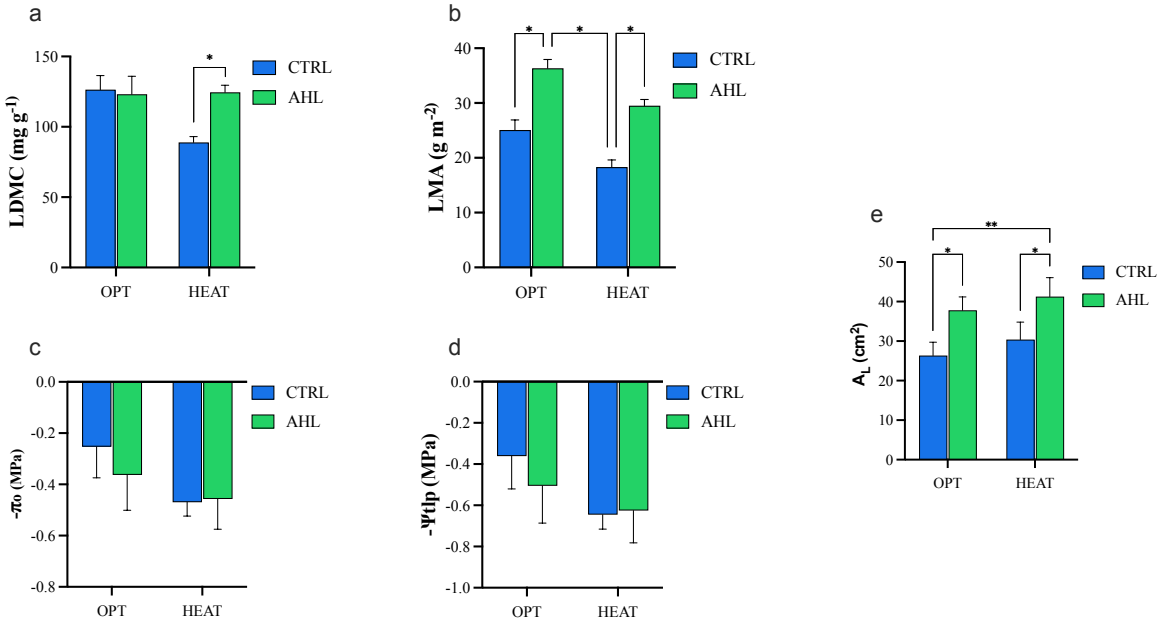


*Figure 6 – Effects of AHL seed priming on leaf structural traits and plant water relations under optimal and heat stress conditions. (a) Leaf dry matter content (LDMC), (b) leaf mass area (LMA), (c) osmotic potential at full turgor (π_0), (d) leaf water potential at the turgor loss point (Ψtlp), and (e) total leaf area (A_l) measured in control (CTRL) and AHL-primed plants grown under optimal temperature (OPT) and heat stress (HEAT) conditions. Asterisks indicate statistically significant differences between treatments (*p < 0.05; **p < 0.001). Data are expressed as mean ± SD (n = 5).*

7.3.3 Stomatal Conductance Dynamics during Recovery

Stomatal conductance to water vapor (g_s), measured after re-irrigation following water stress, differed significantly among treatments. Under optimal temperature, AHL-primed plants showed higher g_s compared to control plants. In heat-stressed controls, g_s remained markedly reduced even after the restoration of irrigation, indicating incomplete functional recovery. Conversely, AHL-primed plants displayed

significantly higher g_s under heat stress after re-irrigation, with values comparable to those measured in optimally grown plants (Figure 7). These results indicate that AHL priming enhanced the recovery of stomatal function following combined heat and water stress.

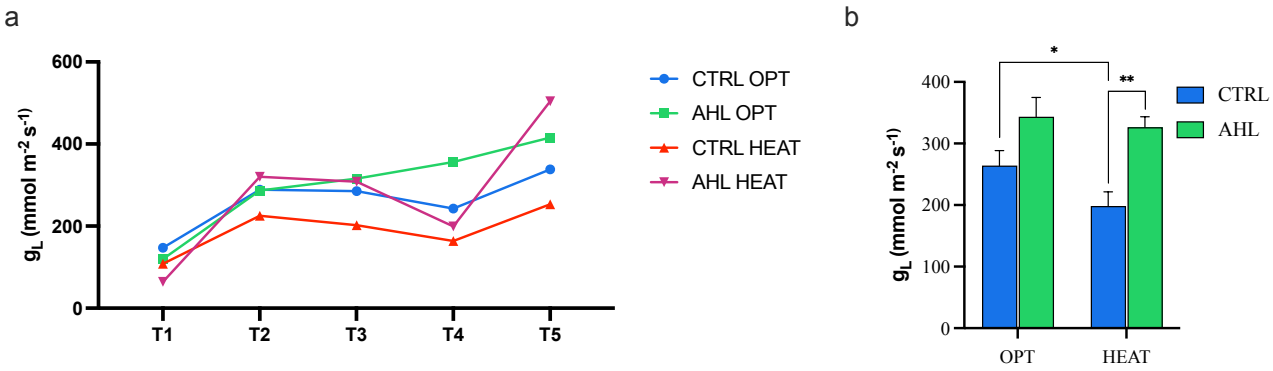


*Figure 7 – post-re-irrigation stomatal conductance to water vapor (g_s) in control and AHL-primed plants. (a) Temporal dynamics of stomatal conductance measured after re-irrigation in plants previously subjected to water stress under optimal and heat stress conditions. (b) Mean stomatal conductance calculated over the post-re-irrigation phase. Asterisks indicate statistically significant differences between control and AHL treatments within the same temperature regime (*p < 0.05; **p < 0.001). Data are expressed as mean ± SD (n = 7).*

7.3.4 Antioxidant Enzyme Activities and Lipid Peroxidation

Antioxidant enzyme activities and lipid peroxidation levels were significantly affected by water stress and seed priming treatment. Before stress imposition, AHL-primed plants already exhibited slightly higher CAT and APX activities compared to control plants, indicating a priming-induced enhancement of basal antioxidant preparedness rather than a stress-driven activation. Following water stress, CAT and APX activities increased in all experimental groups, reflecting enhanced oxidative pressure. However, AHL-primed plants displayed significantly higher antioxidant enzyme

activities than control plants under both optimal and heat stress conditions, indicating a more efficient and coordinated antioxidant response. Lipid peroxidation, estimated as TBARS content, increased markedly in control plants after water stress, particularly in plants growing at higher temperature. In contrast, AHL-primed plants showed significantly lower TBARS levels, indicating reduced membrane damage. Together, these results (Figure 8) demonstrate that AHL seed priming enhances antioxidant capacity, limits oxidative injury, and supports improved physiological recovery following combined heat and water stress.

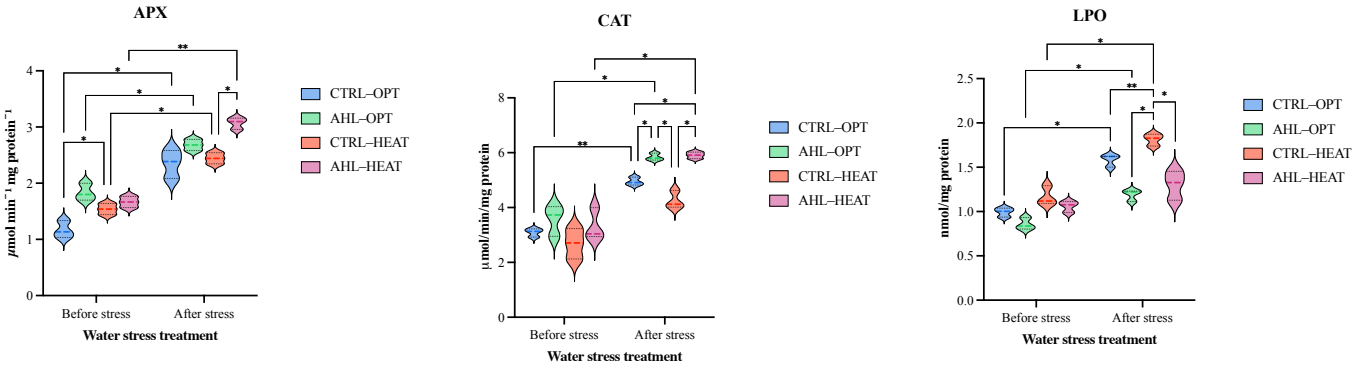


Figure 8 - Activities of catalase (CAT) and ascorbate peroxidase (APX), and levels of lipid peroxidation (LPO, expressed as TBARS content) in leaves of control and AHL-primed plants before and after water stress. AHL-primed plants exhibited enhanced antioxidant enzyme activities and reduced lipid peroxidation following stress, indicating improved oxidative stress management. Data are expressed as mean ± SD.

7.4 Discussion

The present study provides converging evidence that seed priming with an algal-derived aqueous phase from hydrothermal carbonization (AHL) enhances plant performance and tolerance to combined heat and water stress in *Phaseolus vulgaris*. Importantly, AHL functions as a metabolic priming input, enhancing stress resilience through redox-centered regulation rather than via direct hormonal or nutritional effects.

7.4.1 AHL as a Metabolic Interface Rather Than a Simple Biostimulant

Metabolomic profiling revealed that HTC-derived AHL is enriched in central carbon intermediates, amino acids, and redox-related metabolites. Rather than representing a generic mixture of biomass degradation products, the pathway enrichment analysis suggests a functionally relevant profile: AHL mirrors conserved metabolic hubs central to stress acclimation in higher plants. The convergence of glycolysis, TCA cycle, pentose phosphate pathway, glutathione metabolism, and amino acid pathways is unlikely to be incidental, as these routes collectively coordinate ATP production, carbon skeleton availability, nitrogen assimilation, and redox buffering. Increasingly, biostimulant research emphasizes systems-level modulation of primary metabolism over single “active principles” (Zheng et al., 2026; Mashabela et al., 2025). In this context, AHL can be interpreted as a metabolic interface, supplying small molecules that directly interact with plant metabolism and stress-regulatory networks.

Of particular note is the enrichment of, pentose phosphate pathway and glutathione metabolism. The, pentose phosphate pathway –NADPH–glutathione axis

is a central regulator of cellular redox poise under abiotic stress (Zhang et al., 2026; Kruger et al., 2011). The chemical profile of AHL therefore suggests a mechanistic predisposition to enhance redox buffering capacity, a hypothesis corroborated by the observed antioxidant responses.

7.4.2 Priming by AHL Reprograms Basal State and Enhances Stress Resilience

AHL priming did not affect germination, indicating no alteration of early metabolic reactivation or hormonal balance during imbibition. This aligns with previous studies showing that appropriately managed HTC-derived aqueous phases do not inhibit germination in legumes and Brassicaceae (Wang et al., 2020; Celletti et al., 2021; Spagnuolo et al., 2023). The absence of germination effects suggests that AHL does not act as a classical growth regulator. Conversely, elevated basal CAT and APX activities observed prior to stress indicate that AHL establishes a pre-conditioned antioxidant state, a hallmark of priming (Gonzalez Hernandez, 2019). Primed plants maintain defence systems in readiness, enabling faster and stronger activation under stress with minimal metabolic cost.

After stress exposure, enhanced antioxidant enzyme activities in AHL-primed plants, coupled with lower TBARS accumulation, confirm that priming translates into effective oxidative damage control. Reduced lipid peroxidation indicates that AHL does not merely amplify ROS detoxification but preserves membrane integrity and cellular functionality, essential components of resilience (Zandi et al., 2022; Garcia et al., 2014).

Under optimal conditions, AHL-primed plants exhibited increased stem height, basal diameter, leaf number, total leaf area, and dry biomass relative to water-primed

controls. These growth-promoting effects are consistent with reports for algal extracts and other natural biostimulants, which operate through combined nutritional, signalling, and hormone-like mechanisms rather than simple fertilization (Baltazar et al., 2021).

Under heat stress, control plants showed pronounced growth inhibition, reflecting the known impacts of high temperature on cell expansion, carbon assimilation, and biomass accumulation (Kumar et al., 2011; Essemine et al., 2010; Hassan et al., 2021). In contrast, AHL-primed plants maintained significantly higher values across all morphological traits, indicating clear mitigation of thermal growth penalties (Blum, 2017; Rodríguez-Domínguez & Brodribb, 2020)

Biomass partitioning revealed that AHL affected not only total accumulation but also allocation. Primed plants retained higher dry mass in roots, stems, and leaves under heat stress, whereas controls showed marked reductions. This coordinated maintenance of above- and below-ground biomass suggests a functionally advantageous allocation strategy, supporting both carbon gain (via leaves) and water acquisition (via roots) under combined stress (Poorter et al., 2012; Eziz et al., 2017; Blum, 2017; Nardini, 2022). The coordinated increase in leaf volume and LMA, with stable leaf density, further underscores preservation of structural integrity and functional investment.

The morphological advantages observed likely derive from improved redox homeostasis. Heat stress disrupts electron transport chains and generates ROS, constraining cell expansion and protein stability. By enhancing antioxidant systems and potentially increasing NADPH availability via PPP-related pathways, AHL priming may buffer redox perturbations at their source. Higher LMA and stable LDMC

in primed plants support this interpretation, reflecting maintained tissue structural integrity and resistance to oxidative damage (Poorter et al., 2009).

Stomatal conductance measurements further illustrate the functional consequences of priming. In control plants, heat-stressed individuals exhibited persistent stomatal limitation after re-irrigation, indicating incomplete recovery. AHL-primed plants restored gL to near-optimal levels, suggesting improved guard cell functionality. Effective stomatal reopening requires ATP-driven ion transport and controlled ROS signaling, both of which are facilitated by enhanced antioxidant capacity (Murata et al., 2015).

7.5 Conclusion

This study demonstrates that seed priming with an algal-derived aqueous phase from hydrothermal carbonization (AHL) enhances plant performance and tolerance to combined heat and water stress in *Phaseolus vulgaris*. AHL acts as a metabolic priming agent, reprogramming basal metabolic and antioxidant pathways to establish a pre-conditioned state that improves redox homeostasis, preserves tissue structure, and maintains biomass allocation under stress. These coordinated effects limit cellular and membrane damage, support rapid recovery of stomatal and hydraulic function, and sustain growth and gas exchange during and after stress, reflecting a robust priming-induced "stress memory."

Unlike conventional fertilizers, AHL does not function primarily through nutrient supply but as a metabolic conditioner that enhances resilience and recovery capacity. From an applied perspective, these findings underscore the potential of algal-derived HTC aqueous phases, often considered waste streams, as valuable biostimulant resources within a circular economy framework. By demonstrating multi-level enhancement of plant stress tolerance, this study provides mechanistic support for the valorization of HTC by-products as sustainable tools to improve crop performance in the face of climate change.

7.6 References

Abate, E., Nardini, A., Petruzzellis, F., & Trifilò, P. (2021). Too dry to survive: Leaf hydraulic failure in two *Salvia* species can be predicted on the basis of water content. *Plant Physiology and Biochemistry, 166*, 215–224.

Anjum, N.A.; Ahmad, I.; Rodrigues, S.M.; Henriques, B.; Cruz, N.; Coelho, C.; Pacheco, M.; Duarte, A.C.; Pereira, E. Eriophorum Angustifolium and Lolium Perenne Metabolic Adaptations to Metals- and Metalloids-Induced Anomalies in the Vicinity of a Chemical Industrial Complex. Environ. Sci. Pollut. Res. 2013, 20, 568–581.

Baltazar, M., Correia, S., Guinan, K. J., Sujeeth, N., Bragança, R., & Gonçalves, B. (2021). Recent advances in the molecular effects of biostimulants in plants: An overview. Biomolecules, 11(8), 1096.

Bradford, M.M. A Rapid and Sensitive Method for the Quantitation of Microgram Quantities of Protein Utilizing the Principle of Protein-Dye Binding. Anal. Biochem. 1976, 72, 248–254.

Blum, A., 2017. Osmotic adjustment is a prime drought stress adaptive engine in support of plant production. *Plant Cell Environ.* 40, 4–10.

Calvo, P., Nelson, L., & Kloepper, J. W. (2014). Agricultural uses of plant biostimulants. *Plant and Soil, 383*(1–2), 3–41.

Celletti, S., Lanz, M., Bergamo, A., Benedetti, V., Basso, D., Baratieri, M., Cesco, S., Mimmo, T., 2021. Evaluating the aqueous phase from hydrothermal carbonization of cow manure digestate as possible fertilizer solution for plant growth. *Front. Plant Sci.* 12, 687434.

Chen, K., Arora, R., 2013. Priming memory invokes seed stress-tolerance. *Environ. Exp. Bot.* 94, 33–45.

Choudhury, S., Panda, P., Sahoo, L., & Panda, S. K. (2017). Reactive oxygen species signaling in plants under abiotic stress. *Plant Signaling & Behavior, 12*(1), e1332541.

Deolu-Ajayi, A. O., Van der Meer, I. M., Van der Werf, A., & Karlova, R. (2022). The power of seaweeds as plant biostimulants to boost crop production under abiotic stress. *Plant, Cell & Environment, 45*(9), 2537–2553.

Dhindsa, R.S.; Plumb-dhindsa, P.; Thorpe, T.A. Leaf Senescence: Correlated with Increased Levels of Membrane Permeability and Lipid Peroxidation, and Decreased Levels of Superoxide Dismutase and Catalase. J. Exp. Bot. 1981, 32, 93–101.

Duarte, B.; Santos, D.; Marques, J.C.; Caçador, I. Impact of Heat and Cold Events on the Energetic Metabolism of the C3 Halophyte Halimione Portulacoides. Estuar. Coast. Shelf Sci. 2015, 167, 166–177.

Essemine, J., Ammar, S., & Bouzid, S. (2010). Impact of heat stress on germination and growth in higher plants: Physiological, biochemical and molecular

repercussions and mechanisms of defence. Journal of Biological Sciences, 10(6), 565-572.

Eziz, A., Yan, Z., Tian, D., Han, W., Tang, Z., & Fang, J. (2017). Drought effect on plant biomass allocation: A meta-analysis. *Ecology and Evolution, 7*(24), 11002–11010.

FAO, 2020. *The State of World Fisheries and Aquaculture 2020*. FAO, Rome, Italy.

García, J. J., López-Pingarrón, L., Almeida-Souza, P., Tres, A., Escudero, P., García-Gil, F. A., ... & Bernal-Pérez, M. (2014). Protective effects of melatonin in reducing oxidative stress and in preserving the fluidity of biological membranes: a review. Journal of pineal research, 56(3), 225-237.

Gill, S. S., & Tuteja, N. (2010). Reactive oxygen species and antioxidant machinery in abiotic stress tolerance in crop plants. *Plant Physiology and Biochemistry, 48*(12), 909–930.

González Hernández, A. I. (2019). New approaches to control Pseudomonas syringae disease in tomato plants.

Hasanuzzaman, M., Bhuyan, M. H. M. B., Zulfiqar, F., Raza, A., Mohsin, S. M., Mahmud, J. A., Fujita, M., & Fotopoulos, V. (2020). Reactive oxygen species and antioxidant defense in plants under abiotic stress: Revisiting the crucial role of a universal defense regulator. *Antioxidants, 9*(8), 681.

Hassan, M. U., Chattha, M. U., Khan, I., Chattha, M. B., Barbanti, L., Aamer, M., ... & Aslam, M. T. (2021). Heat stress in cultivated plants: Nature, impact, mechanisms, and mitigation strategies—A review. *Plant Biosystems-An International Journal Dealing with all Aspects of Plant Biology*, *155*(2), 211-234.

IPCC, 2014. *Climate Change 2014: Mitigation of Climate Change*. Contribution of Working Group III to the Fifth Assessment Report of the Intergovernmental Panel on Climate Change. Cambridge University Press, Cambridge, UK.

Keunen, E., Peshev, D., Vangronsveld, J., Van Den Ende, W., & Cuypers, A. (2013). Plant sugars are crucial players in the oxidative challenge during abiotic stress: Extending the traditional concept. *Plant, Cell & Environment, 36*(7), 1242–1255.

Khan, W., Rayirath, U. P., Subramanian, S., Jithesh, M. N., Rayorath, P., Hodges, D. M., Critchley, A. T., Craigie, J. S., Norrie, J., & Prithiviraj, B. (2009). Seaweed extracts as biostimulants of plant growth and development. *Journal of Plant Growth Regulation, 28*(4), 386–399.

Krüger, A., Grüning, N. M., Wamelink, M. M., Kerick, M., Kirpy, A., Parkhomchuk, D., ... & Ralser, M. (2011). The pentose phosphate pathway is a metabolic redox sensor and regulates transcription during the antioxidant response. Antioxidants & redox signaling, 15(2), 311-324.

Kumar, S., Kaur, R., Kaur, N., Bhandhari, K., Kaushal, N., Gupta, K., ... & Nayyar, H. (2011). Heat-stress induced inhibition in growth and chlorosis in mungbean

(Phaseolus aureus Roxb.) is partly mitigated by ascorbic acid application and is related to reduction in oxidative stress. Acta Physiologiae Plantarum, 33(6), 2091-2101.

Langone, M., Basso, D., 2020. Process waters from hydrothermal carbonization of sludge: Characteristics and possible valorization pathways. *Int. J. Environ. Res. Public Health* 17, 6618.

Latique, S., Chernane, H., Mansori, M., & El Kaoua, M. (2013). Seaweed liquid fertilizer effect on physiological and biochemical parameters of bean plant (*Phaseolus vulgaris* L.) under drought stress. *Journal of Stress Physiology & Biochemistry, 9*(2), 254–264.

Leng, L., Zhang, W., Leng, S., Chen, J., Yang, L., Li, H., Jiang, S., Huang, H., 2020. Bioenergy recovery from wastewater produced by hydrothermal processing biomass: Progress, challenges, and opportunities. *Sci. Total Environ.* 748, 142383.

Maniscalco, M.P., Volpe, M., Messineo, A., 2020. Hydrothermal carbonization as a valuable tool for energy and environmental applications: A review. *Energies* 13, 4098.

Mashabela, M. D., Terefe, T., Kerchev, P., Sitole, L., & Mhlongo, M. I. (2025). Next-generation biostimulants: molecular insights, digital integration, and regulatory frameworks for sustainable agriculture. Frontiers in plant science, 16, 1710899.

Mittler, R. (2017). ROS are good. *Trends in Plant Science, 22*(1), 11–19.

Nardini, A. (2022). Hard and tough: The coordination between leaf mechanical resistance and drought tolerance. *Flora, 288*, 152023.

Nardini, A., Battistuzzo, M., & Savi, T. (2021). Shoot desiccation and hydraulic failure: A dangerous synergy in drought-induced tree mortality. *Tree Physiology, 41*(2), 225–234.

Paparella, S., Araújo, S.S., Rossi, G., Wijayasinghe, M., Carbonera, D., Balestrazzi, A., 2015. Seed priming: State of the art and new perspectives. *Plant Cell Rep.* 34, 1281–1293.

Pereira, P., Pereira, J. L., Marques, A., Marques, C., Brandão, F., Cesário, R., Frankenbach, S., Serôdio, J., Gonçalves, F. J. M., Canário, J., & Pacheco, M. (2024). Redox Homeostasis Disclosed in the Saltmarsh Plant Halimione portulacoides upon Short Waterborne Exposure to Inorganic Mercury. Toxics, 12(3), 211.

Petruzzellis, F.; Savi, T.; Bacaro, G.; Nardini, A. A Simplified Framework for Fast and Reliable Measurement of Leaf Turgor Loss Point. Plant Physiol. Biochem. 2019, 139, 395–399.

Poorter, H., Niklas, K. J., Reich, P. B., Oleksyn, J., Poot, P., & Mommer, L. (2012). Biomass allocation to leaves, stems and roots: Meta-analyses of interspecific variation and environmental control. *New Phytologist, 193*(1), 30–50.

Resco de Dios, V., Roy, J., Ferrio, J. P., Alday, J. G., Landais, D., Milcu, A., & Gessler, A. (2018). Processes driving nocturnal transpiration and implications for estimating land evapotranspiration. *Scientific Reports, 8*, 12760.

Rodríguez-Domínguez, C. M., & Brodribb, T. J. (2020). Declining root water transport drives stomatal closure in olive under moderate water stress. *New Phytologist, 225*(1), 126–134.

Rouphael, Y., & Colla, G. (2020). Biostimulants in agriculture. *Frontiers in Plant Science, 11*, 40.

Spagnuolo, D., Bressi, V., Chiofalo, M. T., Morabito, M., Espro, C., Genovese, G., Iannazzo, D., & Trifilò, P. (2023). Using the aqueous phase produced from hydrothermal carbonization process of brown seaweed to improve the growth of *Phaseolus vulgaris*. *Plants, 12*(14), 2745.

Srivastava, A. K., Kumar, J. S., & Suprasanna, P. (2021). Seed 'primeomics': Plants memorize their germination under stress. *Biological Reviews, 96*(4), 1723–1743.

Stemann, J., Putschew, A., Ziegler, F., 2013. Hydrothermal carbonization: Process water characterization and effects of water recirculation. *Bioresour. Technol.* 143, 139–146.

Teranishi, Y.; Tanaka, A.; Osumi, M.; Fukui, S. Catalase Activities of Hydrocarbon-Utilizing Candida Yeasts. Agric. Biol. Chem. 1974, 38, 1213–1220.

Tiryakioglu, M.; Eker, S.; Ozkutlu, F.; Husted, S.; Cakmak, I. Antioxidant Defense System and Cadmium Uptake in Barley Genotypes Differing in Cadmium Tolerance. J. Trace Elem. Med. Biol. 2006, 20, 181–189.

Trifilò, P., Raimondo, F., Nardini, A., Lo Gullo, M. A., & Salleo, S. (2004). Drought resistance of *Ailanthus altissima*: Root hydraulics and water relations. *Tree Physiology, 24*(1), 107–114.

Wang, X., Zhang, X., Li, J., & Guo, Y. (2020). Effects of hydrothermal carbonization process water on seed germination and seedling growth of cabbage. *Journal of Cleaner Production, 256*, 120353.

Wang, Y.-S., Zhang, J.-L., Chen, Y.-J., Posch, B.C., Yang, D., He, P.-C., Zhu, S.-D., Ning, Q.-R., Lu, L.-X., Zhang, H.-P., Wang, Z., Liu, M.-Y., Chen, H., Ye, Q. and Liu, H. (2026), Leaf economic traits link drought and heat tolerance of woody species in two contrasting hydrothermal habitats. New Phytol.

Waqas, M.A., Kaya, C., Riaz, A., Farooq, M., Nawaz, I., Wilkes, A., Li, Y., 2019. Potential mechanisms of abiotic stress tolerance in crop plants induced by thiourea. *Front. Plant Sci.* 10, 1336.

Yakhin, O. I., Lubyanov, A. A., Yakhin, I. A., & Brown, P. H. (2017). Biostimulants in plant science: A global perspective. *Frontiers in Plant Science, 7*, 2049.

Zandi, P., & Schnug, E. (2022). Reactive oxygen species, antioxidant responses and implications from a microbial modulation perspective. Biology, 11(2), 155.

Zhang, Z., Li, Z., Jiao, F., Zhang, H., Chen, J., & Wang, M. (2026). The pentose phosphate pathway influences maize radicle growth through regulating reactive oxygen species levels. Crop Design, 100131.

Zheng, C., Ma, H., Sun, H., Tao, D., Zhao, H., Gao, S., & Zhang, Y. (2026). Integrative Strategies for Promoting Plant Salt Tolerance: Root Interactions, Microbial Inoculants, and Biostimulants.

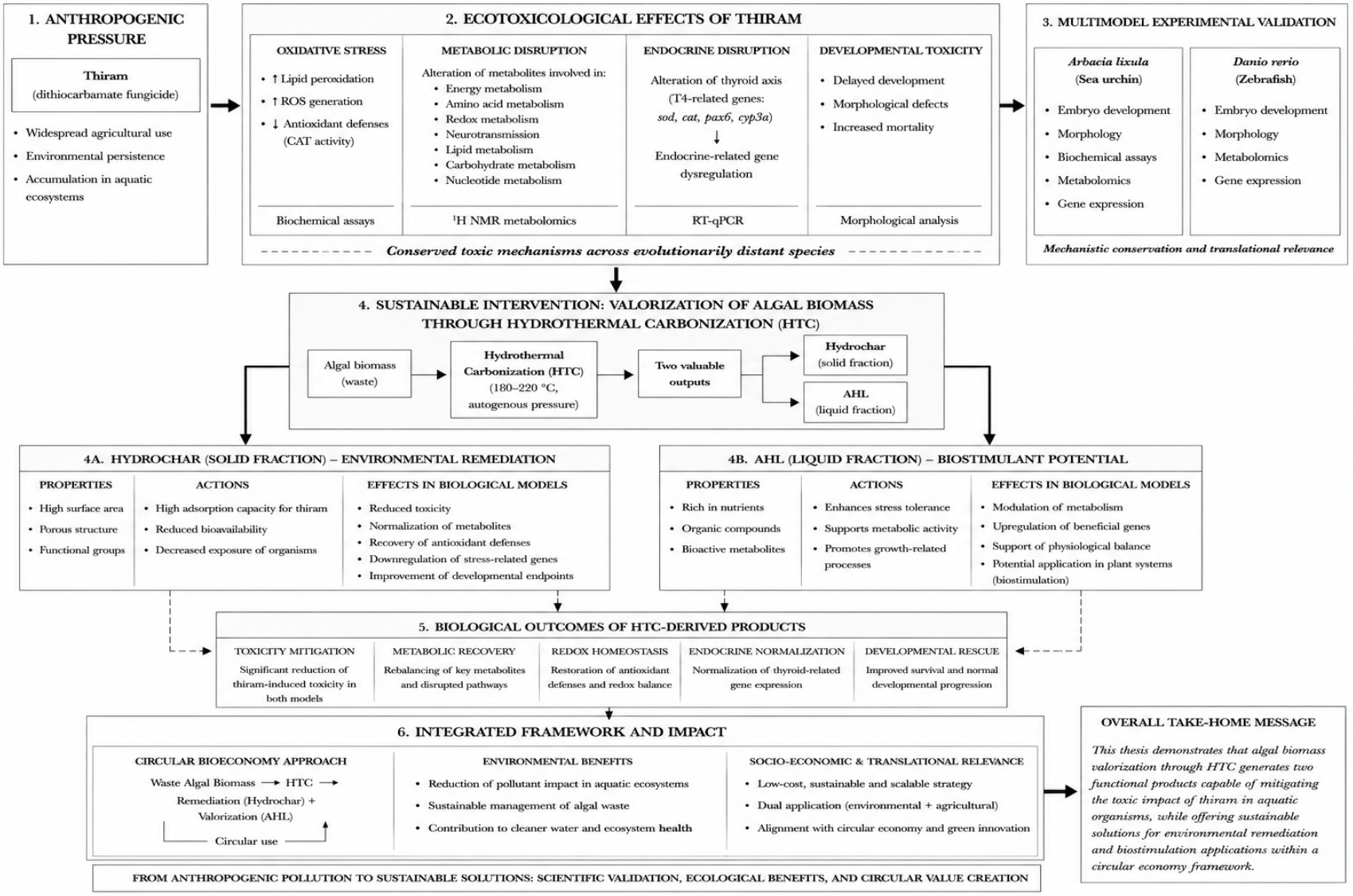
CHAPTER 8

General conclusion

8.1 General conclusion

The results presented in this thesis demonstrate that the fungicide thiram exerts consistent and biologically relevant toxic effects on early developmental stages of aquatic organisms across phylogenetically distant models. In both the sea urchin *Arbacia lixula* and the zebrafish *Danio rerio*, thiram exposure induced marked developmental toxicity, including increased mortality, delayed or arrested embryogenesis, morphological abnormalities, and profound biochemical, molecular, and metabolic alterations at concentrations well below those associated with acute lethality. These findings highlight the high sensitivity of embryonic development to sublethal chemical stress and confirm the suitability of both models for investigating ecotoxicological risk. At the mechanistic level, the integrated analysis of oxidative stress markers, transcriptional responses, and metabolomic profiles revealed that thiram acts as a multifactorial stressor, disrupting redox homeostasis, energy metabolism, and developmentally relevant regulatory pathways. Notably, particular alterations were observed in molecular targets associated with thyroid hormone–related signaling, supporting the role of thiram as an endocrine-disrupting compound capable of interfering with evolutionarily conserved pathways that regulate growth and development in both invertebrates and vertebrates. These results reinforce the ecological relevance of thyroid-related disruption as a sensitive mechanism underlying pesticide-induced developmental toxicity. A central outcome of this work is the demonstration that algal-derived hydrochar, produced through hydrothermal carbonization of waste biomass, effectively mitigates the toxic effects exerted by thiram in both *Arbacia lixula* and *Danio rerio*. Hydrochar treatment significantly reduced developmental abnormalities, attenuated oxidative and endocrine-related

molecular perturbations, and promoted a partial restoration of altered metabolic profiles, indicating a reduction in thiram bioavailability and biological impact. The consistency of these protective effects across distinct biological models supports the robustness of hydrochar as an eco-sustainable adsorbent for pesticide mitigation in aquatic environments. The results obtained in this thesis support the potential use of algal-derived hydrochar as a sustainable adsorbent for the mitigation of pesticide contamination in aquatic environments, suggesting its possible integration into water treatment strategies aimed at reducing the bioavailability of hazardous compounds. In parallel, the HTC-derived aqueous liquid (AHL) was shown to exert beneficial effects on plant growth and stress tolerance, acting as a natural biostimulant capable of enhancing physiological and metabolic resilience under adverse conditions. Together, these findings demonstrate the dual valorization of HTC products, in which the solid fraction is employed for contaminant mitigation while the liquid fraction is repurposed to support plant performance. Taken together, the results of this thesis provide experimental evidence that hydrothermal carbonization represents a versatile and sustainable platform capable of addressing environmental contamination through an integrated pollution–mitigation approach. By transforming waste algal biomass into functional materials with distinct and complementary applications, this work contributes to the development of circular strategies that simultaneously reduce environmental risk, promote resource efficiency, and support ecosystem resilience.


1. ANTHROPOGENIC PRESSURE
Thiram
(dithiocarbamate fungicide)
• Widespread agricultural use
• Environmental persistence
• Accumulation in aquatic ecosystems
2. ECOTOXICOLOGICAL EFFECTS OF THIRAM
OXIDATIVE STRESS
• ↑ Lipid peroxidation
• ↑ ROS generation
• ↓ Antioxidant defenses (CAT activity)
Biochemical assays
METABOLIC DISRUPTION
Alteration of metabolites involved in:
• Energy metabolism
• Amino acid metabolism
• Redox metabolism
• Neurotransmission
• Lipid metabolism
• Carbohydrate metabolism
• Nucleotide metabolism
¹H NMR metabolomics
ENDOCRINE DISRUPTION
Alteration of thyroid axis (T4-related genes: sod, cat, pax6, cyp3a)
↓
Endocrine-related gene dysregulation
RT-qPCR
DEVELOPMENTAL TOXICITY
• Delayed development
• Morphological defects
• Increased mortality
Morphological analysis
Conserved toxic mechanisms across evolutionarily distant species
3. MULTIMODEL EXPERIMENTAL VALIDATION
Arbacia lixula (Sea urchin)
• Embryo development
• Morphology
• Biochemical assays
• Metabolomics
• Gene expression
Danio rerio (Zebrafish)
• Embryo development
• Morphology
• Metabolomics
• Gene expression
Mechanistic conservation and translational relevance
4. SUSTAINABLE INTERVENTION: VALORIZATION OF ALGAL BIOMASS THROUGH HYDROTHERMAL CARBONIZATION (HTC)
Algal biomass (waste)
Hydrothermal Carbonization (HTC) (180–220 °C, autogenous pressure)
Two valuable outputs
Hydrochar (solid fraction)
AHL (liquid fraction)
4A. HYDROCHAR (SOLID FRACTION) – ENVIRONMENTAL REMEDIATION
PROPERTIES
• High surface area
• Porous structure
• Functional groups
ACTIONS
• High adsorption capacity for thiram
• Reduced bioavailability
• Decreased exposure of organisms
EFFECTS IN BIOLOGICAL MODELS
• Reduced toxicity
• Normalization of metabolites
• Recovery of antioxidant defenses
• Downregulation of stress-related genes
• Improvement of developmental endpoints
4B. AHL (LIQUID FRACTION) – BIOSTIMULANT POTENTIAL
PROPERTIES
• Rich in nutrients
• Organic compounds
• Bioactive metabolites
ACTIONS
• Enhances stress tolerance
• Supports metabolic activity
• Promotes growth-related processes
EFFECTS IN BIOLOGICAL MODELS
• Modulation of metabolism
• Upregulation of beneficial genes
• Support of physiological balance
• Potential application in plant systems (biostimulation)
5. BIOLOGICAL OUTCOMES OF HTC-DERIVED PRODUCTS
TOXICITY MITIGATION
Significant reduction of thiram-induced toxicity in both models
METABOLIC RECOVERY
Rebalancing of key metabolites and disrupted pathways
REDOX HOMEOSTASIS
Restoration of antioxidant defenses and redox balance
ENDOCRINE NORMALIZATION
Normalization of thyroid-related gene expression
DEVELOPMENTAL RESCUE
Improved survival and normal developmental progression
6. INTEGRATED FRAMEWORK AND IMPACT
CIRCULAR BIOECONOMY APPROACH
Waste Algal Biomass → HTC → Remediation (Hydrochar) + Valorization (AHL)
Circular use
ENVIRONMENTAL BENEFITS
• Reduction of pollutant impact in aquatic ecosystems
• Sustainable management of algal waste
• Contribution to cleaner water and ecosystem health
SOCIO-ECONOMIC & TRANSLATIONAL RELEVANCE
• Low-cost, sustainable and scalable strategy
• Dual application (environmental + agricultural)
• Alignment with circular economy and green innovation
OVERALL TAKE-HOME MESSAGE
This thesis demonstrates that algal biomass valorization through HTC generates two functional products capable of mitigating the toxic impact of thiram in aquatic organisms, while offering sustainable solutions for environmental remediation and biostimulation applications within a circular economy framework.
FROM ANTHROPOGENIC POLLUTION TO SUSTAINABLE SOLUTIONS: SCIENTIFIC VALIDATION, ECOLOGICAL BENEFITS, AND CIRCULAR VALUE CREATION

8.2 Future perspectives

Future research should broaden the application of hydrochar-based mitigation strategies to additional environmental contaminants, including pesticide mixtures and emerging pollutants, under environmentally realistic exposure scenarios. Extending this approach to further aquatic model organisms, both invertebrates and vertebrates, would help assess the robustness and generalizability of hydrochar-mediated mitigation across different levels of biological complexity. From an agronomic perspective, the potential of HTC-derived aqueous liquids (AHL) as plant biostimulants should be further explored by testing their effectiveness across different plant species and stress conditions. In particular, evaluating AHL-induced resilience under both abiotic and biotic stresses, especially those associated with climate change, will be essential to define their role in sustainable agriculture. From an application and sustainability standpoint, scaling up hydrothermal carbonization processes and evaluating HTC-derived products in mesocosm or field-based systems represent key steps toward real-world implementation. Assessing hydrochar performance under dynamic and continuous-flow conditions may support its integration into wastewater treatment plants as a low-impact, bio-based material for tertiary treatment and contaminant polishing. Finally, within a circular economy framework, this approach can be extended to HTC products derived from different algal species and other organic waste biomasses. Comparative feedstock analyses may identify optimal biomass–product combinations for specific environmental and agricultural applications, contributing to flexible and sustainable strategies for addressing environmental pollution, climate change–related stressors, and resource recovery.